

Facies architecture, paleodischarge, and the variability of confluence scours in Cretaceous Rivers: Ferron Sandstone, Utah and Torrivio Sandstone, New Mexico, USA
By: SANDEEP SHARMA, M.Sc., B. Sc.
A Thesis Submitted to the School of Graduate Studies in Partial Fulfillment of the Requirements for the Doctor of Philosophy Degree
McMaster University © Copyright by Sandeep Sharma, September 2025

McMaster University Doctor of Philosophy (2025)

Hamilton, Ontario, Canada (School of Geography and Earth Sciences)

TITLE: Facies architecture, paleodischarge, and the variability of

confluence scours in Cretaceous Rivers: Ferron Sandstone,

Utah and Torrivio Sandstone, New Mexico, USA

AUTHOR: Sandeep Sharma

M. Sc. (Geology)

Banaras Hindu University

SUPERVISOR: Dr. Janok P. Bhattacharya

Professor and Susan Cunningham Research Chair in

Geology

NUMBER OF PAGES: xx, 170

Lay Abstract

The current thesis is focussed on quantitative estimation of the total sediment transported by a river system and to match that with the volume of sediment deposited in downstream sink, like a delta or a submarine fan. These estimations and predictions are of economic importance, like in hydrocarbon exploration they can help in predicting the total sand volume or reservoir volume and mudstone volume or source-rock volume. Quantitative reconstruction of river channels and channel belt deposits is also useful for characterising ground water aquifers; especially aquifers wherein stacking and spatial distribution of sandstone bodies might control aquifer volume and flow pathways. Novel use of images acquired using drones, aka UAVs, helped in building virtual three-dimensional outcrops to aid the study. This is particularly helpful where outcrops are shear vertical cliffs and hence difficult to access. The study also showed that statistical methods, like the Monte-Carlo simulation, can be successfully applied in geological studies.

Abstract

This thesis is focused on the integration of facies architectural analysis with 3D drone imagery, to provide quantitative analysis of ancient North American Cretaceous river systems. Paleo-digital elevation models were used for estimating drainage area, consistent with previous paleogeographic reconstructions. Monte-Carlo simulations, in combination with physics-based, empirically-derived equations, were used to estimate paleodischarge and downstream sediment volumes. This represents novel use of datasets and methods in quantitative estimation of ancient fluvial systems. This quantitative approach has broad implications for source-to-sink scaling relationships, such as predicting ancient drainage areas, that can be important in paleotectonic and paleogeographic reconstructions, as well as prediction of downstream sink volumes, which have economic importance, as these estimations can be used in hydrocarbon exploration in predicting the volumes of both the reservoir as well as the source rocks. These are also useful for characterizing aquifers to assess aquifer volume and flow pathways. This thesis also addresses a number of on-going scientific debates. The lack of braided rivers imaged using 3D seismic data has raised questions about the preservability of braided river deposits. This thesis provides an unequivocal example of a braided fluvial system from the late Cretaceous Torrivio Sandstone in New Mexico, USA. There is also some debate on how to distinguish autogenic scours from allogenic scour surfaces in ancient systems, with implications for identifying regional sequences. This thesis presents examples of a wide variety of autogenic fluvial scour surfaces, including bar-top hollows, bar-scale confluence scours and channel scours, ranging from normal small-scale channel confluence scours to larger tributary junction scours. The criteria described in this thesis enable the distinction of autogenic scours from regional allogenic incised valley surfaces that define sequence boundaries. The thesis also addresses the long debated concept of "Big River" systems. Integration of qualitative facies architecture analysis with quantitative estimates, derived using novel datasets and methods, show that the scale of major depositional elements can be used to estimate the size and scale of formative rivers and help to distinguish deposits of continental-scale river systems from the smaller rivers documented herein.

Acknowledgments

I would like to begin by expressing my sincere gratitude to my academic supervisor, Dr. Janok Bhattacharya, for guiding me throughout the long path of my PhD. I would like to thank him for his continued support, patience and enthusiasm. I am also grateful for the patience, support and guidance of my supervisory committee members, Dr. Carolyn Eyles and Dr. Joseph Boyce, throughout the period of my research.

I would like to thank the undergraduate students Zachary Waller, Monica Walecki, Curtis Ferron, Andrew Stockford, Tanisha Sharma and Rachel Nelson who worked tirelessly in the field assisting me. I would also like to thank David Kynaston for helping with drone imaging of outcrops.

This research was funded with the generous support of the Susan Cunningham Research Chair at McMaster University, Quantitative Sedimentology Laboratories, with funding from NSERC. Permission for this research was provided by the Bureau of Indian Affairs, Navajo Region, Gallup, New Mexico, USA.

Above all, I think if there's one person who is single-handedly responsible for my successfully finishing this thesis, that person is my wife. If it wasn't for her unwavering support, sacrifices and love, I wouldn't be here. I would also like to thank my therapist for helping me though this long and extremely difficult phase of life. Special mention goes to my beloved pooch Kaia, whose introduction in my life rekindled hope for a successful finish.

Table of Contents

Lay Ab	stract		iii
Abstrac	et		iv
Acknow	wledgn	nents	V
Table o	f Cont	ents	vi
List of	Tables		ix
List of	Figures	5	X
Declara	ition of	Academic Achievement	xix
Chapter	r 1		1
Intro	ductio	n	1
1.1	Resear	ch Objectives	4
1.2	Thesis	Organization	7
Refe	erences		8
Chapter	r 2		. 14
		sink sediment budget analysis of the Cretaceous Ferron Sandstone, Utah he Fulcrum approach	
2.1	Introdu	action	. 15
2.2	Study	area	. 17
2.3	Metho	dology	. 21
	2.3.1	Estimation of bankfull channel dimensions	. 22
	2.3.2	Estimation of bankfull discharge	. 23
	2.3.3	Estimation of mean annual sediment discharge	. 26
	2.3.4	Estimation of mass balance across the fulcrum	. 27
2.4	Result	S	. 27
	2.4.1	Estimation of bankfull channel dimensions	. 28
	2.4.2	Estimation of bankfull discharge	. 32
	2.4.3	Estimation of mean annual sediment discharge	. 36
	2.4.4	Estimation of mass balance across the fulcrum	. 36
2.5	Discus	sion	. 39
	2.5.1	Sediment escape	. 39

		2.5.2	Errors and uncertainties	40
		2.5.3	Evaluation of uncertainty using Monte Carlo simulation	43
	2.6	Conclu	usions	47
	Ref	erences		48
Ch	apte	er 3		56
	Fac		nitecture and paleohydraulics of the late Cretaceous Torrivio Sandston Mexico, USA	
	3.1	Introd	uction	57
		3.1.1	The Torrivio Sandstone, regional setting and previous work	58
	3.2	Study	area and methodology	61
	3.3	Result	s	69
		3.3.1	Litho-facies classification	69
		3.3.2	Architectural elements	72
		3.3.3	Nature of fluvial system in the Torrivio Sandstone	84
		3.3.4	Paleohydraulic calculations	93
	3.4	Discus	ssion	102
		3.4.1	Number of channels in the Torrivio River	102
		3.4.2	Mean annual discharge	106
		3.4.3	Drainage area	113
		3.4.4	Was Torrivio a "big river"?	115
	3.5	Conclu	usions	117
	Ref	erences		118
Ch	apte	er 4		134
	Sca	le of co	influence scours in the late Cretaceous Torrivio Sandstone, NM, USA.	134
	4.1	Introd	uction	135
	4.2	Conflu	ience morphology	136
	4.3	The To	orrivio Sandstone, regional setting and previous work	138
	4.4	Study	area and methodology	138
	4.5	Beddin	ng geometry of DS-2	140
			of confluence scours in the Torrivio Sandstone	142

	4.6.1.	Confluence scours downstream of braid bars	142
	4.6.2.	Channel confluence scours.	145
4.7	Discus	sion	149
	4.7.1.	Confluence scours or incised valleys?	149
	4.7.2.	Relative scour depth	151
4.8	Conclu	nsions	154
Refe	erences		155
Chapte	r 5		162
Con	clusion	ıs	162
5.1	Future	directions	165
Refe	erences		167

List of Tables

Table 2.1. Estimation of paleohydrology, discharge, and sediment volume for the Ferron
trunk valley
Table 2.2. Range of input variables (as in Eq. 2.6) used in the Monte Carlo simulations
based probabilistic estimation and the resulting P10, P50, and P90 values for mean annual
bedload volume (m ³) highlighting the range of possible outcomes44
Table 3.1. Major lithofacies classes for the Torrivio Sandstone in the study area70
Table 3.2. Deterministic palaeohydrological estimation of the main zone of the Torrivio
Sandstone
Table 3.3. Major Input variables from analogous river systems for bankfull duration and RI
used in the Monte-Carlo simulation. Please see the text for source of the data110
Table 3.4. The results of the Monte Carlo simulations-based estimation and the resulting
$P10$, $P50$, and $P90$ values (90% certainty) for mean annual bedload volume (m^3) highlight
the range of possible outcomes.

List of Figures

Figure 2.1. A) Paleogeographic map showing the location of deltaic wedges of the Western Interior Seaway during the Turonian, including the Ferron Notom delta (red stippled)
(modified after Bhattacharya et al. 2016); B) Stratigraphic position of the Ferron Sandstone (after Fielding 2010)
Figure 2.2. A) Dip and B) strike stratigraphy of the Ferron Notom delta showing the constituent parasequences, parasequence sets, and sequences (modified after Zhu et al. 2010), the Ferron outcrop belt shown is in the inset. C) The paleogeographic map of PS-6 showing the wave-influenced, river-dominated delta fed by an incised valley (Ahmed et al. 2014). Also shown are the areal extent of the depositional sink (in black polygon) and the projected downdrift extension of the shoreface (in red polygon) of PS-6. See text for details.
Figure 2.3. The fulcrum workflow for mass balance (after Holbrook and Wanas 2014)21
Figure 2.4. Diagram illustrating the threshold for initiation of motion and suspension for a range of particle parameters (from van Rijn 1984b). The critical mobility parameter, used in the estimation of u_{*cr} , is obtained from the van Rijn range at a particle parameter of 15 (black bars). See text for details.
Figure 2.5. Histogram for distribution of vertical thickness of cross-bed sets from Richards (2014). The mean cross-bed set thickness is 0.18 m
Figure 2.6. Measured section showing the vertically amalgamated fluvial channel stories in PS-6 (Richards 2014). The maximum thickness of the channel as observed in the outcrop is approximately 6 m, which is very close to the thickness (5.5 m) estimated in the current study.
Figure 2.7. Architectural elements observed at marine-to-nonmarine transition in the Ferron Notom Delta at south Cainville, Utah USA. The accretion surfaces observed in the meander belts in Sequence 2 are shown above the sequence boundary (SB 2 in red). The widths of accretion surfaces have been used to estimate the range of bankfull channel widths in the

fulcrum calculation (modified after Zhu (2010)) (PF, Prodelta fines; PH, Prodelta
hyperpycnites; SS, Storm sheets; FS, Frontal splay; TC, Terminal distributary channel; AF,
Abandoned channel; MA, Mouth-bar accretion)31
Figure 2.8. Isopach map of Parasequence 6 overlaid with the sink area polygon (blue). For
Parasequence 6, the total bedload sediment volume in the sink area, corrected for 20%
porosity, is approx. two-thirds of the bedload sediment volume passing through the
fulcrum. See text for details
Figure 2.9. Plot of percentage of suspended load transported in 2% or 7.3 days (Ms ₂) against
basin area. For Ferron, with an area of 50,000 km ² , this percentage is about 50%. (From
Meybeck et al. 2003)
Figure 2.10. The results of the Monte Carlo simulation showing A) the lognormal
probability distribution for the bankfull bedload discharge (Q_{tbf}), the annual bankfull
duration (t_{bd}) , and the proportion of annual sediment load carried during the bankfull period
(b); B) the frequency distribution of mean annual sediment load (Q_{mas}) after 1000
realizations; and C) sensitivity plot for inputs to the Q_{mas} calculation
Figure 3.1. Late Coniacian (87 Ma) paleogeography of the Western Interior Seaway
showing the schematic of the Torrivio Rivers (blue lines) with their catchment located
within the Mogollon Highlands. (Reconstruction and paleolatitude after Roberts and
Kirschbaum 1995; Blakey 2014; and Ferron 2019)59
Figure 3.2. High resolution sequence stratigraphic reconstruction of the Gallup Sandstone
and the younger Torrivio Sandstone. The area covered in the current study is shown by the
black rectangle (Lin et al. 2019).
Figure 3.3. A) Outcrop map of Torrivio and Gallup Sandstone around the town of Gallup,
New Mexico, USA. The measured sections done throughout the current campaign are
represented by red circles while those used here are shown by black circles. B) Location
map of strike (Yellow) and dip (Black) sections used in the current study. The section
shown in white is used for channel-width estimation in Fig. 3.2764

Figure 3.4. Close-up of 3D model built using high-resolution drone images. A) Three points
are selected on a suitable cross-lamina and a surface is drawn through it to estimate the
azimuth using three-point solution (Hasbergen 2012). B) The same structure is shown in
the actual drone image. Please refer to the text for model details
Figure 3.5. Cumulative curve for grain size distribution in the A) Lower (main) zone and B) Upper zone of the Torrivio Sandstone
Figure 3.6. Major litho-facies associations found in the Torrivio Sandstone. A) Fr: massive mudstone with rootlets; B) Fl: mudstone dominated heterolithic deposit in overbank; C) Ripples and ripple cross-laminations (Sr) towards channel abandonment; D) St with smaller Sp units towards the top (left) and Sp as confluence fill (right); E) GI: granules and pebbles lining the channel base (left) and Gt: granules lining cross-laminae (right). The hammer is
30 cm long
Figure 3.7. Major architecture elements and the associated litho-facies associations found in the Torrivio Sandstone. Fl: overbank and/or abandoned channel deposit, Sr: ripples or ripple-cross laminated sandstone, Sp: planar-cross stratified sandstone, St: trough cross stratified sandstone, Gl: granules and pebbles at channel base, UB: unit bar, CB: compound
bar, HO: confluence fill or hollow element
Figure 3.8. Examples of completely preserved channel stories in SS-2. These have been used as proxy for bankfull channel depth estimation
Figure 3.9. Channel-fill dominated by mudstone with lenses of ripple-laminated sandstone in SS-1. The overall percentage of sandstone decreases upwards74
Figure 3.10. 4th order cross-bar channel truncating bars in SS-3. The channel is filled with trough cross-stratified units (St) at the base and planar cross-stratified units (Sp) at the top. The blue box highlights its position in the interpreted cross section
Figure 3.11. Un-interpreted and interpreted sections showing unit bars and compound bar filling in the 4th order and 5th order channels in SS-2. Although planar cross-stratification
(Sp) is the common facies, trough cross-stratification (St) is also present

Figure 3.12. Un-interpreted and interpreted section of SS-3, showing Unit bar with Sp and
sigmoidal reactivation surfaces truncating the laminae. The location of this figure is shown
by Box-3 (blue) on Fig. 3.18
Figure 3.13. Un-interpreted and interpreted section of SS-1, showing the hierarchy of bars. UB-Unit bar; CB-Compound bar. Also shown are the small-scale cross-sets representing dunes riding over the bar complex
Figure 3.14. Compound bar with Sp and convex-to-sigmoidal reactivation surfaces truncating the laminae. The location of this figure is shown by Box-1 (Blue) in SS-1 in Fig. 3.16
Figure 3.15. DS-2 showing three units within the Torrivio Sandstone separated from the Gallup non-marine unit by a sequence boundary of 7th order. A large downstream migrating bar represents the main Torrivio unit while the upper Torrivio unit shows
evidence of downstream migration of fluvial point bars. The section is oriented relative to the outcrop with the solid arrows highlighting paleo-flow direction and dashed arrows showing the paleo-accretion direction. This section is described in detail in Chapter 479
Figure 3.16. SS-1 showing the lower braided unit and the upper sinuous single-channel unit. Mounded geometries emphasize the braided nature of the river system in the lower main unit, as does a 2.25 m thick foreset deposited in a channel-confluence scour (CS). Higher up in the braided section, bars migrating at higher angles relative to the mean paleoflow direction can be seen. Internal architecture of the mud-dominated channel fill is shown in Fig. 3.9. The section is oriented relative to the outcrop with downward arrows coming out of the paper while others point in oblique direction to the left of the paper. See Fig. 3.15 for legends and symbols
Figure 3.17. SS-2 showing braid bars with mounded geometries. Bar-scale confluence scour (CS) with 7 cross-set units. Also, present is the bar-top hollow element with a single set of cross-set. Bars migrating laterally into the channel can be seen in the upper zone of

the Torrivio Sandstone (LA). Dashed arrows represent paleo-accretion direction. Refer to
Fig. 3.15 for legends and symbols. Box-2 is described in detail in Fig. 3.20A and B83
Figure 3.18. SS-3 showing bar-scale confluence (CS) fill with 6 units of cross-stratification
Mounded geometry of the braid bars in the lower unit and point bars in the upper unit is
evident. The internal geometry of the cross-bar channel is shown on Fig. 3.10. Reactivation
surfaces within unit bars can be seen in Box-3, the details of which are shown in Fig. 3.12
See Fig. 3.15 for legends and symbols.
Figure 3.19. Multiple tabular units of splay deposits lying below a 5th order channel. These units are sharp based and contain occasional local scour and generally taper out in the down-flow direction (yellow arrow).
Figure 3.20. A) Bidirectional cross beds and vertical burrows in the Gallup non-marine unit. See text for details. B) Teredolites burrows associated with coal, suggesting a woodground substrate. The carbonaceous mudstone shows prominent rootlets
Figure 3.21. A) "Giant" cross-set in SS-2 associated with braid bars accreting on slip-face of a large bank-attached bars or alternate bars. The location of the section is highlighted by blue box-2 in SS-2 in Fig. 3.17. B) Line diagram of the "giant" cross-set in SS-2 showing intrasets and backsets. See text for details.
Figure 3.22. A) Oblique dip section with a 2 m thick foreset showing small-scale channel confluence. B) Steeply inclined bar, which reaches a thickness of up to 3.9 m, possibly prograding into a channel confluence scour. Location of the measured section is encircled on the map in the inset.
Figure 3.23. 3D block diagram showing the braided nature of the Torrivio Sandstone. The architectural elements drawn represent features seen in the outcrops, but no scale intended
Figure 3.24. The upper Torrivio unit at SS-2 showing fluvial point bars (in blue) laterally migrating into 5th order channel. The solid arrow indicates paleoflow direction (median 20°) whereas the dashed arrow represents the paleoaccretion direction (315°)

Figure 3.25. The lower (orange) and upper (blue) sub-units within the Torrivio section at
SS-3. The lower unit is distinctly laterally migrating while the bars in the upper unit are
migrating obliquely into the channel. The solid arrow indicates paleoflow direction whereas
the dashed arrow represents the accretion direction92
Figure 3.26. Cumulative distribution curve for dune-scale cross-sets from the main braided
zone of the Torrivio Sandstone. Median cross-set thickness is 21 cm (black dotted line).
95
Figure 3.27. Satellite image of a section of the Rakaia River, Canterbury, NZ showing the
channel hierarchy. (A) the channel belt (yellow line) while (B) and (C) are the major and
minor threads respectively
Figure 3.28. Outcrop section normal to the regional paleo flow. The whole outcrop is
approx. 800 m wide, which is enough to measure major channels. The 5th order channels
(in Blue) numbered 1, 2 and 3 are 180 m, 190 m and 340 m wide respectively97
Figure 3.29. Semi-log plot of bedforms as function of flow depth and velocity for a given
range of sandstone grain sizes. Here, the flow velocity for the Torrivio Sandstone (braided
unit) varies from 1.25 to 1.5 m/s, which closely follows the empirically derived values. See
text for details. Modified after Rubin and McCulloch (1980)100
Figure 3.30. Fluvial planform regime diagram (Parker 1976). The braided unit of the
Torrivio plots within the zone with 1-2 braids, highlighting that the Torrivio was probably
a weakly braided system (S-Slope, F-Froude number, $H_{\text{bf}}\text{-Bankfull}$ channel depth (m) and
B _{bf} -Bankfull channel width (m).
Figure 3.31. Log plot of stream power vs grain size (Kleinhans and van den Berg 2011)
highlighting that the main unit of the Torrivio Sandstone (Blue star) was deposited by a
weakly braided river
Figure 3.32. Paleo-Koppen climate zone distribution during the Turonian (A) and
Coniacian-Santonian (B) time. The corresponding zoomed-in section around the current
area of interest highlights a tropical wet climate (Af/Am). Paleo-climate study by Burgener

et al. (2023). As/Aw = tropical savannah; BSh = hot steppe, BSk = cold steppe, BWh = hot
desert, BWk = cold desert; Ca = temperate, humid subtropical, Cb = temperate, maritime
temperate, Cc = temperate, maritime subarctic; Da = continental, hot summer, Db =
continental, warm summer, Dc/Dd = continental, subarctic; E = polar106
Figure 3.33. Modern Koppen climate zone distribution map. Humid-subtropical climate is
represented by Cfa. Also plotted are the locations of the modern analogs from the sub-
tropical humid climates used in this study (www.gloh2o.org/koppen/)107
Figure 3.34. Flow duration curves for the River Po (A) and Brazos River (B) showing the
percentage of time their respective bankfull discharge was exceeded. See text for details.
Figure 3.35. A) The result of the Monte-Carlo simulation showing the range of P10, Median
and P90 values within 90% certainty window. B) Sensitivity of different parameters on the
outcome of the annual bedload discharge (m ³). The conversion of the instantaneous to mean
annual bankfull duration is the most sensitive factor in estimating the mean annual bedload
volume
Figure 3.36. Distribution and assumption charts for the variables used in the Monte-Carlo
simulation. Qtbf and Tbd follow log-normal distribution while the 1/b factor follows a
triangular distribution. See text for explanation
Figure 3.37. Paleogeographic reconstruction at Coniacian (~88.8 Ma) showing the Torrivio
drainage (after Ferron 2019). An approx. drainage area of 75,000 km² can be reasonably
estimated from the above reconstruction
Figure 4.1. Schematic diagram showing the confluence geometry and morphological units.
Q1 and Q2 represent discharge of the incoming channels, θ is the confluence angle, A
represents the confluence scour, B is the bar downstream of the confluence, C is the flow
separation bar, and D represents the tributary mouth bar (modified after Bristow et al.
(1993))

Figure 4.2. The measured sections done throughout the study campaign are represented by
red circles while the sections with confluences are shown by the black circles. Outcrop map
of Torrivio New Mexico, USA is modified after Nummedal and Molenaar, 1995. The
tributary channel confluence is present at DS-2, small-scale channel confluence can be seen
at DS-1 and SS-1 while bar-scale confluence can be seen at SS-2 and SS-3
Figure 4.3. The main unit in DS-2 consists of a large downstream migrating bar. The
oblique relationship between the paleo-flow and paleo-accretion direction within the main
unit is highlighted in the Rose diagrams. The upper Torrivio unit shows evidence of
downstream migrating fluvial point bar. The section is oriented relative to the outcrop with
the solid arrows highlighting paleo-flow direction and dashed arrows showing the paleo-
accretion direction
Figure 4.4. SS-2 showing braid bars with mounded geometries. Bar-scale confluence scour
(CS) with 7 cross-set units. Refer to Fig. 4.3 for legends and symbols143
Figure 4.5. SS-3 showing bar-scale confluence (CS) fill with 6 units of cross-stratification.
See Fig. 4.3 for legends and symbols
Figure 4.6. SS1 showing a 2.25 m thick foreset dipping at a steep angle into a small-scale
channel-confluence scour (CS). See Fig. 4.3 for legends and symbols146
Figure 4.7. A) Oblique dip section with a 2 m thick foreset showing small-scale channel
confluence. B) Steeply inclined bar, which reaches a thickness of up to 3.9 m, prograding
into a channel confluence scour
Figure 4.8. Cumulative probability distribution of the cross-set thickness at the tributary
junction (A) and at upstream channels (B). The median cross-set thickness at the tributary
junction is twice that at upstream channels. Also, the value of the thickest cross-set at the
tributary confluence is almost three-times that at upstream channels. All the measurements
are in cm. Distribution generated by the Data Analysis tool of the Oracle Crystal ball in MS
Excel 148

Figure 4.9. Digital elevation map showing the confluences of the Padma and Jamuna rivers
(A) and Padma and Upper Meghna rivers (B) respectively. The geographical location of
the area within Bangladesh is shown in the inset. The DEM used here is ASTER GDEM
v3 with a resolution of 1arc
Figure 4.10. Multiple scours can be seen at the confluence of the Jamun and Padma rivers
Each of these scours is deeper than the average depth of either of the two rivers, with the
main confluence being approx. 8 km long and 1.4 km wide. Data provided by British
Geological Survey materials © UKRI [2013-14]
Figure 4.11. The confluence of the Padma River with the Upper Meghna tributary. The
main confluence is approx. 6 km long and 900 m wide and has a scour which is close to 60
m deep. Data provided by British Geological Survey materials © UKRI [2013-14]153

Declaration of Academic Achievement

This thesis describes the research that I conducted under the guidance of Dr. Janok Bhattacharya, my PhD advisor, with assistance from Dr. Carolyn Hope Eyles and Dr. Joseph Boyce, on the supervisory committee. It is in integrated article format. The manuscripts for this thesis have been published, submitted, or prepared for final submission to peer-reviewed journals.

I used several software tools to accomplish my research projects: Microsoft office suite of software was used for calculations and thesis writing; Oracle Crystal Ball for Monte-Carlo simulations, QGIS was used for spatial data analyses and map preparation; and Adobe Illustrator and Photoshop were used for drafting measured sections and bedding diagrams.

Chapter 2: The content presented in this Chapter is published in:

Sharma, S., Bhattacharya, J.P., and Richards, B., 2017, Source-to-sink sediment budget analysis of the Cretaceous Ferron Sandstone, Utah, U.S.A., using the Fulcrum approach: Journal of Sedimentary Research, v. 87, no. 6, p. 594–608, doi: 10.2110/jsr.2017.23.

The measured sections used in this study were obtained by Dr. Bhattacharya's former MSc student Benjamin Richards, while all the analysis was carried out by me. I also drafted the text and figures for the paper and Dr. Bhattacharya helped improve the manuscript with expert reviews.

Chapter 3: The content of this chapter is drafted to be submitted as a journal article:

Sharma, S., and Bhattacharya, J.P., 2025, Facies architecture and paleohydraluics of the late Cretaceous Torrivio Sandstone, New Mexico, USA (in prep).

All the measured sections and two-dimensional photomosaics using GigaPan were obtained by me while the acquisition of the drone photos was carried out with the help of David Kynaston. The three-dimensional model building and extraction of high-resolution Orthomosaic were carried out by me. I drafted the text and prepared all the figures while Dr. Bhattacharya provided invaluable edits.

Chapter 4: This chapter has been drafted for submission as a journal paper:

Sharma, S., and Bhattacharya, J.P., 2025, Scale of confluence scours in the late Cretaceous Torrivio Sandstone, NM, USA (in prep).

All the data was acquired by me except for the drone photos, which were acquired with the help of Curtis Ferron and Rachel Nelson. I drafted the text and prepared all the figures while Dr. Bhattacharya helped by providing expert reviews.

Chapter 1

Introduction

Early facies models (e.g., Walker 1976) were largely qualitative and focused more on documenting the nature of depositional environments and their stratigraphic expressions especially as expressed in one-dimensional (1D) vertical measured sections. The introduction of facies architectural approaches emphasized geomorphic elements (e.g., Allen 1983; Miall 1985) with improved ability to interpret the nature of depositional systems, and particularly the nature of bars and channels in fluvial systems. This has now led to more quantitative estimates of ancient sedimentary systems. This revolution in sedimentological analysis of ancient fluvial systems has also evolved with larger scale sequence stratigraphic analysis that allows linkages between individual river deposits and their downstream sinks.

More recently this has led to the source-to-sink concept. Facies architecture analysis provides quantitative data that can be used to assess the size and scaling of depositional systems and to perform source-to-sink sediment budget analysis. Source-to-sink concepts, applied to ancient systems, provide quantitative estimates of paleodischarge and sediment budgets and are critical to establish scaling relationships between various components of a source-to-sink system, from source area to dispersal system (Bhattacharya et al. 2016). Paleodischarge studies of deep time systems have been used in estimating drainage areas that can be key in plate tectonic reconstructions, as well as in estimations of ancient climates (Bhattacharya and Tye 2004, Bhattacharya and MacEachern 2009, Davidson and North 2009). In source-to-sink studies, observations from one part of a linked depositional system, such as a fluvial trunk channel, can help make predictions about the other parts of the system such as down-dip shorelines or submarine fans (Bhattacharya et al. 2016). Both subsurface data and outcrop information can be used to predict and/or extrapolate upstream controls on stratigraphic architectures as well as the size of the rivers and volume of sediment delivered to depositional sinks (Bhattacharya et al. 2016; Lin and Bhattacharya

2016; Sharma et al. 2017). These predictions are of economic importance as well. In hydrocarbon exploration, quantitative source-to-sink analysis can be used to predict reservoir and source-rock volumes. Quantitative reconstruction of fluvial channels and channel belt deposits is also important for characterizing aquifers; especially alluvial aquifers wherein stacking and spatial distribution of channel and channel belt sandstone are a major control on aquifer volume and flow pathways (Van Dijk et al. 2016).

Quantitative estimation of channel dimensions is required to differentiate confluence scours from mean channel scours and incised valleys. Quantitative estimates of channel depth and channel slope are critical to define the backwater limit (calculated by channel depth divided by slope), and this has important implications for predicting channel and channel belt behavior and its stratigraphic expression. The backwater limit can also be used to predict heterogeneity of associated reservoirs and aquifers.

Changes in the river planform can be explained by using specific stream power and median grain size (Van den Berg 1995; Kleinhans and van den Berg 2011). The specific stream power is a function of width-average discharge and slope, which are the outcomes of quantitative source-to-sink analysis. For a given grain size, the increase in the specific stream power results in increased sediment transport, which results in changes in channel planform (Van den Berg 1995).

Different approaches to estimating sediment flux and establishing mass balance across linked source-to-sink system have been established. These include, in addition to others, (i) the empirical BQART model of Syvitski and Milliman (2007), which studies the contribution of drainage area, catchment lithology, relief, temperature and discharge to sediment load; (ii) the scaling relationship between different geomorphological elements of a linked system (Somme et al. 2009) and (iii) more recently the "fulcrum" approach (Holbrook and Wanas 2014), which is essentially based on the premise that over a given period of time, the total mass passing through a cross section of a trunk valley should be equal to that delivered from the source and to the sediment deposited in the sink (Holbrook and Wanas 2014). The fulcrum approach was tested in this research on the Ferron Sandstone, Utah, USA (Li et al. 2010; Zhu et al. 2012; Richards 2014). The availability of a high-resolution sequence stratigraphic framework, as well as chronometric control from

dating of bentonites, allowed individual rivers to be linked to downstream delta, shoreface and prodelta deposits (parasequences), allowing fulcrum estimates to be matched to measured sink volumes. The effects of annual bankfull duration and their recurrence intervals on the annual sediment volume was studied with the help of Monte-Carlo simulation based statistical method. This was done to capture the range of uncertainty in the annual bedload discharge estimation. The annual bankfull duration and the corresponding recurrence interval are one of the largest uncertainties in the fulcrum method. The results of this statistical exercise are presented in Chapter 2. This was one of the first studies to employ a Monte-Carlo statistical method to constrain the range of uncertainty in the estimation of the annual sediment load.

Recently, one of the most discussed topics amongst fluvial sedimentologists has been what constitutes a "Big River" (Miall and Jones 2003; Miall 2006; Fielding 2007; Lewin and Ashworth 2014). Quantitative estimates of dimensions of sandstone depositional elements from outcrop-based studies are required to distinguish deposits of big rivers from average rivers and are addressed in this thesis. To identify trunk versus distributary or tributary channels, size and scale of channel bodies, and their proxies (such as thickness of fining upward channel fills, and dune-scale cross set thickness) is critical. This is also required to distinguish channels formed in incised valleys from un-incised systems, and this is also critical for identifying sequences.

Following the application of the fulcrum method to an existing data set (the Ferron Sandstone), the next step was to identify a new field study site. The late Cretaceous Torrivio Sandstone was chosen as a new field study site for this research because its extensively exposed outcrops provide an excellent opportunity to map the different elements of a source-to-sink system in both dip and strike orientation (Nummedal and Molenaar 1995; Lin et al. 2019; Lin et al. 2021; Wu et al. 2022). In addition, this study of the Torrivio Sandstone was completed in conjunction with simultaneous studies, conducted as part of the McMaster Universities' Quantitative Sedimentology Laboratories, by Lin et al. (2019 and 2021) and Wu et al. (2022) that established a robust regional sequence stratigraphic framework of the Gallup Sandstone, with new chronometric control on bentonites that enable a source-to sink analysis. This study focused on the nature and size

of the more proximal feeder channel systems in the Torrivio that were hypothesized to be linked to the down-dip shorelines to establish a closed source-to-sink system. This used the same approach taken in our study of the Ferron Sandstone, but with an additional component of original fieldwork. Furthermore, it was apparent from a search of the scientific literature on different clastic wedges of the Cretaceous Interior seaway that qualitative and quantitative characterization of the Torrivio Rivers was lacking (Hohman 1986; Flores et al. 1991; Miall 1992). Although, a general braided nature of deposition has been proposed for the Torrivio Sandstone, other interpretations include deposition by a sinuous single-channel (e.g., Miall 1992). There has not been any attempt to carry out a quantitative estimation of the size and paleohydraulics of the rivers that formed the Torrivio Sandstone. This study aims to address these disparate previous interpretations.

To help with this study, novel data and approaches were used. For example, UAV images were used to make three-dimensional (3D) models of outcrops. This enabled analysis of inaccessible vertical outcrops that provide information on the dimension of key architectural elements, such as bars and channels, that are essential in making quantitative paleohydraulic analyses. The UAV data also provided 3D outcrop models that allowed us to use three-point solutions, previously used in structural geology applications (Hasbergen 2012), to estimate paleocurrent directions from cross beds imaged in the 3D models. The paleocurrent data is crucial in interpreting the bedding architecture and channel and bar types in the outcrop cliff faces that are used to make accurate interpretations of the fluvial style (i.e., single versus multi-thread, braided versus meandering). Although some of the previous studies interpreted plan view style based on the bedding geometry (e.g., Miall 1992), these studies lacked the all-important paleocurrent data that allows the orientation of cliff exposures relative to flow direction to be established and without which, interpretations of plan-view can be highly speculative.

1.1 Research Objectives

1. Testing the fulcrum approach to establishing mass-balance in a linked source-to-sink system. An identified Ferron trunk river (Richards 2014) was used as the fulcrum point across which a mass-balance was established using empirical equations and outcrop data

(Richards 2014). Statistical methods were employed to constrain the uncertainty in the paleodischarge and sediment volume estimates of individual parasequences within a well-established chronometric and sequence stratigraphic framework. The estimated sediment volumes were then compared with mapped volumes of sandstone and mudstone in sedimentary sinks to test the fulcrum method and improve its uncertainties and errors.

2. Establishing facies architecture and planform style of ancient river systems responsible for the deposition of the late Cretaceous Torrivio Sandstone. Historically, alluvial channels have been grouped into distinct classes of straight, meandering, braided and anastomosed (Leopold and Wolman 1957), although more recent studies have established that that is not the case and they are represented by a continuum of planform geometries (Nanson and Knighton 1996; Bridge 2003; Kleinhans and van den Berg 2011). Changes in planform can be explained in terms of stream power (Ω) , which is a function of river discharge and slope ($\Omega = \rho gQS$, where ρ is density; g is the acceleration due to gravity, constant at 9.8 m/s²; Q is discharge and S is the channel slope). An increase in stream power generally favours a more braided planform (van den Berg 1995; Kleinhans and van den Berg 2011). It has been shown that meandering streams dominate global river morphologies, accounting for almost 70% of the world's fluvial systems (Li et al. 2025). However, studies of both modern (Coleman 1969; Klassen and Vermeer 1988; Sarker et al. 2003; Sarker and Thorne 2006) and ancient systems (Willis 1993; Willis and Behrensmeyer 1994, 1995; Khan et al. 1997; Bridge 2003; Adams and Bhattacharya 2005) have recorded extensive braided river deposits. Despite this, braided river systems have not been documented in studies using 3D seismic data which has sometimes led to the suggestion that braided rivers are rarely preserved in ancient deposits (Holbrook and Allen 2021),especially in 3D seismic data. One way to explain this apparent lack of braided fluvial deposits in seismic studies is the lack of impedance contrast between generally uniform sand-rich layers within their deposits and also because these rivers can also produce cutbank patterns, which can lead to their mis-interpretation as meandering systems (Holbrook and Allen 2021). Studies on ancient fluvial depositional systems, such as the Torrivio, may provide a valuable case study of a braided ancient stream deposit.

Previous interpretations of the braided nature of the Torrivio Sandstone (Molenaar 1973, 1977; Hohman 1986; Flores et al. 1991) have mostly relied upon the coarse-grained conglomeratic nature of the deposits, and the lack of floodplain mudstones, as opposed to producing detailed bedding diagrams showing mounded geometries of the mid-channel bars with bi-directional downlaps, as shown in this study. The Torrivio also provides opportunities to investigate the various scales of scour surfaces, and especially confluence scours that should be the dominant features of braided fluvial systems (Hein and Walker 1977; Bristow 1993; Adams and Bhattacharya 2005; Smith et al. 2019; Gibling at al. 2023).

- 3. Quantitative characterization of the Torrivio Sandstone to establish the size and scale of the formative system and paleodischarge estimates. Multiple methods of paleohydraulic and paleodischarge estimates were used to provide independent estimates, that can be used to assess the uncertainty and accuracy of the various quantitative techniques currently used in paleohydraulic reconstructions. A novel Monte-Carlo simulation based statistical approach was used to provide a range of values for annual water and sediment discharge. Data from climate-binned modern analogs were used to address the uncertainty in paleodischarge estimates.
- 4. Deciphering the scales of confluence scours in the Torrivio Sandstone. Different scales of confluence scours, ranging from those occurring downstream of a mid-channel bar to those occurring where smaller chute-channels meet the main channel, to major tributary channel junction scours, should be common features in braided streams, but are not well documented in ancient fluvial systems (Smith et al. 2019). These scours should be deeper than the mean bankfull channel depth. Proxies used to estimate flow depth, such as channel fill thickness and dune-scale cross set thickness, may be significantly thicker in confluence scour fills than those formed by dunes in typical braid bars, and thus should not be considered as representative of the mean bankfull flow depth. Thus, differentiating confluence scour fills is significant for accurate estimation of paleohydraulic parameters to determine sediment transport strength, paleodischarge, and sediment flux of a fluvial system (Bhattacharya and Tye 2004; Holbrook and Wanas 2014; Bhattacharya et al. 2016; Lin and Bhattacharya 2016; Sharma et al. 2017). Also, it is important to distinguish

confluence scours, which are autogenic in nature, from incised valleys, which are allogenic features and typically much more extensive in a geographical area (Ullah et al. 2015).

1.2 Thesis Organization

This thesis is a "sandwich" type thesis in which the main body of the thesis (Chapter 2 to 4) consists of published or soon-to-be-published papers.

Chapter 2: Sharma, S., Bhattacharya, J.P. and Richards, B., 2017. Source-to-sink sediment budget analysis of the Cretaceous Ferron Sandstone, Utah, USA, using the fulcrum approach. Journal of Sedimentary Research, 87(6), pp. 594 - 608.

The measured sections used in this study were obtained by former MSc student Benjamin Richards, while all the analysis was carried out by Sandeep Sharma (author of this thesis). Sandeep Sharma also drafted the text and figures for the paper and Dr. Bhattacharya helped improving the manuscript with expert reviews.

Chapter 3: Facies architecture and paleohydraluics of the late Cretaceous Torrivio Sandstone, New Mexico, USA.

This campaign focused on outcrops around the town of Gallup, New Mexico, covering a length of approximately 70 km, with the help of 40 measured sections and multiple high-resolution photomosaics. All the measured sections and two-dimensional (2D) photomosaics using GigaPan were obtained by the author, while the acquisition of the drone photos was carried out with the help of David Kynaston. The 3D model building and extraction of high-resolution Orthomosaic were carried out by the author. The author drafted the text and prepared all the figures while Dr. Bhattacharya provided invaluable edits.

Chapter 4: Scale of confluence scours in the late Cretaceous Torrivio Sandstone, NM, USA.

19 measured sections and 5 photomosaics were directly used in this study. All the data was acquired by the author except for the drone photos, which were acquired with the help of Curtis Ferron and Rachel Nelson. The author drafted the text and prepared all the figures while Dr. Bhattacharya provided helped by providing expert reviews.

References

- Adams, M.M. and Bhattacharya, J.P., 2005. No change in fluvial style across a sequence boundary, Cretaceous Blackhawk and Castlegate Formations of central Utah, USA. Journal of Sedimentary Research, 75(6), pp.1038-1051.
- Allen, J.R.L., 1983. Studies in fluviatile sedimentation: bars, bar-complexes and sandstone sheets (low-sinuosity braided streams) in the Brownstones (L. Devonian), Welsh Borders. Sedimentary Geology, 33(4), pp.237-293.
- Bhattacharya, J.P., and Tye, R.S., 2004, Searching for modern Ferron analogs and application to subsurface interpretation, in Chidsey T.C. Jr., Adams, R.D., and Morris, T.H. eds., The Fluvial-Deltaic Ferron Sandstone: Regional to Wellbore Analog for Fluvial-Deltaic Reservoir Modeling: American Association of Petroleum Geologists, Studies in Geology, 50, p. 39–57.
- Bhattacharya, J.P., Copeland, P., Lawton, T.F. and Holbrook, J., 2016. Estimation of source area, river paleodischarge, paleoslope, and sediment budgets of linked deeptime depositional systems and implications for hydrocarbon potential. Earth-Science Reviews, 153, pp.77-110.
- Bhattacharya, J.P., and MacEachern, J.A., 2009, Hyperpycnal rivers and prodeltaic shelves in the Cretaceous Seaway of North America: Journal of Sedimentary Research, v. 79, p. 184–209.
- Bridge, J.S., 2003, Rivers and Floodplains: Forms, Processes, and Sedimentary Record: Malden, Massachusetts, Blackwell Science, 491 p.
- Bristow, C.S., 1993. Sedimentology of the Rough Rock: A Carboniferous braided river sheet sandstone in northern England. Geological Society, London, Special Publications, 75(1), pp.291-304.

- Coleman, J.M., 1969. Brahmaputra River: channel processes and sedimentation. Sedimentary geology, 3(2-3), pp.129-239.
- Davidson, S.K., and North, C.P., 2009, Geomorphological regional curves for prediction of drainage area and screening modern analogues for rivers in the rock record: Journal of Sedimentary Research, v. 79, p. 773–792.
- Fielding, C.R., 2007. Sedimentology and stratigraphy of large river deposits: recognition in the ancient record, and distinction from "incised valley fills". Large Rivers: Geomorphology and Management, pp.97-113.
- Flores, R.M., Hohman, J.C. and Ethridge, F.G., 1991. Heterogeneity of Upper Cretaceous Gallup sandstone regressive fades, Gallup Sag, New Mexico.
- Gibling, M.R., Jia, R., Gastaldo, R.A., Neveling, J. and Rochín-Bañaga, H., 2023. Braided-river architecture of the Triassic Swartberg member, Katberg Formation, South Africa: Assessing age, fluvial style, and paleoclimate after the end-Permian extinction. Journal of Sedimentary Research, 93(10), pp.741-775.
- Hasbargen, L.E., 2012. A test of the three-point vector method to determine strike and dip utilizing digital aerial imagery and topography.
- Hein, F.J. and Walker, R.G., 1977. Bar evolution and development of stratification in the gravelly, braided, Kicking Horse River, British Columbia. Canadian Journal of Earth Sciences, 14(4), pp.562-570.
- Hohman, J.C., 1986. Depositional Model of Coal-bearing, Upper Cretaceous Gallup Sandstone, Gallup Sag Area, New Mexico (Doctoral dissertation, Colorado State University).
- Holbrook, J., and Wanas, H., 2014, A fulcrum approach to assessing source-to-sink mass balance using channel paleohydrologic parameters derivable from Common fluvial data sets with an example from the Cretaceous of Egypt: Journal of Sedimentary Research, v. 84, p. 349–372.
- Holbrook, J.M. and Allen, S.D., 2021. The case of the braided river that meandered: Bar assemblages as a mechanism for meandering along the pervasively braided Missouri River, USA. Bulletin, 133(7-8), pp.1505-1530.

- Khan, I.A., Bridge, J.S., Kappelman, J. and Wilson, R., 1997. Evolution of Miocene fluvial environments, eastern Potwar plateau, northern Pakistan. Sedimentology, 44(2), pp.221-251.
- Klassen, G.J. and Vermeer, K., 1988. Channel characteristics of the braiding Jamuna River, Bangladesh. In International Conference on River Regime. Hydraulics Research Limited, Wallingford, Oxon UK. 1988. p 173-189. 16 fig, 1 tab, 13 ref..Leclair, S.F., and Bridge, J.S., 2001, Quantitative interpretation of sedimentary structures formed by river dunes: Journal of Sedimentary Research, v. 71, p. 713–716.
- Kleinhans, M.G. and van den Berg, J.H., 2011. River channel and bar patterns explained and predicted by an empirical and a physics-based method. Earth Surface Processes and Landforms, 36(6), pp.721-738.
- Leopold, L.B., Wolman, M.G., 1957. River channel patterns braided, meandering and straight. U.S. Geol. Surv. Prof. Pap. 282B, 39–85.
- Lewin, J. and Ashworth, P.J., 2014. Defining large river channel patterns: Alluvial exchange and plurality. Geomorphology, 215, pp.83-98.
- Li, W., Bhattacharya, J.P., and Campbell, C., 2010, Temporal evolution of fluvial style in a compound incised-valley fill, Ferron "Notom Delta", Henry Mountains Region, Utah (U.S.A.): Journal of Sedimentary Research, v. 80, p. 529–549.
- Li, Y., Zhang, Y., Zheng, N., Li, L., Ji, H., Bao, Z. and Feng, Z., 2025. Global classification of river morphology based on inland water dynamics characterization and digital elevation data. Scientific Reports, 15(1), p.14258.
- Lin, W., and Bhattacharya, J.P., 2016, Estimation of Source-to-Sink Mass Balance and Depositional Systems Dominated Sediment Budgets by a Fulcrum Approach Assessment Using Channel Paleohydrologic Parameters: Cretaceous Dunvegan Formation: American Association of Petroleum Geologists, Search and Discovery article#41852.
- Lin, W., Bhattacharya, J.P. and Stockford, A., 2019. High-resolution sequence stratigraphy and implications for cretaceous glacioeustasy of the Late Cretaceous Gallup System, New Mexico, USA. Journal of Sedimentary Research, 89(6), pp.552-575. Miall, A.D.,

- 1985. Architectural-element analysis: a new method of facies analysis applied to fluvial deposits.
- Lin, W., Kynaston, D., Ferron, C., Bhattacharya, J.P. and Matthews, W., 2021. Depositional and sequence stratigraphic model of transgressive shelf sandstone: The Late Cretaceous Tocito Sandstone, San Juan Bain, New Mexico, USA. Journal of Sedimentary Research, 91(4), pp.415-432.
- Miall, A.D., 1977. Lithofacies types and vertical profile models in braided river deposits: a summary.
- Miall, A.D., 1985. Architectural-element analysis: a new method of facies analysis applied to fluvial deposits.
- Miall, A.D., 1992. Sedimentology of a sequence boundary within the nonmarine Torrivio Member, Gallup Sandstone (Cretaceous), San Juan Basin, New Mexico.
- Miall, A.D. and Jones, B.G., 2003. Fluvial architecture of the Hawkesbury sandstone (Triassic), near Sydney, Australia. Journal of Sedimentary Research, 73(4), pp.531-545.
- Miall, A.D., 2006. Reconstructing the architecture and sequence stratigraphy of the preserved fluvial record as a tool for reservoir development: A reality check. AAPG bulletin, 90(7), pp.989-1002.
- Molenaar, C.M., 1973. Sedimentary facies and correlation of the Gallup Sandstone and associated formations, northwestern New Mexico.
- Molenaar, C.M., 1977. The Pinedale oil seep-an exhumed stratigraphic trap in the southwestern San Juan Basin. In San Juan Basin III: New Mexico Geol. Soc. Guidebook, 28th Field Conference (p. 243).
- Nummedal, D. and Molenaar, C.M., 1995. Sequence stratigraphy of ramp-setting strand plain successions: the Gallup Sandstone, New Mexico.
- Nanson, G.C. and Knighton, A.D., 1996. Anabranching rivers: their cause, character and classification. Earth surface processes and landforms, 21(3), pp.217-239.
- Richards, B.H., 2014, Fluvial to marine succession in a compound incised valley system in the Ferron Notom delta, Utah: M.Sc. Thesis: University of Houston, Houston, Texas, USA., 56 p.

- Sambrook Smith, G.H., Nicholas, A.P., Best, J.L., Bull, J.M., Dixon, S.J., Goodbred, S., Sarker, M.H. and Vardy, M.E., 2019. The sedimentology of river confluences. Sedimentology, 66(2), pp.391-407.
- Sarker, M.H., Huque, I., Alam, M. and Koudstaal, R., 2003. Rivers, chars and char dwellers of Bangladesh. International Journal of River Basin Management, 1(1), pp.61-80.
- Sarker, M.H. and Thorne, C.R., 2006. Morphological response of the Brahmaputra–Padma–Lower Meghna River system to the Assam earthquake of 1950. Braided Rivers: process, deposits, ecology and management, 36, pp.289-310.
- Sharma, S., Bhattacharya, J.P. and Richards, B., 2017. Source-to-sink sediment budget analysis of the Cretaceous Ferron Sandstone, Utah, USA, using the fulcrum approach. Journal of Sedimentary Research, 87(6), pp.594-608.
- Sømme, T.O., Helland-Hansen, W., Martinsen, O.J. and Thurmond, J.B., 2009. Relationships between morphological and sedimentological parameters in source-to-sink systems: A basis for predicting semi-quantitative characteristics in subsurface systems. Basin Research, 21(4), pp.361-387.
- Syvitski, J.P. and Milliman, J.D., 2007. Geology, geography, and humans battle for dominance over the delivery of fluvial sediment to the coastal ocean. The Journal of Geology, 115(1), pp.1-19.
- Ullah, M. S., Bhattacharya, J. P., and Dupre, W. R., 2015, Confluence scours versus incised valleys: Examples from the Cretaceous Ferron Notom Delta, Southeastern Utah, USA: Journal of Sedimentary Research, v. 85, p. 445-458.
- Van den Berg, J.H., 1995. Prediction of alluvial channel pattern of perennial rivers. Geomorphology, 12(4), pp.259-279.
- Van Dijk, W.M., Densmore, A.L., Sinha, R., Singh, A. and Voller, V.R., 2016. Reduced-complexity probabilistic reconstruction of alluvial aquifer stratigraphy, and application to sedimentary fans in northwestern India. Journal of Hydrology, 541, pp.1241-1257.
- Walker, R.G., 1976. Facies model-3. Sandy fluvial systems. Geoscience Canada, 3(2), pp.101-109.
- Willis, B., 1993. Ancient river systems in the Himalayan foredeep, Chinji Village area, northern Pakistan. Sedimentary geology, 88(1-2), pp.1-76.

- Willis, B.J. and Behrensmeyer, A.K., 1994. Architecture of Miocene overbank deposits in northern Pakistan. Journal of Sedimentary Research, 64(1b), pp.60-67.
- Willis, B.J. and Behrensmeyer, A.K., 1995. Fluvial systems in the Siwalik Miocene and Wyoming paleogene. Palaeogeography, Palaeoclimatology, Palaeoecology, 115(1-4), pp.13-35.
- Wu, T., Bhattacharya, J.P. and Jung-Ritchie, L., 2022. Sequence stratigraphic interpretation in marginal marine settings by the approach of parasequence-thickness-to-sandstone-fraction ratio: Case studies of the Gallup and Ferron outcrops in the Western Interior Basin, USA. Journal of Sedimentary Research, 92(2), pp.67-94.
- Zhu, Y., Bhattacharya, J.P., Li, W., Lapen, T.J., Jicha, B.R., and Singer, B.S., 2012, Milankovitch-scale sequence stratigraphy and stepped forced regressions of the Turonian Ferron Notom Deltaic Complex, South-Central Utah, U.S.A.: Journal of Sedimentary Research, v. 82, p. 723–746.

Chapter 2

Source-to-sink sediment budget analysis of the Cretaceous Ferron Sandstone, Utah using the Fulcrum approach

Chapter 2 matches sediment fluxes, estimated to have passed through the trunk channel of an ancient river system, with mapped downstream sediment volumes in a deltaic sink, providing a test of the recently developed fulcrum approach of source-to-sink analysis. This chapter uses field measurements (such as channel depth, width, and grain size) to estimate paleodischarge in an ancient trunk channel of the Cretaceous Ferron Sandstone in Central Utah. The estimates of instantaneous discharge are then integrated over the geological duration of the river to estimate the total sediment volume delivered to downstream deltaic sinks to balance the estimated sediment flux. The bankfull channel depths, calculated using the scaling relationship between the flow depth and the mean dune height, vary from 3.3 m to 5.5 m with an average depth of 4.4 m. The corresponding bankfull channel width estimates vary from 50 m to 80 m, with an average value of 65 m, calculated using scaling relationship between channel width and the width of accretion surfaces. Water discharge calculated for these bankfull dimensions vary from 2.7×10^2 m^3/s to 8.6×10^2 m^3/s , also indicating that these rivers were routinely capable of generating hyperpycnal flows. The instantaneous sediment discharge reaching the fulcrum was calculated using established sediment transport equations. These instantaneous discharge values were first converted to mean annual sediment volume using the bankfull event durations, recurrence intervals, and a factor for the proportion of the total annual sediment load transported during the bankfull period, based on empirical relationships from modern climate analogs, and then projected over the average time duration of individual parasequences in the Ferron Notom clastic wedge, which is approximately 14 kyr. The mass balance across the fulcrum reveals that the average bedload sediment volume derived from the source (about 3 km³) matches with that deposited in the sink within a factor of two. However, underestimation of the bedload volume in the sink suggests sediment escape beyond the limits of currently mapped sink area. Previous models for the Ferron indicate

significant SE deflection of sediment due to wave reworking, which may account for the missing sandy sediment. It is also possible that there is an overestimation of time duration for individual valleys, resulting in higher sink-volume estimation and larger source-to-sink mass imbalance. A probabilistic estimation, based on Monte Carlo simulations, was used to test the sensitivity of key parameters used in converting bankfull discharge to mean annual discharge. The P10, P50 (median), and P90 values for the average annual bedload volume (Q_{mas}) are 9.1×10^4 m³, 1.7×10^5 m³, and 3.7×10^5 m³, respectively. A Q_{mas} value between P50 and P90 yields a source-to-sink balance for bedload volume.

This study establishes a mass balance across the fulcrum with a reduced range of uncertainty for the various parameters used. Uncertainty associated with bankfull channel dimensions has been reduced through inclusion of detailed outcrop data. The uncertainty in estimating average annual sediment volume (Q_{mas}) from bankfull events is approx. within a factor of four. This uncertainty can be further reduced by incorporating a more robust global-discharge dataset from modern analog river systems. Despite many assumptions and uncertainties, our study shows that the fulcrum method appears to be capable of balancing sediment budgets to within at least an order of magnitude in deeptime sedimentary systems.

2.1 Introduction

Outcrop and subsurface data have been used for paleohydrologic calculations for ancient systems, including estimates of catchment areas and bankfull discharge (Davidson and North 2009). Such calculations are used to make comparisons between ancient depositional systems (Bhattacharya and Tye 2004; Bhattacharya and MacEachern 2009; Li et al. 2010; Holbrook and Wanas 2014). Major factors affecting accuracy of discharge estimates for ancient systems include lack of climate information (especially the average duration of bankfull events), limited age control, and lack of knowledge of both catchment area and sediment routing pathways (Davidson and North 2009; Holbrook and Wanas 2014). Our analysis is based on the premise that over a given period of time, the total mass passing through a cross section of a trunk valley should be equal to that delivered from the source

and to the sediment deposited in the sink, constituting the "fulcrum approach to source-to-sink analysis" (Holbrook and Wanas 2014). The fulcrum approach does not require knowledge of source and basin area and relief (Holbrook and Wanas 2014), although this information may improve the estimate, but information about paleoclimate is critical. Since this method compares the amount of sediment passing through the fulcrum to that in the sink, it does not need to account for the amount of sediment already stored in the areas upstream of the fulcrum, nor does it require the depositional sink to be a closed system (Holbrook and Wanas 2014). However, balancing fulcrum estimates with downdip sediment volumes requires a closed sink.

The present study performs a source-to-sink sediment-budget analysis for a welldocumented compound valley system and its downstream delta deposit in the mid-Turonian Ferron Sandstone of Utah, USA (Li et al. 2010; Li and Bhattacharya 2013; Ullah et al. 2015), using the fulcrum approach. The Ferron Sandstone provides a suitable opportunity to test the fulcrum technique because it is extensively exposed and well studied. The previous stratigraphic analysis allows specific valleys and their contained channel deposits to be linked to mapped downstream shoreface and deltaic parasequences (Fielding 2010; Li et al. 2010; Zhu et al. 2012). Previous chronometric analysis also allows estimation of the duration of sequences in the Ferron wedge (Zhu et al. 2012). The fulcrum was chosen in a previously identified and mapped trunk valley, and the amount of sediment passing through it is estimated using paleohydrologic measurements from the preserved channel deposits integrated over the estimated timespan of the valley during which sediment was delivered to the deltaic sink. This estimate is then compared with the volume of sediment deposited in the downstream deltaic systems (sinks) that were mapped in previous studies (Li et al. 2010; Zhu et al. 2012). The ability to compare mapped downstream sediment volumes with the flux estimates of the fulcrum method provides the opportunity to test the utility of the fulcrum method.

2.2 Study area

The Ferron Sandstone Member belongs to the Mancos Shale Formation. It overlies the Tununk Shale Member and is followed up by the Blue Gate Shale Member (Garrison and van den Bergh 2004). The Ferron Sandstone was deposited in a foreland basin along the western margins of the Cretaceous Interior Seaway of North America during the Late Cretaceous (Garrison and van den Bergh 2004) (Fig. 2.1A). The Ferron Sandstone is made up of three clastic wedges including the Vernal, Last Chance, and Notom delta complex (Gardner et al. 2004; Garrison and van den Bergh 2004). Amongst these, the Notom and Vernal deltas are the oldest (Garrison and van den Bergh 2004).

Detailed facies analysis has established that the Ferron Notom fluvio-deltaic system contains linked nonmarine river-dominated delta plain and shallow marine facies associations (Peterson and Ryder 1975; Garrison and van den Bergh 2004; Fielding 2010; Li et al. 2010). (Fig. 2.1B). Through ⁴⁰Ar/³⁹Ar dating of Sanidine crystals from bentonite beds, Zhu et al. (2012) established a mid-Turonian age of deposition for the Notom deltaic wedge, ranging from 91.3 +/- 0.77 Ma to 90.6 +/- 0.25 Ma, and covering approximately 620,000 years. Palynological studies have established an ever-wet tropical to subtropical climate regime (Akyuz et al. 2015).

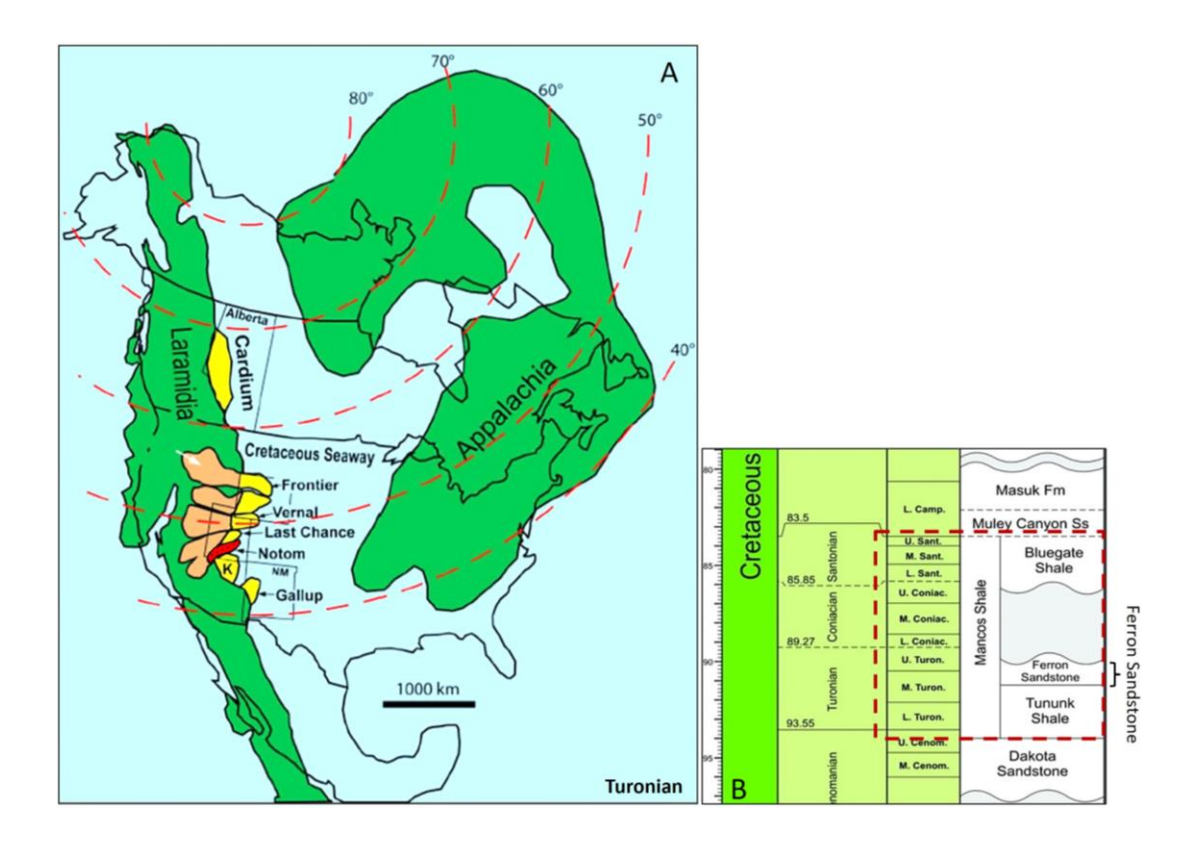


Figure 2.1. A) Paleogeographic map showing the location of deltaic wedges of the Western Interior Seaway during the Turonian, including the Ferron Notom delta (red stippled) (modified after Bhattacharya et al. 2016); B) Stratigraphic position of the Ferron Sandstone (after Fielding 2010).

The Ferron Notom deltaic complex is subdivided into six sequences, eighteen parasequence sets, and forty-three parasequences (Li et al. 2010; Zhu et al. 2012) (Fig. 2.2A). Assuming roughly equal sequence durations, the total time was divided by the number of sequences, which would suggest that each sequence was about 100 kyr in duration, and that parasequences were deposited on the order of 14 – 20 kyr (Zhu et al. 2012). The origin of high-frequency, Milankovitch-scale stratigraphic cycles have been attributed to glacio-eustasy (Zhu et al. 2012) although the role of tectonics is also documented (Fielding 2011).

Out of the six sequences, the older sequences, 3 through 6, are predominantly marine, whereas the youngest, Sequence 1, is entirely fluvial. The sediment-budget analysis in this paper is focused on Sequence 2 (Fig. 2.2), which is the only sequence in which the

landward incised valleys can be linked to the coeval shoreline systems (Li et al. 2010; Zhu et al. 2012). Sequence 2 consists of parasequence sets 7 through 4. Parasequence sets 7 and 4 (PS7 and PS4) have only one parasequence each, whereas parasequence sets 6 and 5 (PS6 and PS5) have three and two parasequences, respectively (Zhu et al. 2012). The constituent parasequences of PS6 can be seen in the strike section. Detailed stratigraphic correlations (Li et al. 2010; Zhu et al. 2012) have established a proximal incised-valley system feeding the falling-stage and lowstand systems of PS7 and PS6 respectively (Fig. 2.2).

Previous studies presented detailed paleogeographic maps of PS6 (Fig. 2.2C), and these show an incised valley feeding a large, river-dominated delta lobe, flanked by wave-dominated shoreface deposits (Li et al. 2011; Ahmed et al. 2014). We assume that the northern shoreface deposit consists of sand supplied by rivers farther north and carried to the Notom delta by longshore drift, representing the updrift margin of an asymmetrical, wave-influenced delta (Bhattacharya and Giosan 2003; Li et al. 2011). This sandstone body is thus not considered to be a part of the Notom source-to-sink system and was not included in our sediment budget analysis. Although it was not possible to fully correlate and map the prodeltaic mudstone facies, the limits of sandstone in the river-dominated delta lobe in the middle of the map is reasonably well constrained (Fig. 2.2, Zhu et al. 2012; Ahmed et al. 2014). We also project a wave-dominated shoreface south of the river-dominated delta lobe (Fig. 2.2C), and this sediment is considered as part of the PS6 source-to-sink system and is thus incorporated in our sediment-budget analysis. We thus have a reasonably well-constrained estimate of the volume of sand in the deltaic and shoreface sinks fed by the river in the valley.

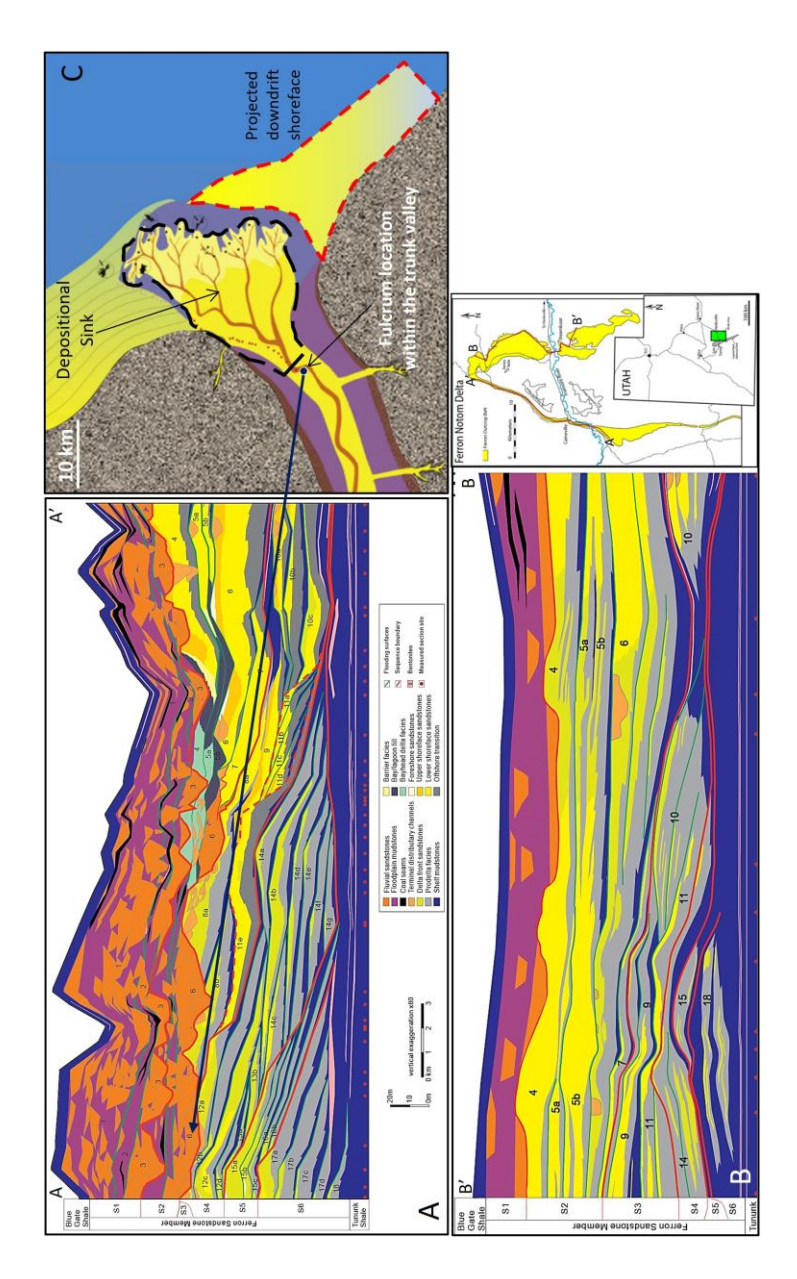


Figure 2.2. A) Dip and B) strike stratigraphy of the Ferron Notom delta showing the constituent parasequences, parasequence sets, and sequences (modified after Zhu et al. 2010), the Ferron outcrop belt shown is in the inset. C) The paleogeographic map of PS-6 showing the wave-influenced, river-dominated delta fed by an incised valley (Ahmed et al. 2014). Also shown are the areal extent of the depositional sink (in black polygon) and the projected downdrift extension of the shoreface (in red polygon) of PS-6. See text for details.

2.3 Methodology

The complete fulcrum workflow (Fig. 2.3) is divided into four steps: i) estimation of bankfull channel dimensions (depth and width), ii) estimation of instantaneous bankfull water and sediment discharge, iii) estimation of mean annual sediment discharge, and iv) estimation of the mass balance over a longer geological time frame (Holbrook and Wanas 2014).

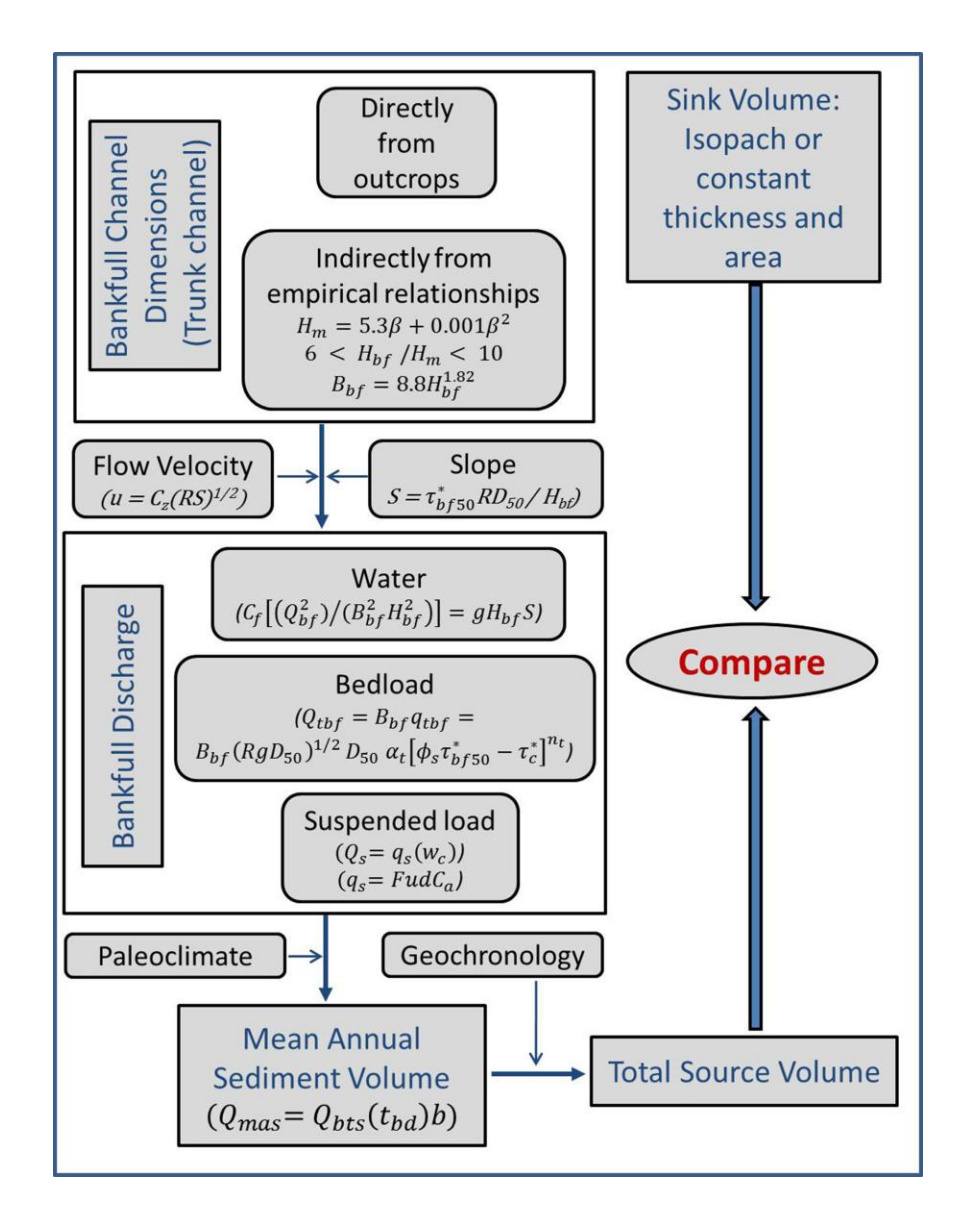


Figure 2.3. The fulcrum workflow for mass balance (after Holbrook and Wanas 2014).

2.3.1 Estimation of bankfull channel dimensions

Bankfull channel depth, i.e., the depth at bankfull discharge beyond which the discharge overflows onto the floodplain (Leopold et al. 1964), and the corresponding bankfull channel width, can be estimated directly by measuring completely preserved channel stories from outcrop or subsurface data (Bridge and Tye 2000; Bridge 2003). Care was taken in outcrops, particularly in cases recording multiple episodes of cut and fill, such as with incised-valley deposits with amalgamated vertical successions that may record incomplete story preservation (Bridge and Tye 2000; Holbrook and Wanas 2014).

In addition to observation of preserved channel stories, empirical relationships between the bedform height and the flow depth can also be used as an independent check to estimate the bankfull flow depth (Bridge and Tye 2000; LeClair and Bridge 2001; Bhattacharya and Tye 2004). The cross-bed set thickness of a fluvial deposit can be related to the dune height (Eq. 2.1), which in turn is related to the flow depth at the time of dune migration (Bridge 1997; LeClair et al. 1997). LeClair and Bridge (2001) (Eq. 2.1) proposed a relationship between cross-bed set thickness and dune height, based on flume experiments and modern rivers like the Calamus River in Nebraska and the Baal River in the Netherlands:

$$H_m = 5.3\beta + 0.001\beta^2 \tag{2.1}$$

where H_m is the mean dune height and $\beta = S_m/1.8$; S_m is the mean vertical thickness of cross-bed set.

The mean cross-bed set thickness should not include data from any anomalously thick cross-bed sets (Bhattacharya and Tye 2004). The bankfull flow depth (H_{bf}) is estimated to be 6-10 times the mean dune height (LeClair and Bridge 2001; Holbrook and Wanas 2014). Multiplying the mean dune height by 6 and 10 delineates the lower and upper limits of channel-depth estimates (LeClair and Bridge 2001). Channel width (B_{bf}) can be measured either directly from outcrops or estimated using empirical relationships, such as those proposed by Bridge and Mackey (1993) for single-thread channel systems (Eq. 2.2),

$$B_{bf} = 8.8 H_{bf}^{1.82} (2.2)$$

2.3.2 Estimation of bankfull discharge

Once the bankfull channel depth and width are estimated, the corresponding water and sediment discharges can be calculated using well-established flow transport equations (van Rijn 1984b; Parker 2004; Wright and Parker 2004).

The bankfull flow velocity is related to the dimensionless bankfull Chézy resistance coefficient (C_{zbf}) wherein $u = C_{zbf} \sqrt{(gH_{bf}S)}$ (Parker 2004, 2008), a form of Chézy relation for flow velocity (Parker 2008). Since velocity at bankfull conditions is given by $u = Q_{bf}$ / $B_{bf}H_{bf}$, and $C_{zbf} = (C_f)^{-1/2} g^{-1/2}$ (Parker 2008), combining these two will result in Eq. 2.3, which can be used to calculate bankfull water discharge (Parker 2004; Holbrook and Wanas 2014).

$$C_f = [(Q_{bf}^2)/(B_{bf}^2 H_{bf}^2)] = gH_{bf}S$$
 (2.3)

where, C_f is dimensionless Chézy friction coefficient),

$$C_f^{-\frac{1}{2}} = (8.1) \left(\frac{H_{bf}}{k_s}\right)^{\frac{1}{6}},$$
 (2.3a)

and
$$S ext{ (Slope)} = \frac{\left(\tau_{bf50}^*\right)(RD_{50})}{H_{bf}}$$
 (2.3b)

Eq. 2.3a is a modified form of the Manning-Strickler equation (Parker 2004; Wright and Parker 2004) where, $k_S = 3D_{90} + 1.1\Delta(1 - e^{-25\psi})$ if bedforms are present; Δ is the bedform height; $\psi = \Delta / \lambda$ where $\lambda = 7.3H_{bf}$ is the bedform wavelength (Holbrook and Wanas 2014). In Eq. 2.3b, τ_{bf50}^* is the dimensionless shear stress, which is assumed to be 1.86 for sandbed rivers (Dade and Friend 1998; Parker et al. 1998; Parker 2004). R is the submerged dimensionless relative density, estimated at 1.65 for quartz sand grains in water of standard

density; D_{50} is the median grain size and g is acceleration due to gravity at 9.8 m/s² (Parker 2004; Holbrook and Wanas 2014).¹

Bankfull bedload discharge is calculated using Eq. 2.4 (Parker 2004).

$$Q_{tbf} = B_{bf} q_{tbf} = B_{bf} (RgD_{50})^{1/2} D_{50} \alpha_t [\phi_s \tau_{bf50}^* - \tau_c^*]^{n_t}, \tag{2.4}$$

where q_{tbf} is the bedload discharge per unit width, $\alpha_t = \frac{\alpha_{EH}}{c_f}$, $\alpha_{EH} = 0.05$, $n_t = 2.5$, $\phi_S = 1$, and $\tau_c^* = 0$ (Parker et al. 1998; Parker 2004; Holbrook and Wanas 2014). Details about the constants in Eq. 2.4 are available in Engelund and Hansen (1967).

The suspended-load discharge (Q_s) is calculated using Eq. 2.5 and 2.5a (van Rijn 1984b; Parker 2004; Wright and Parker 2004).

$$Q_s = q_s(B_{bf}) (2.5)$$

$$q_s$$
 (suspended – sediment discharge per unit width) = $FudC_a$ (2.5a)

where, F (suspension factor) = $\frac{\left(\left[\frac{a}{d_m}\right]^{Z'} - \left[\frac{a}{d_m}\right]^{1.2}\right)}{\left(\left[1 - \left(\frac{a}{d_m}\right)\right]^{Z'} \left[1.2 - Z'\right]\right)}$, with a (reference level) = $0.05 \times H_{bf}$

(Garcia and Parker 1991; Wright and Parker 2004), Z' (suspension parameter) = $v_s/\beta ku_*$; u (mean flow velocity) = $C_Z(RS)^{0.5}$, C_Z (standard Chézy resistance coefficient) = $(g)^{0.5}8.1\left(\frac{H_{bf}}{k_s}\right)^{\frac{1}{6}}$, R (hydraulic radius of channel) = $\frac{area}{wetted\ perimeter}$, and d_m is the bankfull channel depth (= H_{bf}) (van Rijn 1984b; Parker 2004). In the calculation of the suspension parameter, $Z' = \frac{v_s}{\beta ku_*}$, v_s is the settling velocity, β (coefficient related to diffusion of

¹ In the original paper by Holbrook and Wanas (2014) the parameter R was incorrectly assigned the dimensions of g/cm^3 , which we have corrected here.

sediment particles) = $1 + 2\left[\frac{v_s}{u_*}\right]^2$, where u_* (overall bed shear velocity) = $\left(gH_{bf}S\right)^{0.5}$, k is the von Kármán constant ~ 0.4 (van Rijn 1984b).

 C_a is the suspended-sediment concentration at a reference depth (a) and is calculated using Eq. 2.5b (Wright and Parker 2004).

$$C_a = \frac{(AZ_u^5)}{(1 + (A/0.3)Z_u^5)} \tag{2.5b}$$

where $A = 5.7 \times 10^{-7}$, $Z_u = \left(\frac{u_{*s}}{v_s}\right) Re_p^{0.6} S^{0.7}$, u_{*s} (bed shear velocity) = $\left(gH_{bf}S\right)^{0.5}$, v_s (settling velocity) = $10\left(\frac{v}{D_s}\right) \left\{ \left[1 + \left(\frac{0.01(s-1)gD_s^3}{v^2}\right)\right]^{0.5} - 1 \right\}$, $Re_p = \frac{(RgD_{50})^{0.5}D_{50}}{v}$, R = 1.65, and $v = 1 \times 10^{-6}$ m²/s (van Rijn 1984b; Parker 2004). The above equation for settling velocity (v_s) is valid for suspended-sediment particle size (D_s) between 100 and 1000 μ m (van Rijn 1984b). D_s represents the sediment particle size that can be kept in suspension (van Rijn 1984b; Holbrook and Wanas 2014). D_s can be calculated using the equation,

$$\frac{D_S}{D_{50}} = 1 + 0.011(\sigma_S - 1)(T - 25), \tag{2.5c}$$

where σ_s (standard deviation of grain size) = $0.5 \left(\frac{D_{84}}{D_{50}} + \frac{D_{16}}{D_{50}}\right)$, and T (transport – stage parameter) = $[(u'_*)^2 - (u_*_{cr})^2]/(u_*_{cr})^2$, with u'_* (bed shear velocity related to grains) = $\left(\frac{g^{0.5}}{c_z}\right)u$ and u_*_{cr} as critical bed shear velocity, which can be estimated from the Shields diagram (Fig. 2.4) using an appropriate suspension value (van Rijn 1984b). In this study, u_*_{cr} is estimated to be 0.031 using a critical mobility parameter from the middle of the van Rijn range (0.1 at particle parameter, D_* of 15) for initiation of suspension and then solving for u_*_{cr} using the equation on the Y axis $(u^2_*_{cr}/(s-1)gD_{50})$ (van Rijn 1984b; Holbrook and Wanas 2014). The particle parameter can be calculated using $D_* = D_{50} \left[\frac{(s-1)g}{v^2}\right]^{1/3}$ where s is the specific dimensionless density of 1.65 and v is the kinematic viscosity of the fluid = 1×10^{-6} m²/s for water at 20° C (van Rijn 1984b).

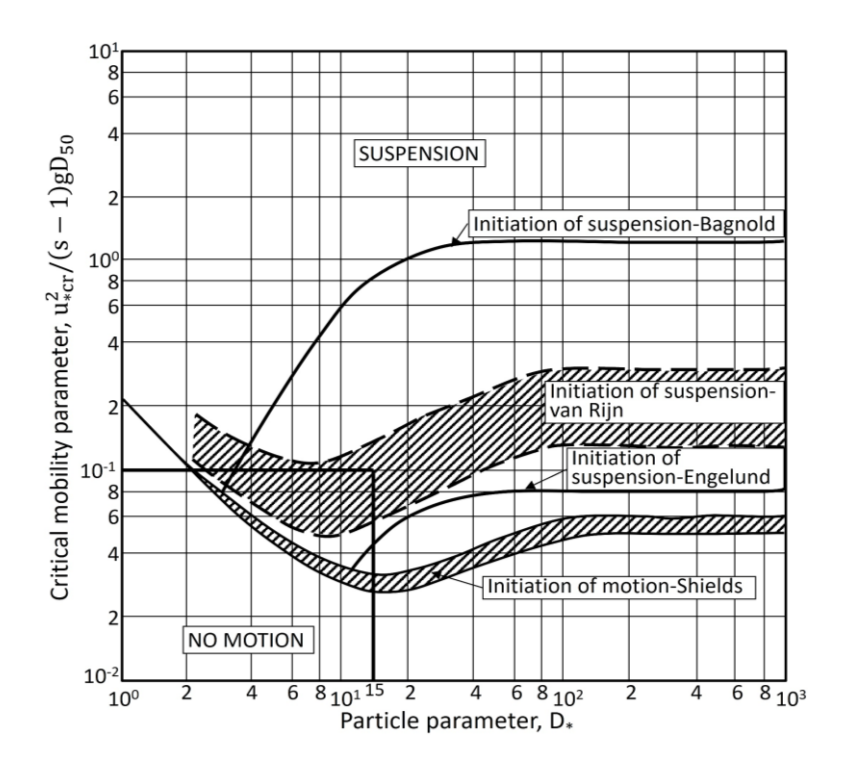


Figure 2.4. Diagram illustrating the threshold for initiation of motion and suspension for a range of particle parameters (from van Rijn 1984b). The critical mobility parameter, used in the estimation of u_{*cr} , is obtained from the van Rijn range at a particle parameter of 15 (black bars). See text for details.

These discharge calculations are based on analysis of the coarser-grained bedload fraction, which we assume to be moving during flood periods. The predominance of dune-scale bedforms, versus upper flow regime bedforms, such as low-amplitude bedwaves or antidunes, suggests that calculated velocities, and consequently discharge, represent flood discharge, rather than mean or average discharge. The mean annual discharge is estimated below.

2.3.3 Estimation of mean annual sediment discharge

After calculations of the bankfull sediment discharge, the next step is to calculate the mean annual sediment discharge using Eq. 2.6 (Holbrook and Wanas 2014).

$$Q_{mas} = Q_{bts}(t_{bd})b (2.6)$$

where Q_{mas} is the total annual sediment discharged in one year, Q_{bts} is the average total bankfull sediment discharge rate, t_{bd} is the mean annual bankfull discharge duration obtained by dividing the annual bankfull event duration by its recurrence interval (RI), which is the average number of years between bankfull events of a given magnitude, and b is a dimensionless multiplier representing the inverse of the proportion of the total annual sediment load carried during the mean annual bankfull duration (Meybeck et al. 2003; Holbrook and Wanas 2014).

2.3.4 Estimation of mass balance across the fulcrum

The mean annual sediment discharge, when projected over the duration of the stratigraphic interval under study, gives an estimate of the sediment volume crossing the fulcrum. This sediment volume can then be compared with the volume of sediment deposited in the sink, estimated either by assuming a constant mean thickness value over the area of interest or using an isopach map (Bhattacharya et al. 2016). These sediment volumes can be compared with the sediment-flux estimates to evaluate the balance of sediment budgets between source and sink. In this example, we focus on the sand budget, as this is better constrained by previous maps and cross sections (Fig. 2.2; Ahmed et al. 2014).

2.4 Results

In this study, the Fulcrum approach to establish source-to-sink mass balance was applied to a trunk channel deposit in an incised valley belonging to Sequence 2 in the Ferron Notom deltaic wedge. This trunk valley was correlated to the shoreline systems of parasequences 6 and 7 (Fig. 2.2). The paleodischarge estimates were integrated over the amount of time associated with one of the parasequences fed by the river and compared with the volume of sand mapped in the parasequence (Fig. 2.2).

2.4.1 Estimation of bankfull channel dimensions

The average cross-bed set thickness reported from the fluvial channel is 0.185 m (Richards 2014). This average value is derived from a set of 45 values of cross-bed set thickness (Fig. 2.5), which yields a mean dune height (H_m) of 0.54 m, calculated using Eq. 2.1.

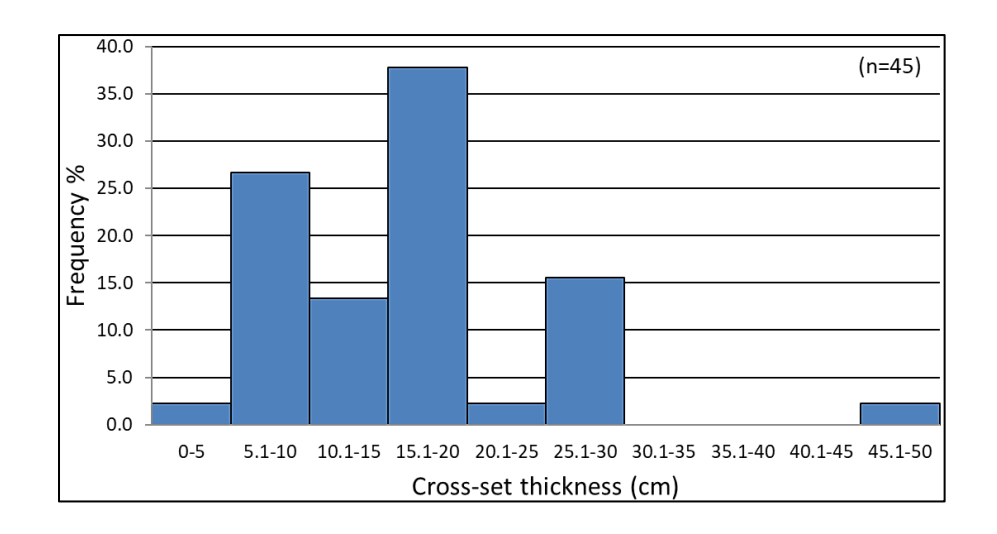


Figure 2.5. Histogram for distribution of vertical thickness of cross-bed sets from Richards (2014). The mean cross-bed set thickness is 0.18 m.

The statistical test of the viability of this method of using cross-bed thickness to determine the mean dune height requires that the ratio of standard deviation to mean of the cross-bed set thicknesses should be 0.88 (\pm 0.3) (Bridge and Tye 2000). This ratio in the current study is \sim 0.5, which is less than the limit mentioned by Bridge and Tye (2000). This suggests that the cross-bed sets were formed by migration of dunes that did not undergo large variation in their form (Bridge and Tye 2000). This is the reason why we have used only one value of mean dune height instead of a range. Following LeClair and Bridge's (2001) conclusion that the ratio of bankfull channel depth to mean dune height (H_{bf}/H_m) varies between 6 and 10, the bankfull channel depth (H_{bf}) is estimated to range from 3.3 m to 5.5 m, which may represent the low and high range of values for bankfull channel depth. The estimated average bankfull channel depth of 4.4 m is the arithmetic mean of these two values. The outcrop measured sections also show that Sequence 2 comprises a multi-story amalgamated channel system. The thickest preserved stories are also on the order of < 6 m

(Richards 2014) (Fig. 2.6), suggesting channel depths on that order. Zhu et al. (2012) also document channel thalweg depths of 7 m to 9 m in Sequence 2. Since the average bankfull channel depth is considered to be one-half of the bankfull thalweg depth (LeClair and Bridge 2001), the mean bankfull channel depths estimated from storey thickness range from 3.5 m to 4.5 m, which matches the bankfull depths estimated independently from the LeClair and Bridge (2001) method.

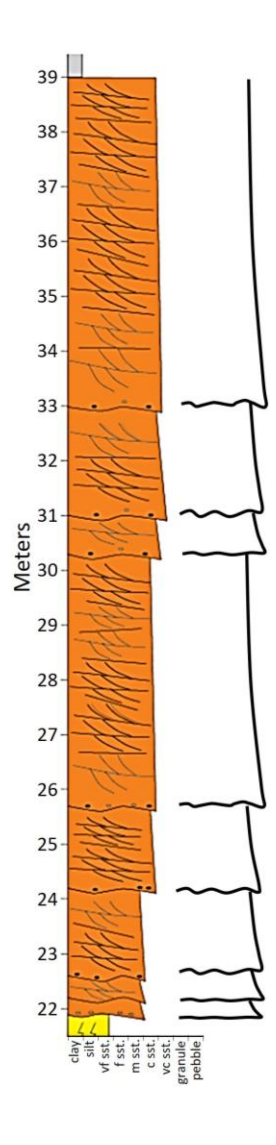


Figure 2.6. Measured section showing the vertically amalgamated fluvial channel stories in PS-6 (Richards 2014). The maximum thickness of the channel as observed in the outcrop is approximately 6 m, which is very close to the thickness (5.5 m) estimated in the current study.

Using these bankfull channel depths, the range of bankfull channel widths (B_{bf}) , estimated via Eq. 2.2, range from 76 m to 192 m, with a mean value of 128 m. However, none of the previous outcrop studies, where channel cross sections can be directly observed, have reported estimated bankfull channel width to be more than 80 m to 100 m (Zhu et al. 2012; Richards 2014). Similarly, the maximum bankfull channel widths reported from the younger Sequence 1 are also rather less than 100 m (Li et al. 2010; Bhattacharyya et al. 2015; Ullah et al. 2015; Wu et al. 2015). Therefore, it appears that the empirical equations are likely to yield overestimates of channel widths for the current study.

Another way of calculating the bankfull channel width is to use the width of accretion surfaces observed in meander belts, which represent 50% to 80% of channel width (Bridge 2003; Bhattacharya et al. 2016). Using an accretion-surface width of 40 m, as observed in Sequence 2 by Zhu (2010) (Fig. 2.7), bankfull channel width is estimated to range from 50 m to 80 m with a mean value of 65 m.

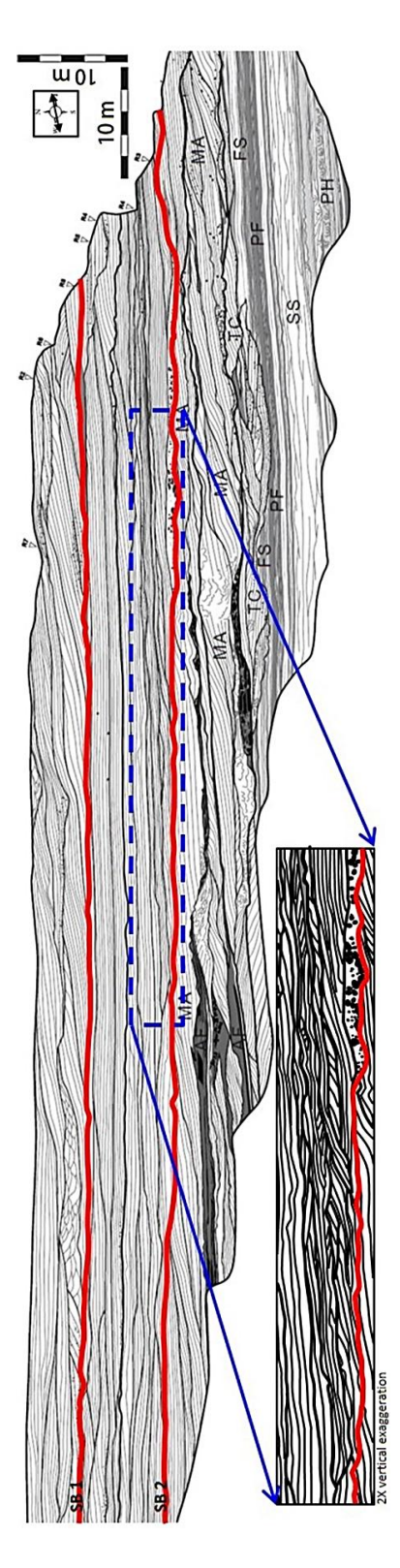


Figure 2.7. Architectural elements observed at marine-to-nonmarine transition in the Ferron Notom Delta at south Cainville, Utah USA. The accretion surfaces observed

in the meander belts in Sequence 2 are shown above the sequence boundary (SB 2 in red). The widths of accretion surfaces have been used to estimate the range of bankfull channel widths in the fulcrum calculation (modified after Zhu (2010)) (PF, Prodelta fines; PH, Prodelta hyperpycnites; SS, Storm sheets; FS, Frontal splay; TC, Terminal distributary channel; AF, Abandoned channel; MA, Mouth-bar accretion).

2.4.2 Estimation of bankfull discharge

The D_{50} grain size is 0.6 mm, also estimated using the outcrop data of Richards (2014). For the estimated channel dimensions, the slope (S) for the Ferron, estimated using the Shields criterion via Eq. 2.3b, ranges from 5.6 x 10^{-4} to 3.4 x 10^{-4} , with an average value of 4.2 x 10^{-4} . A somewhat higher slope value of 9.2 x 10^{-4} was arrived at using the stratigraphic approach of measuring the elevation drop of channel bases in the valley along a depositional-dip cross section hung from a flattened lower bentonite datum (Bhattacharya et al. 2016). This is assumed to approximate the slope of the fluvial longitudinal profile, but the actual river slope may be a factor of two lower than the fluvial long profile, depending on its sinuosity.

The bankfull water discharge (Q_{bf}) is calculated using Eq. 2.3 for a range of values of bankfull channel depths, widths, and slopes. The low, average, and high estimates of bankfull water discharge are 2.7×10^2 m³/s, 5.2×10^2 m³/s, and 8.6×10^2 m³/s, respectively. Similar bankfull discharge estimates have also been reported from the Ferron in earlier studies (Li et al. 2010; Bhattacharya et al. 2016).

Regional hydraulic-geometry curves, or simply regional curves, are used extensively in hydrological estimations of extant river systems (Leopold and Maddock 1953; Andrews 1980; Doll et al. 2002). These regional curves show how the channel dimensions vary with discharge as a power function at a given river cross section (Leopold and Maddock 1953). These relationships can be expressed as (Leopold and Maddock 1953),

$$y = aQ^b (2.7)$$

where y can be average channel depth, width, or velocity and Q is water discharge in ft^3 /s (Leopold and Maddock 1953).

These regional curves have also been used for paleohydrological estimations for ancient depositional systems (Davidson and North 2009). Using regional hydraulic-geometry curves from similar paleo-latitudes and humid subtropical climatic regimes, Davidson and North (2009) reported a range of possible values of bankfull discharge for the Ferron River from the younger Last Chance delta, exposed farther north. Using McCandless' (2003) geomorphic curve for the Maryland Coastal Plain and a bankfull channel depth range of 5 – 9 m, they calculated bankfull discharge to vary from 3.5×10^2 m³/s to 13.6×10^2 m³/s. The choice of the geomorphic curve was driven by the fact that the latitude of the Maryland rivers is similar to the inferred paleolatitude of the Ferron rivers (Ryer and McPhillips 1983; Davidson and North 2009). We calculated a range of values of bankfull discharge using the relationship between the bankfull channel depth and discharge from McCandless (2003) for streams in the Maryland Coastal Plain (Eq. 2.8).

Mean depth (ft) =
$$0.32(Q_{bkf})^{0.4}$$
 (2.8)

where Q_{bkf} is the bankfull channel discharge in ft³/s.

Using the low, average, and high estimates of bankfull channel depth (from Eq. 2.8), we calculated bankfull discharge values of 1.8×10^2 m³/s, 3.8×10^2 m³/s, and 6.7×10^2 m³/s, respectively, for the Notom delta. These bankfull discharge values fall within the range of bankfull discharges calculated using the fulcrum approach.

The total bankfull bedload discharge (Q_{tbf}) is estimated by multiplying the bankfull channel width by the bedload discharge per unit width (q_{tbf}) using Eq. 2.4. The bedload discharge (Q_{tbf}) ranges from 0.11 m³/s to 0.34 m³/s, with an average estimated value of 0.17 m³/s, corresponding to the respective values of channel width established earlier (Table 2.1).

The flow velocity is estimated using the standard Chézy coefficient, slope (as estimated above), and hydraulic radius (*R*). The average flow velocity is 1.7 m/s, with lower and upper bounds at 1.6 m/s and 1.9 m/s, respectively (Table 2.1).

The total suspended-load discharge (Q_s) is estimated by multiplying the estimated suspended discharge per unit width (q_s) by channel width using Eq. 2.5. The suspended-load discharge (Q_s) ranges from 1.2 m³/s to 3.5 m³/s, with an average estimated value of 2.2 m³/s (Table 2.1).

Table 2.1. Estimation of paleohydrology, discharge, and sediment volume for the Ferron trunk valley.

		Bedform				Grain					Bedlo	Bedload Volume		Suspende	Suspended-load Volume Total Sediment Load	Total S	ediment Load
7	Average	Height		Bankfull	Bankfull Bankfull							(m ³)	Suspended-		(m ³)		(m ³)
	Cross-set	Меап		Channel	Channel Channel	(mm)		Average	Average Bankfull Bedload	Bedload		For	load		For		For
I	[hickness	Dune		Depth	Width	(D ₃₀ ,		Flow	Flow Discharge Discharge Mean	Discharge	Mean	combined	Discharge Mean	Mean	combined Mean	Меап	combined
	(S _m)		Height Estimation (H _{bf})	$(\mathbf{H}_{\mathrm{bf}})$	$(\mathbf{B}_{\mathrm{bf}})$	D84,	Slope	Velocity	Slope Velocity (Qbf)	(Q _{tbf})	Annual	(Q _{th} t) Annual duration of (Q _s)	(Q,	annual	annual duration of annual	annual	duration of
	(m)	(Hm) (m)	(Hm) (m) Case	(m)	(m)	D50,	(S)	(m/s)	(m ³ /s)	(m ³ /s)	(Qmas)	$(\mathbf{m}^3/\mathbf{s})$ (Q_{mas}) parasequences	(m ³ /s)	(Qmas)	(Q _{mas}) parasequences (Q _{mas}) parasequences	(Qmas)	parasequences
l	0.18	0.54	Low	3.3	50	3.0, 2.0,	3.0, 2.0, 0.00056 1.6	1.6	270	0.11	1.4×10 ⁵	$0.11 1.4 \times 10^5 4.0 \times 10^9$	1.2	1.5×10 ⁶	1.5×10^6 4.5×10^{10} 1.7×10^6 4.9×10^{10}	1.7×10 ⁶	4.9×10^{10}
			Base	4.4	99	0.6,	0.00042 1.7	1.7	520	0.17	2.2×10 ⁵	$0.17 2.2 \times 10^5 6.2 \times 10^9$	2.2	2.8×10 ⁶	8.0×10^{10} 3.0×10^{6}	3.0×10 ⁶	8.6×10^{10}
			High	5.5	80		0.00034 1.9	1.9	098	0.34	3.0×10^{5}	$0.34 3.0 \times 10^5 8.7 \times 10^9$	3.5	4.4×10 ⁶	4.4×10^6 1.3×10^{11} 4.7×10^6 1.4×10^{11}	4.7×10 ⁶	1.4×10 ¹¹

2.4.3 Estimation of mean annual sediment discharge

In order to establish the sediment balance over the duration of the stratigraphic interval under investigation, the instantaneous sediment discharge rates calculated above need to be projected first over a one-year period and then over the duration of the stratigraphic unit of interest (Holbrook and Wanas 2014). The mean annual discharge (Q_{mas}) for the trunk channel can be calculated using Eq. 2.6.

Empirical compilations reveal a large variation in the year-averaged bankfull duration with a typical average for most modern rivers at about 2% or 7.3 days (Meybeck et al. 2003; Holbrook and Wanas 2014). It has also been shown that approximately 50% of the total annual sediment load can be transported during such bankfull events (Meybeck et al. 2003; Powell et al. 2006). Using these average values for average annual bankfull-event duration and the proportion of the annual sediment load carried during the flood duration based on analog data from modern rivers, the average/ base case annual sediment load (Q_{mas}) for the Ferron channel under study is estimated at 3×10^6 m³ (sum of total annual bedload and suspended load volume of 2.2×10^5 m³ and 2.8×10^6 m³, respectively) with low and high range values of 1.7×10^6 m³ (bedload, 1.4×10^5 m³ and suspended load, 1.5×10^6 m³) and 4.7×10^6 m³ (bedload, 3×10^5 m³ and suspended load, 4.4×10^6 m³), respectively (Table 2.1).

2.4.4 Estimation of mass balance across the fulcrum

High-frequency cyclicity or Milankovitch-scale cyclicity ($10^4 - 10^6$ years) has been reported from the sedimentary records of the Cretaceous Interior basin of North America (Sageman et al. 1997; Meyers et al. 2001; Locklair and Sageman 2008). Zhu et al. (2012) recorded Milankovitch-scale high-frequency cycles in the Ferron Notom Delta and suggested that individual parasequences may correlate to 20,000-year precessional cycles. If the time period of deposition is represented by a 10^4 yr Milankovitch cycle, (approx. 14 kyr for individual parasequences) (Zhu et al. 2012; Bhattacharya et al. 2016), we estimated that the average total sediment volume derived from the source area that would have passed through the fulcrum during the total time duration of parasequences 6 and 7 is

approximately 8.6×10^{10} m³ (86 km³), including a bedload volume of 6.2×10^9 m³ (6.2 km³) and suspended-load volume of 8×10^{10} m³ (80 km³, Table 2.1).

In the absence of mapping of the lateral extent of suspended load represented by prodelta and shelf mudstone facies (Bhattacharya et al. 2016), in this study the mass balance was compared solely for the bedload portion of the total sediment load. The limits of river-fed sand in the large delta lobe of PS6 (Zhu et al. 2012; Ahmed et al. 2014; Li et al. 2015) are shown in a paleogeographic map (Fig. 2.2). An isopach map for the river-dominated delta lobe in PS6 (Figs. 2.2C and 2.8) was created based on the previous paleogeographic maps (Zhu et al. 2012; Ahmed et al. 2014; Zhiyang et al. 2015) and using thickness measurements from Parasequence 6 of Sequence 2 from previously published cross sections (Li et al. 2010; Zhu et al. 2012). Assuming 20% porosity, the volume of mapped sandstone in the delta lobe is approximately 2.1×10^9 m³ (2.1 km³).

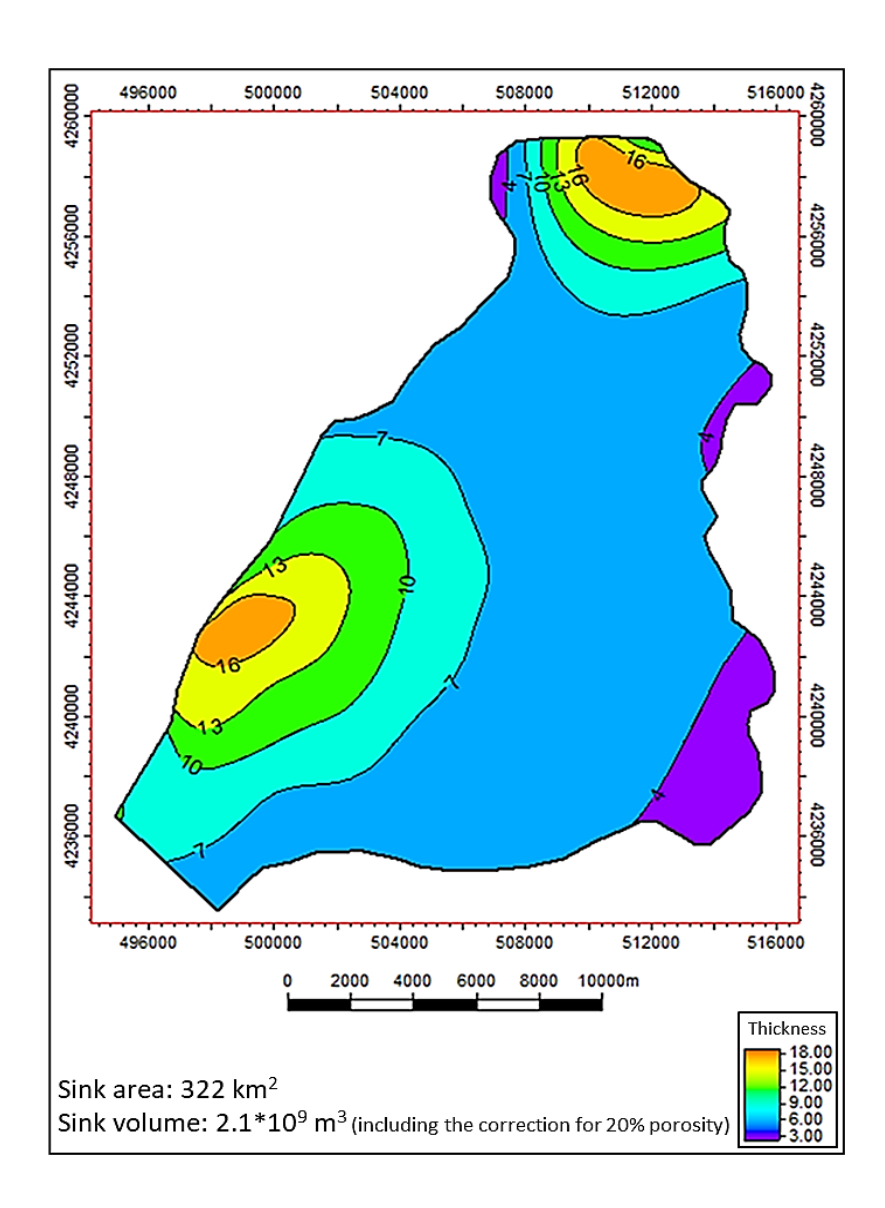


Figure 2.8. Isopach map of Parasequence 6 overlaid with the sink area polygon (blue). For Parasequence 6, the total bedload sediment volume in the sink area, corrected for 20% porosity, is approx. two-thirds of the bedload sediment volume passing through the fulcrum. See text for details.

Regional mapping (Li et al. 2010, 2011; Zhu et al. 2012) has established that the sandstone distribution in PS7 is also restricted to areas similar to that of PS6. The bedload sink volume for PS7 was estimated by considering an average thickness of sandstone at 6 m, derived from measured sections of previous studies (Li et al. 2010; Zhu et al. 2012), and a sink area similar to PS6 (322 km²) along with a porosity correction of 20%. The estimated sandstone volume mapped for PS7 is approximately 1.5×10^9 m³ (1.5 km³). The combined sandstone

volume of the two parasequences is 3.6×10^9 m³ (3.6 km³), which is approximately 3/5 of the sand volume calculated as passing through the fulcrum.

Given the errors and uncertainty of the method, the fulcrum calculations show volumes that are consistent with mapped bedload volumes in the sink. This suggests a well-balanced system and suggests that the approach is robust. However, this and other fulcrum analyses (e.g., Holbrook and Wanas 2014; Lin and Bhattacharya 2017) show a consistent tendency to underestimate bedload volumes by up to a factor of three. In the sections below, we discuss why this may be the case.

2.5 Discussion

2.5.1 Sediment escape

The Ferron Notom fluvio-deltaic wedge has been interpreted as an ancient deposit of an asymmetric wave-dominated delta with strong longshore transport (Bhattacharya and Giosan 2003; Fielding 2010; Li et al. 2011). One of the plausible explanations for the difference between the estimated source and sink sand volumes in the current study could be that there was wave reworking of the sandy delta lobes, which may have carried sediment towards the southeast beyond the limit of the current map area (Fielding 2010). The downdrift extension of the shoreface could have been extensive; for example, 30-70km-long shore-parallel shoreface deposits are documented for areas that lay in between trunk rivers during deposition of the younger Cretaceous Blackhawk Formation (Hampson 2000), and these may be analogous to the Ferron. Considering an 8-km-wide shoreface belt (Taylor and Lovell 1995), an average vertical thickness of 10 m (Zhu et al. 2012), and an alongshore length of 30 – 70 km (Fig. 2.2B), sand volumes transported by waves downdrift of the Ferron river mouths could have been 2.5×10^9 m³ to 5.5×10^9 m³ (2.5 - 5.5 km³), which could readily account for the escaped sand volume of the higher fulcrum estimates presented above. If we consider the lower limit of sand volume transported by waves downdrift $(2.5 \times 10^9 \text{ m}^3)$ and add it to the sink volume estimated above, the resulting sand volume would almost exactly match the total sand volume passing through the fulcrum.

Another mechanism for explaining the difference between the source and the sink volume could be the offshore transport of sand beyond the current sink area via hyperpycnal flows (Bhattacharya and MacEachern 2009; Li et al. 2015). Rivers draining small basins in tectonically active mountainous settings tend to produce hyperpycnal flows (Mulder and Syvitski 1995). These hyperpycnal rivers normally have average discharge values less than 6000 m³/s (Bhattacharya and MacEachern 2009). Considering the flood-discharge values estimated in this study within the framework of the tectonic setting and ever-wet tropical to subtropical paleo-climate (Akyuz et al. 2015), it suggests that the Ferron rivers likely produced frequent hyperpycnal flows, as also shown by Bhattacharya and MacEachern (2009), and these may have contributed to escape of bedload onto the shelf. Recent evaluation of prodelta facies in PS6 shows that there is up to 50% very fine to fine sandstone, which was deposited as hyperpycnites and a variety of potential stormgenerated combined flows (Li et al. 2015). Although these facies were not mapped, sand volumes are likely to be significant and could account for a proportion of the missing bedload. Conversely, much of this very fine sand was likely carried as suspended load and thus may not be relevant to the bedload sediment budget balance.

2.5.2 Errors and uncertainties

Like any other paleohydrological estimation and sediment budget analysis, the fulcrum approach has uncertainties associated with estimation of such factors as bankfull channel dimensions, mean annual bankfull discharge, and mean annual sediment load. These uncertainties may introduce errors of up to an order of magnitude (Holbrook and Wanas 2014). However, there are ways to reduce the range of uncertainties and/or incorporate them in the final calculation using a probabilistic approach.

Direct field measurements can help to reduce uncertainty in paleohydrological estimates. The measurements of grain size and channel depth used in the current study come from detailed outcrop observations and thus carry low errors, typically less than 10%. Thickness measurements are quite accurate and are precise to within a few centimeters for a meterthick unit (i.e., uncertainty is < 10%). The precision of grain-size measurements using a standard grain size card is 1/2 ϕ , resulting in a maximum uncertainty of about 30%.

Although the number of measurements of cross-bed set thicknesses (n = 45) is somewhat limited, the channel depths calculated using empirical equations based on mean cross-bed set thickness are supported by direct field measurements. This suggests that the error in channel-depth estimation is low. However, channel-width calculations based on empirical equations yield values that are significantly higher than what has been observed in the field (Li et al. 2010; Zhu et al. 2012; Ullah et al. 2015). Empirically derived channel widths may have an error range of about 50% – 100% (Bhattacharya et al. 2016). Channel widths used for paleodischarge estimates in this study are calculated using the width of lateral-accretion surfaces rather than empirical equations. The extent of lateral accretion surfaces can be measured on photomosaics with a precision of about 1 m per 10 m (about 10%), and the interpolation of channel widths from point bar extent may have an uncertainty of about 25%. As a consequence, we estimate that our channel-width estimates from outcrop observations of point-bar dimensions have an uncertainty of about 35%.

Slope calculation based on a constant bankfull Shields number (τ_{bf50}^*) of 1.86, approximated for sand-bed rivers, may vary by a factor of two (Holbrook and Wanas 2014). The range of slope values calculated in this study suggests variation by a factor of less than two. The slope calculated in this study matches those derived from stratigraphic methods by a factor of about two (Bhattacharya et al. 2016). The slope calculations thus have an uncertainty of about 200%. However, it is possible that steeper slopes will persist only for a limited time duration as rivers will tend to degrade towards a lower gradient, especially when incised into unconsolidated sediment, as was the case in the Ferron. So, on a time scale of $\sim 20,000$ years, steeper slopes may have existed only for about 10-15% of the time and the overall slope for rest of the 85-90% time may have been lower. Therefore, the variation in the slope values may be relatively small. Also, fluvial long profiles may not be the same as the actual river slopes, especially for highly sinuous rivers (i.e., the length of the river course may be two times the straight-line distance, resulting in slopes that are 50% lower than the fluvial long profile).

The bankfull Shields number (τ_{bf50}^*) varies with particle Reynolds number, which is a proxy for grain size (Parker 2008; Wilkerson and Parker 2011; Lynds et al. 2014), and this

variation may not be captured by using a constant bankfull Shields number for slope calculations (Lynds et al. 2014). We also calculated slope using Eq. 2.9 (Lynds et al. 2014):

$$S = RD_{50}/H_{bf} \left[\frac{u_{*sf}}{w_s} \left(\frac{W^*}{Re_p} \right)^{\frac{1}{3}} \right]^2$$
 (2.9)

where u_{*sf} is skin-friction shear velocity, w_s is settling velocity, Re_p is particle Reynolds number, $Re_p = (\sqrt{RgD_{50}})D_{50}/v$ (Wilkerson and Parker 2011), and W^* is dimensionless settling velocity, which can be calculated by Eq. 2.9a (Dietrich 1982).

$$W^* = -3.76715 + 1.92944 * (log(D^*) - 0.09815 * (log(D^*)^2 - 0.00575 * (log(D^*)^3 + 0.00056 * (log(D^*)^4)))$$
(2.9a)

where D^* (dimensionless particle size) = $(\rho_s - \rho)gD_{50}^3/\rho v^2$ (Dietrich 1982), and ρ_s and ρ_s are grain density and fluid density, respectively.

The $\frac{u_{*sf}}{w_s}$ ratio can be assumed to be 2.0 after Julien (1998). The resulting slope values range from 2.5 x 10⁻⁴ to 1.5 x 10⁻⁴, with an average value of 1.9 x 10⁻⁴ representing an error factor of less than two. If we consider the whole spectrum of slope values estimated in this study, it shows an uncertainty of approximately 200%.

Holbrook and Wanas (2014), while applying the fulcrum approach to their mass-balance analysis of the Cretaceous Bahariya Formation of Egypt, reported that the biggest uncertainty in their sediment-budget estimation was associated with the conversion of bankfull discharge to the mean annual sediment load, which may introduce an order-of-magnitude error in the estimation. The factors contributing to this uncertainty include the annual bankfull or flood duration, its recurrence interval, and the proportion of the total sediment load carried during the bankfull period (Eq. 2.6). Although using the average values of bankfull duration and recurrence intervals from modern analogs might provide a reasonably gross estimate of mean annual sediment volume, it is also true that there is a large variation in the lower and upper range of these values, which is related to the climatic setting of the river system (Holbrook and Wanas 2014; Bhattacharya et al. 2016). Data

from modern rivers show that the duration of annual bankfull discharge varies from approximately 0.3% to approximately 6.6% per year, which translates into 1 to 24 days (Wolman and Miller 1960; Andrews 1980; Sweet and Geratz 2003; Metcalf 2004; Powell 2006). The recurrence interval also varies from 0.2 to 2 years (McCandless and Everett 2002; McCandless 2003; Sweet and Geratz 2003; Powell et al. 2006). In most cases, approximately 50% of the total annual sediment load is carried during bankfull events (Powell et al. 2006). For drainage basins with an area of the order of 10⁴ km², like the Ferron with an estimated drainage area of about 50,000 km² (Bhattacharya and Tye 2004), 50% of the total suspended solid load can be transported during 2% or 7.3 days of a year, which corresponds to the average bankfull duration (Fig. 2.9) (Meybeck et al. 2003). However, values may also vary from 25% (Powell et al. 2006) to 90% (Nolan et al. 1987).

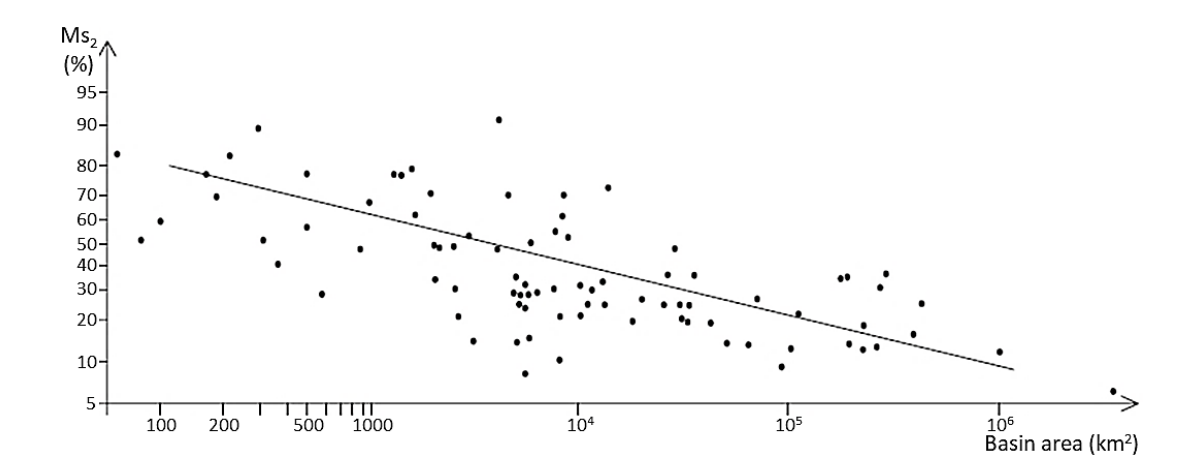


Figure 2.9. Plot of percentage of suspended load transported in 2% or 7.3 days (Ms₂) against basin area. For Ferron, with an area of 50,000 km², this percentage is about 50%. (From Meybeck et al. 2003)

2.5.3 Evaluation of uncertainty using Monte Carlo simulation

In order to understand the sensitivity of these parameters on the calculation of annual bedload volume, a Monte Carlo simulation was run using the Oracle Crystal Ball software, which is a spreadsheet-based application. Monte Carlo simulation involves random sampling of all independent input variables, having a range of uncertainty, to obtain a distribution of ranges of dependent output values through multiple scenarios or iterations

(Vose 1996). Commonly used probability distributions include normal, lognormal, triangular, and uniform (Vose 1996). Random samples for input variables are chosen on the basis of a suitable probability distribution and for each set of input parameters an output set is generated (Raychaudhuri 2008). Each set of output parameters is one iteration or scenario, and the result of thousands of such iterations is a probability distribution of possible outcomes (Raychaudhuri 2008). The results of a simulation can be expressed in terms of P10, P50 (median, unless the distribution is normal, in which case both the mean and median would be same), and P90, which represents the exceedance probability of respective numbers. For example, P90 means that 90% of values exceed the P90 estimate.

Since most of the discharge data for rivers follow a lognormal distribution (Pickup and Warner 1976; Yu and Wolman 1987; Nash 1994; Bowers et al. 2012), a total of 1000 realizations were run using a lognormal distribution for bedload discharge rates (Q_{tbf}), mean annual bankfull duration (t_{bd}) and the dimensionless multiplier (b) (Table 2.2).

Table 2.2. Range of input variables (as in Eq. 2.6) used in the Monte Carlo simulations based probabilistic estimation and the resulting P10, P50, and P90 values for mean annual bedload volume (m³) highlighting the range of possible outcomes.

Estimation Case	Bedload discharge (m ³ /s)	Number of bankfull event days/yr	RI	t _{bd} (s)	b		annual bo	
						P10	P50	P90
Low	0.11	1.0	0.2	432000	4.0	9.1 ×	1.7 ×	3.7 ×
Base	0.17	7.3	1.0	630720	2.0	10^4	10^{5}	10^{5}
High	0.24	24.0	2.0	1036800	1.1	- 3	- 0	- 0

The P10, P50, and P90 values of Q_{mas} are 9.1×10^4 m³, 1.7×10^5 m³, and 3.7×10^5 m³, respectively (Fig. 2.10B), indicating that Q_{mas} estimations vary by a factor of four. An ever-wet tropical to subtropical climate (Akyuz et al. 2015) and the existence of abundant coals (Zhu et al. 2012) support the assumption that the bankfull flow duration for the Ferron

River could have been more than the average of 2% or 7.3 days a year. Therefore, a discharge value higher than the current P50 value may be more realistic. The sensitivity analysis during Monte Carlo simulation (Fig. 2.10C) suggests that the calculations of mean annual sediment load are most sensitive to factor b, suggesting that it might have a value higher than the normally assumed value of 2 for the current study.

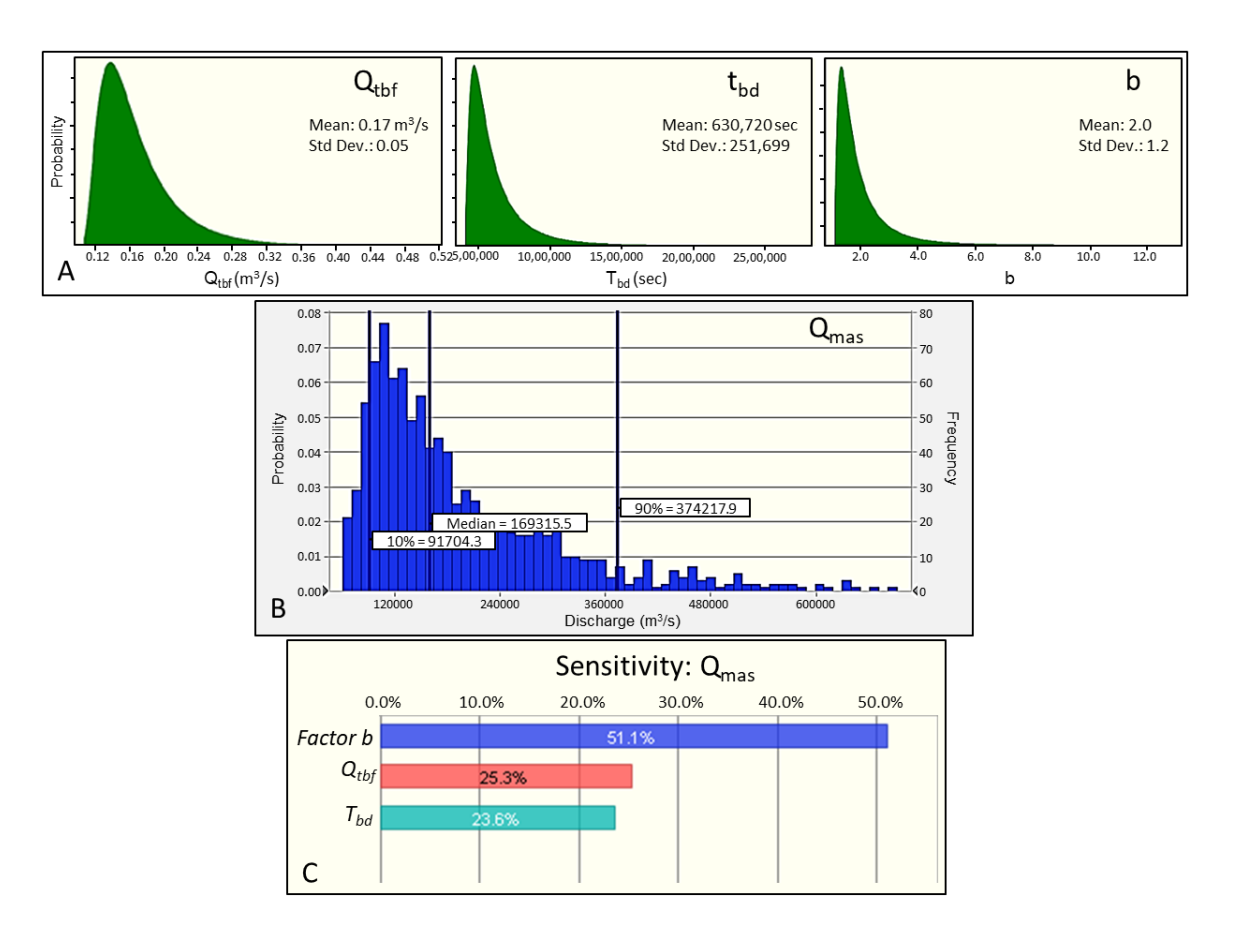


Figure 2.10. The results of the Monte Carlo simulation showing A) the lognormal probability distribution for the bankfull bedload discharge (Q_{tbf}) , the annual bankfull duration (t_{bd}) , and the proportion of annual sediment load carried during the bankfull period (b); B) the frequency distribution of mean annual sediment load (Q_{mas}) after 1000 realizations; and C) sensitivity plot for inputs to the Q_{mas} calculation.

If we consider the P50 value of bedload Q_{mas} to establish a mass balance across the fulcrum for the combined time duration of parasequences 6 and 7, the source-area bedload volume $(4.9 \times 10^9 \text{ m}^3 \text{ or } 4.9 \text{ km}^3)$ is more than 3/4 of the sand volume measured in the associated

parasequences 6 and 7 delta lobes $(3.6 \times 10^9 \,\mathrm{m}^3 \,\mathrm{or}\, 3.6 \,\mathrm{km}^3)$. This difference between source and sink bedload volumes is less than the difference between the respective bedload volumes using the deterministic fulcrum approach. However, consideration of the P90 value results in an overestimation of source-derived bedload volume, suggesting a Q_{mas} in between P50 and P90 values. Therefore, the bankfull event duration and RI for the Ferron might be higher than the typically considered average values, and consequently a higher Q_{mas} value might be more realistic. As mentioned earlier, this is also supported by facies (Zhu et al. 2012) and paleoclimatic studies of the Ferron (Akyuz et al. 2015).

As discussed above, sediment escape by wave reworking alongshore and via hyperpycnal flows could account for underestimation of the sink volume measured in the immediate study area. Radiometric dating (Zhu et al. 2012) restricts the deposition of the Ferron Notom delta to have occurred between 91.25 ± 0.77 Ma and 90.64 ± 0.25 Ma, corresponding to the *Prionocyclus hyatti* and *Prionocyclus macombi* biozones (Cobban et al. 2006). Honoring the Law of Superposition and considering that the average biozone duration in Turonian is about 390,000 years (Garrison and van den Bergh 2004), the total time duration for the Ferron Notom delta may vary from approximately 200,000 to 800,000 years. This represents an uncertainty range of 400%.

Dividing the total time duration for the Ferron Notom delta equally amongst the parasequences results in a calculated duration of approximately 14 kyr for each parasequence (Zhu et al. 2012). In their geochronological assessment, Zhu et al. (2012) also reported the radiometric ages of 90.69 ± 0.34 Ma for a bentonite bed lying slightly below Parasequence 7, and 90.64 ± 0.25 Ma for another bentonite bed above the coal seam in Parasequence 2 (Fig. 2.2A). Considering these two dates alone, the average time duration for each of the five parasequences falling within this time window, including those under current study, is approximately $10 \, \text{kyr}$, which, although within the same order of magnitude as before, narrows down the time interval by 30%. Considering this time duration for a parasequence, the estimated average bedload volume passing through the fulcrum for parasequences 6 and 7 is $4.3 \times 10^9 \, \text{m}^3$ ($4.3 \, \text{km}^3$). The total bedload sink volume of $3.6 \, \text{km}^3$ accounts for $\sim 85\%$ of the source-derived sand volume, which thus represents an

improvement in the source-to-sink mass balance by about 25%. The 10^4 -year time duration associated with a Ferron parasequence is an order of magnitude bigger than the time duration of a single delta lobe in the Mississippi River, which is about 1500 years (Aslan et al. 2005). It is possible that these parasequences are not as long lived, and that there is more time associated with sequence boundaries 1 and 2 (Zhu et al. 2012). But with the current data, it is not possible to improve the chronometric resolution beyond the current level, which results in a relatively long-time duration for parasequences, and hence a larger sink volume. Reducing the time duration for a parasequence to ~ 8.5 kyr results in a mass balance between source and sink bedload volumes. This time assumption would yield a total time duration for the Ferron Notom delta of about 365,000 years, which is still within the range of time duration calculated above.

2.6 Conclusions

The quantitative paleohydrology for the Ferron trunk river, based on the fulcrum approach, yields flood-discharge values in the range of 2.7×10^2 m³/s to 8.6×10^2 m³/s, which support the hypothesis that these rivers were capable of routinely producing hyperpycnal flows (Bhattacharya and MacEachern 2009). The average total sediment volume that likely passed through the fulcrum during the total time duration of parasequences 6 and 7 is estimated to be $\sim 8.6 \times 10^{10}$ m³ (86 km^3), including a bedload volume of 6.2×10^9 m³ (6.2 km^3) and suspended-load volume of 8×10^{10} m³ (80 km^3). The estimated combined bedload volume in the sink for parasequences 6 and 7 is about 3.6×10^9 m³ (3.6 km^3), which is about 60% of the total bedload volume passing through the fulcrum. This is well within the inherent uncertainty of the calculations but nevertheless suggests escape of some bedload fraction. This difference is likely due to wave reworking of the sandy delta lobes and deflection of sediment to the SE beyond the current sink limit, as well as transport of sand farther offshore via hyperpycnal flows. The P50 Q_{mas} value of the probabilistic estimation shows improved source-to-sink mass balance in comparison to the deterministic fulcrum approach. The probabilistic estimation shows that a Q_{mas} between P50 and P90 estimation

is more realistic for the Ferron. This also suggests that the bankfull event duration and RI for the Ferron might be higher than the typical average values.

Paleohydrology and sediment-budget estimations can be used in climate reconstructions, drainage-area estimations, as well as estimates of sediment partitioning between components of a linked source-to-sink system. Knowing the sediment volume passing through the fulcrum location helps in making a first order estimate of reservoir volumes in the sink areas (Bhattacharya et al. 2016). This study demonstrates the application of the fulcrum approach in a source-to-sink analysis, with a reduced range of errors and uncertainties than previous examples (e.g. Holbrook and Wanas 2014) through detailed outcrop work and incorporation of climate data from modern analogs. Although the biggest contributor to error is still the conversion from instantaneous to mean annual sediment load, we have managed to reduce the uncertainty in our estimation. This study also uses Monte Carlo simulation based probabilistic estimations of the sediment load of a stratigraphic system, using a range of values of annual discharge duration and recurrence intervals taken from modern analogs with similar climatic conditions.

References

- Ahmed, S., Bhattacharya, J.P., Garza, D.E., and Li, Y., 2014, Facies architecture and stratigraphic evolution of a river-dominated delta front, Turonian Ferron Sandstone, Utah, USA: Journal of Sedimentary Research, v. 84, p. 97–121.
- Akyuz, I., Warny, S., Famubode, O., and Bhattacharya, J.P., 2015, Palynology of the Upper Cretaceous (Turonian) Ferron Sandstone Member, Utah, USA: identification of marine flooding surfaces and Milankovitch cycles in subtropical, ever-wet, paralic to non-marine palaeoenvironments: Palynology, v. 40, no. 1, p. 122-136.
- Andrews, E.D., 1980, Effective and bankfull discharges of streams in the Yampa River basin, Colorado and Wyoming: Journal of Hydrology, v. 46, p. 311–330.
- Aslan, A., Autin, W.J., and Blum, M.D., 2005, Causes of river avulsion: insights from the late Holocene avulsion history of the Mississippi River, USA: Journal of Sedimentary Research, v. 75, p. 650-664.

- Bhattacharya, J.P., Copeland, P., Lawton, T.F., and Holbrook, J., 2016, Estimation of source area, river paleo-discharge, paleoslope and sediment budgets of linked deeptime depositional systems and implications for hydrocarbons: Earth-Science Reviews, v. 153, p. 77-110.
- Bhattacharya, J.P., and Giosan, L., 2003, Wave-influenced deltas: geomorphological implications for facies reconstruction: Sedimentology, v. 50, p.187-210.
- Bhattacharya, J.P., and MacEachern, J.A., 2009, Hyperpycnal rivers and prodeltaic shelves in the Cretaceous Seaway of North America: Journal of Sedimentary Research, v. 79, p. 184–209.
- Bhattacharya, J.P., and Tye, R.S., 2004, Searching for modern Ferron analogs and application to subsurface interpretation, *in* Chidsey T.C. Jr., Adams, R.D., and Morris, T.H. eds., The Fluvial-Deltaic Ferron Sandstone: Regional to Wellbore Analog for Fluvial-Deltaic Reservoir Modeling: American Association of Petroleum Geologists, Studies in Geology, v. 50, p. 39–57.
- Bhattacharya, P., Bhattacharya, J.P., and Khan, S.D., 2015, Paleo-channel reconstruction and grain size variability in fluvial deposits, Ferron Sandstone, Notom Delta, Hanksville, Utah: Sedimentary Geology, v. 325, p. 17-25.
- Bowers, M.C., Tung, W.W., and Gao, J.B., 2012, On the distributions of seasonal river flows: Lognormal or power law?: Water Resources Research, v. 48, p. 1–12.
- Bridge, J.S., 1997, Thickness of sets of cross-strata and planar strata as a function of formative bedwave geometry and migration: Geology, v. 25, p. 971–974.
- Bridge, J.S., 2003, Rivers and Floodplains; Forms, Processes, and Sedimentary Record: Malden, Massachusetts, Blackwell Science, 491 p.
- Bridge, J.S., and Mackey, S.D., 1993, A theoretical study of fluvial sandstone body dimensions, *in* Flint, S.S., and Bryant, I.D., eds., The Geological Modelling of Hydrocarbon Reservoirs and Outcrop Analogues: International Association of Sedimentologists, Special Publication 15, p. 213–236.
- Bridge, J.S., and Tye, R.S., 2000, Interpreting the dimensions of ancient fluvial channel bars, channels, and channel belts from wireline-logs and cores: American Association of Petroleum Geologists, Bulletin, v. 84, p. 1205–1228.

- Cobban, W.A., Walaszczyk, I., Obradovich, J.D., and McKinney, K.C., 2006, A USGS Zonal Table for the Upper Cretaceous Middle Cenomanian-Maastrichtian of the Western Interior of the United States Based on Ammonites, Inoceramids, and Radiometric Ages: US Geological Survey, Open-File Report- 2006-1250, 45 p.
- Dade, W.B., and Friend, P.F., 1998, Grain-size, sediment-transport regime, and channel slope in alluvial rivers: The Journal of Geology, v. 106, p. 661-676.
- Davidson, S.K., and North, C.P., 2009, Geomorphological regional curves for prediction of drainage area and screening modern analogues for rivers in the rock record: Journal of Sedimentary Research, v. 79, p. 773–792.
- Dietrich, W.E., 1982, Settling velocity of natural particles: Water Resources Research, v. 18, p. 1615–1626.
- Doll, B.A., Wise-Frederick, D.E., Buckner, C.M., Wilkerson, S.D., Harman, W.A., Smith, R.E., and Spooner, J., 2002, Hydraulic geometry relationships for urban streams throughout the Piedmont of North Carolina: Journal of the American Water Resources Association, v. 38, p. 641-651.
- Engelund, F., and Hansen, E., 1967, A Monograph on Sediment Transport in Alluvial Streams: Copenhagen, Technisk Vorlag, 62 p.
- Fielding, C.R., 2010, Planform and facies variability in asymmetric deltas: Facies analysis and depositional architecture of the Turonian Ferron Sandstone in the Western Henry Mountains, South-Central Utah, U.S.A.: Journal of Sedimentary Research, v. 80, p. 455–479.
- Fielding, C.R., 2011, Foreland basin structural growth recorded in the Turonian Ferron Sandstone of the Western Interior Seaway Basin, USA: Geology, v. 39, p. 1107-1110.
- Garcia, M. and Parker, G., 1991, Entrainment of bed sediment into suspension: Journal of Hydraulic Engineering, v. 117, p. 414-435.
- Gardner, M.H., Cross, T.A., and Levorsen, M., 2004, Stacking patterns, sediment volume partitioning, and facies differentiation in shallow-marine and coastal-plain strata of the Cretaceous Ferron Sandstone, Utah, *in* Chidsey T.C., Jr., Adams, R.D., and Morris, T.H., eds., Regional to Wellbore Analog for Fluvial-Deltaic Reservoir Modeling: The

- Ferron Sandstone of Utah: American Association of Petroleum Geologists, Studies in Geology, v. 50, p. 95-124.
- Garrison J.R., JR., and van den Bergh, T.C.V., 2004, High-resolution depositional sequence stratigraphy of the upper Ferron sandstone last chance delta: an application of coal-zone stratigraphy, *in* Chidsey T.C., Jr., Adams, R.D., and Morris, T.H., eds., Regional to Wellbore Analog for Fluvial-Deltaic Reservoir Modeling: The Ferron Sandstone of Utah: American Association of Petroleum Geologists, Studies in Geology, v. 50, p. 125–192.
- Hampson, G.J., 2000, Discontinuity surfaces, clinoforms, and facies architecture in a wave-dominated, shoreface-shelf parasequence: Journal of Sedimentary Research, v. 70, p. 325-340.
- Holbrook, J., and Wanas, H., 2014, A fulcrum approach to assessing source-to-sink mass balance using channel paleohydrologic parameters derivable from common fluvial data sets with an example from the Cretaceous of Egypt: Journal of Sedimentary Research, v. 84, p. 349–372.
- Julien, P.Y., 1998, Erosion and Sedimentation: New York, Cambridge University Press, 280 p.
- Leclair, S.F., and Bridge, J.S., 2001, Quantitative interpretation of sedimentary structures formed by river dunes: Journal of Sedimentary Research, v. 71, p. 713–716.
- Leclair, S.F., Bridge, J.S., and Wang, F., 1997, Preservation of cross-strata due to migration of subaqueous dunes over aggrading and non-aggrading beds: Comparison of experimental data with theory: Geoscience Canada, v. 24, p. 55–66.
- Leopold, L.B. and Maddock, T., 1953, The hydraulic geometry of stream channels and some physiographic implications: U.S. Geological Survey Professional Paper 252, p. 1–57.
- Li, W., Bhattacharya, J.P., and Campbell, C., 2010, Temporal evolution of fluvial style in a compound incised-valley fill, Ferron "Notom Delta", Henry Mountains Region, Utah (U.S.A.): Journal of Sedimentary Research, v. 80, p. 529–549.

- Li, W., Bhattacharya, J.P., Zhu, Y., Garza, D., and Blankenship, E., 2011, Evaluating delta asymmetry using 3D facies architecture and ichnological analysis, Ferron Notom Delta, Capital Reef Utah, USA: Sedimentology, v. 58, p. 478-507.
- Li, Y., and Bhattacharya, J.P., 2013, Facies-architecture study of a stepped, forced regressive compound incised valley in the Ferron Notom delta, Southern Central Utah, USA: Journal of Sedimentary Research, v. 83, p. 206-225.
- Li, Z., Bhattacharya, J.P., and Schieber, J., 2015, Evaluating along-strike variation using thin-bedded facies analysis, Upper Cretaceous Ferron Notom Delta, Utah: Sedimentology, v. 62, p. 2060-2089.
- Lin, W., and Bhattacharya, J.P., 2017, Estimation of source-to-sink mass balance and depositional systems dominated sediment budgets by a fulcrum approach assessment using channel paleohydrologic parameters: Cretaceous Dunvegan Formation: Journal of Sedimentary Research, v. 87, p. 97-116.
- Locklair, R.E., and Sageman, B.B., 2008, Cyclostratigraphy of the Upper Cretaceous Niobrara Formation, western interior, USA: a Coniacian–Santonian orbital timescale: Earth and Planetary Science Letters, 269, p. 540-553.
- Lynds, R.M., Mohrig, D., Hajek, E.A., and Heller, P.L., 2014, Paleoslope reconstruction in sandy suspended-load-dominant rivers: Journal of Sedimentary Research, v. 84, p. 825-836.
- McCandless, T.L., 2003, Maryland Stream Survey: Bankfull Discharge and Channel Characteristics of Streams in the Coastal Plain hydrologic regions: U.S. Fish and Wildlife Service, Annapolis, Maryland, Report CBFO-S03-02.
- McCandless, T.L. and Everett, R.A., 2002, Maryland Stream Survey: Bankfull Discharge and Channel Characteristics in the Piedmont hydrologic region: U.S. Fish and Wildlife Service, Annapolis, Maryland, Report CBFO-S02-01.
- Metcalf, C., 2004, Regional Channel Characteristics for Maintaining Natural Fluvial Geomorphology in Florida Streams: U.S. Fish and Wildlife Service, Panama City, Fisheries Resource Office.

- Meybeck, M., Laroche, L., Dürr, H., and Syvitski, J.P.M., 2003, Global variability of daily total suspended solids and their fluxes in rivers: Global and Planetary Change, v. 39, p. 65–93.
- Meyers, S.R., Sageman, B.B., and Hinnov, L.A., 2001, Integrated quantitative stratigraphy of the Cenomanian-Turonian Bridge Creek Limestone Member using evolutive harmonic analysis and stratigraphic modeling: Journal of Sedimentary Research, v. 71, p. 628-644.
- Mulder, T., and Syvitski, J.P.M., 1995, Turbidity currents generated at river mouths during exceptional discharges to the world oceans: The Journal of Geology, v. 103, p. 285–299.
- Nash, D.B., 1994, Effective sediment-transporting discharge from magnitude-frequency analysis: The Journal of Geology, v. 102, p. 79-95.
- Nolan, K.M., Lisle, T.E., and Kelsey, H.M., 1987, Bankfull discharge and sediment transport in northwestern California, *in* Beschta, R., Blinn, T., Grant, G.E., Swanson, F.J. and Ice, G.G., eds., Erosion and Sedimentation in the Pacific Rim: International Association of Hydrological Sciences, Publication no. 165, p. 439-449.
- Parker, G., 2004, 1D Sediment Transport Morphodynamics with Applications to Rivers and Turbidity Currents: E book, http://www.nced.umn.edu/.
- Parker, G., 2008, Transport of gravel and sediment mixtures, Chapter 3, Sedimentation Engineering, *in* Garcia, M.H., ed., Processes, Measurements, Modeling and Practice: American Society of Civil Engineers, Manuals and Reports on Engineering Practice, no. 110, p. 165-252.
- Parker, G., Paola, C., Whipple, K., and Mohrig, D., 1998, Alluvial fans formed by channelized fluvial and sheet flow, I: Theory: Journal of Hydraulic Engineering, v. 124, p. 985-995.
- Peterson, F., and Ryder, R.T., 1975, Cretaceous rocks in the Henry Mountains region, Utah, and their stratigraphic relation to neighboring regions, *in* Fassett, J.E., ed., Canyonlands Country: Four Corners Geological Society Guidebook 8th Field Conference, p. 167-189.

- Pickup, G., and Warner, R.F, 1976, Effects of hydrologic regime on magnitude and frequency of dominant discharge: Journal of Hydrology, v. 29, p. 51-75.
- Powell, G.E., Mecklenburg, D., and Ward, A., 2006, Evaluating channel-forming discharges: A study of large rivers in Ohio: American Society of Agricultural and Biological Engineers, Transactions, v. 49, p. 35-46.
- Raychaudhuri, S., 2008, Introduction to Monte Carlo Simulation, *in* Mason, S.J., Hill, R.R., Mönch, L., Rose, O., Jefferson, T., and Fowler, J.W., eds., Proceedings of the 2008 Winter Simulation Conference, p. 91-100.
- Richards, B.H., 2014, Fluvial to marine succession in a compound incised valley system in the Ferron Notom delta, Utah: M.Sc. Thesis: University of Houston, Houston, Texas, USA, 56 p.
- Ryer, T.A., and McPhillips, M., 1983, Early Late Cretaceous paleogeography of east-central Utah, *in* Reynolds, M.W., and Dolly, E.D., eds., Mesozoic Paleogeography of the West-central United States: Denver, Rocky Mountain Section, Society of Economic. Paleontologists and Mineralogists, Rocky Mountain Paleogeography Symposium 2, p. 253–272.
- Sageman, B.B., Rich, J., Arthur, M.A., Birchfield, G.E., and Dean, W.E., 1997, Evidence for Milankovitch periodicities in Cenomanian-Turonian lithologic and geochemical cycles, Western Interior USA: Journal of Sedimentary Research, v. 67, p. 286-301.
- Sweet, W.V., and Geratz, J.W., 2003, Bankfull hydraulic geometry relationships and recurrence intervals for North Carolina's Coastal Plain: Journal of the American Water Resources Association, v. 39, p. 861–871.
- Taylor, D.R., and Lovell, R.W., 1995, High-frequency sequence stratigraphy and paleogeography of the Kenilworth member, Blackhawk Formation, Book Cliffs, Utah, USA, *in* van Wagoner, J.C., and Bertram, G.T., eds., Sequence Stratigraphy of Foreland Basin Deposits: Outcrop and Subsurface Examples from the Cretaceous of North America: American Association of Petroleum Geologists, Memoir 64, p. 257–275.
- Ullah, M.S., Bhattacharya, J.P., and Dupre, W.R., 2015, Confluence scours versus incised valleys: Examples from the Cretaceous Ferron Notom Delta, Southeastern Utah, USA: Journal of Sedimentary Research, v. 85, p. 445-458.

- van Rijn, L.C., 1984b, Sediment transport, Part II: Suspended load transport: Journal of Hydraulic Engineering, v. 110, p. 1613-1641.
- Vose, D., 1996, Quantitative Risk Analysis: A Guide to Monte Carlo Simulation Modelling: Chichester, West Sussex, John Wiley & Sons, 729 p.
- Wilkerson, G.V., and Parker, G., 2011, Physical basis for quasi-universal relationships describing bankfull hydraulic geometry of sand-bed rivers: Journal of Hydraulic Engineering, v. 137, p. 739–753.
- Wolman, M.G., and Miller, J.P., 1960, Magnitude and frequency of forces in geomorphic processes: The Journal of Geology, v. 68, p. 54-74.
- Wright, S., and Parker, G., 2004, Flow resistance and suspended load in sand-bed rivers: Simplified stratification model: Journal of Hydraulic Engineering, v. 130, p. 796–805.
- Wu, C., Bhattacharya, J.P., and Ullah, M., 2015, Paleohydrology and 3D facies architecture of ancient point bars, Ferron Sandstone, Notom Delta, South-central, Utah: Journal of Sedimentary Research, v. 85, p. 399-418.
- Yu, B., and Wolman, M.G., 1987, Some dynamic aspects of river geometry: Water Resources Research, v. 23, p. 501-509.
- Zhu, Y., 2010, Sequence Stratigraphy and Facies Architecture of the Cretaceous Ferron Notom Delta Complex, South-Central Utah, U.S.A.: PhD Thesis, University of Houston, Houston, Texas, USA, 144 p.
- Zhu, Y., Bhattacharya, J.P., Li, W., Lapen, T.J., Jicha, B.R., and Singer, B.S., 2012, Milankovitch-scale sequence stratigraphy and stepped forced regressions of the Turonian Ferron Notom Deltaic Complex, South-Central Utah, U.S.A.: Journal of Sedimentary Research, v. 82, p. 723–746.

Chapter 3

Facies architecture and paleohydraulics of the late Cretaceous Torrivio Sandstone, New Mexico, USA

There are many well documented single-thread meandering river depositional systems in the Cretaceous Western Interior Seaway, including the Dunvegan Formation in Alberta, Canada and the Ferron Sandstone Member in Utah, USA. However, detailed work for braided river deposits is far less available. This paper examines deposits of the Torrivio River in New Mexico, that has been previously interpreted as braided largely based on its coarse-grained nature, rather than careful analysis of bar deposits. This study uses data from 18 measured sections and 6 photomosaics to demonstrate that Torrivio shows a change in the formative rivers from weakly-braided multi-channel system to overlying sinuous single-channel system. Paleohydraulic analysis shows that the braided river was about 3-6 m deep and on average 200 m wide. However, a 12 m thick downstream migrating tributary confluence deposit and multiple other deposits of smaller confluence scale can also be found. The braided section is characterized by typical mid-channel and side bars along with multiple channel fills producing a more sheet-like geometry. The overlying sinuous channel was approximately 4 m deep and 40 m wide. The vertical change in the fluvial style is attributed to a decrease in the stream power of the system.

Paleodischarge estimates of the braided section show that the average water discharge was $\sim 1850 \, \text{m}^3/\text{sec}$ whereas the average bedload discharge was $0.27 \, \text{m}^3/\text{s}$. Using suitable climate-binned modern analogs, the average annual bedload volume was estimated to be about $30.2 \, \text{x} \, 10^4 \, \text{m}^3$. A Monte-Carlo simulation was also run to evaluate the effects of bankfull duration and recurrence interval on annual bedload estimates. The annual bedload volume estimates range from $16.2 \, \text{x} \, 10^4 \, \text{m}^3$ to $61.8 \, \text{x} \, 10^4 \, \text{m}^3$, which demonstrates appreciable reduction in the range of uncertainty by using climate-binned modern analogs.

3.1 Introduction

Historically, fluvial facies models emphasize the plan view of the river as a main control on sand body geometry as well as overall stratigraphic architecture, such that meandering rivers are purported to produce mud-dominated strata whereas braided systems are dominated by sandstone and/or conglomerate, with little preserved floodplain (e.g., Cant 1982; Friend 1983; Walker and Cant 1984). The interpretation of plan view was commonly based on the degree of amalgamation of channel fills versus more detailed analysis of bedding patterns in cliff sections, where the orientation of cliffs versus paleoflow allows braid bars and point bars to be distinguished (Bristow 1993a; Bridge and Lunt 2006). In this study we use bedding diagrams, paleocurrents and measured sections to reevaluate the fluvial style of the Torrivio Sandstone in New Mexico, which has previously been interpreted as a braided channel deposit largely based on the coarse-grain size, sandy nature and lack of extensive muddy floodplain and abandoned channel deposits. We will also establish that the Torrivio Sandstone deposits are not exclusively braided in nature and represent a continuum of deposits from braided to meandering.

The late Cretaceous fluvial deposits of the North American Western Interior Seaway have been described in detail in the literature, from the Dunvegan Formation in Alberta, Canada to the Ferron Sandstone in Utah, USA (Plint et al. 2001; Plint and Wadsworth 2003; Kimmerle and Bhattacharya 2018). However, the same level of description is not available for the Torrivio Sandstone, although notable work has been done by Hohman (1986), Flores et al. (1991) and Woods (1992). Most of this work was concentrated in the outcrops in the Gallup Sag area, which is located west of the town of Gallup and what is conspicuously missing from these studies are bedding diagram-based quantitative assessment and paleo-hydraulics and discharge estimation. This study describes and analyses the fluvial deposits of the Torrivio Sandstone in extensively exposed strike-oriented outcrops, located east of the town of Gallup, and provides paleohydraulic and paleodischarge estimations. This would also be one of the very few studies to provide a statistical analysis of paleodischarge and source-to-sink mass balance of an ancient fluvial system through Monte-Carlo simulation (Sharma et al. 2017).

In the last couple of decades, use of ground-penetrating radar (GPR) has greatly aided in the 3D characterization of fluvial deposits (Best et al. 2003; Lunt and Bridge 2004; Sambrook Smith et al. 2006). More recently, drone images have been proven to be quite useful in making 3D models of outcrops, especially where accessibility to the outcrops is difficult (Hayes et al. 2023). High-resolution drone images have also been used in the current study to make 3D models of the outcrops. These models have been used for both qualitative and quantitative characterization of fluvial deposits, ranging from establishing the hierarchy of bounding surfaces to obtaining dimension of sandstone bodies and paleocurrent directions.

3.1.1 The Torrivio Sandstone, regional setting and previous work

The Torrivio and the Gallup Sandstone were deposited in a foreland basin along the western margin of the Cretaceous Interior Seaway of North America (Fig. 3.1). The foreland basin system formed due to the subduction of the oceanic Pacific plate beneath the continental North American plate (DeCelles and Giles 1996; DeCelles 2004). The basin extended for about 3000 km from the Gulf of Mexico in the south to the Arctic in the north (Weimer 1984; Miall et al. 2008). The Gallup Sandstone is one of several major deltaic complexes deposited towards the south-western end of the Western Interior Seaway during the Cretaceous Period (Molenaar 1973, 1974, 1983; Nummedal and Swift 1987; Nummedal 1990; Nummedal and Riley 1991; Nummedal and Molenaar 1995).

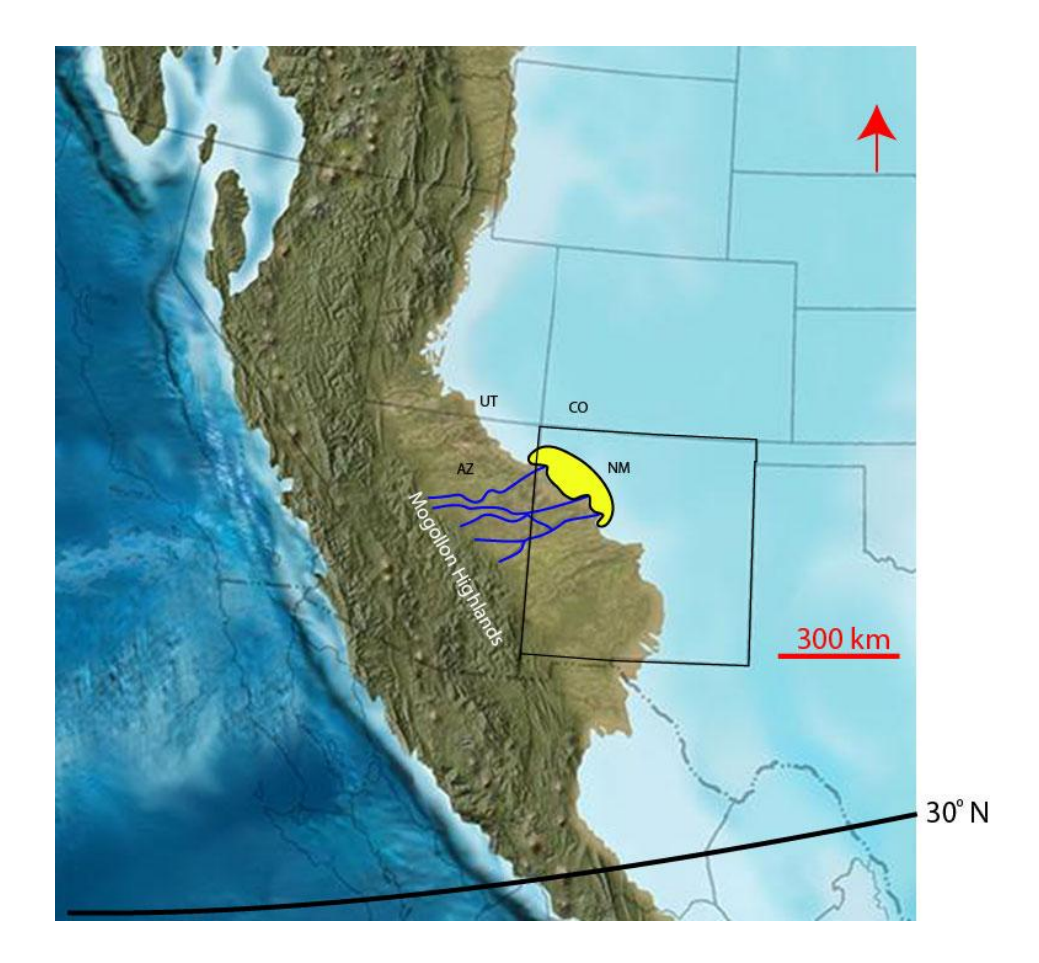


Figure 3.1. Late Coniacian (87 Ma) paleogeography of the Western Interior Seaway showing the schematic of the Torrivio Rivers (blue lines) with their catchment located within the Mogollon Highlands. (Reconstruction and paleolatitude after Roberts and Kirschbaum 1995; Blakey 2014; and Ferron 2019).

Sequence stratigraphic studies of the shallow marine Gallup Sandstone and the associated fluvial deposits, along with the overlying Torrivio Sandstone deposits, have identified 12 high-frequency sequences within the Gallup depositional system (Lin et al. 2019) and concluded that the Torrivio Sandstone is younger than the Gallup Sandstone throughout the San Juan basin (Fig. 3.2).

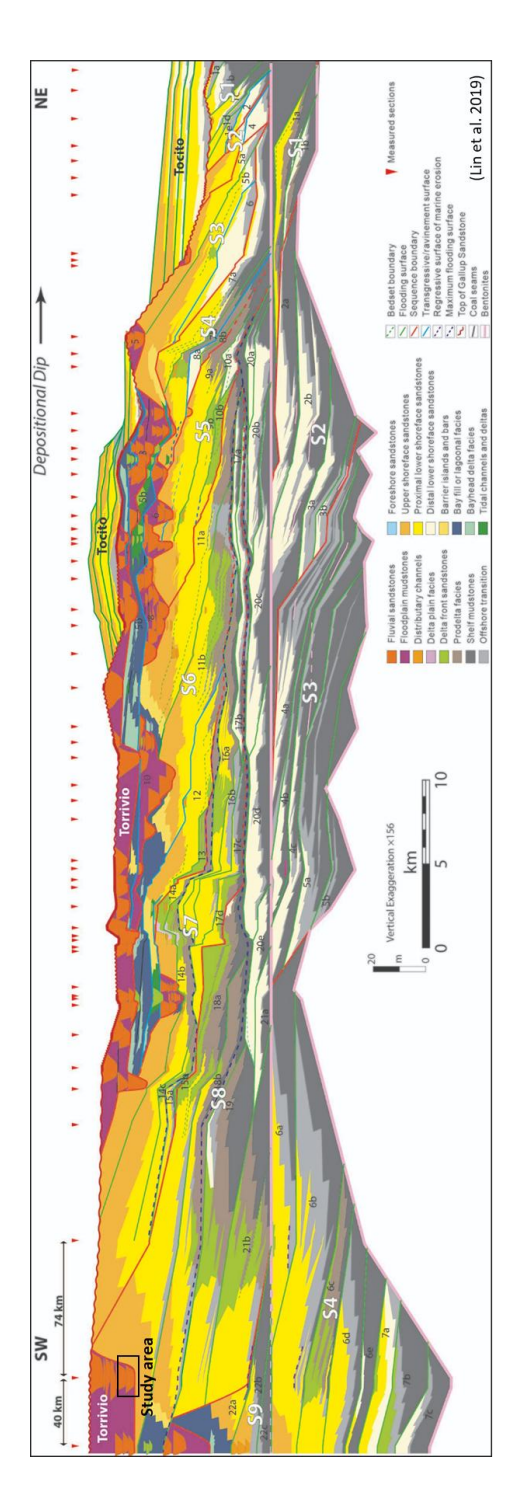


Figure 3.2. High resolution sequence stratigraphic reconstruction of the Gallup Sandstone and the younger Torrivio Sandstone. The area covered in the current study is shown by the black rectangle (Lin et al. 2019).

The Torrivio Sandstone has long been described as a Member of the Crevasse Canyon Formation and is thought to have fed the marine Gallup Sandstone (Molenaar 1973, 1977), although differing hypotheses have also been proposed (Nummedal and Swift 1987, Riley 1993). A U-Pb detrital Zircon-based geochronology of the Gallup Sandstone (Ferron 2019; Lin et al. 2021) confirms that the Torrivio system does not feed the Gallup Sandstone, which in-turn is fed by a fluvial system composed of multiple feeder valleys.

On the basis of coarse-grained conglomeratic nature of the Torrivio deposits, and the lack of floodplain mudstones, the Torrivio Sandstone has been interpreted as deposits of a braided fluvial system (Molenaar 1973, 1977; Hohman 1986, Flores et al. 1991), with a mean northeast paleoflow direction (Hohman 1986). This study reevaluates the fluvial style of the Torrivio using detailed bedding diagrams of cliff exposures, integrated with measured sections and paleocurrent data.

3.2 Study area and methodology

The outcrops of the Torrivio Sandstone cover an extensive area in North-West New Mexico and eastern Arizona, USA (Molenaar 1977; Nummedal and Molenaar 1995) (Fig. 3.3A). The current campaign focused on outcrops around the town of Gallup in New Mexico, covering a length of approximately 70 km, with total of 40 measured sections and multiple high-resolution photo-mosaics. The outcrop belt around the Nose Rock Point provides an excellent opportunity to study these deposits in detail, especially facies architectural analysis along the strike-oriented exposures (Fig. 3.3A).

The outcrops used in this study extend approximately 7 km east from the Nose Rock Point. Twelve measured sections from these strike-oriented outcrops were used here. In addition, two dip-oblique sections were also used for facies architecture analysis (Fig. 3.3B). High-resolution 2D photo-mosaics were developed using images captured with a digital single-lens reflex (DSLR) camera mounted over a Gigapan Epic Robot. This instrument facilitates taking zoomed-in, high resolution images, with sufficient overlap (approx. 1/3rd in this study) between them to cover the whole outcrop in detail. These images were then imported

into the Gigapan Stitch software to merge to generate sections ready to be interpreted, with minimal geometric distortion.

UAVs or drones have proven to be useful in geological studies, especially in areas where outcrop accessibility is an issue (Harrald et al. 2021). The 3D models built using drone-captured images have resolution high enough to estimate vertical and lateral dimensions of sedimentary structures at different scales and may also be used to derive paleocurrent information (Harrald et al. 2021). The UAV used in this study was a DJI-Phantom Pro equipped with a 20-megapixel CMOS sensor camera. The UAV flight paths were designed to provide complete coverage of outcrops. The UAV was set to take images every two seconds to maintain approx. 70% overlap between successive images. Six to nine Ground Control Points (GCPs) were placed on outcrops to ensure proper scaling and georeferencing of images. The number and placement of these GCPs were determined with the objective of covering the corner points and center of the outcrop to ensure maximum accuracy in the final model.

The images were imported into the Pix4D Mapping, a drone mapping software, as jpeg files. Multiple tie points were used in the initial processing for enhanced 3D control within the model. These points include GCPs and automatic tie points that the software identifies based on key features of the outcrop. These points help in making the densified point clouds, containing 3D points for model building. All the information regarding their spatial position and RGB color is stored. The densified point cloud is needed for measurements, like distance and volume. Major factors which determine the resolution of these models and eventually their utility in visualization include:

1) The Ground Sampling Distance (GSD), which measures the distance between the centers of two successive pixels and is inversely proportional to the spatial resolution. In simpler terms, bigger GSD values will produce less visible details. The GSD values for 3D-models used in this study are high enough to allow for visualization of sedimentary structures and estimation of paleocurrent directions. For example, in one of the models (DS-2, described later), the GSD is 0.74 cm or 0.29 inches.

- 2) Image calibration, which can be define as the percentage of calibrated images out of the total images taken. In the same example, 630 out of a total of 635 images (99%) could be calibrated.
- 3) Key points per image or the number of characteristic points detected in an image. Generally, 10,000 key points per image is considered good. In our example, there are more than 15,000 key points per image.

All of these properties reflect the good quality of 3D models used in the current study.

Two-dimensional orthomosaics or orthogonal sections were extracted and used for making bedding diagrams. For smaller outcrops, extracting a single orthomosaic was sufficient to develop a 2D section for interpretation. However, for large outcrops with curved surfaces, multiple perpendicular orthogonal sections were extracted, keeping enough overlap between them. These were then stitched together in Adobe Photoshop to generate sections, which were used to draft bedding diagrams in Adobe Illustrator.

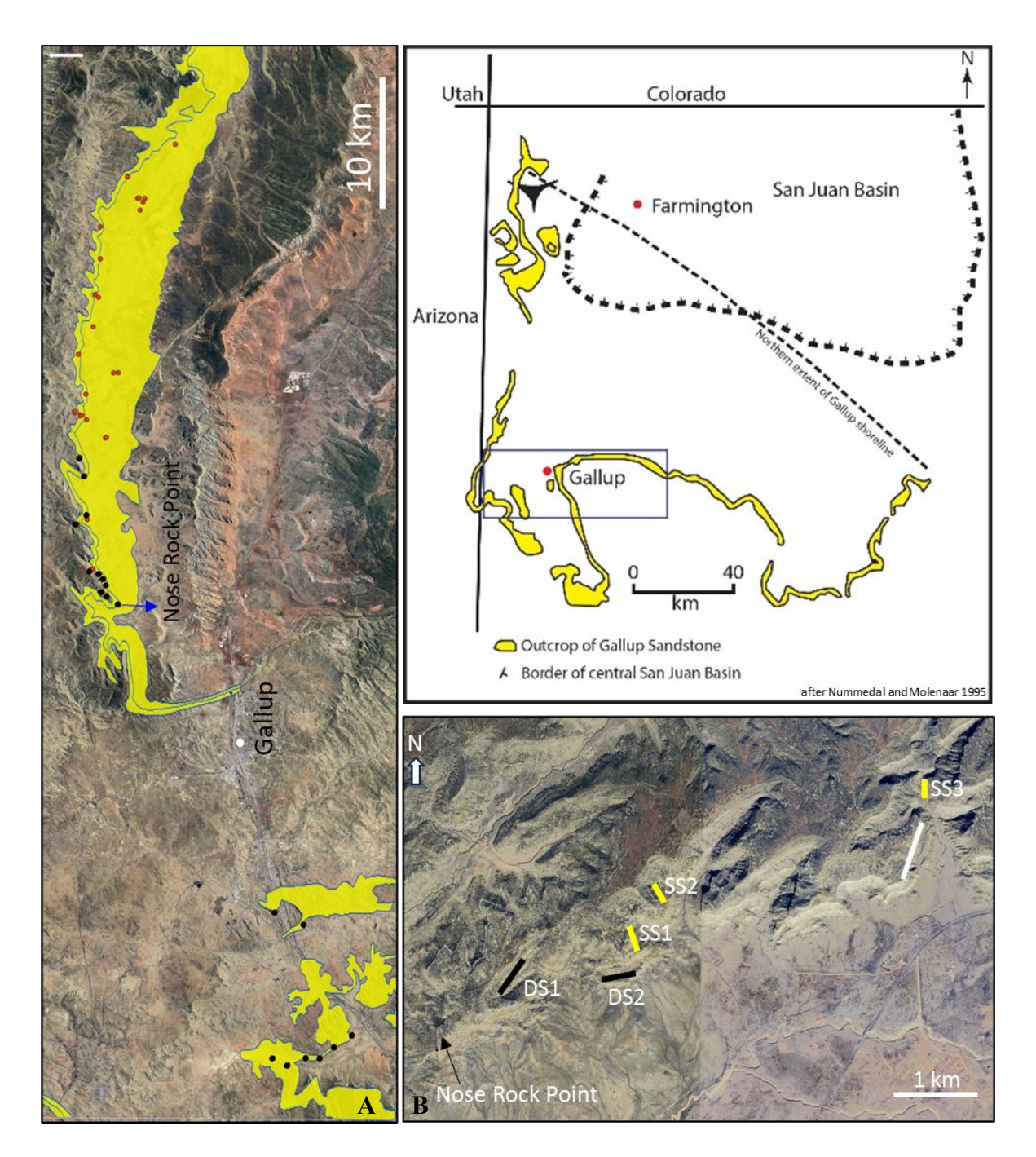


Figure 3.3. A) Outcrop map of Torrivio and Gallup Sandstone around the town of Gallup, New Mexico, USA. The measured sections done throughout the current campaign are represented by red circles while those used here are shown by black circles. B) Location map of strike (Yellow) and dip (Black) sections used in the current study. The section shown in white is used for channel-width estimation in Fig. 3.27.

Facies architectural analysis of outcrops involved mapping of bounding surfaces to delineate constituent bars and channels. These surfaces were named using the nomenclature and bounding surface hierarchy of Miall (1985). The highest seventh order surface is represented by erosional bases of individual valleys, mapped on photo-mosaics and extended from measured section through extensive field correlations. These surfaces are characterized by the presence of ripped-up mudstone clasts and extra-formational conglomerate. Sixth order surfaces mark erosional bases of channel belts, which separate mudstone and/or siltstones from rippled cross-bedded sandstones above. Fifth order surfaces mark the erosive bases of major channels. The erosional bases of minor channels and macroforms form fourth order surfaces, while bar accretion and bar-bounding surfaces mark the third order surfaces. Co-set bounding surfaces are second order surfaces while lamina-set bounding surfaces are first-order surfaces (Miall 1985). The litho-facies were identified taking into consideration the lithology and sedimentary structures. The hierarchy of bounding surfaces, along with depositional geometry and lithofacies association lead to the identification of different architectural elements that can be used to establish a depositional model for the system (Allen 1983; Miall 1985, 1988, 1996; Sprague et al. 2005).

Paleocurrent data were obtained using dune-scale cross beds and rib and furrow structures. In addition to this, paleocurrent data were also obtained from dune-scale cross sets visible in the high-resolution drone images. This involved identifying clear cross sets and measuring the X and Y coordinates and height at three points on a single cross stratum and then using them for dip-azimuth estimations using a three-point vector method (Fig. 3.4) implemented in the MS-Excel (Hasbargen 2012). The three-point calculations closely matched readings taken in the field and the differences between the two estimates, even with an error range of 10-20%, did not significantly affect the final geological model.

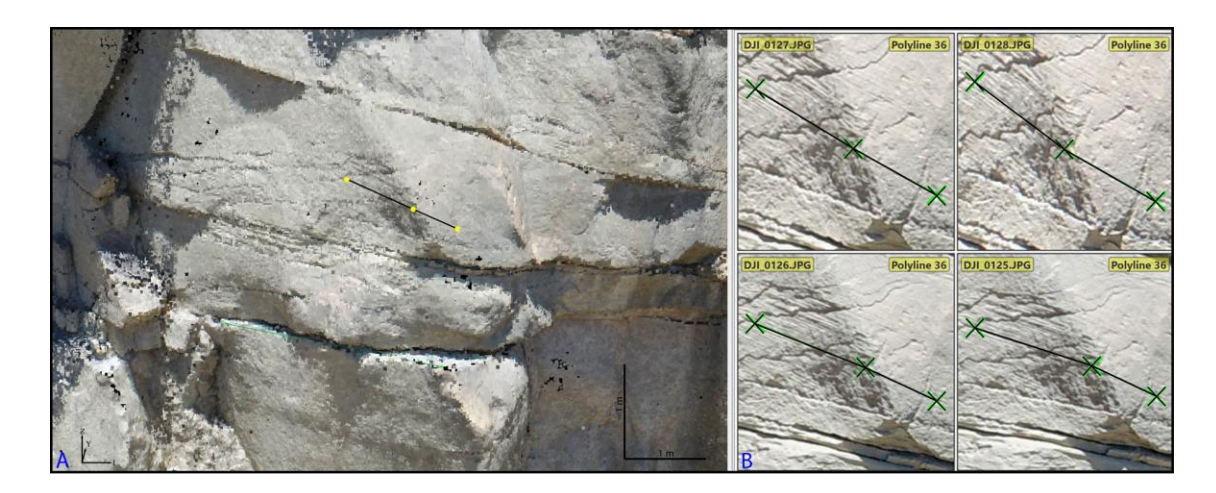


Figure 3.4. Close-up of 3D model built using high-resolution drone images. A) Three points are selected on a suitable cross-lamina and a surface is drawn through it to estimate the azimuth using three-point solution (Hasbergen 2012). B) The same structure is shown in the actual drone image. Please refer to the text for model details.

The grain size was measured directly in the outcrops, with the help of standard grain-size card. Care was taken to measure every distinct unit to highlight vertical grain-size trends, if any. These grain size measurements were included in drafting the measured sections. The individual measurements were then averaged using a vertical moving window of 50 cm, but care was observed to not cross depositional boundaries and include dissimilar facies. These average values were then used to generate the cumulative grain size curve.

The grain size for the lower zone of the Torrivio Sandstone, as estimated from measured sections, ranges from fine-to-coarse grained, with a median (D₅₀) value of 0.38 mm, which corresponds to medium-upper sandstone (Fig. 3.5A). The D₅₀ grain size value for the upper zone of the Torrivio Sandstone is 0.21 mm, corresponding to fine-upper sandstone (Fig. 3.5B). Granules and pebbles could also be found occurring at the channel base in both the zones and were also found flanking the laminae of the cross-bed sets in the lower zone. Similar observations have also been reported in previous studies (Hohman 1986; Flores et al. 1991; Nummedal and Molenaar 1995).

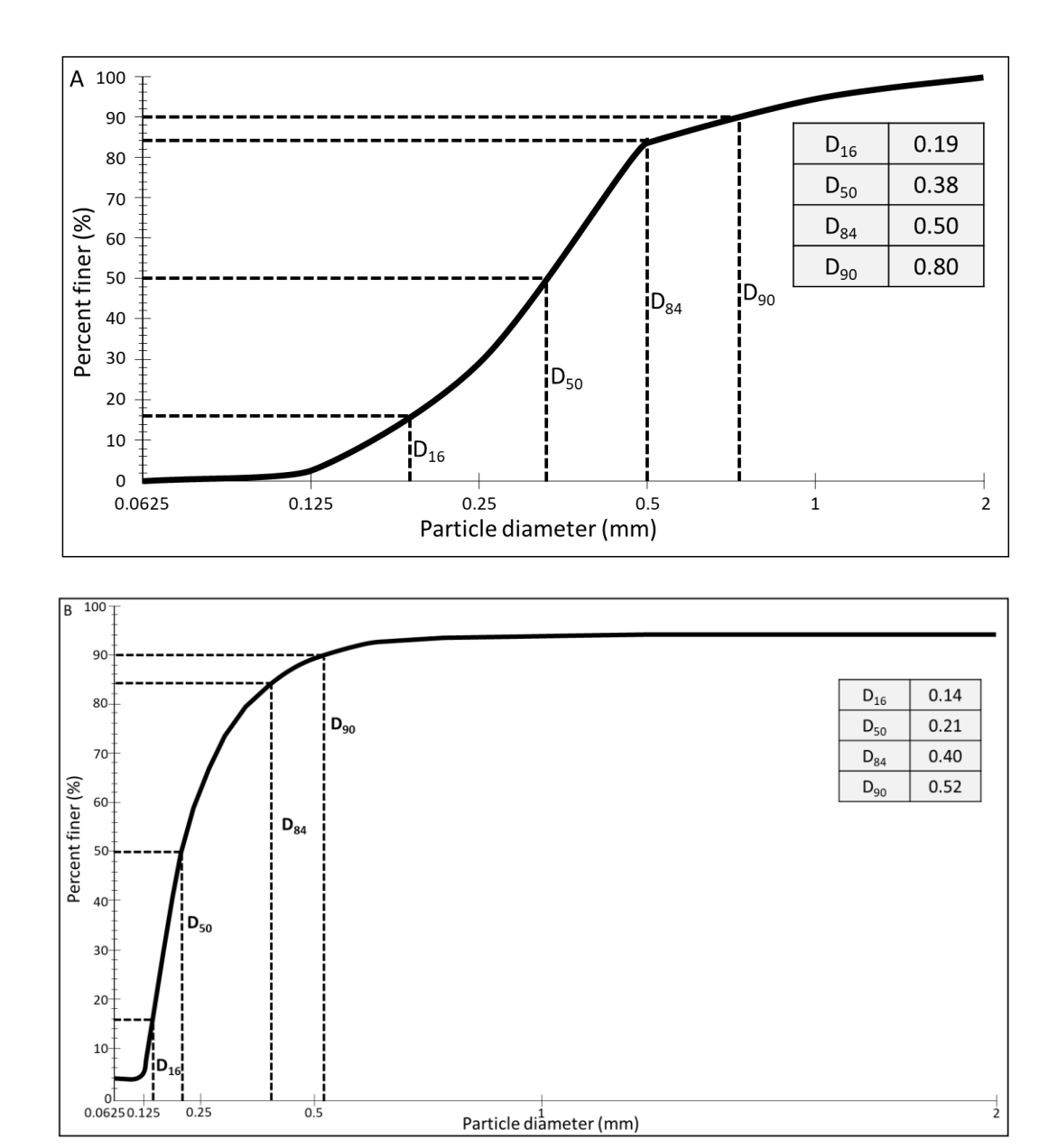


Figure 3.5. Cumulative curve for grain size distribution in the A) Lower (main) zone and B) Upper zone of the Torrivio Sandstone.

In order to estimate the annual water and sediment discharge, the bankfull discharge duration and its recurrence interval need to ascertained (Searcy 1959; Holbrook and Wanas 2014). Since these parameters are not available for the ancient systems, information from suitable climate-binned modern analogs can be used (Holbrook and Wanas 2014; Bhattacharya et al. 2016; Lin and Bhattacharya 2016; Sharma et al. 2017) The bankfull discharge duration (i.e. the number of days a flow overtops the channel to extend into the

floodplain), can be estimated by plotting the flow duration curve (FDC) (Searcy 1959; Vogel et al. 1994). An FDC is essentially a cumulative frequency curve showing the amount of time a discharge of a given magnitude is either equaled or exceeded over a given period of time (Searcy 1959). The type of discharge or streamflow data used in this plot could be daily, weekly or monthly for a particular river basin (Searcy 1959; Vogel et al. 1994). The streamflow data is arranged with respect to their increasing magnitude and then cumulated. The time (in percentage) for each class is then computed (Searcy 1959). The cross-plot between the cumulative discharge and percentage time is plotted with the former as the ordinate axis and the latter as the abscissa (Searcy 1959).

The size and scale of a river, its water discharge and total sediment load, scale with the catchment area (Schumm and Hadley 1961; Wilson 1972; Milliman 1980; Milliman and Meade 1983; Milliman and Syvitski 1992; Milliman 1997). The climate of the basin and its relief play important roles in the sediment yield of the river, which is defined as the sediment load per unit area (Milliman and Syvitski 1992; Milliman 1997). The relationship between water discharge and drainage area was given by Syvitski and Milliman (2007),

$$Q = kA^m (3.1)$$

where, Q is the water discharge in m³/s, A is the drainage area in km², k is a constant equal to 0.075 and m is an exponent of 0.8. The k and m values depend on the runoff values for different climate zones (Eide et al. 2018). The equation can thus be simplified into:

$$Q = RoA \tag{3.2}$$

where, Q is the water discharge in km³/year, A is the drainage area in $10^6 \times \text{km}^2$ and runoff (Ro) is in mm/km/year (Nyberg et al. 2021).

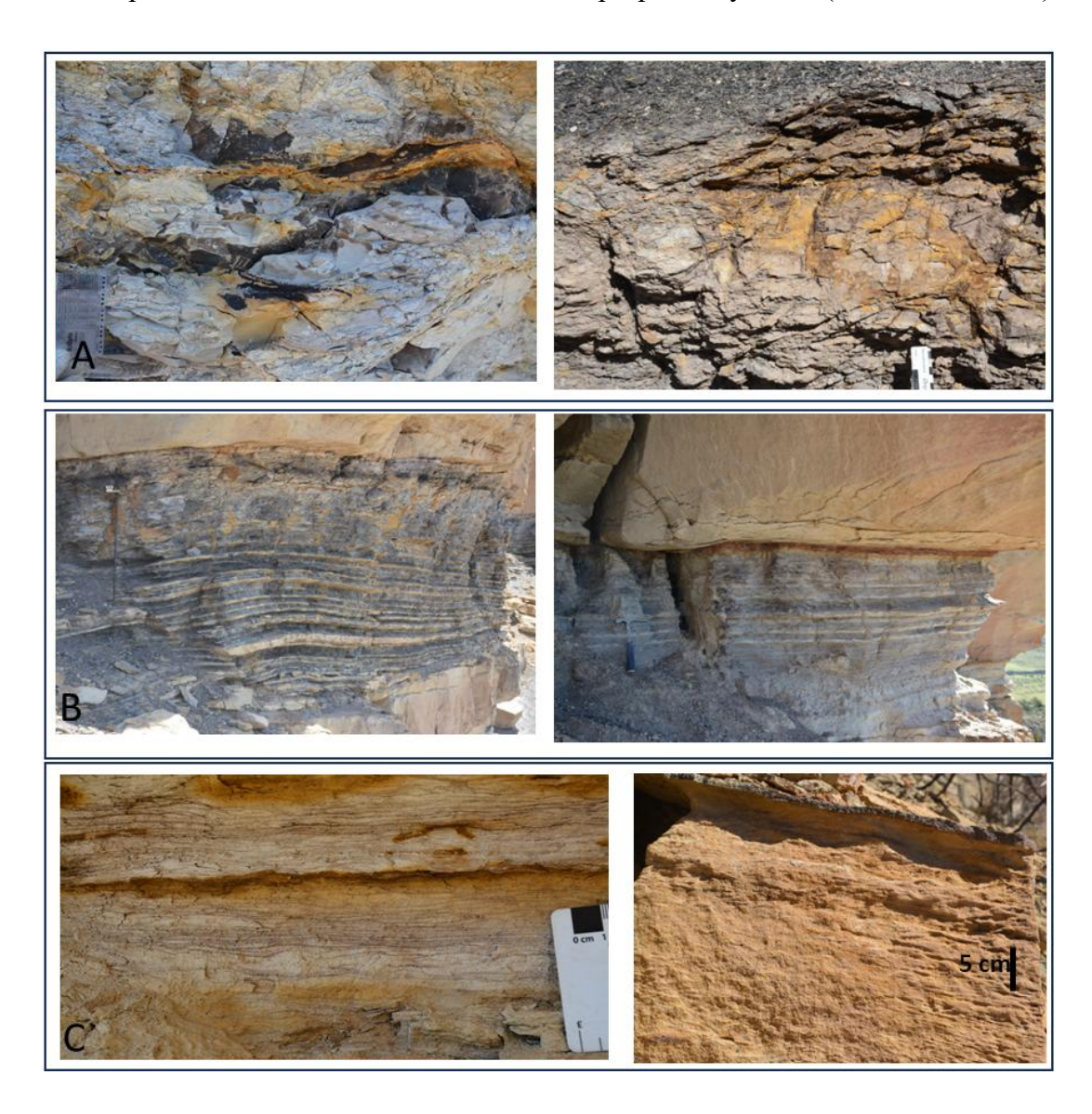
Two independent methods were used to estimate the drainage area of the Torrivio River. The first method used paleogeographic reconstruction, aided with detrital Zircon (DZ) petrographic analysis, proposed by Ferron (2019) and Lin et al. (2021). The second method used regional geomorphic relationships from climate-binned modern fluvial systems (Davidson and North 2009).

3.3 Results

The observations made on the outcrops are defined below.

3.3.1 Litho-facies classification

Seven major litho-facies associations were identified (Fig. 3.6) based on their characteristic lithology, sedimentary structure and bedding geometry and are listed in Table 3.1. Most of the description follows the classification scheme proposed by Miall (1977, 1978, 1996).



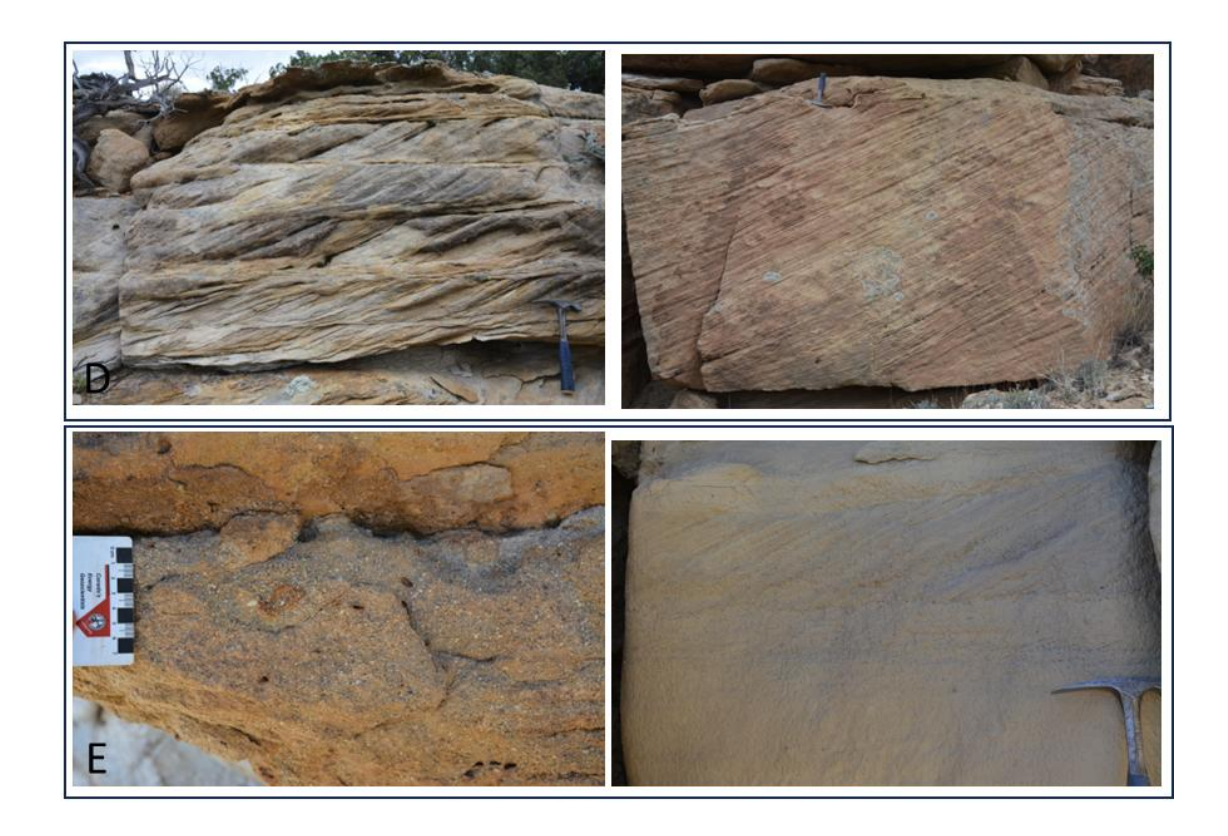


Figure 3.6. Major litho-facies associations found in the Torrivio Sandstone. A) Fr: massive mudstone with rootlets; B) Fl: mudstone dominated heterolithic deposit in overbank; C) Ripples and ripple cross-laminations (Sr) towards channel abandonment; D) St with smaller Sp units towards the top (left) and Sp as confluence fill (right); E) GI: granules and pebbles lining the channel base (left) and Gt: granules lining cross-laminae (right). The hammer is 30 cm long.

Table 3.1. Major lithofacies classes for the Torrivio Sandstone in the study area.

Facies code	Description	Interpretation
Fr	Massive mudstone with rootlets.	Incipient soil.
Fl	Mudstone-dominated facies with very-fine grained rippled and/or ripple-cross laminated, and occasionally parallel laminated sandstone, interbedded with mudstone. The top of this facies is often incised by 6th- and/or 5th-order	Overbank, abandoned channel and/or floodplain deposits.

	surfaces. These can be a few centimeters to more than a meter thick and laterally persistent for a few meters.	
Sr	Very fine-grained sandstone with ripples and ripple cross-laminations. These occur towards the top of channel fill or within the floodplain deposits.	Represents deposition in the lower flow regime, reflecting channel abandonment fill or in overbank splays where they form tabular units.
St	Medium-to-coarse grained sandstone with trough-cross stratification. The set thickness varies from 5 to 40 cm with co-set thicknesses sometime exceeding a meter. Grains generally fine upward. These are often associated with overlying planar cross-bedded (Sp) units.	The smaller cross-beds represent deposition in the lower flow regime associated with migration of sinuous crested 3D dunes, whereas the thicker units represent deposition at low angle bar fronts (Smith 1970).
Sp	Fine-to-coarse grained sandstone with planar cross stratification and fining upward trends. These are often tabular in geometry with thickness varying from 5 cm to more than 3 m.	Represents deposition associated with migration of straight crested 2D dunes and bars. Thicker units are interpreted as confluence scour fills.
Gl	Deposits represented by granules and pebbles occurring at the base of a channel.	Because this facies occurs just above scour bases, mostly 5th- order, this may represent channel lag deposits.
Gt	Deposits represented by granules flanking the laminae of cross-bed sets, fining upward trend observed.	Products of high energy bedload transport within channels.

3.3.2 Architectural elements

The architectural elements fall within three main groups, which are defined as 1) larger channel element, 2) smaller within-channel elements and 3) overbank elements (Miall 1996; Miall and Jones 2003). These elements are shown schematically in Fig. 3.7 and in outcrop sections.

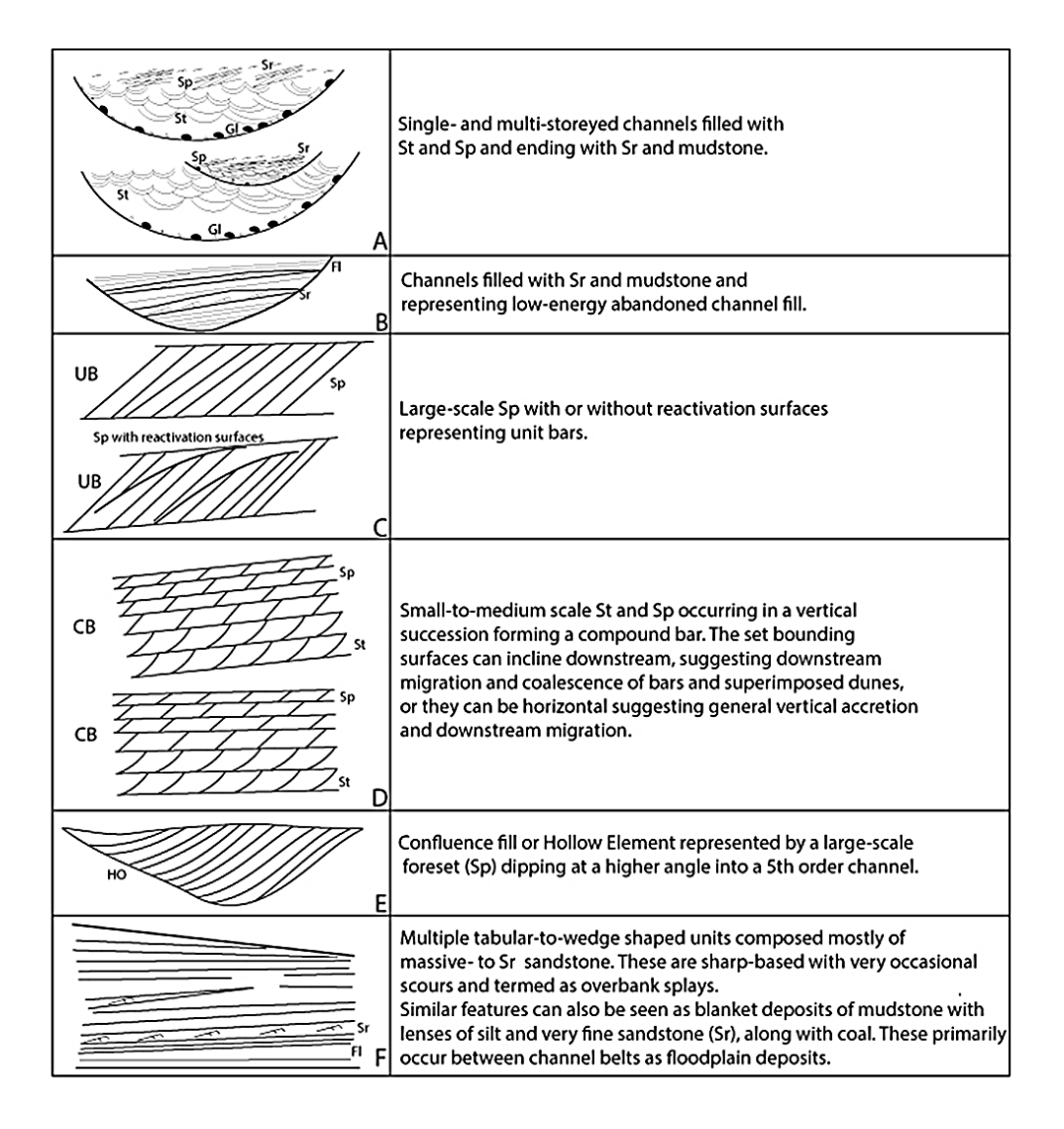


Figure 3.7. Major architecture elements and the associated litho-facies associations found in the Torrivio Sandstone. Fl: overbank and/or abandoned channel deposit, Sr: ripples or ripple-cross laminated sandstone, Sp: planar-cross stratified sandstone, St: trough cross stratified sandstone, Gl: granules and pebbles at channel base, UB: unit bar, CB: compound bar, HO: confluence fill or hollow element.

These groups can be further divided into multiple individual elements as described below.

1. Channel Element

i. Channels filled with sandstone: These predominantly lenticular deposits are represented by flat-to-erosive, concave up, 5th order bounding surfaces and, in a few cases, 4th order surfaces (Miall 1996). These can be a single story or consist of multiple stories with grain size and cross-set thickness decreasing upward in individual stories. Completely preserved channel stories can be seen in the strike cross-section 2 (SS-2) (Fig. 3.8). From the erosive base up, there are massive sandstones with some intraformational conglomerates. Trough cross-stratified (St) lower bar sandstones and planar cross-stratified (Sp) upper bar sandstones follow. The laminae of the cross sets are sometimes lined with granular sand. The thickness of individual cross sets decreases upward, and the overall grain size also fines up. These cross-stratified units are overlain by fine-grained ripple-and/or ripple cross laminated sandstones, progressing into siltstone and mudstone dominated overbank facies (Fl). The progressive thinning of cross-bedded units and fining of grain size suggest gradual decrease in the strength of the in-filling flows (Bridge 2003). The channel bases are often lined with granules and pebbles (Gl). The channels can be single- or multi-storied.

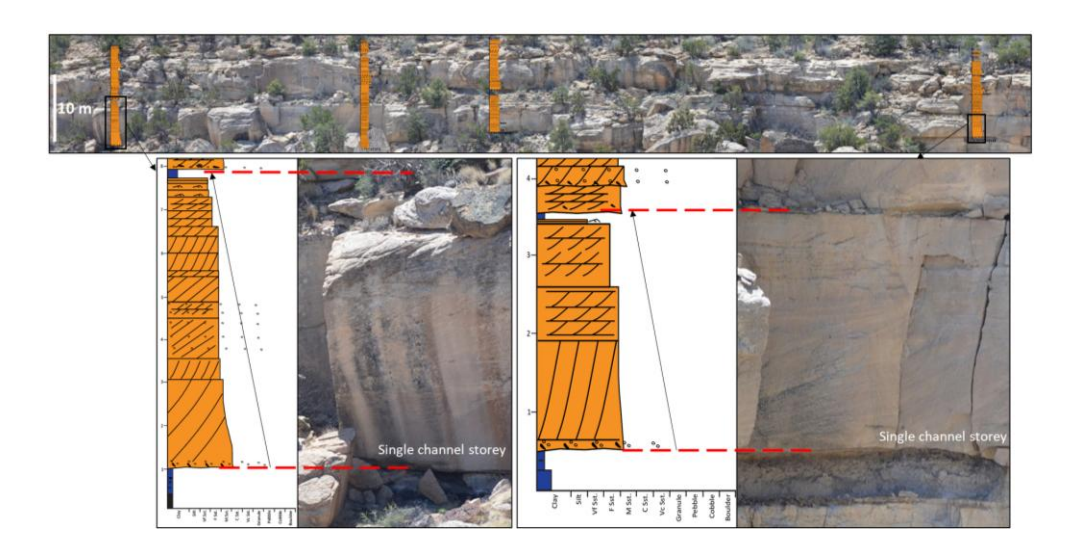


Figure 3.8. Examples of completely preserved channel stories in SS-2. These have been used as proxy for bankfull channel depth estimation.

ii. Channels filled with sandstone and mudstone: These are represented by sandstone, typically ripple-laminated (Sr) with occasional cross-bedding, and muddy overbank deposits (Miall 1996; Hjellbakk 1997). These are mostly lenticular shaped and bounded by 5th order scour bases. A good example of this is seen in SS-1 (Fig. 3.9), where older side bar deposits appear to be truncated by a channel. The overall percentage of sandstone decreases upwards with mudstone or silty-mudstone lithology dominating the fill. As this facies association is mostly dominated by mudstone with occasional sandstone lenses, these are interpreted as low energy abandoned channel deposits (Miall 1996; Hjellbakk 1997).

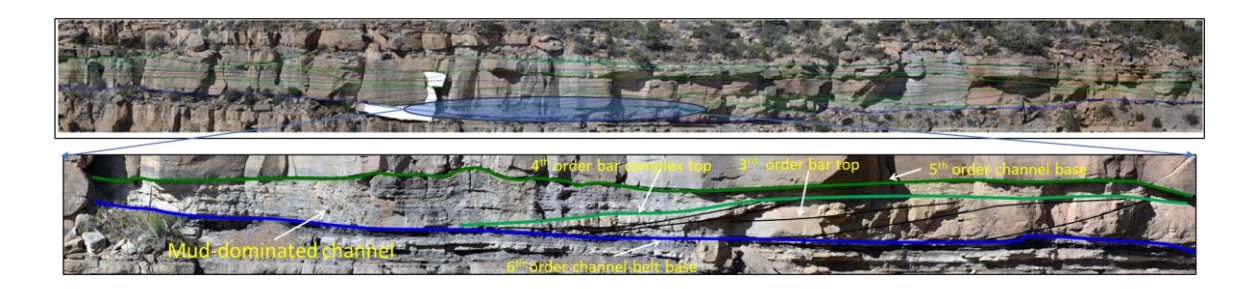


Figure 3.9. Channel-fill dominated by mudstone with lenses of ripple-laminated sandstone in SS-1. The overall percentage of sandstone decreases upwards.

iii. *Chute or cross-bar channel*: Occasionally, as shown in SS-3 (Fig. 3.10), a small channel bounded by a 4th order scour base can be seen cutting into the uppermost parts of the bars. In this example, this channel is less than a meter deep. This is referred to as a cross-bar channel or chute channel (Bridge 2003). Units of trough cross-stratified sandstone occur at the base and smaller planar-cross bedded units occur towards the top. These cross-sets would scale with the flow depth in this particular channel and not with the mean channel depth. This channel is topped by a 5th order surface.

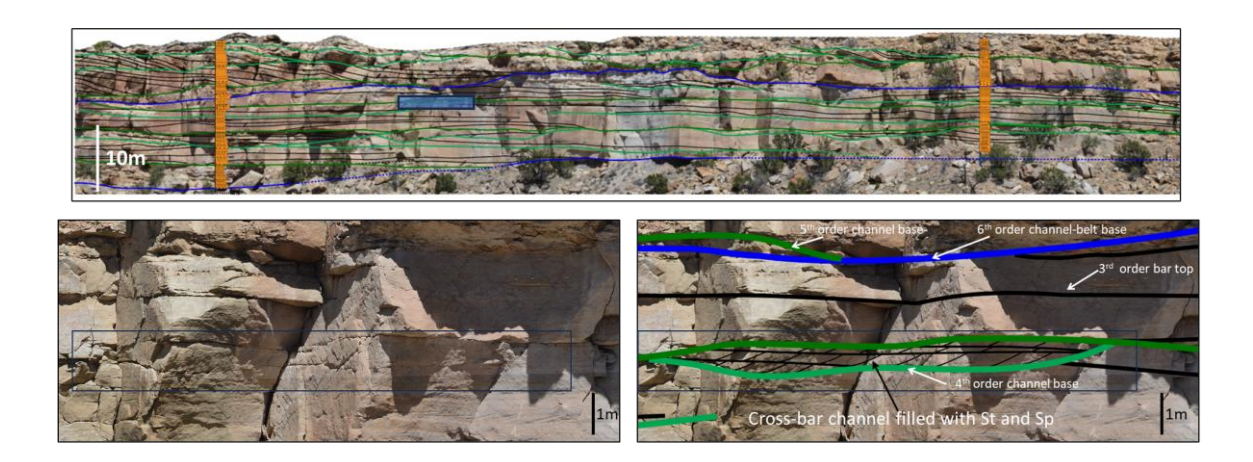


Figure 3.10. 4th order cross-bar channel truncating bars in SS-3. The channel is filled with trough cross-stratified units (St) at the base and planar cross-stratified units (Sp) at the top. The blue box highlights its position in the interpreted cross section.

2. Within Channel Element

i. Unit bars (UB): Bars with relatively simple depositional morphologies are defined as unit bars (Smith 1974, 1978). In the Torrivio outcrops, these are generally represented by tabular units with planar (Sp) and trough (St) cross-bedded sandstone. These units are bounded by 3rd order bar bounding surfaces (Miall 1996; Hjellbakk 1997) and range in thickness from \sim 0.6 m to 2 m and can be laterally continuous for a few tens of meters (Fig. 3.11).

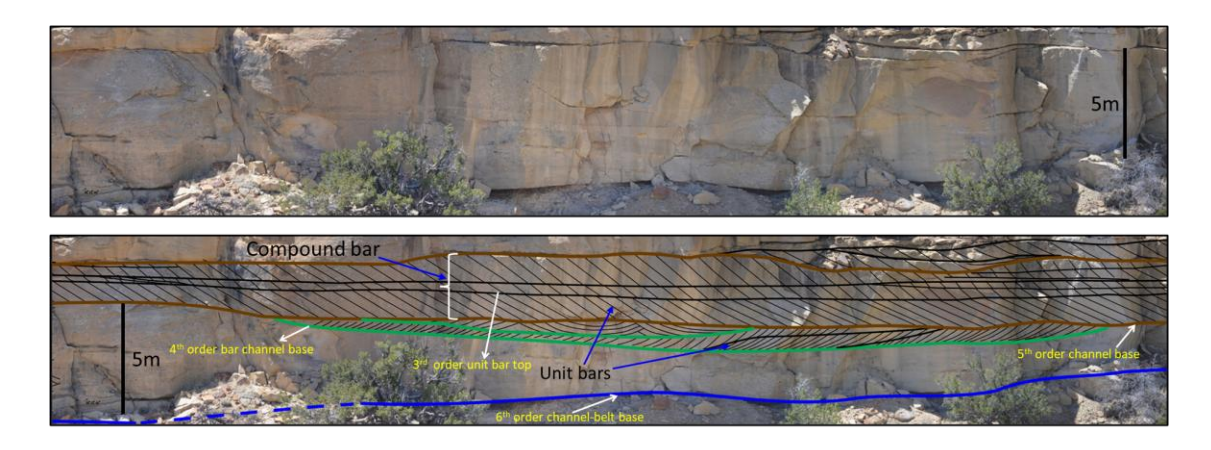


Figure 3.11. Un-interpreted and interpreted sections showing unit bars and compound bar filling in the 4th order and 5th order channels in SS-2. Although

planar cross-stratification (Sp) is the common facies, trough cross-stratification (St) is also present.

These bars generally point in the downstream direction but may also be at a relatively higher angle to the mean flow direction as explained in the forthcoming section. The planar cross-strata are often truncated by reactivation surfaces, which are sigmoidal in appearance (Fig. 3.12). These could represent the "planar-convex minor contact" of Allen (1983). These reactivation surfaces generally highlight local discordance in current strength and/or sediment supply (Allen 1983). The tabular units are interpreted to represent downstream migration of braid bars (Bridge 2003).



Figure 3.12. Un-interpreted and interpreted section of SS-3, showing Unit bar with Sp and sigmoidal reactivation surfaces truncating the laminae. The location of this figure is shown by Box-3 (blue) on Fig. 3.18.

ii. Compound Bars (CB): These tabular sandstone bodies are characterized by the presence of stacked sandstone units (unit bars) (Fig. 3.11, 3.13 and 3.14), which could be both planar (Sp) and trough (St) cross-stratified (Hjellbakk 1997; Lunt and Bridge 2004; Bridge and Lunt 2006; Ashworth et al. 2011). The thickness of the whole unit ranges from slightly less than a meter to more than 3 meters. Individual medium-scale cross sets range from 10 cm to 50 cm in thickness and the thickness generally decreases upwards. The large-scale cross-sets could be more than one meter thick and are sometimes overlain by dune-

scale cross sets. The set bounding surfaces are commonly inclined downstream, suggesting downstream migration and coalescence of bars and superimposed dunes, or they can be horizontal, suggesting general vertical accretion and downstream migration (Hjellbakk 1997).

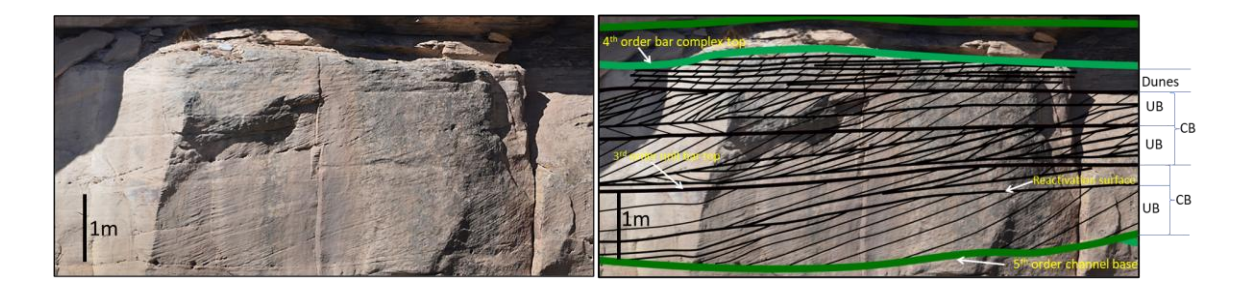


Figure 3.13. Un-interpreted and interpreted section of SS-1, showing the hierarchy of bars. UB-Unit bar; CB-Compound bar. Also shown are the small-scale cross-sets representing dunes riding over the bar complex.

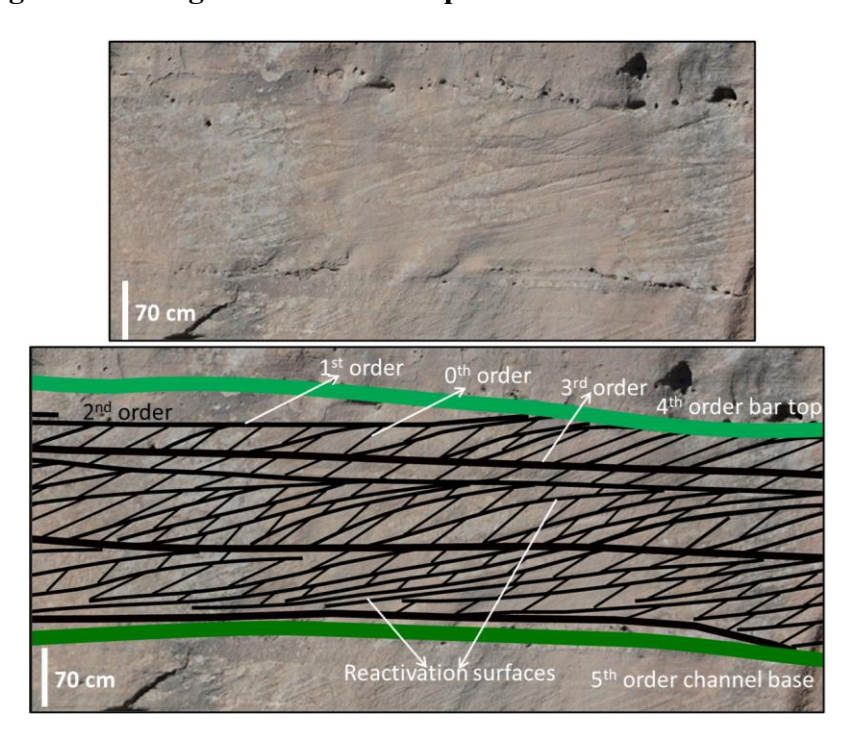


Figure 3.14. Compound bar with Sp and convex-to-sigmoidal reactivation surfaces truncating the laminae. The location of this figure is shown by Box-1 (Blue) in SS-1 in Fig. 3.16.

- iii. Hollow Element or Confluence deposit (HO): These units are represented by deposits of different scales filling the scour, ranging from simple bar scale to channel confluence scale, consisting of a single out-sized foreset unit or a compound bar representing single story deposit respectively (Fig. 3.15, 3.16 and 3.17) These deposits scale with the confluence scour and not with the average channel scour (Miall and Jones 2003; Ullah et al. 2015).
- iv. *Lateral Accretion (LA)*: These comprise tabular to wedge shaped geometrical units (Fig. 3.17 and 3.18) where the 3rd order bar bounding surfaces dip at a higher angle to the flow direction represented by cross bed sets and the whole unit is bounded by a 5th order base. The bars may or may not have silt/mudstone drapes.

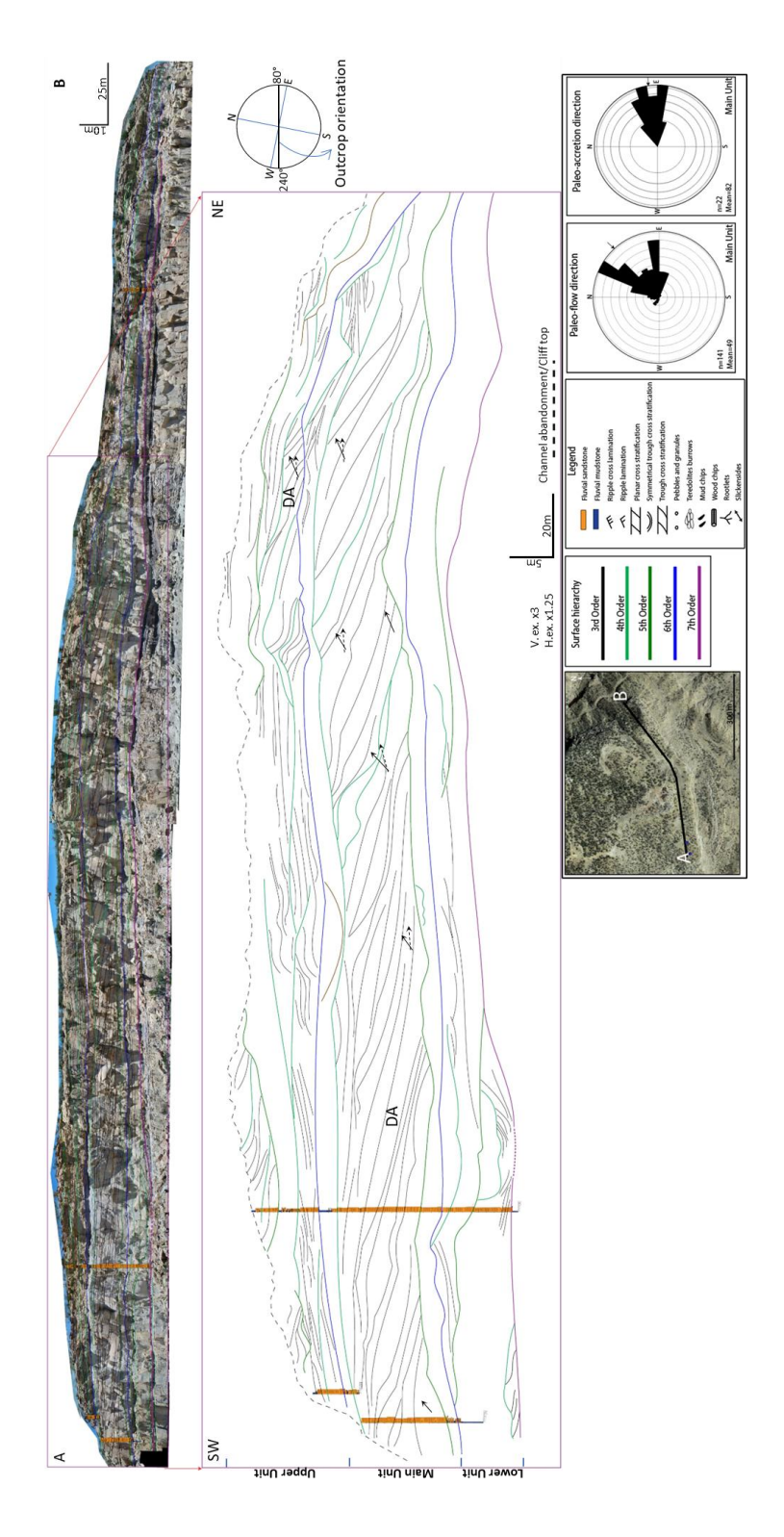


Figure 3.15. DS-2 showing three units within the Torrivio Sandstone separated from the Gallup non-marine unit by a sequence boundary of 7th order. A large

downstream migrating bar represents the main Torrivio unit while the upper Torrivio unit shows evidence of downstream migration of fluvial point bars. The section is oriented relative to the outcrop with the solid arrows highlighting paleoflow direction and dashed arrows showing the paleo-accretion direction. This section is described in detail in Chapter 4.

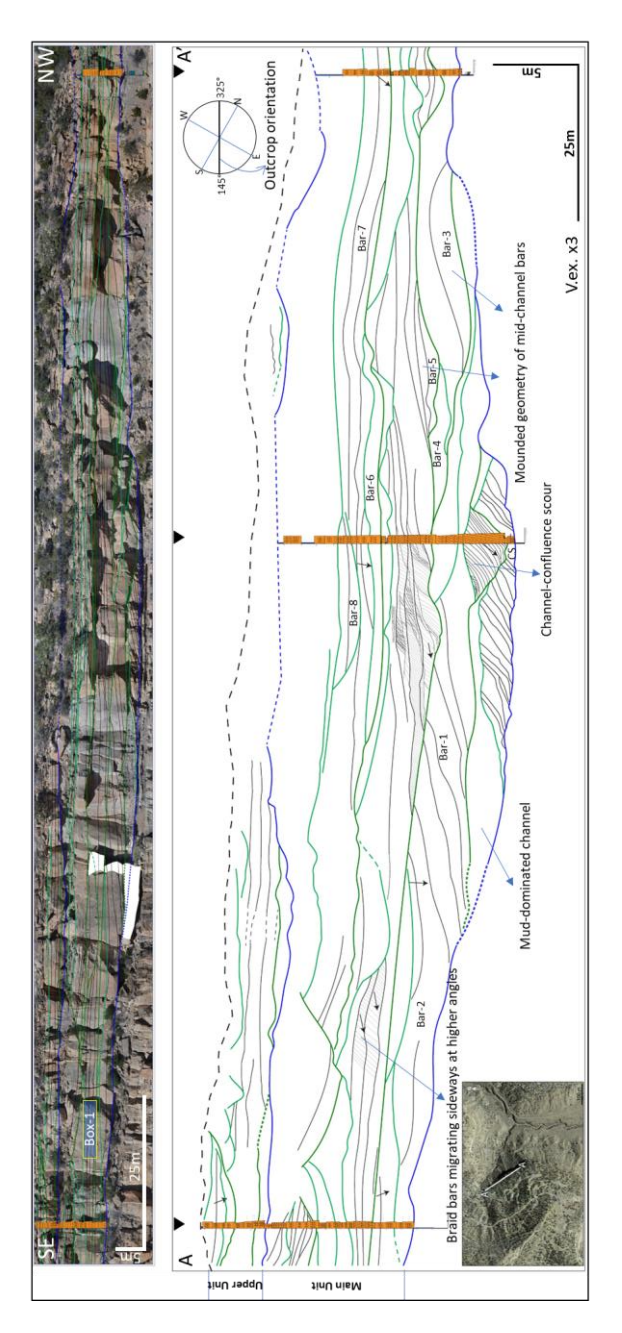


Figure 3.16. SS-1 showing the lower braided unit and the upper sinuous singlechannel unit. Mounded geometries emphasize the braided nature of the river system

in the lower main unit, as does a 2.25 m thick foreset deposited in a channel-confluence scour (CS). Higher up in the braided section, bars migrating at higher angles relative to the mean paleo-flow direction can be seen. Internal architecture of the mud-dominated channel fill is shown in Fig. 3.9. The section is oriented relative to the outcrop with downward arrows coming out of the paper while others point in oblique direction to the left of the paper. See Fig. 3.15 for legends and symbols.

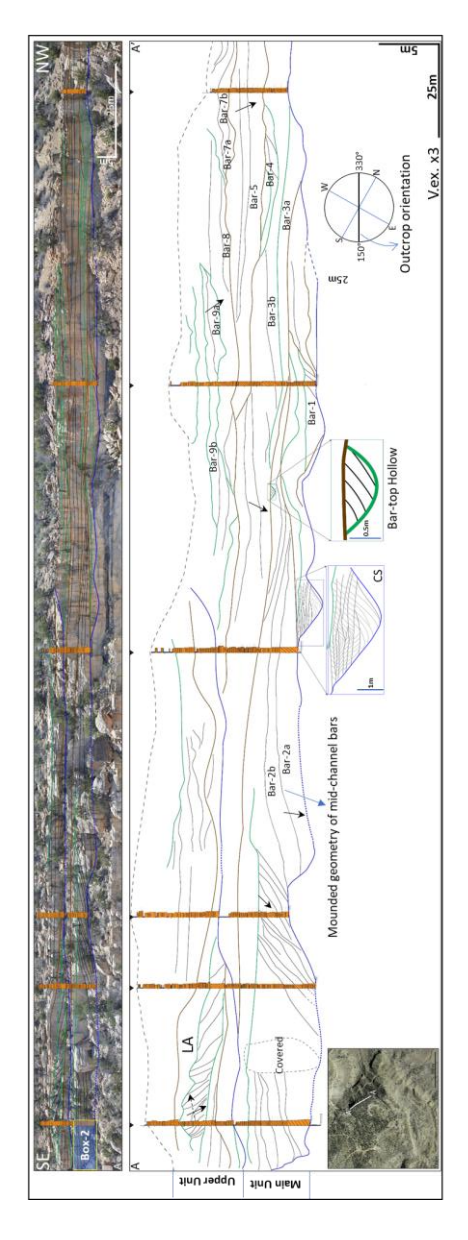


Figure 3.17. SS-2 showing braid bars with mounded geometries. Bar-scale confluence scour (CS) with 7 cross-set units. Also, present is the bar-top hollow element with a

single set of cross-set. Bars migrating laterally into the channel can be seen in the upper zone of the Torrivio Sandstone (LA). Dashed arrows represent paleo-accretion direction. Refer to Fig. 3.15 for legends and symbols. Box-2 is described in detail in Fig. 3.20A and B.

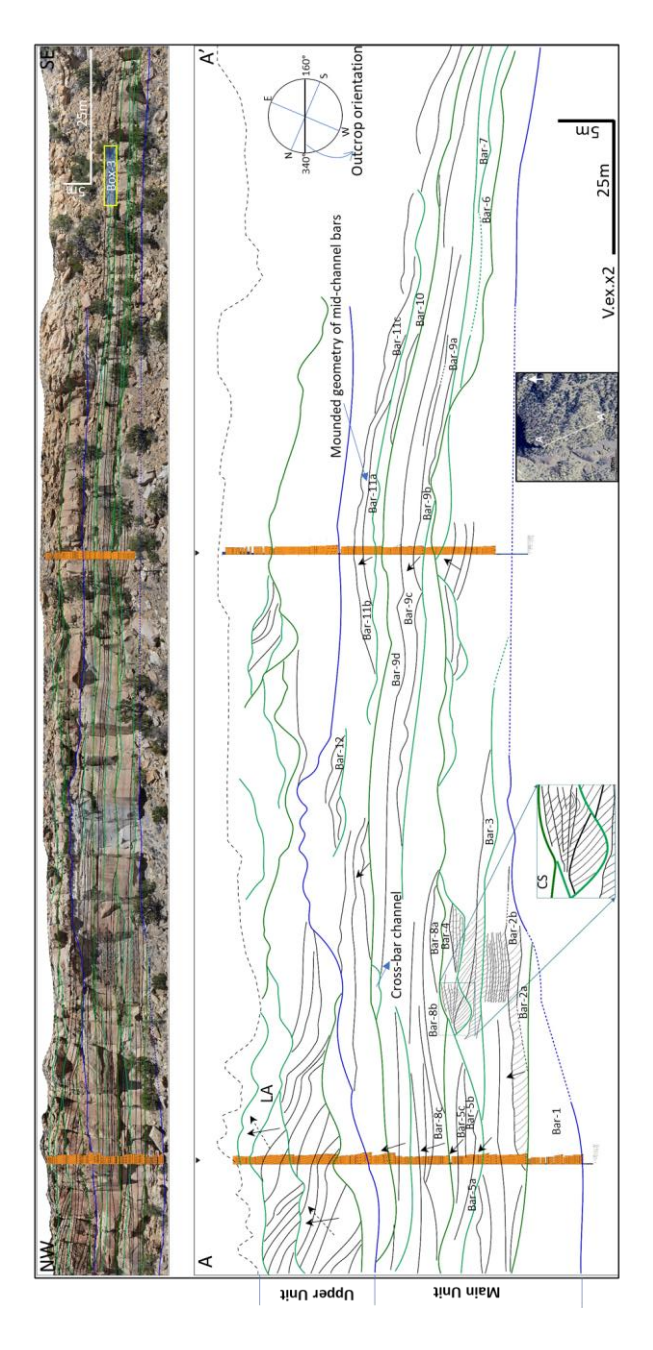


Figure 3.18. SS-3 showing bar-scale confluence (CS) fill with 6 units of cross-stratification. Mounded geometry of the braid bars in the lower unit and point bars

in the upper unit is evident. The internal geometry of the cross-bar channel is shown on Fig. 3.10. Reactivation surfaces within unit bars can be seen in Box-3, the details of which are shown in Fig. 3.12. See Fig. 3.15 for legends and symbols.

3. Overbank Element

- i. *Splay*: These comprise multiple tabular units composed mostly of massive to ripple-cross laminated (Sr) very-fine grained sandstone (Fig. 3.19). These units are sharp-based with rare scours, sandwiched between floodplain mudstone, which could be organic-rich, coaly (Burns et al. 2019). Individual sandstone bodies are 30 cm to 50 cm thick, occasionally reaching up to 90 cm thick. Their extent in the flow-parallel and flow-perpendicular directions is approximately 30 m to 40 m and 10 m to 20 m respectively. These are interpreted to be deposits of overbank splays, which over-top the levees and flow out onto the floodplain mudstone (Fischer et al. 2008; Burns et al. 2019).
- ii. *Floodplain deposit*: These are represented by blanket deposits of mudstone with lenses of silt and very fine sandstone (Sr), along with coal. These primarily occur between channel belt deposits.



Figure 3.19. Multiple tabular units of splay deposits lying below a 5th order channel. These units are sharp based and contain occasional local scour and generally taper out in the down-flow direction (yellow arrow).

3.3.3 Nature of fluvial system in the Torrivio Sandstone

In the study area, the Torrivio Sandstone is interpreted to be separated from the underlying Gallup Sandstone by a 7th order sequence boundary (Miall 1992) (Fig. 3.15). This unit of the Gallup Sandstone has traditionally been described as "non-marine" (Molenaar 1983; Nummedal and Molenaar 1995). However, the medium-grained and cross bedded Gallup Sandstone shows signatures like bi-directional cross beds of possible tidal origin and Ophiomorpha trace fossils (Fig. 3.20A). Miall (1992) also reported similar observations in the same area. This unit is separated from the overlying Torrivio Sandstone by a laterally extensive layer rich in the Teredolites ichnofacies, wood remnants and coal, suggesting a "woodground substrate" (Bromley et al. 1984) (Fig. 3.20B). This might suggest presence of a subaerial unconformity at the base of the Torrivio Sandstone (Miall 1992; Pemberton et al. 2004; Lin et al. 2019).



Figure 3.20. A) Bidirectional cross beds and vertical burrows in the Gallup non-marine unit. See text for details. B) Teredolites burrows associated with coal, suggesting a woodground substrate. The carbonaceous mudstone shows prominent rootlets.

The thickest Torrivio section (~35 m) is seen at DS-2, which can be divided into 3 distinct units, separated by two 6th order surfaces (Fig. 3.15). The lower unit is approx. 7 m thick,

while the main and the upper units are approx. 16 m and 12 m thick respectively. The lower unit pinches out to the east of the outcrop. The lower Torrivio unit is separated from the main unit by a 6th order channel-belt bounding surface (Miall 1996), which is rich in floodplain facies with mudstone, carbonaceous matter, wood chips and rootlets (Fig. 3.15).

A distinct hierarchy of bounding surfaces can be identified (Miall 1985). There are channel belt bounding 6th order surfaces followed by major and minor channel bounding surfaces of 5th- and 4th-order respectively (Miall 1985). Most of the 5th and 4th order scour surfaces are undulating and give rise to sheet sandstone like architecture made up of downstream, lateral and obliquely migrating bars (Miall 1985; Miall 1993) (Fig. 3.16 to 3.18). A small, symmetrical bowl-shaped concave-up feature can be seen truncating one of the midchannel bars in SS-2 (Fig. 3.17). It is about 0.5 m thick at its deepest point and filled with a single cross-set dipping at a steeper angle. Similar features, although at larger scale, have been described as "bar-top hollows" from the modern braided river systems of the Brahmaputra River (Bristow 1993b) and the South Saskatchewan River (Best et al. 2006). These channels occur only at the bar tops and should therefore be distinguished from the formative channels of a system, particularly while estimating paleo-channel dimensions (Best et al. 2006).

Unit bars or simple bars (Smith 1974, 1978; Allen 1983), represented by solitary large-scale cross stratification bounded by 3rd order surfaces, are abundant (Fig. 3.11). The cross stratification is often intersected by convex-up to sigmoidal reactivation surfaces (Collinson 1970; Jones 1977; Allen 1983). Reactivation surfaces can also be seen intersecting foresets in stacked cross-bedded units (compound bars) particularly in SS-1 (Fig. 3.12 to 3.14). Similar reactivation surfaces were originally interpreted as the erosive surfaces produced due to low stage changes in bars in the snow-fed Tana River, Norway (Collinson 1970), where the discharge can be infrequent and flashy. However, Allen (1973) and later McCabe and Jones (1977) established that these surfaces can form even at constant stage. In the current study, multiple convex-to-sigmoidal reactivation surfaces occur close together and cannot be ascribed to changing flow stages. Also, as described in the section below, the climatic conditions at the time of deposition of the Torrivio

Sandstone were largely humid, sub-tropical with frequent rainy days (Burgener et al. 2023), suggesting that the discharge was not flashy. Thus, it can be argued that the reactivation surfaces seen here were more likely formed by changing flow strength at constant flow stage (McCabe and Jones 1977).

Downstream accreting bars, where the bar bounding surfaces dip in the same direction as the foresets (Bristow 1993a; Miall 1993), are present in all the strike sections. A good example of this is shown by bar-2 in SS-2 (Fig. 3.17) where, a compound mid channel bar growth forms a low amplitude mounded geometry, represented by 3rd order bounding surfaces, which dip obliquely on to the 5th order channel base, thus forming bi-directional downlaps (Willis 1993 a and b; Adams and Bhattacharya 2015). The complete succession of bar growth, however, is not preserved as it is eroded by a younger channel. Similar mounded geometries can also be seen in SS-1 (Fig. 3.16) and in SS-3 (Fig. 3.18).

Besides the above, there are bars, both unit and compound, which show tabular geometry with planar cross-sets dipping at a high angle to the regional paleo flow (NE). In SS-1 (Fig. 3.16), such bars are present towards the southeastern edge of the outcrop and their foresets trend in a general SE direction (median of 120°). The foresets in these units are truncated by convex reactivation surfaces (Fig. 3.13 and 3.14). These bars occur higher up in the succession and may suggest channel switching within the braid belt that may in turn reflect the topography resulting from the long-term channel stacking (Bristow 1993a).

Most of the cross stratification (St and Sp) varies in thickness from smaller dune to larger bar scale, 5 cm to approx. 1 m. However, occasionally, trough cross stratifications can reach thickness values significantly more than 2 m. As seen in SS-2 (Fig. 3.21A), these "giant" (McCabe 1977) concave cross strata, dipping only slightly oblique to the down-current direction, merge with the erosive base at a very low angle. Normal grading is common and a few of the cross laminae are lined with coarser sandstones and show fining upward trends within the set. These are particularly common lower in the unit. Occurring towards the top of the unit, there are undulatory bedforms with small-scale cross stratification, lying within the large-scale cross sets (Fig. 3.21B). These can be interpreted as "intrasets" of Collinson (1968). These intrasets can be seen dipping in the up-current

direction. These large-scale cross strata can be interpreted to represent accretion on slip-faces of large bank-attached bars or alternate bars (McCabe 1977). The smaller up-current dipping sets could be "antidune backsets" and represent deposition in the upper flow regime (Fig. 3.21B) (Fielding 2006).

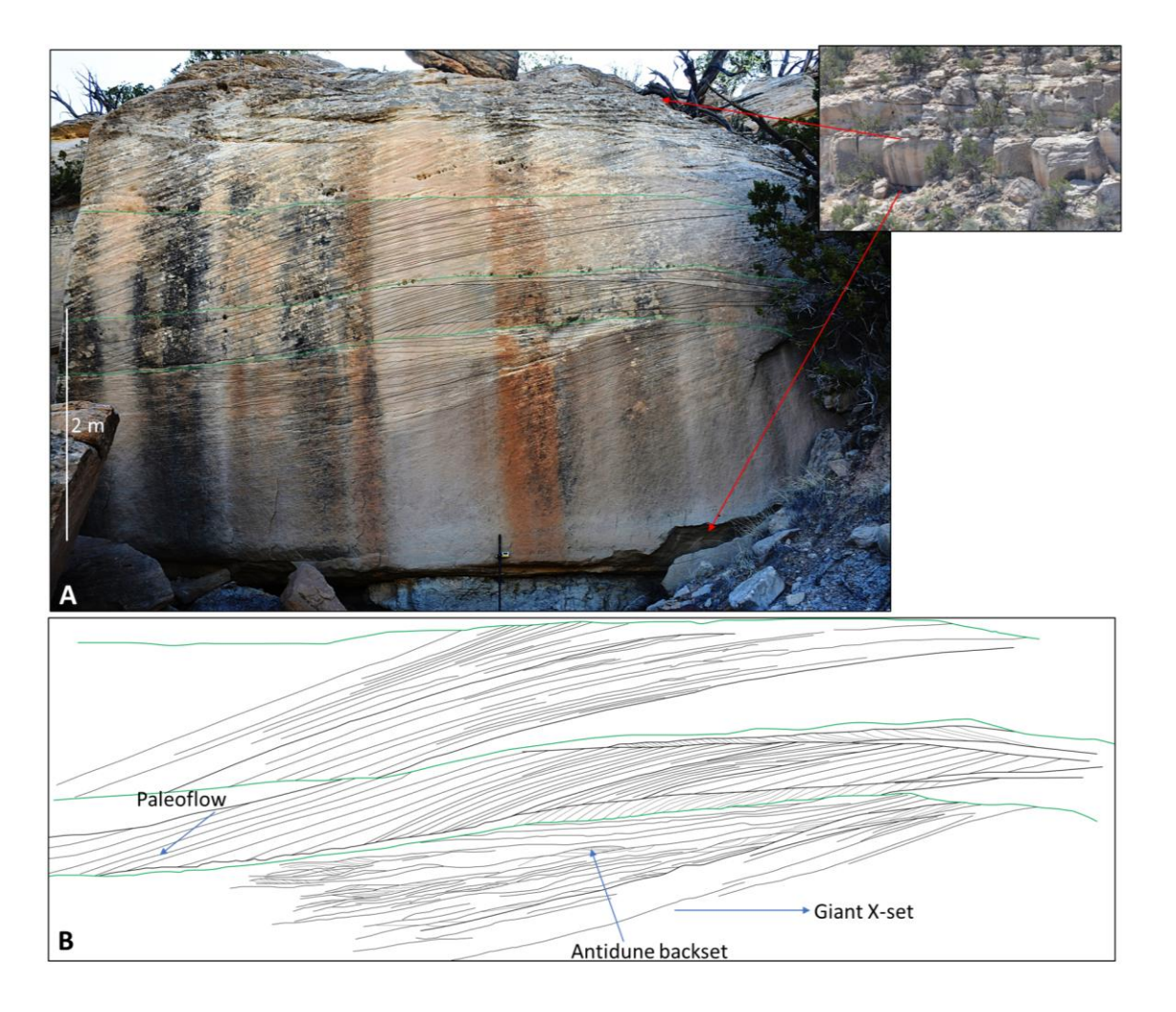


Figure 3.21. A) "Giant" cross-set in SS-2 associated with braid bars accreting on slip-faces of a large bank-attached bars or alternate bars. The location of the section is highlighted by blue box-2 in SS-2 in Fig. 3.17. B) Line diagram of the "giant" cross-set in SS-2 showing intrasets and backsets. See text for details.

The amalgamated nature of the sandstone bodies seen in all the above cross sections indicates that the Torrivio River wasn't largely an avulsive and/or distributive system (Blum and Tornqvist 2000; Blum 2013) and was possibly landward of the "backwater"

limit" (Paola and Mohrig 1996). The presence of a large tributary confluence scour further strengthens the conclusion as it shows that the system was still tributive in nature. The backwater length, the length over which base-level changes transmit signals upstream (Paola and Mohrig 1996), can be estimated by dividing the mean channel depth by the slope and this value for the Torrivio is approximately 20 km (Wu et al.2022; Yperen at al. 2024).

Different scales of confluence deposits are also documented within the main unit of the Torrivio Sandstone. These range from simple, small-scale confluences occurring downstream of mid-channel bars to large-scale tributary confluences. The smaller scale channel confluences are represented by a single set of oversized foresets dipping obliquely into the scour. The large foresets represent the avalanching face of a channel mouth bar moving into the scour hole, represented by an erosional 5th order surface (Best 1988; Bristow et al. 1993; Sambrook Smith et al. 2019). These steeply dipping avalanche faces are characteristic of smaller scale junctions, such as those occurring downstream of a chute or cross-bar channel and those that occur at discordant-bed confluences (Parsons et al. 2008; Leite Ribiero et al. 2012; Rhoads 2020). A good example of this is seen in the lower middle section of SS-1 (Fig. 3.16), where a 2.25 m thick cross-set fills an erosive scour base (5th order) at very high angle and is flanked by side bar deposits. The sandstone shows a fining-upward grain size trend, as seen in the measured section. Another example is seen in dip section-1 (DS-1), where an approximately 2 m thick foreset can be seen filling the interpreted confluence scour (Fig. 3.22A). A 3.9 m thick steeply inclined foreset is yet another example of a channel confluence fill (Fig. 3.22B).

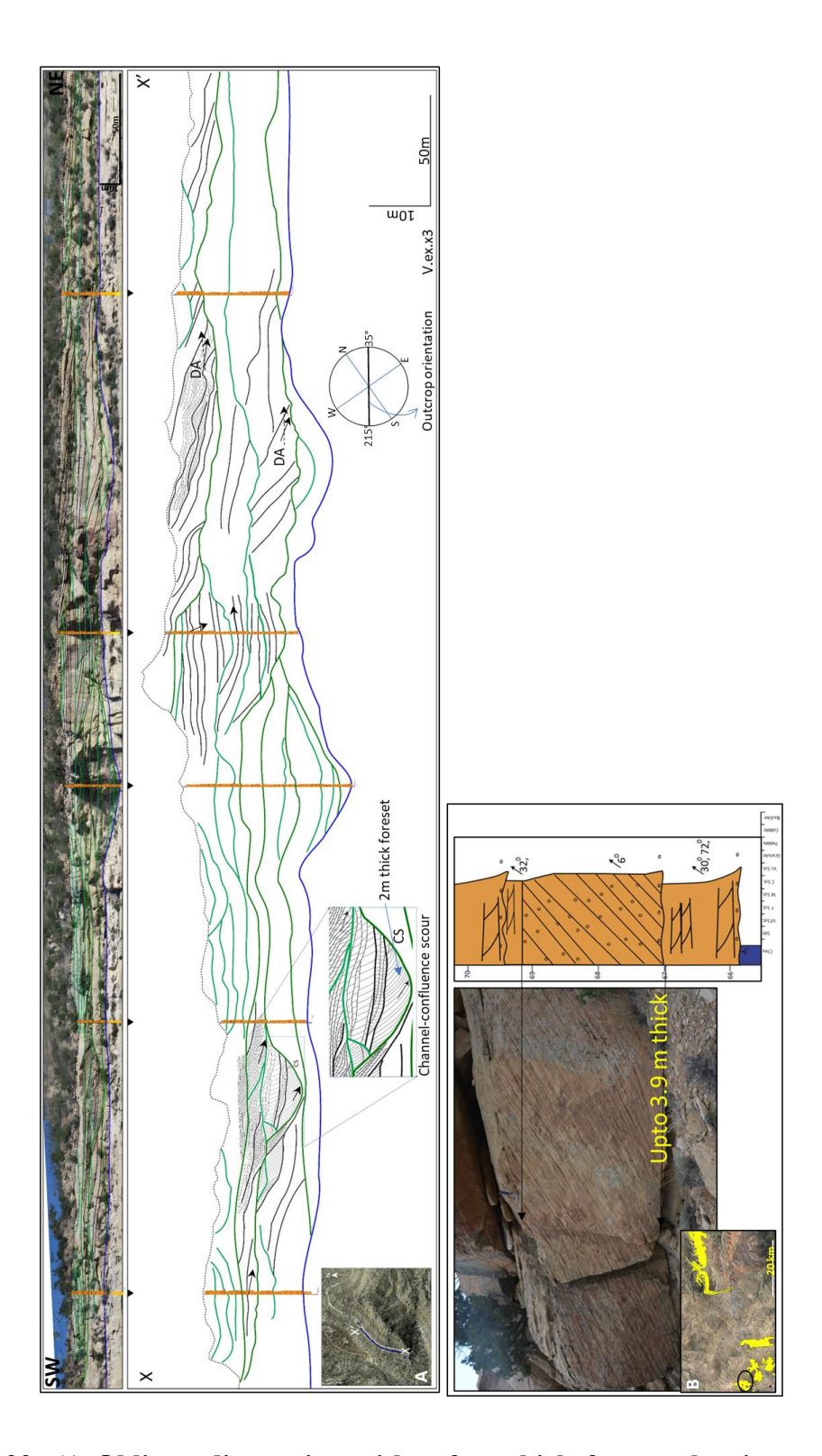


Figure 3.22. A) Oblique dip section with a 2 m thick foreset showing small-scale channel confluence. B) Steeply inclined bar, which reaches a thickness of up to 3.9 m,

possibly prograding into a channel confluence scour. Location of the measured section is encircled on the map in the inset.

We know that bars scale to channel flow depth, but the bars present in these confluence zones will reflect the depth of the confluence and not that of the average bankfull conditions (Bridge 2003; Smith et al. 2019). Hence, proper identification of these out-sized units is required for correct channel depth estimation.

At the other end of the spectrum of the scale of channel-confluence deposits is a single 12 m thick, downstream accreting bar observed in DS-2 (Fig. 3.15). Since the bankfull channel depth, as represented by completely preserved single channel fill, varies from 3 to 6 m in the Torrivio outcrop, such an anomalously thick single channel fill is considered very unlikely to represent deposition by an average channel and thus most likely represents a bar at a junction where a tributary channel meets the main channel or just further downstream of the junction point (Smith et al. 2019). This architectural element is discussed in greater detail in Chapter 4.

To summarize, the scour bases within the lower unit are mostly 5th order surfaces while 4th order surfaces represent only minor scours. These surfaces are relatively flat to gently undulating with multiple amalgamated stories of channel deposits, often incomplete, and overlain by bars giving rise to a broad sheet-like geometry (Miall 1993; Gibling 2006). The mid-channel bars show characteristic mounded geometry with bi-directional downlap (Adams and Bhattacharya 2015). The laterally accreting bars do not show silt/mudstone draping and the thickness of the cross sets do not show appreciable change. Therefore, the lower unit of the Torrivio Sandstone is interpreted as the deposit of a braided fluvial system. A block diagram (Fig. 3.23) shows all the major architectural elements found in the braided section of the Torrivio Sandstone.

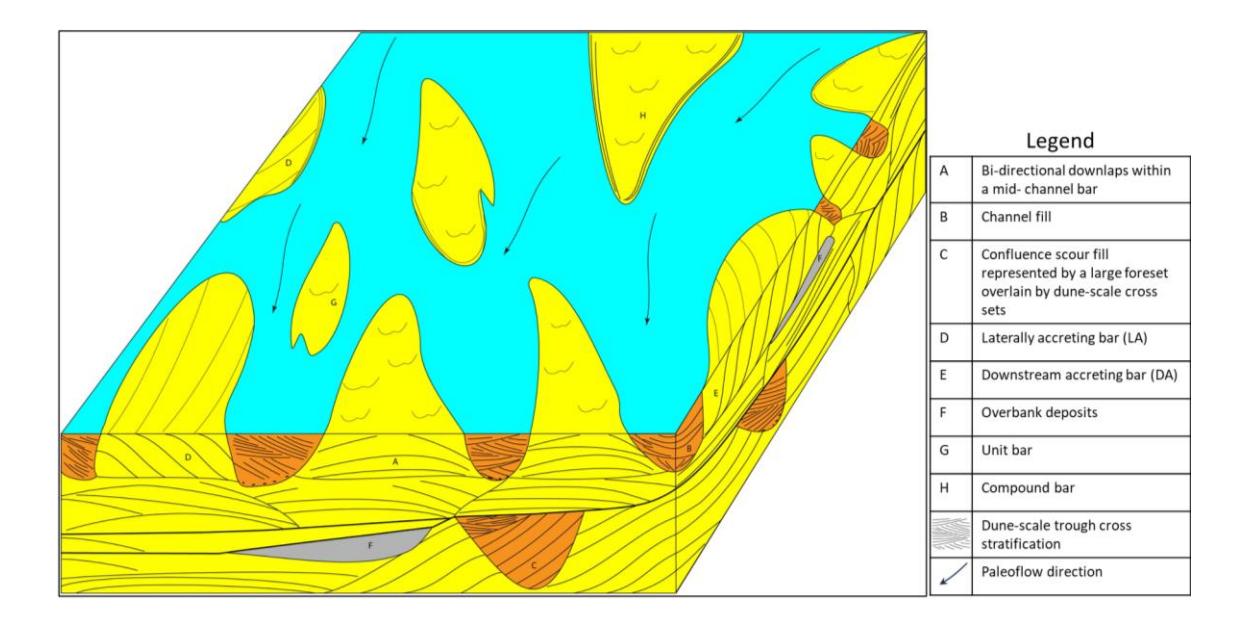


Figure 3.23. 3D block diagram showing the braided nature of the Torrivio Sandstone. The architectural elements drawn represent features seen in the outcrops, but no scale is intended.

Above the braided fluvial deposits of the lower unit and separated from it by a 6th order channel-belt surface and floodplain facies, lies the upper unit. This unit is relatively thinner, and its outcrop is not extensively exposed in the current study area. The median grain size of sandstone in this unit is 0.21 mm, which is finer than the lower unit, although coarser sediments can be seen lining the 5th order surfaces. Trough cross stratified sandstone is the dominant facies. Most of the channel fills show fining upward successions along with reduction in the thickness of the cross sets. In SS-2 and SS-3, 3rd order bar accretion surfaces can be seen migrating into channels with 5th order scour bases. In SS-2 (Fig. 3.24), the median direction of accretion is 315° (n = 5) while the flow direction remains NE (median-20°, n = 6). In SS-3 (Fig. 3.25), there are two subunits showing preferred migration of bar deposits. The lower subunit shows a median bar migration direction of 120° (n = 6) while the flow direction is again NE (median-55°, n = 3). The upper subunit, however, shows an oblique relationship between the accretion and flow direction, with a median accretion direction of 80°. The measurements in SS-3 are from the 3D-models built with drone images. The accretion surfaces in both outcrop sections are draped with finer silty

deposits. These observations suggest that these deposits were most probably from a laterally migrating single thread channel.

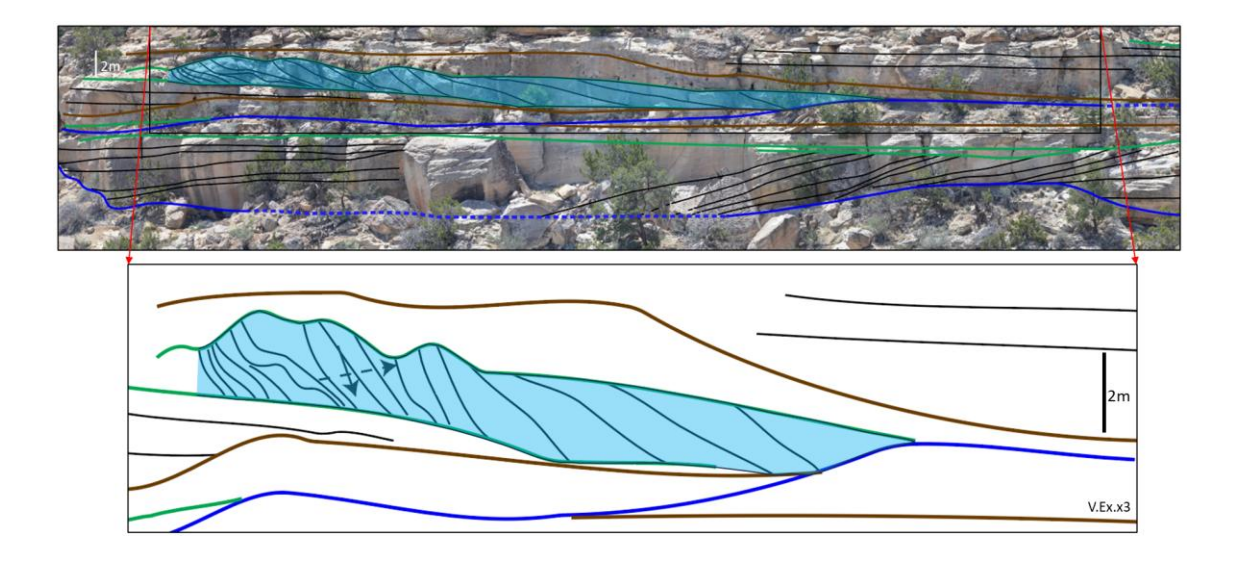


Figure 3.24. The upper Torrivio unit at SS-2 showing fluvial point bars (in blue) laterally migrating into 5th order channel. The solid arrow indicates paleoflow direction (median-20°) whereas the dashed arrow represents the paleoaccretion direction (315°).

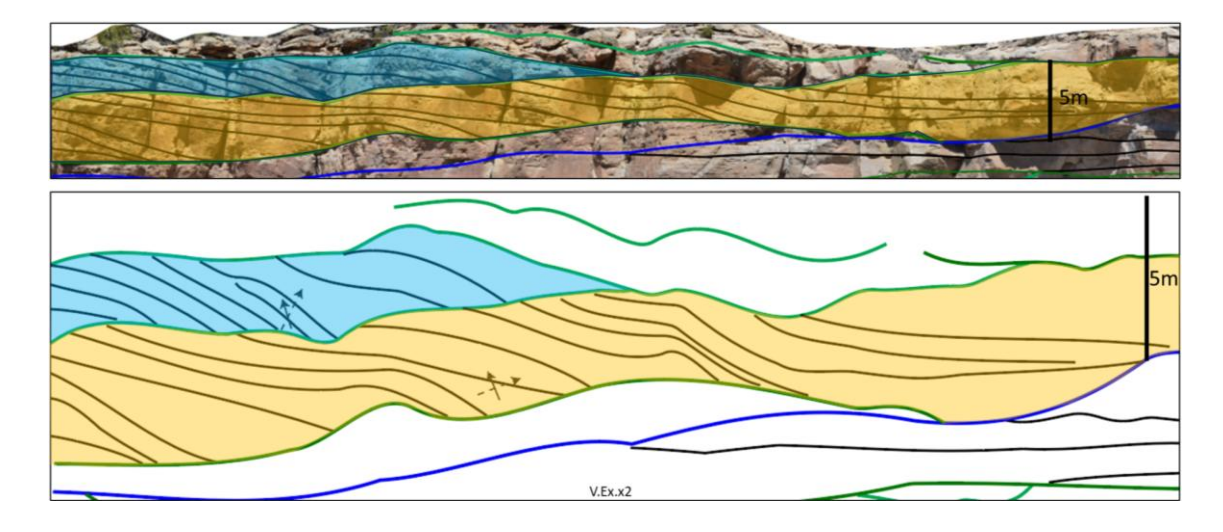


Figure 3.25. The lower (orange) and upper (blue) sub-units within the Torrivio section at SS-3. The lower unit is distinctly laterally migrating while the bars in the upper unit are migrating obliquely into the channel. The solid arrow indicates paleoflow direction whereas the dashed arrow represents the accretion direction.

3.3.4 Paleohydraulic calculations

The bankfull channel depth has been defined as the depth at bankfull discharge, beyond which the discharge overflows onto the floodplain (Leopold et al. 1964) and the corresponding channel width as bankfull channel width. It is possible to measure flow depths in the ancient systems directly from the outcrops wherein a completely preserved finning upward succession representing a channel story can be taken as a proxy for the bankfull depth (Bridge and Tye 2000; Bridge 2003; Bhattacharya and Tye 2004). Empirical relationships between the bedform height and the flow depth can also be used to estimate the bankfull flow depth (Bridge and Tye 2000; LeClair and Bridge 2001; Bhattacharya and Tye 2004). The dune-scale cross-set thickness of a fluvial deposit can be related to the formative dune height (Eq. 3.3), which in turn is related to the flow depth at the time of dune migration (Bridge 1997; LeClair et al. 1997; Bridge and Tye 2000; LeClair and Bridge 2001; Bhattacharya and Tye 2004). Bankfull channel width can be estimated directly from the strike-oriented outcrops by tracing the erosional base of the channel to the point where it merges with the flood plain/overbank facies (Bhattacharya et al. 2016). Empirical relationships also exist to estimate the bankfull channel widths (Leopold and Maddock 1953; Bridge and Mackey 1993). In the case of meandering fluvial systems, the width of the laterally accreting surfaces, as seen in the strike-oriented sections, represent about 50% to 80% of the bankfull channel width (Bridge 2003; Donselaar and Overeem 2008; Bhattacharya et al. 2016).

Multiple studies on ancient systems, particularly from the Cretaceous Western Interior Seaway, have carried out paleohydraulic estimations to establish sediment flux, source-to-sink mass balance and to make comparisons between different ancient systems (Holbrook and Wanas 2014; Bhattacharya et al. 2016; Lin and Bhattacharya 2016; Sharma et al. 2017). The following section describes the paleohydraulic calculation for the Torrivio River in detail.

1. Bankfull channel dimensions

i. Bankfull channel depth: The completely preserved channel storey thickness has been used as a proxy for the bankfull channel depth (d_m) (Bridge and Mackey 1993). However, care must be taken to not include confluence scours represented by single outsized foresets and bars. The measured storey thickness was corrected for compaction by a factor of 10% (Ethridge and Schumm 1978) to obtain the original bankfull depth. The measured storey thickness varies from 3 m to 6 m (n = 8), which gives a range of bankfull channel depths of 3.3 m to 6.6 m. An average value of 5 m has been taken to represent mean of the above range for bankfull channel depth.

The bankfull channel depth was also estimated using an average cross-set thickness of 21 cm (n = 700) (Fig. 3.26), and empirical relationship of LeClair and Bridge (2001) (Eq. 3.3). To test whether the dune height can be used to estimate the channel depth, the coefficient of variation i.e. the ratio of standard deviation (S_d) to the mean value (S_m) of the cross-set thickness values was estimated. The ratio of S_d/S_m was 0.71, which closely follows the range of 0.88 (\pm 0.3) given by Bridge and Tye (2000).

$$H_m = 5.3\beta + 0.001\beta^2 \tag{3.3}$$

where H_m is the mean dune height and $\beta = \frac{S_m}{1.8}$; S_m is the mean vertical thickness of cross-bed set. The cross-bed set thickness of a fluvial deposit can be related to the dune height (Eq. 3.3), and eventually to the flow depth (Bridge 1997; LeClair et al. 1997). The bankfull channel depth can scale to about 6 to 10 times the mean dune height (LeClair and Bridge 2001). The channel depth derived from the above relationship ranged from 3.7 m to 6.2 m (uncompacted) which follows the outcrop measured depths very closely and is therefore provides an independent quality check.

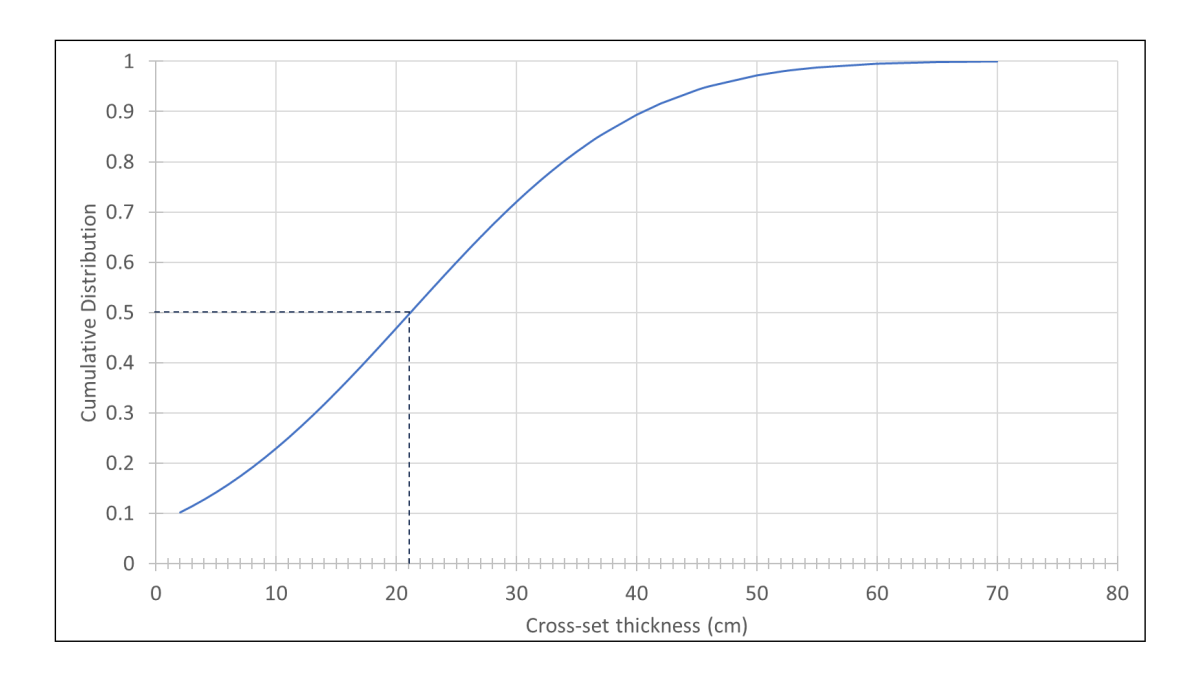


Figure 3.26. Cumulative distribution curve for dune-scale cross-sets from the main braided zone of the Torrivio Sandstone. Median cross-set thickness is 21 cm (black dotted line).

In the upper single sinuous channel zone although most of the point bars are truncated, a few bars are completely preserved, represented by bar roll-over as can be is seen in the lower subunit at SS-3 (Fig. 3.25). The thickest bar here reaches a thickness of approx. 3.5 m and considering that the bar height is typically about 80% of channel depth, a bankfull channel depth of about 4.3 m is estimated (Bridge 2003; Donselaar and Overeem 2008; Wu et al. 2015; Bhattacharya et al. 2016; Sharma et al. 2017).

ii. Bankfull channel width and channel belt width: Within the active part of a braided river, channels can range from the small-scale individual threads to major channels consisting of multiple threads and bars (5th order channels here). The largest scale is that of the channel belt, which may contain multiple major channels, and associated bars and islands (Fig. 3.27) (Bristow 1987; Bridge 1993; Egozi and Ashmore 2009; Limaye 2020).

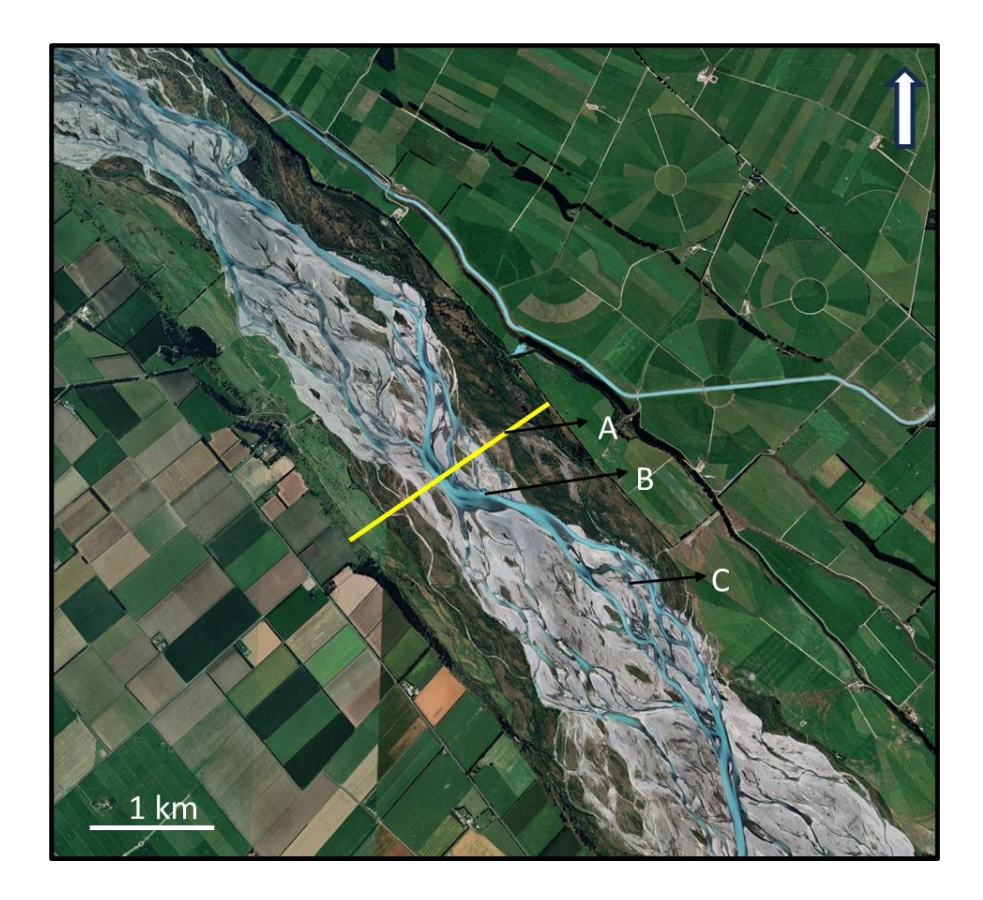


Figure 3.27. Satellite image of a section of the Rakaia River, Canterbury, NZ showing the channel hierarchy. (A) the channel belt (yellow line) while (B) and (C) are the major and minor threads respectively.

It is often difficult to find outcrops which are normal to the paleoflow and continuous enough to map major channels and channel belts. In the current study however, one of the outcrop sections provided a suitable opportunity to map these features (Fig. 3.28). The width of the 5th order channels in this section ranges from approx. 180 m to 340 m. These channels contain smaller 4th order threads and bars.

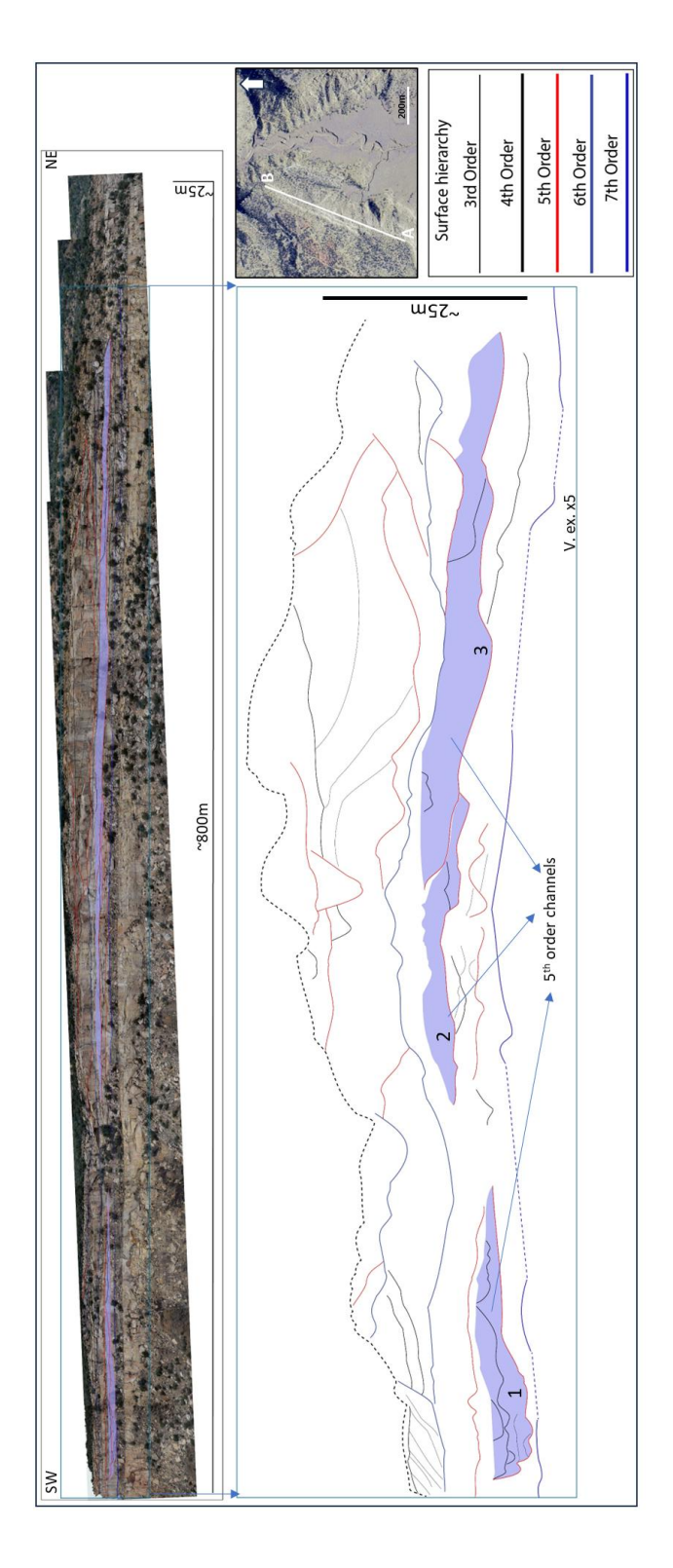


Figure 3.28. Outcrop section normal to the regional paleo flow. The whole outcrop is approx. 800 m wide, which is enough to measure major channels. The 5th order channels (in Blue) numbered 1, 2 and 3 are 180 m, 190 m and 340 m wide respectively.

Empirical relationships were also used to estimate the bankfull channel width (B_{bf}) and channel belt width (B_{cwbf}) for multi-thread rivers, given by Leopold and Maddock (1953, Eq. 3.4) and Bridge and Mackey (1993, Eq. 3.5) respectively.

$$B_{bf} = 42d_m^{1.11} (3.4)$$

$$B_{cwbf} = 192d_m^{1.37} (3.5)$$

The bankfull channel width was estimated to range from 169 m to 335 m, with a mean value of 251 m for the respective values of d_m estimated above. These values closely follow those observed directly from the outcrop. The respective values for the bankfull channel belt width were estimated to be 921 m and 1710 m and 1315 m. The estimation of channel belt width is important to constrain the number of active channels that might have transported the sediments, especially in ancient systems where suitable modern analogs are to be used to estimate the number of active channels (Egozi and Ashmore 2009). The bankfull width/thickness ratio estimated here for the respective mean value is close to 50, which follows the guide range of values given by Gibling (2006).

The average width of the accretion surface in the upper zone at SS-3 is 26 m (n = 2). Considering that the width of the accretion surfaces represents 50% to 80% of the channel width (Bridge 2003; Bhattacharya et al. 2016), the width of the channel ranges from about 32 m to 52 m at SS-3.

2. Slope

Slope was calculated using the median grain (D_{50}), bankfull channel depth (d_m) and the dimensionless shear stress (τ_{bf50}^*), the value of which is 1.86 for sand-bed rivers (Parker 2004; Wilkerson and Parker 2011).

$$S(Slope) = \frac{(\tau_{bf50}^*)^{(RD_{50})}}{H_{bf}}$$
(3.6)

R in the above equation is the submerged dimensionless relative density, the value of which is 1.65 for quartz sand grains in water of standard density (Parker 2004). The dimensionless

shear stress (τ_{bf50}^*) is assumed to be 1.86 for sand-bed rivers like the Torrivio (Parker et al. 1998; Dade and Friend 1998; Parker 2004).

The value of slope estimated using Eq. 3.6 varies from 3.3×10^{-4} to 1.8×10^{-4} , with a mean value of 2.3×10^{-4} .

The average slope value for the upper zone is estimated to be 1.5 x10⁻⁴. The change in Torrivio planform from braided to sinuous single channel can be explained using specific stream power, which is a function of width-averaged discharge, slope and median grain size (Van den Berg 1995). The reduction in the median grain size and slope, as mentioned above, could be explained by decreasing discharge and local changes in the fluvial long profile respectively (Bridge 2003), although distinguishing their individual signals might be difficult.

3. Mean flow velocity

The mean flow velocity (u) is calculated using the Eq. 3.7 (Parker 2004, 2008):

$$u = C z_{bf} \sqrt{g H_{bf} S} \tag{3.7}$$

Where, Cz_{bf} is the dimensionless bankfull Chézy resistance coefficient and is related to the dimensionless Chézy friction coefficient (C_f) by the following equation:

$$Cz_{bf} = (C_f)^{-1/2}$$
 (3.7a)

$$C_f^{-\frac{1}{2}} = (8.32) \left(\frac{H_{bf}}{k_s}\right)^{\frac{1}{6}}$$
 (3.7b)

The value for k_s can be determined using the Eq. 3.7c:

$$k_s = 3D_{S_{90}} + 1.1\Delta (1 - e^{-25\psi})$$
 (3.7c)

The Eq. 3.7c satisfies conditions where bedforms are present; Δ is the bedform height; $\psi = \frac{\Delta}{\lambda}$ where $\lambda = 7.3 H_{bf}$ is the bedform wavelength (Parker 2004; Holbrook and Wanas 2014). The acceleration due to gravity (g) is 9.8 m/s².

The mean flow velocity for the bankfull channel depth and width estimated above ranges from 1.2 m/s to 1.5 m/s, with a mean value of 1.4 m/s. Another way to estimate the mean flow velocity is to use the 3D bedform phase diagram (Rubin and McCulloch 1980). For a 3–6 m deep channel with a mean grain size of 0.38 mm (medium sand), the mean flow velocity would be in the region of 1–1.5 m/s (Fig. 3.29). This provides an independent check for the empirical estimation of mean flow velocity.

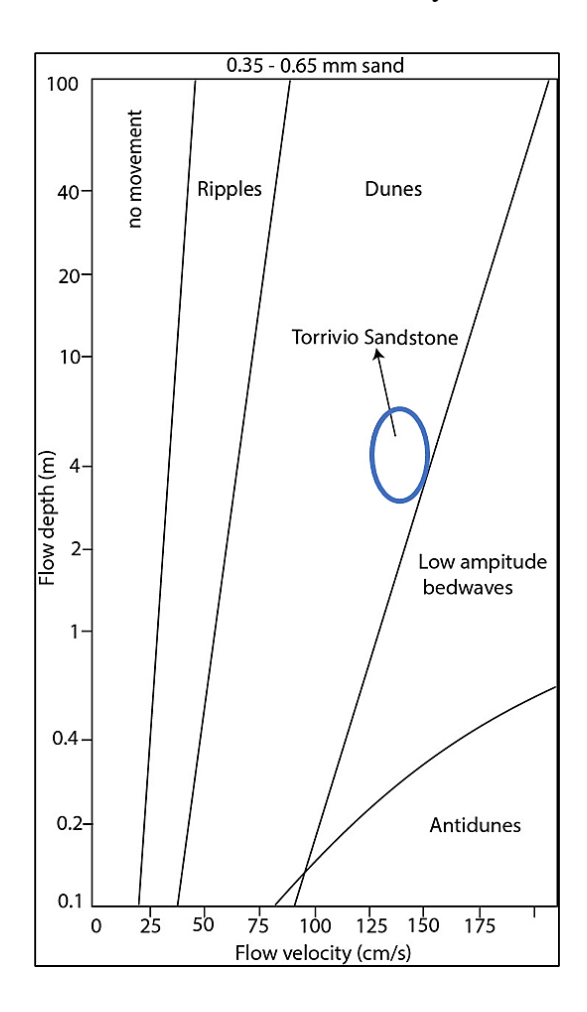


Figure 3.29. Semi-log plot of bedforms as function of flow depth and velocity for a given range of sandstone grain sizes. Here, the flow velocity for the Torrivio

Sandstone (braided unit) varies from 1.25 to 1.5 m/s, which closely follows the empirically derived values. See text for details. Modified after Rubin and McCulloch (1980).

4. Bankfull discharge

The water discharge for bankfull channel dimensions (Q_{bf}) was calculated using the following equation (Parker 2004, 2008):

$$C_f[(Q_{hf}^2)/(B_{hf}^2 H_{hf}^2)] = gH_{hf}S$$
(3.8)

The bankfull water discharge ranges from 785–3483 m³/s, with a mean value of 1850 m³/s for respective bankfull channel dimensions.

5. Bankfull sediment load discharge

The suspended load discharge was estimated using Eq. 3.9 and 3.9a (van Rijn 1984; Parker 2004; Wright and Parker 2004):

$$Q_s = q_s(B_{bf}) (3.9)$$

$$q_s(suspended - sediment \ discharge \ per \ unit \ width) = FudC_a$$
 (3.9a)

These equations and input parameters have been described in detail in Chapter 2. For the respective values of the bankfull channel width, the suspended load discharge varies from $0.7-2.7 \text{ m}^3/\text{s}$, with a mean value of $1.5 \text{ m}^3/\text{s}$.

The bedload discharge was calculated using the Parker (2004) transport equation (please refer to chapter-2 for details of the following equation):

$$Q_{tbf} = B_{bf} q_{tbf} = B_{bf} (RgD_{50})^{1/2} D_{50} \alpha_t [\phi_s \tau_{bf50}^* - \tau_c^*]^{n_t}$$
(3.10)

The values of bedload discharge range from 0.18–0.36 m³/s, with a mean of 0.27 m³/s. This gives the total sediment discharge of approximately 0.9 m³/s, 1.7 m³/s and 3 m³/s for the minimum, mean and maximum bankfull channel widths respectively.

The results of the deterministic palaeohydrological estimation of the main zone of the Torrivio Sandstone is presented in Table 3.2.

Table 3.2. Deterministic palaeohydrological estimation of the main zone of the Torrivio Sandstone

Avg. Cross Set Thickness (m)	Bedform Height (m)	H _{bf} (outcrop) (m)	B _{bf} (outcrop) (m)	B _{bf} (Leopold and Maddock 1953) (m)	Slope	Grain Size (mm) (D90, D84, D50, D16,)	Mean flow velocity (m/s)	<i>Q_{bf}</i> (m ³ /s)	Q_{tbf} (m³/s)
0.21	0.62	3.5	180	169	3.3x10 ⁻⁴	1.6,1.0,0.38,0.16	1.2	785	0.18
		5	260	251	2.3x10 ⁻⁴		1.4	1850	0.27
		6.5	340	335	1.8x10 ⁻⁴		1.5	3483	0.36

3.4 Discussion

3.4.1 Number of channels in the Torrivio River

The estimation of total discharge for single-thread rivers in ancient systems is reasonably well-documented in the literature (Bhattacharya and Tye 2004; Holbrook and Wanas 2014; Bhattacharya et al. 2016; Lin and Bhattacharya 2016; Sharma et al. 2017). However, the same for multi-thread rivers is less common (Hampson et al. 2013). This might be because it is difficult to ascertain the total number of channels involved in actively carrying water and sediment in a multi-thread river, and how the proportion of that is divided into the constituent channels, directly from an outcrop.

To overcome this challenge, information from modern multi-thread fluvial systems and results from experimental studies can be used. The number of channels in a system, or the braiding intensity, is generally proportional to the river size (Ashmore 2022.) For example, in the Brahmaputra River in Bangladesh, the number of active channels shows a positive correlation with channel-belt width (Takagi et al. 2007), and the same relationship was also observed in the Jamuna and Padma of Bangladesh (Sarker and Thorne 2006; Sarker et al. 2014).

The number of channels involved in active sediment transport, defined as the active braiding intensity (BI_A), exists as a subset of the total number of channels in a multi-thread system, defined as the total braiding intensity (BI_T) (Bertoldi et al. 2009; Egozi and Ashmore 2009). Bertoldi et al. (2009) carried out experimental work with coarse sand (D₅₀ = 0.63 mm) and varying longitudinal slope and discharge and documented that the ratio BI_A/ BI_T ranges from 0.2 to 0.6. A similar range of values from 0.3 to 0.5 was also reported by Egozi and Ashmore (2009) in their experimental study. Bertoldi et al. (2009) used well-sorted sand-sized particles and varied the slope and discharge conditions whereas Egozi and Ashmore's (2009) experiment was suited for coarser particles (D₅₀ = 1.2 mm), with constant discharge but varying slope. Since, the finer sand particles have a lower threshold of critical shear stress and hence higher mobility, the range of values for the BI_A/ BI_T as reported by Bertoldi et al. (2009) might be closer to sand-bed rivers like the Torrivio.

Takagi et al. (2007) reported that the total number of channels (BI_T) in the Jamuna River varies from 1 to 12, although values over 5 are rare. Considering the BI_A/ BI_T ratio of 0.2 - 0.6 (Bertoldi et al. 2009), the number of active channels in the Brahmaputra should range from 2 to 6. Since the channel-belt width in the Torrivio Sandstone is considerably smaller than the Brahmaputra River, the total number of channels should also be considerably fewer. Therefore, it seems very likely that the number of active channels in the Torrivio River should not be significantly more than 2. Also, the bankfull W/D ratio for the Torrivio River channels hover around the lower range of values (approx. 50) typical of the multithread rivers (Gibling 2006). These observations might suggest that the Torrivio was not a particularly large, braided river with a higher channel count. The same observation is also made when the Torrivio is placed on the cross plot of the ratio of slope/Froude number and bankfull width/ depth (Parker 1976). The Torrivio plots in the section of braided rivers with only 1-2 braids (Fig. 3.30).

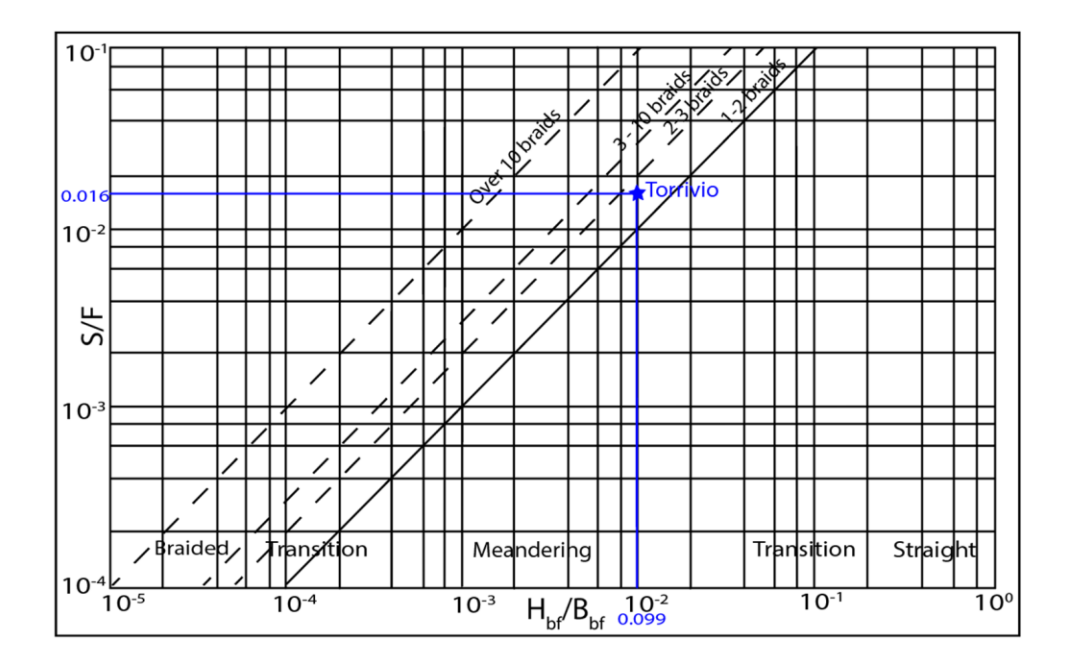


Figure 3.30. Fluvial planform regime diagram (Parker 1976). The braided unit of the Torrivio plots within the zone with 1-2 braids, highlighting that the Torrivio was probably a weakly braided system (S-Slope, F-Froude number, H_{bf}-Bankfull channel depth (m) and B_{bf}-Bankfull channel width (m).

van den Berg (1995) proposed that the specific stream power (ω_{pv} , in kW/m²) can be used to distinguish alluvial channel patterns. This observation was later updated to include meandering streams with scrolls, and chute channels (Kleinhans and van den Berg 2011). They proposed the following equation to calculate the specific stream power for sand-bed rivers:

$$\omega_{pv} = \rho g Q S / W_r \tag{3.11}$$

where, ρ is the density of water in kg/m³, g is the acceleration due to gravity (9.8 m/s²), Q is the bankfull discharge (m³/s), S is the slope and W_r is the pattern-independent reference width and $W_r = \alpha \sqrt{Q_{bf}}$, α is 4.7 for sand-bed systems where D₅₀ < 2 mm. The specific stream power of the Torrivio River, at the mean bankfull discharge of 1850 m³/s and D₅₀ grain size of 0.38 mm, is estimated to be approximately 21 W/m², which plots very close to the line separating the single- and multi-thread channels (Fig. 3.31). This is consistent with the Parker (1976) method and again suggests that the Torrivio River was probably a

weakly braided river system. All these observations indicate that the number of active channels in the Torrivio could be close to 1 to 2.

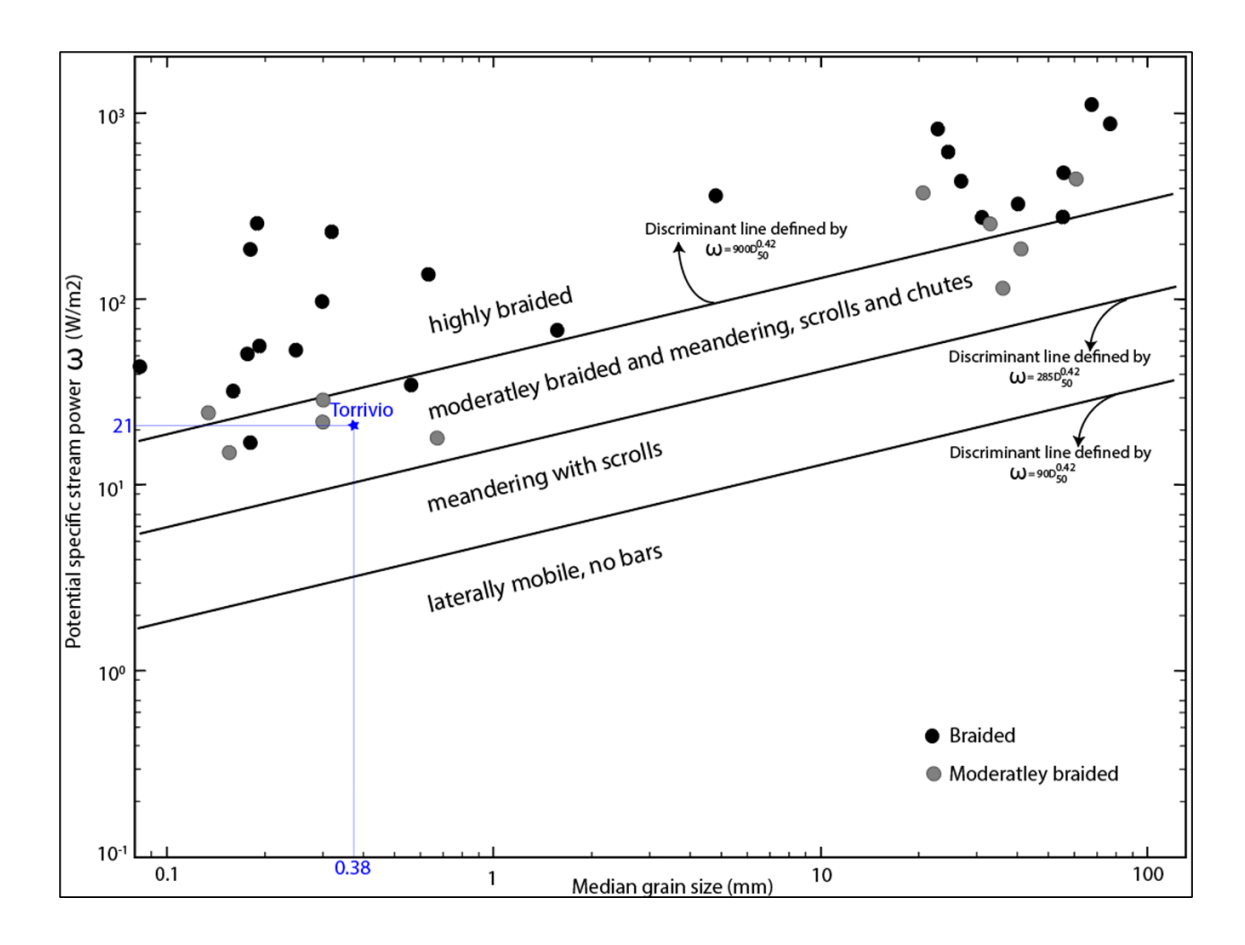


Figure 3.31. Log plot of stream power vs grain size (Kleinhans and van den Berg 2011) highlighting that the main unit of the Torrivio Sandstone (Blue star) was deposited by a weakly braided river.

It has been observed, both in the field (Mosley 1983) and in experimental setups (Stojic et al. 1998; Bertoldi and Tubino 2007; Egozi and Ashmore 2009), that most of the discharge in a multi-channel system is restricted to a single main channel. The main channel can account for approx. $3/4^{th}$ of the total discharge (Mosley 1983; Egozi and Ashmore 2009). If we consider that the mean estimations of channel dimensions and discharge (1850 m³/s) for the Torrivio River, as described earlier, represent the main channel and $3/4^{th}$ of the total possible discharge, and the conclusion that the Torrivio is a weakly braided system with

two threads, the total mean discharge for the braided Torrivio river is estimated to be about 2466 m³/s.

3.4.2 Mean annual discharge

The conversion of the instantaneous discharge to annual discharge involves knowing the annual bankfull event duration (Holbrook and Wanas 2014), which varies considerably, as discussed in Chapter 2. However, the range of uncertainty in this estimation, particularly for deep-time systems, can be reduced if data from modern analogs are used (Davidson and North 2009). This would obviously involve knowing the paleoclimate of the basin in question. The paleo-Koppen climate classification by Burgener et al. (2023) and the paleoprecipitation model of Valdes et al. (2020) for Santonian and Coniacian ages identify a wet, tropical humid climate for the Torrivio drainage basins (Fig. 3.32).

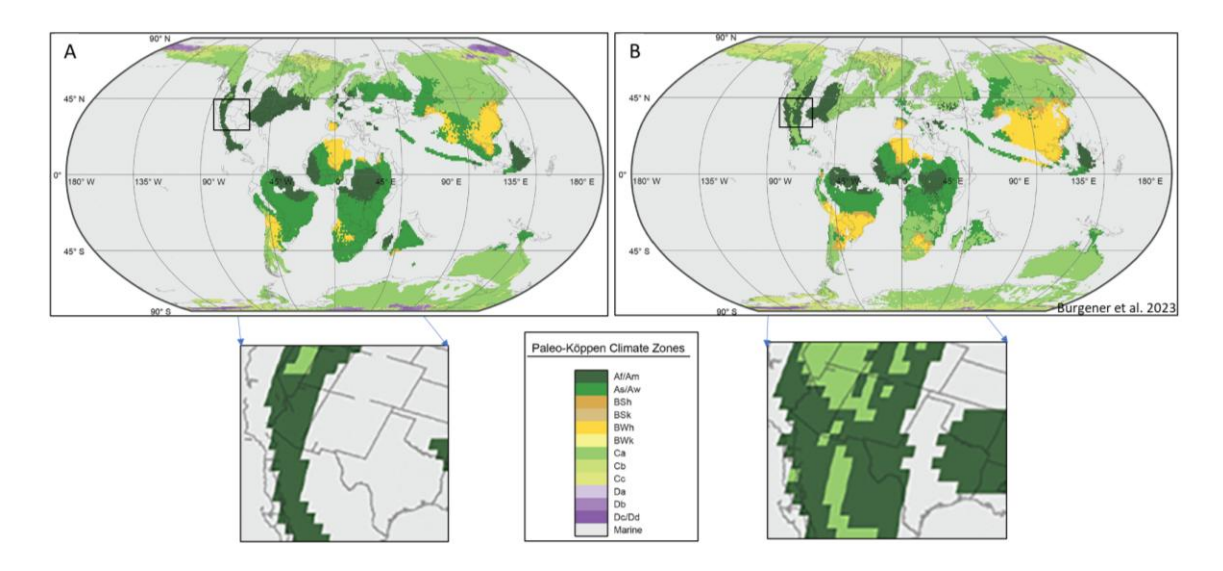


Figure 3.32. Paleo-Koppen climate zone distribution during the Turonian (A) and Coniacian-Santonian (B) time. The corresponding zoomed-in section around the current area of interest highlights a tropical wet climate (Af/Am). Paleo-climate study by Burgener et al. (2023). As/Aw = tropical savannah; BSh = hot steppe, BSk = cold steppe, BWh = hot desert, BWk = cold desert; Ca = temperate, humid subtropical, Cb = temperate, maritime temperate, Cc = temperate, maritime subarctic; Da = continental, hot summer, Db = continental, warm summer, Dc/Dd = continental, subarctic; E = polar.

The petrographic analysis of the Torrivio Sandstone (Lin et al. 2021) documented that the sandstone composition varied from 59 – 74%, 19 – 33% and 6 – 15% for Quartz, Feldspar and lithic (QFL) fragments respectively. This range of QFL composition has been reported to suggest humid climate provenance (Suttner and Dutta 1986). This observation, coupled with the fact that coal is found abundantly associated with the Torrivio Sandstone (Hohman 1986; Flores et al. 1991), is consistent with a humid climate for the Torrivio drainage system. The paleogeographic reconstruction of the Cretaceous Western Interior Seaway for the Santonian-Coniacian time places the Torrivio fluvial system between 30° N and 50° N paleo-latitude (Blakey 2014, Blakey and Ranney 2017; Burgener et al. 2023). In the modern Koppen climate classification (Peel et al. 2007), this range of latitude is characterized by wet, tropical and humid climate similar to that found in the eastern and south-eastern USA, and northern Italy (Fig. 3.33) and suitable analogs have been taken from these geographical areas, as explained below.

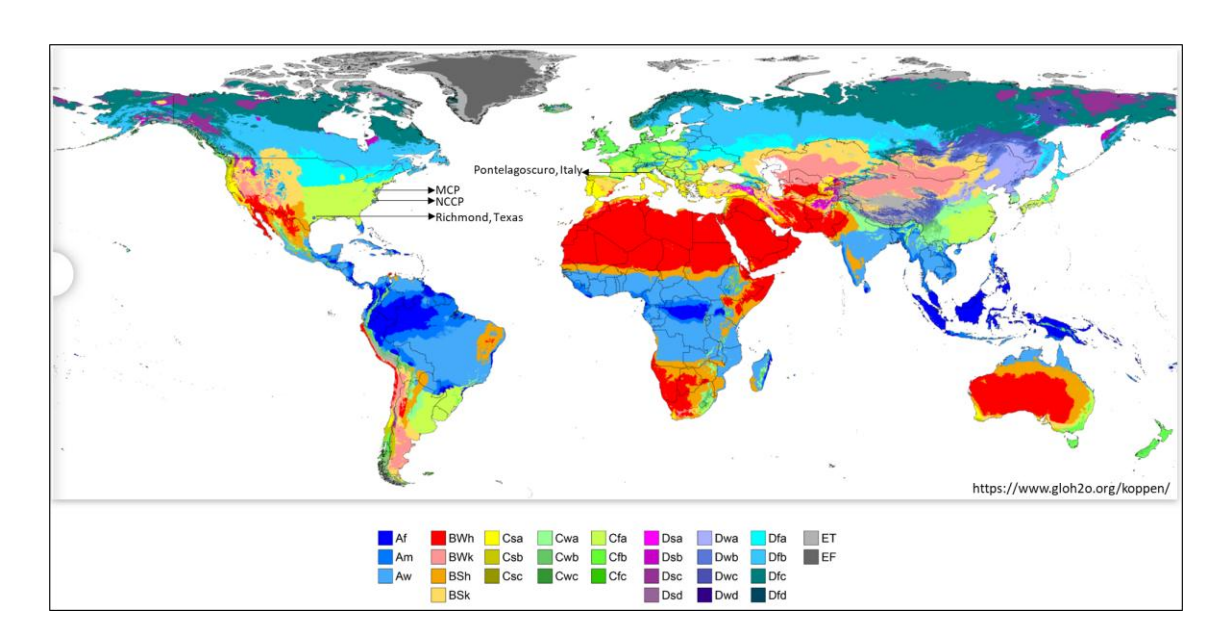


Figure 3.33. Modern Koppen climate zone distribution map. Humid-subtropical climate is represented by Cfa. Also plotted are the locations of the modern analogs from the sub-tropical humid climates used in this study (www.gloh2o.org/koppen/).

Information is available for bankfull periods for smaller catchments in Maryland, Delaware, North Carolina, USA, and larger catchments, such as the Brazos River in Texas, USA and Po River at Pontelagoscuro in Italy. Sweet and Geratz (2003) estimated that for the smaller catchments in the North Carolina coastal plains (NCCP), the annual bankfull event duration ranges from 1.4 days to 18 days, with a simple mean of approx. 6 days. Recurrence interval (RI) for the coastal plain catchments of Virginia and Maryland (MCP) ranges from 1 to 2 years, with a mean value of 1.5 years (Krstolic and Chaplin 2007). A global study of bankfull return period (Liu et al. 2024), binned with respect to the climate of the basin, documented a median RI of 1 year for tropical climates.

The bankfull discharge for the Po River at the Pontelagoscuro station has been estimated to be about 4000 m³/s (Lanzoni et al. 2015). The RI for bankfull floods has been estimated to be 1.25 years (Borhani et al. 2020) and 1.58 years (Billi and Fazzini 2017). The mean daily discharge data for the Po River is available at the Global Runoff Data Center website (GRDC) at station Pontelagoscuro (station no. 6348800) for a six-year period from January 1980 to December 1985. We used this data to generate the flow duration curve (Fig. 3.34A) and observed that the bankfull discharge of 4000 m³/s was equaled or exceeded 4.8% of times or approx. 17 days.

Strom (2013) reported a bankfull discharge of 40000 f³/s or 1133 m³/s for the Brazos River at the Richmond station in Texas, USA using data from 1966 – 1986, he also estimated the RI for the bankfull event to be 1.5 years. RI values ranging from 1 to 2 years have also been reported for the Lower Brazos at Richmond (Philips 2015). The bankfull duration is estimated to range from 5 to 11 days (Hudson and Mossa 1997; Strom 2013). We used the mean daily discharge data from the USGS website for the Brazos River at Richmond station no. 08114000, from 1966 to 1986 and produced a flow duration curve (Fig. 3.34B), which shows that the bankfull discharge of 40000 f³/s or 1133 m³/s was equaled or exceeded 2.6% of time or approximately 10 days. A similar value of approx. 2% or 7 days in a year has also been reported by Andrews (1980) for the same period at Richmond station.

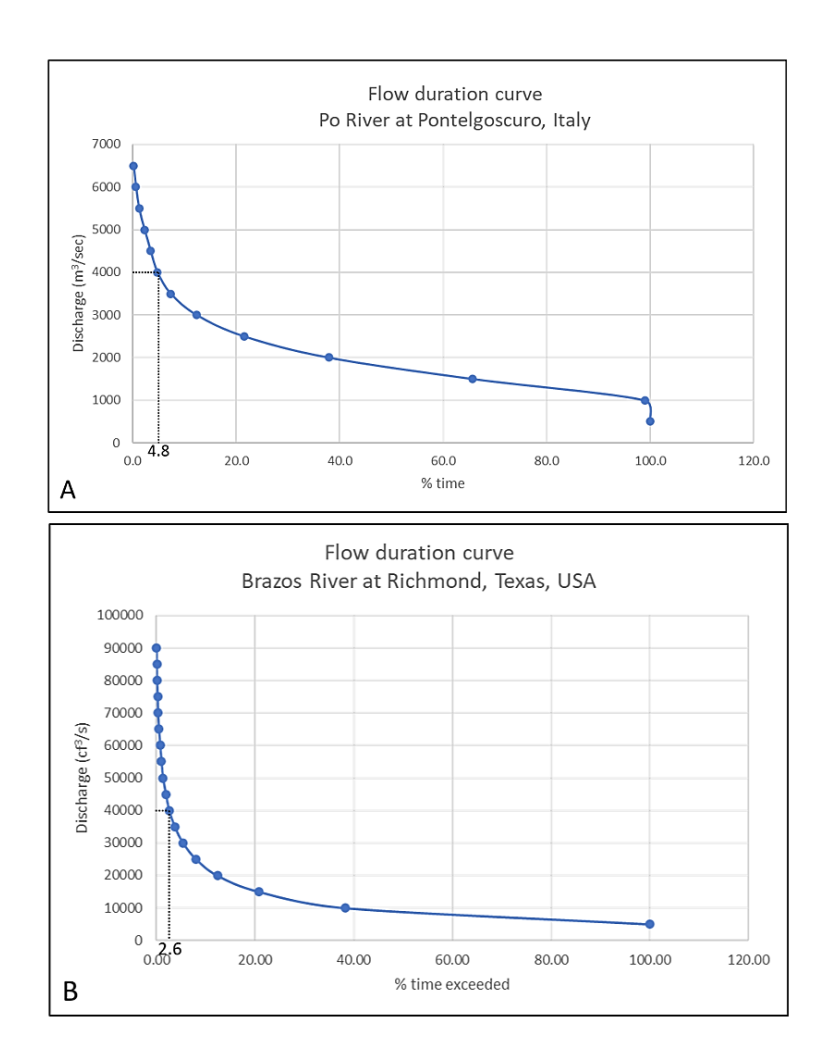


Figure 3.34. Flow duration curves for the River Po (A) and Brazos River (B) showing the percentage of time their respective bankfull discharge was exceeded. See text for details.

It is, therefore, clear from the above-mentioned analog data that there's a considerable variability in the annual bankfull discharge estimation. If the objective is to estimate the annual bedload discharge, another factor to consider is the proportion of bedload which is carried by the river during bankfull duration. In a global study, Meybeck et al. (2003) observed that for drainage basins with area of the order of $10^4 \, \mathrm{km^2}$, approximately half of the annual bedload is carried during the bankfull period. Strom (2013) reported similar values of 52 - 54% for their study on the Brazos River at Richmond.

The mean annual discharge can be estimated using the following equation:

$$Q_{mas} = Q_{bt}(t_{bd})b (3.12)$$

where Q_{mas} is the mean annual bedload discharge, Q_{bt} is the rate of bankfull bedload discharge, t_{bd} is the mean annual bankfull duration (ratio of bankfull duration/RI) and b is the inverse of the proportion of bedload transported during the bankfull duration (Holbrook and Wanas 2014).

To capture the range of possible values for the annual bedload discharge (volume in m³), a Monte-Carlo simulation was run. The input variables for the simulation have been listed in Table 3.3. Data from most of the natural processes, including river discharge data, follow a log-normal distribution (Pickup and Warner 1976; Yu and Wolman 1987; Nash 1994; Bowers et al. 2012; Sharma et al. 2017), a similar approach was also followed here to calculate the mean annual discharge. However, a triangular distribution was adopted for *b* as the average value of 2 is well-established and a maximum of 2.5 and a minimum of 1.7 were considered to provide a range. A total of 1000 realizations were run. The results of the simulation are presented in Table 3.4.

Table 3.3. Major Input variables from analogous river systems for bankfull duration and RI used in the Monte-Carlo simulation. Please see the text for source of the data.

River System	Bankfull	Duration	Recurrence Interval (RI)		
	Min.	Max.	Min.	Max.	
Po, Italy	NA	**7	1.25	1.58	
Brazos, USA	5	11	1.5	1.5	
*NCCP, USA	1.4	18	NA	**1.2	
Santa Lucia, Uruguay	NA	**35	NA	**1.01	

^{*}North Carolina Coastal Plain; **Average value

Table 3.4. The results of the Monte Carlo simulations-based estimation and the resulting P10, P50, and P90 values (90% certainty) for mean annual bedload volume (m³) highlight the range of possible outcomes.

Estimation	Bedload discharge (m³/s)	Number of bankfull event (days/yr)	RI	<i>t</i> _{bd} (s)	b	Mean annual bedload volume (Q_{mas}, m^3)			
Case						P10	P50	P90	
Low	0.18	1.4	1.01	119762.4	2.5				
Base	0.27	9.7	1.36	635294.1	2.0	16.2×10^4	30.2×10^4	61.8×10^4	
High	0.36	18	1.58	984303.8	1.7				

It is clear that there is still a range in the value of the annual bedload discharge (m³), but the range itself has reduced markedly. In their study of the Ferron Rivers, Sharma et al. (2017) reported that the Q_{mas} values varied by more than a factor of four whereas in this study it varies by a factor of less than four (Fig. 3.35A). This improvement in the confidence of prediction is due to the application of data from suitable modern analogs binned with similar climatic conditions. However, the biggest contribution to the range of Q_{mas} values comes from the t_{bd} (Fig. 3.35B) and its effects can be mitigated by bringing in more analog data. The distribution and assumption of the variables used in the estimation of annual bedload volume are shown in Fig. 3.36.

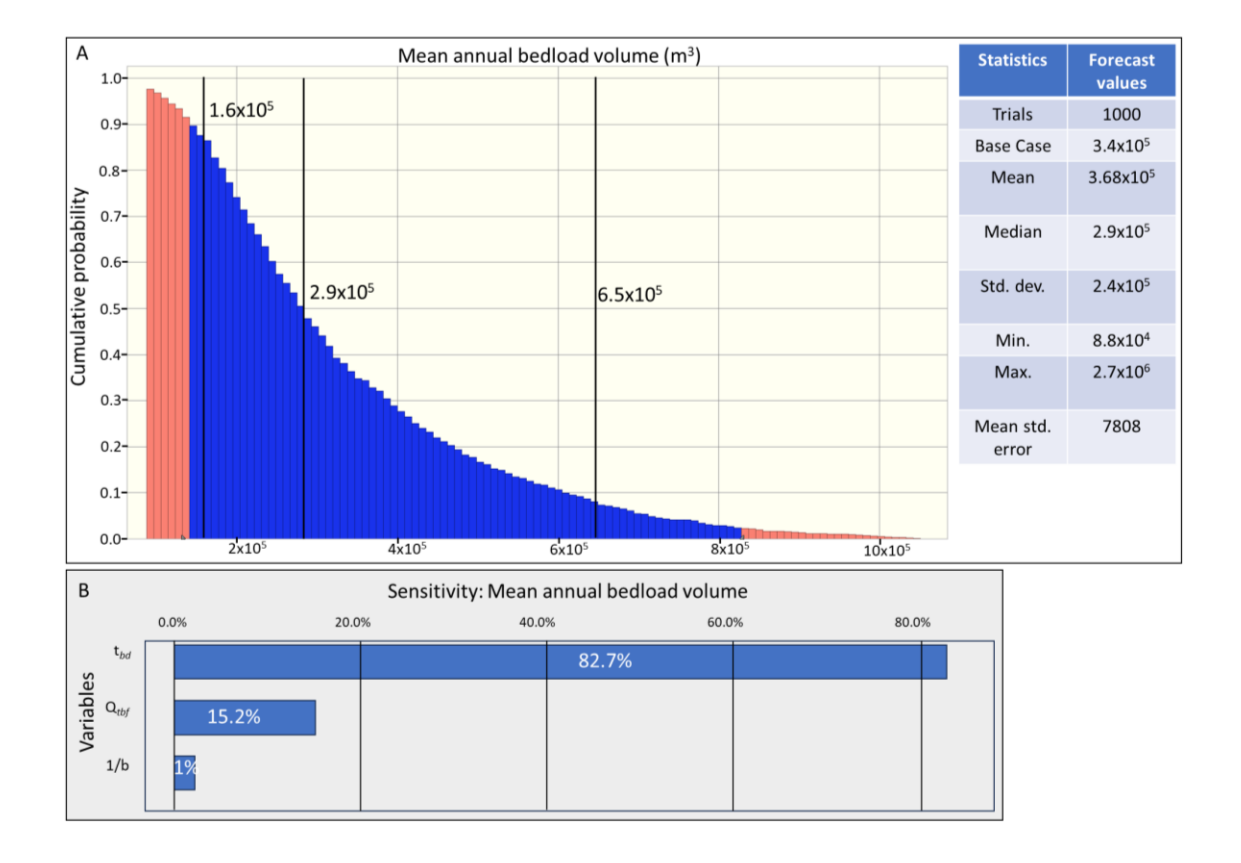


Figure 3.35. A) The result of the Monte-Carlo simulation showing the range of P10, Median and P90 values within 90% certainty window. B) Sensitivity of different parameters on the outcome of the annual bedload discharge (m³). The conversion of the instantaneous to mean annual bankfull duration is the most sensitive factor in estimating the mean annual bedload volume.

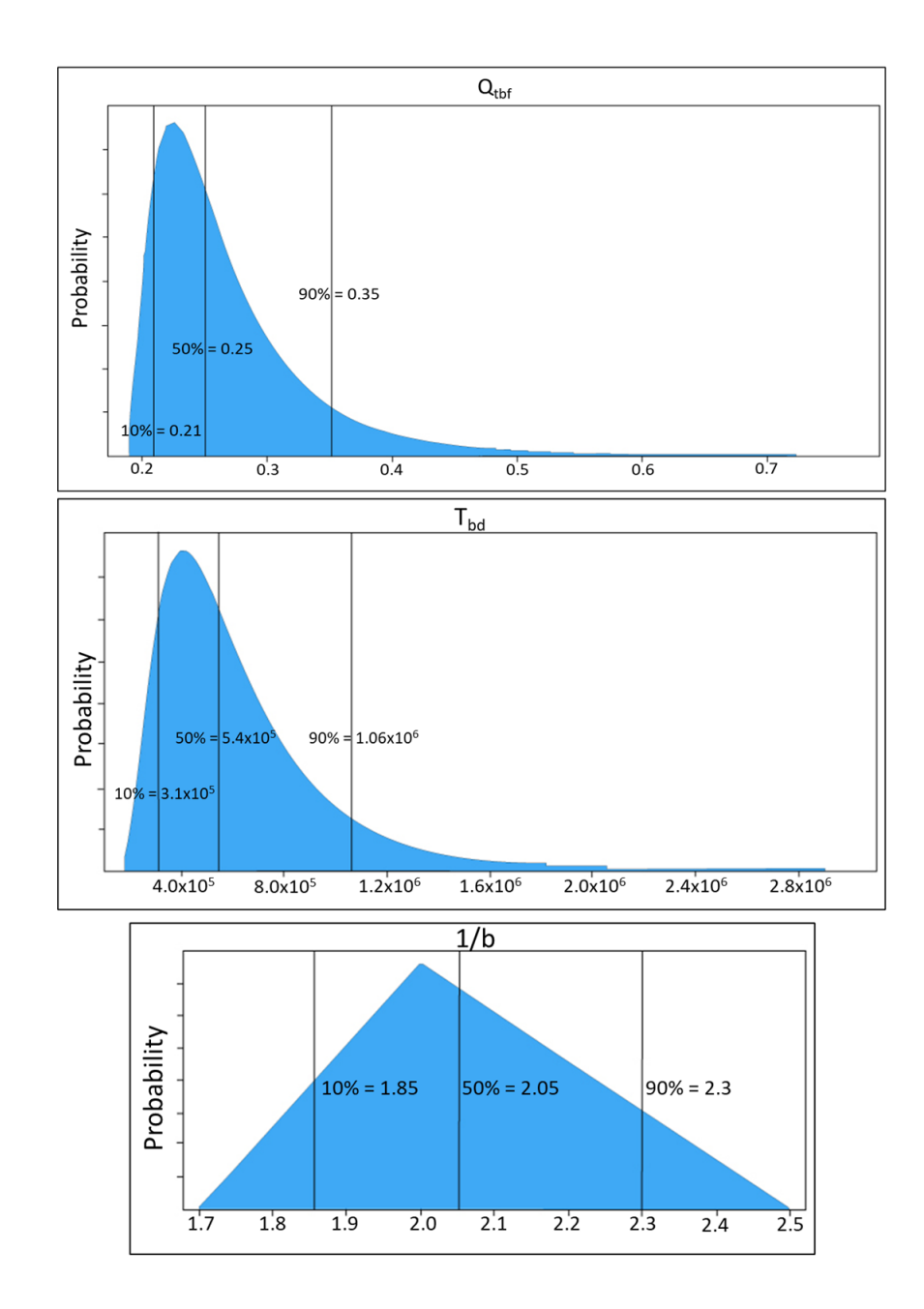


Figure 3.36. Distribution and assumption charts for the variables used in the Monte-Carlo simulation. Q_{tbf} and T_{bd} follow log-normal distribution while the 1/b factor follows a triangular distribution. See text for explanation.

3.4.3 Drainage area

Suitable modern analogs can also be very useful in estimating paleo-drainage areas (Davidson and North 2009). Regional curves, from catchments belonging to similar

climatic settings, have been used to constrain the range of values for drainage areas (McCandless 2003; Sweet and Geratz 2003; Metcalf 2004; Metcalf and Shaneyfelt 2005; Krstolic and Chaplin 2007; Davidson and North 2009; Jones 2017). Using the relationship (Eq. 3.13) between bankfull discharge and drainage for the Po River (Eq. 8 in Billi and Fazzini (2017)) and the range of bankfull discharge values for the Torrivio River described above, the drainage area for the Torrivio River was estimated at 26000 km², with probable minimum and maximum estimates at approximately 10500 km² to 51000 km² respectively.

$$Q_{bf} = 0.0669A + 82.762 \tag{3.13}$$

where Q_{bf} is the bankfull discharge in m³/s and A is the drainage area in km².

Using a similar relationship (Eq. 3.14) from the Brazos River at Richmond (Raines 1998) gives a range of catchment area values of approximately 13200 km², 55600 km² and 161000 km².

$$Q_{bf} = 173A^{0.595} (3.14)$$

where discharge and area units are in f³/s and miles² respectively.

Detrital Zircon and petrographic analysis (Ferron 2019; Lin et al. 2021) places the most likely source for Torrivio rivers towards the Mogollon Highlands in the south and southwest direction. Their analysis concluded that the rivers feeding the Gallup Sandstone were older than the Torrivio rivers and most likely sourced from the Sevier fold and thrust belt (Dickinson and Suczek 1979). Using their paleogeographic reconstruction for the Coniacian period (Fig. 3.37), the Torrivio drainage area can be reasonably estimated to be about 70,000 – 75,000 km². This is close to the higher values estimated using regional geomorphic relationships described above.

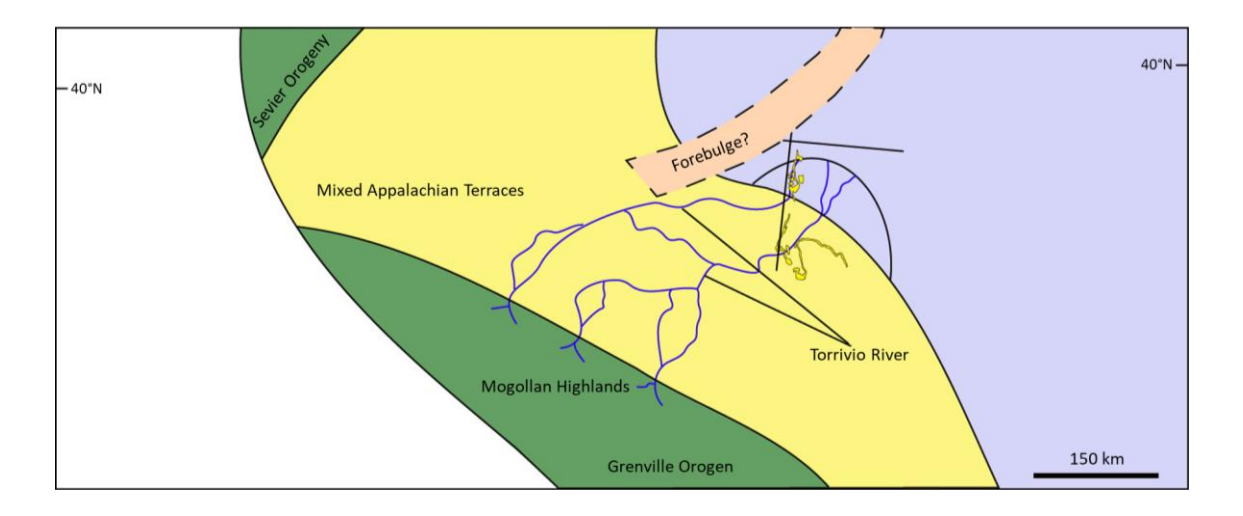


Figure 3.37. Paleogeographic reconstruction at Coniacian (~88.8 Ma) showing the Torrivio drainage (after Ferron 2019). An approx. drainage area of 75,000 km² can be reasonably estimated from the above reconstruction.

3.4.4 Was Torrivio a "big river"?

Big rivers have typically been defined based on their water and sediment discharge and the size of the drainage basin (Potter 1978). These parameters can be readily assessed in modern river systems, e.g. the Brahmaputra River (Bristow 1987, 1993; Thorne et al. 1993; Best and Ashworth 1997; Best et al. 2003) and the Amazon River (Mertes et al. 1996; Vital et al. 1998; Archer 2005). But these are very difficult to determine accurately in the rock record, as explained in this study. However, the scale of major depositional elements might help in estimating the size and scale of the formative rivers (Miall 2006; Fielding 2008).

On average, the bankfull channel depth in the Torrivio Sandstone is about 5 m, with the deepest scour reaching a depth of 12 m, which represents a tributary-channel confluence. The Triassic Hawkesbury Sandstone of the Sydney Basin in eastern Australia has been interpreted to be deposited by a large braided system (Rust and Jones 1987; Miall and Jones 2003). In their study, Miall and Jones (2003) documented that the Hawkesbury channels were 5-10 m deep while the confluence scours were up to 20 m deep. Although at first glance, the depths of the channels in the Torrivio Sandstone and the Hawkesbury Sandstone

might seem relatable, if we compare the widths of the 5th order channels, it becomes clear that this is not actually the case. The widest 5th order channel in the Torrivio Sandstone is ~350 m while that in the Hawkesbury Sandstone is ~2700 m (Miall and Jones 2003). The respective width-to-depth ratio would be ~70 for the Torrivio Sandstone and 540 for the Hawkesbury Sandstone, which is close to an order of magnitude larger than the Torrivio Sandstone. Thus, it is crucial to define major architectural elements to compare two depositional systems.

If we consider the modern Brahmaputra River, the 5th order channels are typically about 10-12 m deep, although maximum scour depths of close to 50 m have been recorded (Best and Ashworth 1997). The bars within these channels would be about 7 m thick and 1-2 km wide (Ashworth et al. 2000; Best et al. 2003). Bankfull width-to-thickness ratio would be close to 700 (Thorne et al. 1993), which means channel width of more than 2 km. Although, these bars and channels would undergo changes due to channel migration and avulsion before preservation, these values could still be an order of magnitude larger than the Torrivio Sandstone.

The outcrops of the Campanian-age Castelgate Sandstone in the Book Cliffs of Utah, expose deposits of a braided system reaching a height of about 80 m (Fouch et al. 1983; Miall 1993; Olsen et al. 1995). Although at a glance deposits of this thickness might suggest that the Castlegate River was a big river system, architectural analysis highlights that the outcrop essentially represents stacked channel belt complexes (McLaurin and Steel 2007). Based on fully preserved barforms, the paleochannel depth was estimated to range from 1.5 to 8 m, with an average depth of 4.1 m (Miall 1993; Lynds and Hajek 2006). McLaurin and Steel (2007) reported paleochannel depths in the range of 4.6 to 7.7 m and width of 143 to 365 m. These average value of the channel dimensions match closely with that of the Torrivio River. Therefore, it would be prudent to conclude that big deposits do not necessarily mean big formative rivers.

3.5 Conclusions

Multiple types of data have been used in this study to ascertain and describe the type of fluvial system that existed at the time of deposition of the Torrivio Sandstone. The deposits of the Torrivio River are not exclusively braided in nature, as has been reported in previously published studies (Hohman 1986; Flores et al. 1991). The Torrivio River was essentially a mixed system, showing evolution from a pre-dominantly braided system to a more sinuous, single-channel system over time. This change possibly reflects a reduction in the stream power of the formative rivers. The braided unit of the Torrivio Sandstone was deposited by a river, which was approximately 5 m deep, and 250 m wide, contained within a channel belt about 1350 m wide. The dominant architectural elements include:

- 1. Channel elements: Sandstone-dominated channel; mudstone-dominated channel with some sandstone and smaller chute or cross-bar channels.
- 2. Within channel elements: Unit bars; compound bars and hollow elements or confluence scour fill. Lateral and downstream accreting elements.
- 3. Overbank elements: Splay and floodplain deposits.

The braided section is characterized typically by mounded mid-channel bars, along with multiple side bars and channel fills producing a broadly sheet-like geometry. Also common are confluence scour deposits, ranging from simple bar-scale to large tributary confluence scale. Paleohydraulic estimations suggest that the average slope of the system was approx. 2.3 x10⁻⁴ and the mean flow velocity was 1.4 m/s. The mean values for the bankfull water discharge, the suspended load discharge and the bedload discharge are ranges 1850 m³/s, 1.5 m³/s and 0.27 m³/s, respectively. It has also been demonstrated that the Torrivio River was possibly a weakly braided system with number of active channels not likely exceeding two.

The overlying single channel deposits show fining of the median grain size as well as reduction in the channel width, suggesting a reduction in stream power and hence vertical change in the planform geometry. The formative channel was about 5 m deep and 10 - 27 m wide. The catchment area for the Torrivio River was estimated to be approx. $75,000 - 100,000 \text{ km}^2$. These values closely follow those previously published.

The study also shows that the range of uncertainty in the estimation of annual water and sediment discharge can be reduced by using climate-binned modern analogs. To capture this uncertainty in the annual bedload volume (m^3), a Monte-Carlo simulation-based estimation was also carried out. The P10, P50 and P90 case numbers for the bedload volume are 16.2×10^4 , 30.2×10^4 and 61.8×10^4 m³, respectively. The major source of this uncertainty still is the conversion of the instantaneous discharge to mean annual discharge using the bankfull duration days and their respective recurrence interval. More climate-binned information from modern analogs can help improve the discharge estimates of ancient systems.

References

- Adams, M.M. and Bhattacharya, J.P., 2005. No change in fluvial style across a sequence boundary, Cretaceous Blackhawk and Castlegate Formations of central Utah, USA. Journal of Sedimentary Research, 75(6), pp. 1038–1051.
- Allen, J.R.L., 1973. Features of cross-stratified units due to random and other changes in bed forms. Sedimentology, 20(2), pp. 189–202.
- Allen, J.R.L., 1983. Studies in fluviatile sedimentation: bars, bar-complexes and sandstone sheets (low-sinuosity braided streams) in the Brownstones (L. Devonian), Welsh Borders. Sedimentary Geology, 33(4), pp. 237–293.
- Andrews, E.D., 1980, Effective and bankfull discharges of streams in the Yampa River basin, Colorado and Wyoming: Journal of Hydrology, v. 46, p. 311–330.
- Archer, A.W., 2005. Review of Amazonian depositional systems. Fluvial sedimentology VII, pp.17-39.
- Ashmore, P., 2022. Braiding. In: Shroder, J.J.F. (Ed.), Treatise on Geomorphology, vol. 6. Elsevier, Academic Press, pp. 517–543, doi: 10.1016/B978-0-12-409548-9.12086-X.
- Ashworth, P.J., Best, J.L., Roden, J.E., Bristow, C.S. and Klaassen, G.J., 2000. Morphological evolution and dynamics of a large, sand braid-bar, Jamuna River, Bangladesh. Sedimentology, 47(3), pp. 533–555.

- Ashworth, P.J., Sambrook Smith, G.H., Best, J.L., Bridge, J.S., Lane, S.N., Lunt, I.A., Reesink, A.J., Simpson, C.J. and Thomas, R.E., 2011. Evolution and sedimentology of a channel fill in the sandy braided South Saskatchewan River and its comparison to the deposits of an adjacent compound bar. Sedimentology, 58(7), pp.1860-1883.
- Bertoldi, W. and Tubino, M., 2007. River bifurcations: Experimental observations on equilibrium configurations. Water Resources Research, 43(10).
- Bertoldi, W., Zanoni, L. and Tubino, M., 2009. Planform dynamics of braided streams. Earth Surface Processes and Landforms, 34(4), pp.547-557.
- Best, J.L., 1988. Sediment transport and bed morphology at river channel confluences. Sedimentology, 35(3), pp.481-498.
- Best, J.L. and Ashworth, P.J., 1997. Scour in large braided rivers and the recognition of sequence stratigraphic boundaries. Nature, 387(6630), pp.275-277.
- Best, J.L., Ashworth, P.J., Bristow, C.S. and Roden, J., 2003. Three-dimensional sedimentary architecture of a large, mid-channel sand braid bar, Jamuna River, Bangladesh. Journal of Sedimentary Research, 73(4), pp.516-530.
- Best, J., Woodward, J., Ashworth, P., Smith, G.S. and Simpson, C., 2006. Bar-top hollows: a new element in the architecture of sandy braided rivers. Sedimentary Geology, 190(1-4), pp.241-255.
- Bhattacharya, J.P., and Tye, R.S., 2004, Searching for modern Ferron analogs and application to subsurface interpretation, in Chidsey T.C. Jr., Adams, R.D., and Morris, T.H. eds., The Fluvial-Deltaic Ferron Sandstone: Regional to Wellbore Analog for Fluvial-Deltaic Reservoir Modeling: American Association of Petroleum Geologists, Studies in Geology, 50, p. 39–57.
- Bhattacharya, J.P., Copeland, P., Lawton, T.F. and Holbrook, J., 2016. Estimation of source area, river paleo-discharge, paleoslope, and sediment budgets of linked deeptime depositional systems and implications for hydrocarbon potential. Earth-Science Reviews, 153, pp.77-110.
- Billi, P. and Fazzini, M., 2017. Global change and river flow in Italy. Global and Planetary Change, 155, pp.234-246.

- Blakey, R.C., 2014. Paleogeography and paleotectonics of the western interior seaway, Jurassic-Cretaceous of North America. Search and Discovery, 30392, p.72.
- Blakey, R.C. and Ranney, W.D., 2017. Ancient landscapes of western North America: A geologic history with paleogeographic maps. Springer.
- Borhani, S., Hosseiny, H. and Strom, K., 2020. Effective discharge calculations: Comparison of classic methods with a morphodynamic model on a reach of the Po River (Italy). In River Flow 2020 (pp. 685-693). CRC Press.
- Bowers, M.C., Tung, W.W., and Gao, J.B., 2012, On the distributions of seasonal river flows: Lognormal or power law?: Water Resources Research, v. 48, p. 1–12.
- Bridge, J.S., 1993. The interaction between channel geometry, water flow, sediment transport and deposition in braided rivers. Geological Society, London, Special Publications, 75(1), pp.13-71.
- Bridge, J.S., 1997, Thickness of sets of cross-strata and planar strata as a function of formative bedwave geometry and migration: Geology, v. 25, p. 971–974.
- Bridge, J.S., 2003, Rivers and Floodplains: Forms, Processes, and Sedimentary Record: Malden, Massachusetts, Blackwell Science, 491 p.
- Bridge, J.S., and Mackey, S.D., 1993, A theoretical study of fluvial sandstone body dimensions, in Flint, S.S., and Bryant, I.D., eds., The Geological Modelling of Hydrocarbon Reservoirs and Outcrop Analogues: International Association of Sedimentologists, Special Publication 15, p. 213–236.
- Bridge, J.S., and Tye, R.S., 2000, Interpreting the dimensions of ancient fluvial channel bars, channels, and channel belts from wireline-logs and cores: American Association of Petroleum Geologists, Bulletin, v. 84, p. 1205–1228.
- Bridge, J.S. and Lunt, I.A., 2006. Depositional models of braided rivers (Vol. 36, pp. 11-50). Oxford, UK: Blackwell Publishing.
- Bristow, C.S., 1987. Brahmaputra River: channel migration and deposition. In: Ethridge, F.G., Flores, R.M., Harvey, M.D. (Eds.), Recent Developments in Fluvial Sedimentology. Society of Economic Paleontologists and Mineralogists, vol. 39. Special Publication, pp. 63–74.

- Bristow, C.S., 1993a. Sedimentology of the Rough Rock: A Carboniferous braided river sheet sandstone in northern England. Geological Society, London, Special Publications, 75(1), pp.291-304.
- Bristow, C.S., 1993b. Sedimentary structures exposed in bar tops in the Brahmaputra River, Bangladesh. Geological Society, London, Special Publications, 75(1), pp.277-289.
- Bristow, C.S., Best, J.L. and Roy, A.G., 1993. Morphology and facies models of channel confluences. Alluvial Sedimentation, pp.89-100.
- Bromley, R.G., Pemberton, S.G. and Rahmani, R.A., 1984. A Cretaceous woodground: the Teredolites ichnofacies. Journal of Paleontology, pp.488-498.
- Burgener, L., Hyland, E., Reich, B.J. and Scotese, C., 2023. Cretaceous climates: Mapping paleo-Köppen climatic zones using a Bayesian statistical analysis of lithologic, paleontologic, and geochemical proxies. Palaeogeography, Palaeoclimatology, Palaeoecology, 613, p.111373.
- Burns, C.E., Mountney, N.P., Hodgson, D.M. and Colombera, L., 2019. Stratigraphic architecture and hierarchy of fluvial overbank splay deposits. Journal of the Geological Society, 176(4), pp.629-649.
- Cant, D. J., 1982, Fluvial facies models, in P. A. Scholle and D. Spearing, eds., Sandstone depositional environments: AAPG Memoir 31, p. 115–138.
- Collinson, J.D., 1968. Deltaic sedimentation units in the Upper Carboniferous of northern England. Sedimentology, 10(4), pp.233-254.
- Collinson, J.D., 1970. Bedforms of the Tana River, Norway. Geografiska Annaler: Series A, Physical Geography, 52(1), pp.31-56.
- Dade, W.B., and Friend, P.F., 1998, Grain-size, sediment-transport regime, and channel slope in alluvial rivers: The Journal of Geology, v. 106, p. 661-676.
- Davidson, S.K., and North, C.P., 2009, Geomorphological regional curves for prediction of drainage area and screening modern analogues for rivers in the rock record: Journal of Sedimentary Research, v. 79, p. 773–792.

- DeCelles, P.G., 2004. Late Jurassic to Eocene evolution of the Cordilleran thrust belt and foreland basin system, western USA. American Journal of Science, 304(2), pp.105-168.
- DeCelles, P.G. and Giles, K.A., 1996. Foreland basin systems. Basin research, 8(2), pp.105-123.
- Dickinson, W.R. and Suczek, C.A., 1979. Plate tectonics and sandstone compositions. AAPG Bulletin, 63(12), pp.2164-2182.
- Donselaar, M.E. and Overeem, I., 2008. Connectivity of fluvial point-bar deposits: An example from the Miocene Huesca fluvial fan, Ebro Basin, Spain. AAPG bulletin, 92(9), pp.1109-1129.
- Egozi, R. and Ashmore, P., 2009. Experimental analysis of braided channel pattern response to increased discharge. Journal of Geophysical Research: Earth Surface, 114(F2).
- Eide, C.H., Müller, R. and Helland-Hansen, W., 2018. Using climate to relate water discharge and area in modern and ancient catchments. Sedimentology, 65(4), pp.1378-1389.
- Ethridge, F.G. and Schumm, S.A., 1977. Reconstructing paleochannel morphologic and flow characteristics: methodology, limitations, and assessment.
- Ferron, C., 2019. Detrital Zircon Signal Inversion in the Cretaceous Southwestern US Interior Seaway-A Case Study from the Gallup System New Mexico (master's dissertation).
- Fielding, C.R., 2006. Upper flow regime sheets, lenses and scour fills: extending the range of architectural elements for fluvial sediment bodies. Sedimentary Geology, 190(1-4), pp.227-240.
- Fielding, C.R., 2007. Sedimentology and stratigraphy of large river deposits: recognition in the ancient record, and distinction from "incised valley fills". Large Rivers: Geomorphology and Management, pp.97-113.
- Fisher, J.A., Krapf, C.B., Lang, S.C., Nichols, G.J. and Payenberg, T.H., 2008. Sedimentology and architecture of the Douglas Creek terminal splay, Lake Eyre, central Australia. Sedimentology, 55(6), pp.1915-1930.

- Flores, R.M., Hohman, J.C. and Ethridge, F.G., 1991. Heterogeneity of Upper Cretaceous Gallup sandstone regressive fades, Gallup Sag, New Mexico.
- Fouch, T.D., Lawton, T.F., Nichols, D.J., Cashion, W.B. and Cobban, W.A., 1983. Patterns and timing of synorogenic sedimentation in Upper Cretaceous rocks of central and northeast Utah. Rocky Mountain Section (SEPM).
- Friend, P.F., 1983. Towards the field classification of alluvial architecture or sequence. Modern and ancient fluvial systems, pp.345-354.
- Gibling, M.R., 2006. Width and thickness of fluvial channel bodies and valley fills in the geological record: a literature compilation and classification. Journal of sedimentary Research, 76(5), pp.731-770.
- Hampson, G.J., Jewell, T.O., Irfan, N., Gani, M.R. and Bracken, B., 2013. Modest change in fluvial style with varying accommodation in regressive alluvial-to-coastal-plain wedge: Upper Cretaceous Blackhawk Formation, Wasatch Plateau, central Utah, USA. Journal of Sedimentary Research, 83(2), pp.145-169.
- Harrald, J.E., Coe, A.L., Thomas, R.M. and Hoggett, M., 2021. Use of drones to analyse sedimentary successions exposed in the foreshore. Proceedings of the Geologists' Association, 132(3), pp.253-268.
- Hasbargen, L.E., 2012. A test of the three-point vector method to determine strike and dip utilizing digital aerial imagery and topography.
- Hayes, D.A., Botterill, S.E., Ranger, M.J. and Gingras, M.K., 2023. Fluvial character and architecture of an outcrop using sedimentology combined with UAV-based modeling, Cretaceous McMurray Formation, NE Alberta, Canada. Journal of Sedimentary Research, 93(5), pp.273-292.
- Hjellbakk, A., 1997. Facies and fluvial architecture of a high-energy braided river: the Upper Proterozoic Seglodden Member, Varanger Peninsula, northern Norway. Sedimentary Geology, 114(1-4), pp.131-161.
- Hohman, J.C., 1986. Depositional Model of Coal-bearing, Upper Cretaceous Gallup Sandstone, Gallup Sag Area, New Mexico (Doctoral dissertation, Colorado State University).

- Holbrook, J., and Wanas, H., 2014, A fulcrum approach to assessing source-to-sink mass balance using channel paleohydrologic parameters derivable from Common fluvial data sets with an example from the Cretaceous of Egypt: Journal of Sedimentary Research, v. 84, p. 349–372.
- Hudson, P.F. and Mossa, J., 1997. Suspended sediment transport effectiveness of three large, impounded rivers, US Gulf Coastal Plain. Environmental Geology, 32, pp.263-273.
- Jones, C.M., 1977. Effects of varying discharge regimes on bed-form sedimentary structures in modern rivers. Geology, 5(9), pp.567-570.
- Jones, E.R., 2017. Probabilistic source-to-sink analysis of the provenance of the California paleoriver: implications for the early Eocene paleogeography of western North America.
- Kimmerle, S. and Bhattacharya, J.P., 2018. Facies, backwater limits, and paleohydraulic analysis of rivers in a forced-regressive, compound incised valley, Cretaceous Ferron Sandstone, Utah, USA. Journal of Sedimentary Research, 88(2), pp.177-200.
- Kleinhans, M.G. and van den Berg, J.H., 2011. River channel and bar patterns explained and predicted by an empirical and a physics-based method. Earth Surface Processes and Landforms, 36(6), pp.721-738.
- Krstolic, J.L. and Chaplin, J.J., 2007. Bankfull regional curves for streams in the non-urban, non-tidal coastal plain physiographic province, Virginia and Maryland (No. 2007-5162). Geological Survey (US).
- Lanzoni, S., Luchi, R. and Pittaluga, M.B., 2015. Modeling the morphodynamic equilibrium of an intermediate reach of the Po River (Italy). Advances in Water Resources, 81, pp.95-102.
- Leclair, S.F., Bridge, J.S., and Wang, F., 1997, Preservation of cross-strata due to migration of subaqueous dunes over aggrading and non-aggrading beds: Comparison of experimental data with theory: Geoscience Canada, v. 24, p. 55–66.
- Leclair, S.F. and Bridge, J.S., 2001. Quantitative interpretation of sedimentary structures formed by river dunes. Journal of Sedimentary Research, 71(5), pp.713-716.

- Leite Ribeiro, M., Blanckaert, K., Roy, A.G. and Schleiss, A.J., 2012. Flow and sediment dynamics in channel confluences. Journal of Geophysical Research: Earth Surface, 117(F1).
- Leopold, L.B. and Maddock, T., 1953. The hydraulic geometry of stream channels and some physiographic implications (Vol. 252). US Government Printing Office.
- Leopold, L.B., Wolman, M.G. and Miller, J.P. (1964) Fluvial Processes in Geomorphology. Freeman, San Francisco, 522 p.
- Limaye, A.B., 2020. How do braided rivers grow channel belts?. Journal of Geophysical Research: Earth Surface, 125(8), p.e2020JF005570.
- Lin, W., and Bhattacharya, J.P., 2016, Estimation of Source-to-Sink Mass Balance and Depositional Systems Dominated Sediment Budgets by a Fulcrum Approach Assessment Using Channel Paleohydrologic Parameters: Cretaceous Dunvegan Formation: American Association of Petroleum Geologists, Search and Discovery article#41852.
- Lin, W., Bhattacharya, J.P. and Stockford, A., 2019. High-resolution sequence stratigraphy and implications for cretaceous glacioeustasy of the Late Cretaceous Gallup System, New Mexico, USA. Journal of Sedimentary Research, 89(6), pp.552-575. Miall, A.D., 1985. Architectural-element analysis: a new method of facies analysis applied to fluvial deposits.
- Lin, W., Kynaston, D., Ferron, C., Bhattacharya, J.P. and Matthews, W., 2021. Depositional and sequence stratigraphic model of transgressive shelf sandstone: The Late Cretaceous Tocito Sandstone, San Juan Bain, New Mexico, USA. Journal of Sedimentary Research, 91(4), pp.415-432.
- Liu, Y., Wortmann, M., Hawker, L., Neal, J., Yin, J., Santos, M.S., Anderson, B., Boothroyd, R., Nicholas, A., Smith, G.S. and Ashworth, P., 2024. Global Estimation of River Bankfull Discharge Reveals Distinct Flood Recurrences Across Different Climate Zones.
- Lunt, I.A. and Bridge, J.S., 2004. Evolution and deposits of a gravelly braid bar, Sagavanirktok River, Alaska. Sedimentology, 51(3), pp.415-432.

- Lynds, R. and Hajek, E., 2006. Conceptual model for predicting mudstone dimensions in sandy braided-river reservoirs. AAPG bulletin, 90(8), pp.1273-1288.
- McCandless, T.L., 2003, Maryland Stream Survey: Bankfull Discharge and Channel Characteristics of Streams in the Coastal Plain hydrologic regions: U.S. Fish and Wildlife Service, Annapolis, Maryland, Report CBFO-S03-02.
- McCabe, P.J., 1977. Deep distributary channels and giant bedforms in the Upper Carboniferous of the Central Pennines, northern England. Sedimentology, 24(2), pp.271-290.
- McCabe, P.J. and Jones, C.M., 1977. Formation of reactivation surfaces within superimposed deltas and bedforms. Journal of Sedimentary Research, 47(2), pp.707-715.
- McLaurin, B.T. and Steel, R.J., 2007. Architecture and origin of an amalgamated fluvial sheet sand, lower Castlegate Formation, Book Cliffs, Utah. Sedimentary Geology, 197(3-4), pp.291-311.
- Mertes, L.A., Dunne, T. and Martinelli, L.A., 1996. Channel-floodplain geomorphology along the Solimões-Amazon river, Brazil. Geological Society of America Bulletin, 108(9), pp.1089-1107.
- Metcalf, C., 2004, Regional Channel Characteristics for Maintaining Natural Fluvial Geomorphology in Florida Streams: U.S. Fish and Wildlife Service, Panama City, Fisheries Resource Office.
- Metcalf, C. and Shaneyfelt, R., 2005. Alabama riparian reference reach and regional curve study. US Fish and Wildlife Service, Panama City Fisheries Resource Office. Panama City, FL.
- Meybeck, M., Laroche, L., Dürr, H., and Syvitski, J.P.M., 2003, Global variability of daily total suspended solids and their fluxes in rivers: Global and Planetary Change, v. 39, p. 65–93.
- Miall, A.D., 1978. Lithofacies types and vertical profile models in braided rivers: a summary. In: Miall, A.D. (Ed.), Fluvial Sedimentology.: Memoir, 5. Canadian Society of Petroleum Geologists, Calgary, pp. 597–604.

- Miall, A.D., 1985. Architectural-element analysis: a new method of facies analysis applied to fluvial deposits.
- Miall, A.D., 1988. Architectural elements and bounding surfaces in fluvial deposits: anatomy of the Kayenta Formation (Lower Jurassic), southwest Colorado. Sedimentary Geology, 55(3-4), pp.233-262.
- Miall, A.D., 1992. Sedimentology of a sequence boundary within the nonmarine Torrivio Member, Gallup Sandstone (Cretaceous), San Juan Basin, New Mexico.
- Miall, A.D., 1993. The architecture of fluvial-deltaic sequences in the upper Mesaverde Group (Upper Cretaceous), Book Cliffs, Utah. Geological Society, London, Special Publications, 75(1), pp.305-332.
- Miall, A.D., 1996. The stratigraphic architecture of fluvial depositional systems. The Geology of Fluvial Deposits: Sedimentary Facies, Basin Analysis, and Petroleum Geology, pp.251-309.
- Miall, A.D., 2006. Reconstructing the architecture and sequence stratigraphy of the preserved fluvial record as a tool for reservoir development: A reality check. AAPG bulletin, 90(7), pp.989-1002.
- Miall, A.D., Catuneanu, O., Vakarelov, B.K. and Post, R., 2008. The Western interior basin. Sedimentary basins of the world, 5, pp.329-362.
- Miall, A.D. and Jones, B.G., 2003. Fluvial architecture of the Hawkesbury sandstone (Triassic), near Sydney, Australia. Journal of Sedimentary Research, 73(4), pp.531-545.
- Milliman, J.D., 1980. Sedimentation in the Fraser River and its estuary, southwestern British Columbia (Canada). Estuarine and Coastal Marine Science, 10(6), pp.609-633.
- Milliman, J.D. and Meade, R.H., 1983. World-wide delivery of river sediment to the oceans. The Journal of Geology, 91(1), pp.1-21.
- Milliman, J.D. and Syvitski, J.P., 1992. Geomorphic/tectonic control of sediment discharge to the ocean: the importance of small mountainous rivers. The journal of Geology, 100(5), pp.525-544.
- Molenaar, C.M., 1973. Sedimentary facies and correlation of the Gallup Sandstone and associated formations, northwestern New Mexico.

- Molenaar, C.M., 1974, Correlation of the Gallup Sandstone and associated formations, upper cretaceous, eastern San Juan and Acoma Basins, New Mexico. In Ghost Ranch: New Mexico Geological Society Guidebook, 25th Field Conference (pp. 251-258).
- Molenaar, C.M., 1977. The Pinedale oil seep-an exhumed stratigraphic trap in the southwestern San Juan Basin. In San Juan Basin III: New Mexico Geol. Soc. Guidebook, 28th Field Conference (p. 243).
- Molenaar, C.M., 1983. Major depositional cycles and regional correlations of Upper Cretaceous rocks, southern Colorado Plateau and adjacent areas. Rocky Mountain Section (SEPM).
- Mosley, M.P., 1983. Response of braided rivers to changing discharge. Journal of Hydrology (New Zealand), pp.18-67.
- Nash, D.B., 1994, Effective sediment-transporting discharge from magnitude-frequency analysis: The Journal of Geology, v. 102, p. 79-95.
- Nummedal, D., 1990, Sequence stratigraphic analysis of upper Turonian and Coniacian strata in the San Juan basin, New Mexico, U.S.A., in R.N. Ginsburg and B. Beaudoin, eds., Cretaceous resources, events and rhythms: Dordrecht, Kluwer Publishing, p. 33–46.
- Nummedal, D. and Molenaar, C.M., 1995. Sequence stratigraphy of ramp-setting strand plain successions: the Gallup Sandstone, New Mexico.
- Nummedal, D. and Riley, G.W., 1991. Origin of late Turonian and Coniacian unconformities in the San Juan basin.
- Nummedal, D. and Swift, D.J., 1987. Transgressive stratigraphy at sequence-bounding unconformities: some principles derived from Holocene and Cretaceous examples.
- Nyberg, B., Helland-Hansen, W., Gawthorpe, R., Tillmans, F. and Sandbakken, P., 2021. Assessing first-order BQART estimates for ancient source-to-sink mass budget calculations. Basin Research, 33(4), pp.2435-2452.
- Olsen, T., Steel, R., Hogseth, K., Skar, T. and Roe, S.L., 1995. Sequential architecture in a fluvial succession; sequence stratigraphy in the Upper Cretaceous Mesaverde Group, Prince Canyon, Utah. Journal of Sedimentary Research, 65(2b), pp.265-280.

- Parker, G., 1976. On the cause and characteristic scales of meandering and braiding in rivers. Journal of fluid mechanics, 76(3), pp.457-480.
- Parker, G., 2004, 1D Sediment Transport Morphodynamics with Applications to Rivers and Turbidity Currents: E book, http://www.nced.umn.edu/.
- Parker, G., 2008, Transport of gravel and sediment mixtures, Chapter 3, Sedimentation Engineering, in Garcia, M.H., ed., Processes, Measurements, Modeling and Practice: American Society of Civil Engineers, Manuals and Reports on Engineering Practice, no. 110, p. 165–252.
- Parsons, D.R., Best, J.L., Lane, S.N., Kostaschuk, R.A., Hardy, R.J., Orfeo, O., Amsler, M.L. and Szupiany, R.N., 2008. Large river channel confluences. River confluences, tributaries and the fluvial network, pp.73-91.
- Peel, M.C., Finlayson, B.L. and McMahon, T.A., 2007. Updated world map of the Köppen-Geiger climate classification. Hydrology and earth system sciences, 11(5), pp.1633-1644.
- Pemberton, S.G., MacEachern, J.A. and Saunders, T., 2004. Stratigraphic applications of substrate-specific ichnofacies: delineating discontinuities in the rock record.
- Phillips, J.D., 2015. Hydrologic and geomorphic flow thresholds in the Lower Brazos River, Texas, USA. Hydrological sciences journal, 60(9), pp.1631-1648.
- Pickup, G., and Warner, R.F, 1976, Effects of hydrologic regime on magnitude and frequency of dominant discharge: Journal of Hydrology, v. 29, p. 51-75.
- Plint, A.G., McCarthy, P.J. and Faccini, U.F., 2001. Nonmarine sequence stratigraphy: updip expression of sequence boundaries and systems tracts in a high-resolution framework, Cenomanian Dunvegan Formation, Alberta foreland basin, Canada. AAPG bulletin, 85(11), pp.1967-2001.
- Plint, A.G. and Wadsworth, J.A., 2003. Sedimentology and palaeogeomorphology of four large valley systems incising delta plains, western Canada Foreland Basin: Implications for mid-Cretaceous sea-level changes. Sedimentology, 50(6), pp.1147-1186.
- Potter, P.E., 1978. Significance and origin of big rivers. The Journal of Geology, 86(1), pp.13-33.

- Raines, T.H., 1998. Peak-discharge frequency and potential extreme peak discharge for natural streams in the Brazos River basin, Texas (Vol. 98, No. 4178). US Department of the Interior, US Geological Survey.
- Riley, Gregory Wayne, "Origin of a Coarse-Grained Shallow Marine Sandstone Complex: The Coniacian Tocito Sandstone, Northwestern New Mexico. (Volumes 1 and 2)." (1993). LSU Historical Dissertations and Theses. 5541.
- Rhoads, B.L., 2020. River dynamics: Geomorphology to support management. Cambridge University Press.
- Roberts, L.N.R. and Kirschbaum, M.A., 1995. Paleogeography of the Late Cretaceous of the Western Interior of middle North America: Coal distribution and sediment accumulation (No. 1561). US Government Printing Office.
- Rubin, D.M. and McCulloch, D.S., 1980. Single and superimposed bedforms: a synthesis of San Francisco Bay and flume observations. Sedimentary Geology, 26(1-3), pp.207-231.
- Rust, B.R. and Jones, B.G., 1987. The Hawkesbury Sandstone south of Sydney, Australia; Triassic analogue for the deposit of a large, braided river. Journal of Sedimentary Research, 57(2), pp.222-233.
- Sambrook Smith, G.H., Ashworth, P.J., Best, J.L., Woodward, J. and Simpson, C.J., 2006. The sedimentology and alluvial architecture of the sandy braided South Saskatchewan River, Canada. Sedimentology, 53(2), pp.413-434.
- Sambrook Smith, G.H., Nicholas, A.P., Best, J.L., Bull, J.M., Dixon, S.J., Goodbred, S., Sarker, M.H. and Vardy, M.E., 2019. The sedimentology of river confluences. Sedimentology, 66(2), pp.391-407.
- Sarker, M.H. and Thorne, C.R., 2006. Morphological response of the Brahmaputra–Padma–Lower Meghna River system to the Assam earthquake of 1950. Braided Rivers: process, deposits, ecology and management, 36, pp.289-310.
- Sarker, M.H., Thorne, C.R., Aktar, M.N. and Ferdous, M.R., 2014. Morpho-dynamics of the Brahmaputra–Jamuna River, Bangladesh. Geomorphology, 215, pp.45-59.

- Schumm, S.A. and Hadley, R.F., 1961. Progress in the application of landform analysis in studies of semiarid erosion (Vol. 437). US Department of the Interior, Geological Survey.
- Searcy J. K., 1959 Flow-duration curves. U.S. Geological Survey water supply paper 1542-A. U.S. Geological Survey, Washington, D.C.
- Sharma, S., Bhattacharya, J.P. and Richards, B., 2017. Source-to-sink sediment budget analysis of the Cretaceous Ferron Sandstone, Utah, USA, using the fulcrum approach. Journal of Sedimentary Research, 87(6), pp.594-608.
- Smith, N.D., 1974. Sedimentology and bar formation in the upper Kicking Horse River, a braided outwash stream. The Journal of Geology, 82(2), pp.205-223.
- Smith, N. (1978) Some comments on terminology for bars in shallow rivers. In: Fluvial Sedimentology (Ed A.D. Miall), pp. 85-88. Canadian Society of Petroleum Geologists, Calgary, Alberta, Canada.
- Sprague, A.R.G., Garfield, T.R., Goulding, F.J., Beaubouef, R.T., Sullivan, M.D., Rossen, C., Campion, K.M., Sickafoose, D.K., Abreu, V., Schellpeper, M.E. and Jensen, G.N., 2005. Integrated slope channel depositional models: the key to successful prediction of reservoir presence and quality in offshore West Africa. Veracruz, Mexico, Colegio de Ingenenieros Petroleros de México, pp.1-13.
- Stojic, M., Chandler, J., Ashmore, P. and Luce, J., 1998. The assessment of sediment transport rates by automated digital photogrammetry. Photogrammetric Engineering and Remote Sensing, 64(5), pp.387-395.
- Strom, K., 2013. Suspended sediment sampling and annual sediment yield on the lower Brazos River. Department of Civil and Environmental Engineering, University of Houston.
- Suttner, L.J. and Dutta, P.K., 1986. Alluvial sandstone composition and paleoclimate; I, Framework mineralogy. Journal of Sedimentary Research, 56(3), pp.329-345.
- Sweet, W.V, and Geratz, J.W., 2003, Bankfull hydraulic geometry relationships and recurrence intervals for North Carolina's Coastal Plain: Journal of the American Water Resources Association, v. 39, p. 861–871.

- Syvitski, J.P. and Milliman, J.D., 2007. Geology, geography, and humans battle for dominance over the delivery of fluvial sediment to the coastal ocean. The Journal of Geology, 115(1), pp.1-19.
- Takagi, T., Oguchi, T., Matsumoto, J., Grossman, M.J., Sarker, M.H. and Matin, M.A., 2007. Channel braiding and stability of the Brahmaputra River, Bangladesh, since 1967: GIS and remote sensing analyses. Geomorphology, 85(3-4), pp.294-305.
- Thorne, C.R., Russell, A.P. and Alam, M.K., 1993. Planform pattern and channel evolution of the Brahmaputra River, Bangladesh. Geological Society, London, Special Publications, 75(1), pp.257-276.
- Ullah, M. S., Bhattacharya, J. P., and Dupre, W. R., 2015, Confluence scours versus incised valleys: Examples from the Cretaceous Ferron Notom Delta, Southeastern Utah, USA: Journal of Sedimentary Research, v. 85, p. 445-458.
- Valdes, P.J., Scotese, C.R. and Lunt, D.J., 2020. Deep ocean temperatures through time. Climate of the Past Discussions, 2020, pp.1-37.
- Van den Berg, J.H., 1995. Prediction of alluvial channel pattern of perennial rivers. Geomorphology, 12(4), pp.259-279.
- van Rijn, L.C., 1984b, Sediment transport, Part II: Suspended load transport: Journal of Hydraulic Engineering, v. 110, p. 1613-1641.
- Vital, H., Stattegger, K., Posewang, J. and Theilen, F., 1998. Lowermost Amazon River: morphology and shallow seismic characteristics. Marine Geology, 152(4), pp.277-294.
- Vogel, R.M. and Fennessey, N.M., 1994. Flow-duration curves. I: New interpretation and confidence intervals. Journal of Water Resources Planning and Management, 120(4), pp.485-504.
- Walker, R.G. and Cant, D.J., 1984. Sandy fluvial systems. *Facies models*, 1, pp.71-89.
- Weimer, R.J.,1984. Relationship of unconformities, tectonics and sea level changes, Cretaceous Western Interior, United States of America. In: Schlee, J.S. (Eds.), Interregional Unconformities and Hydrocarbon Accumulation. American Association of Petroleum Geologists, memoir 36, 7-36.

- Wilkerson, G.V., and Parker, G., 2011, Physical basis for quasi-universal relationships describing bankfull hydraulic geometry of sand-bed rivers: Journal of Hydraulic Engineering, v. 137, p. 739–753.
- Willis, B., 1993a. Ancient river systems in the Himalayan foredeep, Chinji Village area, northern Pakistan. Sedimentary geology, 88(1-2), pp.1-76.
- Willis, B., 1993b. Evolution of Miocene fluvial systems in the Himalayan foredeep through a two kilometer-thick succession in northern Pakistan. Sedimentary geology, 88(1-2), pp.77-121.
- Wilson, L., 1972. Seasonal sediment yield patterns of US rivers. Water Resources Research, 8(6), pp.1470-1479.
- Wright, S., and Parker, G., 2004, Flow resistance and suspended load in sand-bed rivers: Simplified stratification model: Journal of Hydraulic Engineering, v. 130, p. 796–805.
- Woods, L.J. 1992. Influence of Base-level Change on Coastal Plain, Shelf and Slope Deposition Systems. Unpublished PhD. Dissertation, Colorado State University, Fort Collins, Colorado, 164 p.
- Wu, C., Bhattacharya, J.P. and Ullah, M.S., 2015. Paleohydrology and 3D facies architecture of ancient point bars, Ferron Sandstone, Notom Delta, south-central Utah, USA. *Journal of Sedimentary Research*, 85(4), pp.399-418.
- Yu, B., and Wolman, M.G., 1987, Some dynamic aspects of river geometry: Water Resources Research, v. 23, p. 501-509.

Chapter 4

Scale of confluence scours in the late Cretaceous Torrivio Sandstone, NM, USA

Confluence scours represent the deepest areas in fluvial systems produced by autogenic processes. Although scour fills have a higher probability of being preserved in the rock record, only a few ancient examples have been documented in the literature. In the rock record, confluence deposits can be recognized by the presence of anomalously thick single storey channel fills, which should be bounded at the base by fifth-order erosive channel surfaces and on top by fourth-order surfaces. The deposits may also show single out-sized, steeply dipping foresets filling a scour.

This chapter focuses on braided stream deposits of the late Cretaceous Torrivio Sandstone in north-western New Mexico, USA. These outcrops show a variety of scales of confluence scours and their deposits, ranging from smaller bar-scale deposits, characterized by compound bars consisting of multiple cross-set units, to a larger scale tributary junction. The latter is represented by a single 12 m, downstream migrating bar, bounded by surfaces characteristics of confluence deposits. The much larger scale feature is rare, with only one example found in otherwise continuous cliff exposures and is best explained as a confluence at a tributary junction. The increased accommodation at the site is also shown in the values of the median cross-set thickness (60 cm) and that of the thickest cross-set (2.5 m), which is considerably more than those at the upstream channels at 30 cm and < 1 m respectively. The relative scour depth to confluence angle scaling relationship estimates the confluence angle to be approximately 46°. Detailed architectural analysis and establishing bounding surface hierarchy on cross-sectional geometries exposed in outcrops, as well as identification of outsize scour fills can help distinguish deep confluence deposits from multistorey incised valley fills.

4.1 Introduction

Fluvial confluence scours occur where channel threads converge, such as at confluence zones at the downstream margin of braid bars, or where tributaries join a main channel or another tributary. These are marked scours that are much deeper than the mean bankfull channel depth. Although cross set thickness of dunes has been used to infer channel flow depths (Bridge 1997; LeClair et al. 1997; LeClair and Bridge 2001), cross-set thickness of a confluence scour may be significantly thicker and may not be representative of the mean bankfull flow depth. Thus, differentiating confluence scour fills is significant for accurate estimation of paleohydraulic parameters that can be used to determine sediment transport strength, paleodischarge, and sediment flux of a fluvial system (Bhattacharya and Tye 2004; Holbrook and Wanas 2014; Bhattacharya et al. 2016; Lin and Bhattacharya 2016; Sharma et al. 2017). Confluence scours are autogenic in nature and should be distinguished from incised valleys, which are allogenic and typically much more extensive in area (Ullah et al. 2015).

The deposits of confluence zones should be readily represented in ancient systems, as confluences represent the deepest scours, which increases their likelihood of preservation. However, only a handful of studies on ancient systems have identified deposits associated with confluence scours. This could be due to difficulty in identifying what constitutes their deposits. Previous studies have described the deposits of the confluence scours to include large-scale unit bars, commonly marked by single large-scale foreset beds, bounded by surfaces of higher order (Ullah et al. 2015; Smith et al. 2019), compound bars (Bridge 2003; Smith et al. 2019), or deposits dissected by multiple erosional surfaces (Sieganthaler and Huggenberger 1993).

This outcrop-based study documents confluence scours ranging from simple bar scale to large tributary confluence scour fill in the Late Cretaceous Torrivio Sandstone in northwest New Mexico, USA and in doing so identifies features that can be used in the field to distinguish different scales of confluence fill. Also discussed are the importance of architecture analysis to distinguish deposits of rivers belonging to different scales.

4.2 Confluence morphology

Experimental studies (Smith et al. 2019) have described places in a fluvial system where scours can form. These include, scours formed downstream of a braid bar, scours formed at the outer bend of a channel, which can be formed in single thread meandering streams, scours formed at the junction of two tributaries, and scours formed downstream of the confluence two or more channels (Smith et al. 2019).

Experimental studies have also shown that river channel confluences generally constitute distinct morphological units (Mosley 1976; Best 1988). In larger-scale stream (Fig. 4.1) these include a tributary mouth bar at the junction of two merging channels, a major deep scour hole elongated in the direction of the channel with higher discharge (assuming uneven discharge between the two), a bar downstream of the scour hole, and flow separation bars attached to the channel flanks (Mosley 1976; Best 1988; Bristow et al. 1993; Best and Rhoads 2008).

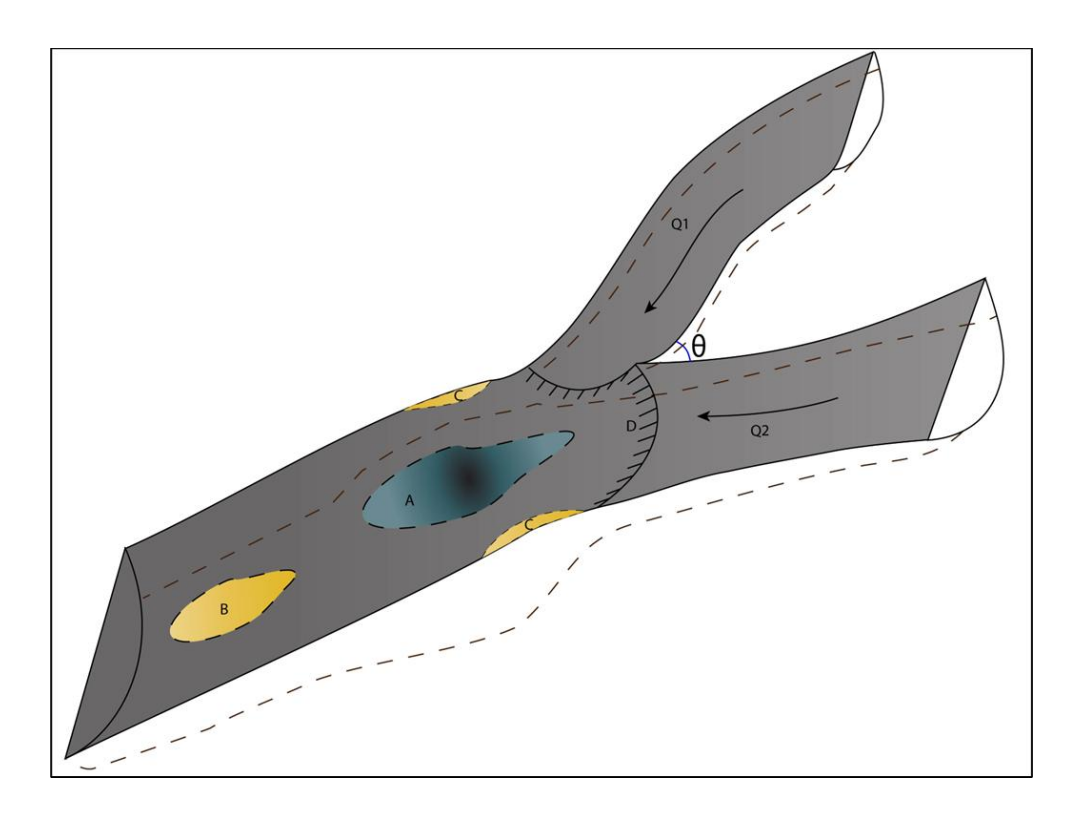


Figure 4.1. Schematic diagram showing the confluence geometry and morphological units. Q1 and Q2 represent discharge of the incoming channels, θ is the confluence

angle, A represents the confluence scour, B is the bar downstream of the confluence, C is the flow separation bar, and D represents the tributary mouth bar (modified after Bristow et al. (1993)).

The overall geometry of the confluence zone is shaped by factors such as (i) the ratio of the discharge of the incoming channels (Mosley 1976; Best 1988), wherein the scour hole either bisects the junction angle, in the case of equal discharge in the two channels or is preferentially elongated to the channel with higher discharge (Mosley 1976). The scour depth increases with the increase in the tributary discharge relative to that of the main channel (Best 1988), and (ii) the junction angle at which the two channels meet (Mosley 1976; Best 1988). The scour depth increases with the angle of confluence, although the increase is nonlinear in nature (Mosley 1976; Best 1988; Ahadiyan et al. 2018). The steepest increase in scouring occurs between 15° and 80° junction angle, while relatively little scouring happens either side of this range (Mosley 1976; Best 1988; Best and Rhoads 2008). It has also been found that at a given junction angle, larger junctions have relatively smaller scour depths (Smith et al. 2005; Best and Rhoads 2008). However, a scour depth of more than 70 m has been documented at the confluence of the Negros and the Solimoes River in Brazil (Ianniruberto et al. 2018). This is much deeper than the average upstream depth of 20 m (Ianniruberto et al. 2018) The mid-channel bar downstream of the confluence scour forms mainly due to flow deceleration and joining of the two channels (Mosley 1976; Best 1986, 1988; Dixon et al. 2018).

Confluence scours and their deposits have been documented in the modern (Ashmore and Parker 1983; Best 1988; Klassen and Vermeer 1988; Ashmore 1993; Biron et al. 1993; Bristow and Best 1993; Bristow et al. 1993; Best and Ashworth 1997; Smith et al. 2005; Dixon et al. 2018) and ancient fluvial systems (Cowan 1991; Huggenberger 1993; Siegenthaler and Huggenberger 1993; Miall and Jones 2003; Heintz et al. 2003; Kostic and Aigner 2007; and Ullah et al. 2015). Confluence scours are typically bounded by a sharp and erosive fifth order surface (Miall 1985) and filled with anomalously thick unit bar foresets, commonly capped by a compound bar deposit (Ullah et al. 2015). However, bar-scale confluences, such as those downstream of braid bars (Smith et al. 2019), may produce deposits that resemble thick fining-up compound bars, with individual cross-sets

decreasing in thickness upwards. Owing to repeated reworking and erosion, the extent of these deposits might be limited with less than ten cross-sets comprising one compound bar (Bridge 2003; Bridge and Lunt 2006; Smith et al. 2019).

4.3 The Torrivio Sandstone, regional setting and previous work

The Torrivio sandstone of the Crevasse Canyon Formation is a mixed-influence river deposit that erosionally overlies the Turonian Gallup Sandstone in the San Juan Basin, New Mexico. It was deposited as part of a number of clastic wedges that built into the western margin of the Cretaceous Interior Seaway of North America (Molenaar 1973, 1974, 1983; Nummedal and Swift 1987; Nummedal 1990; Nummedal and Riley 1991; Nummedal and Molenaar 1995). Further details of the regional setting are given in Chapter 3. Previous work on the Torrivio suggest it was a braided stream, but this was primarily based on its high sandstone content reflecting amalgamation of channel belt deposits (Molenaar 1973, 1977; Hohman 1986, Flores et al. 1991). In Chapter 3, we use detailed bedding diagrams to illustrate that the Torrivio rivers show an evolution from simple braided to single thread. In this paper, we focus on a number of different scales of confluence scours that are well represented, and their implications for fluvial sequence stratigraphy and interpretation of paleohydraulics.

4.4 Study area and methodology

Multiple sections, both strike and dip oriented, show features characteristic of the confluence scour fill. Sections SS-1, SS-2, SS-3, DS-1 and DS-2 are used in this chapter, with specific focus on DS-2, which lies approx. 3 km east of Nose Rock Point (Fig. 4.2). The litho-facies classification, identification of architectural elements and the approach to generating bedding diagrams have been described in the previous chapter.

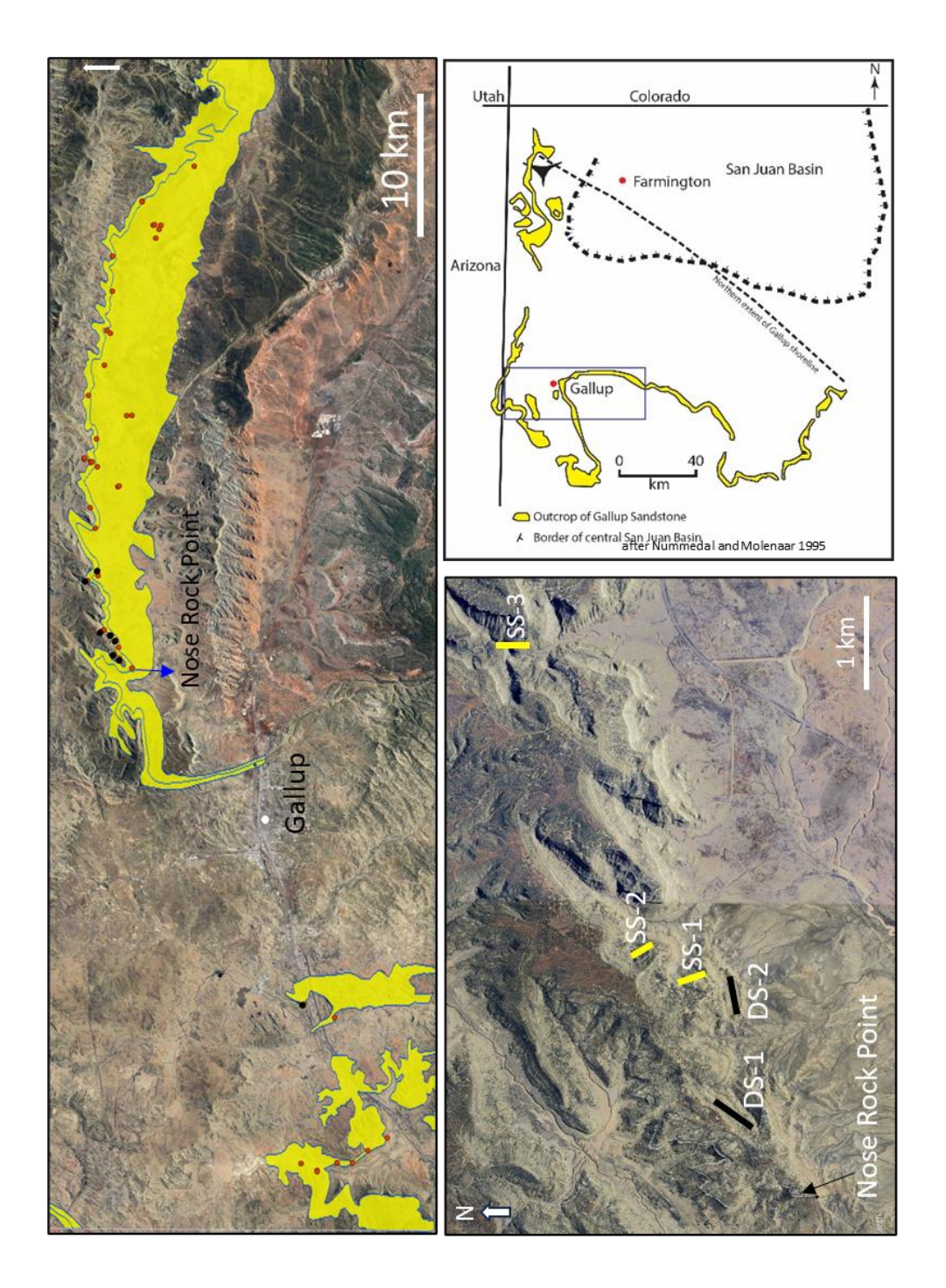


Figure 4.2. The measured sections done throughout the study campaign are represented by red circles while the sections with confluences are shown by the black circles. Outcrop map of Torrivio New Mexico, USA is modified after Nummedal and Molenaar, 1995. The tributary channel confluence is present at DS-2, small-scale

channel confluence can be seen at DS-1 and SS-1 while bar-scale confluence can be seen at SS-2 and SS-3.

4.5 Bedding geometry of DS-2

The main unit of the Torrivio Sandstone at DS-2 (Fig. 4.3) is represented by a single downstream migrating bar, which is approximately 12 m thick. The downstream migration of the bars was established by studying the relationship between the 3rd order bar bounding surfaces and the cross sets therein (Miall 1988). The bars are migrating to the east, with a median of 82° (n = 22) whereas the paleo-flow direction is due north-east, with a median of 49° (n = 141) (Fig. 4.3). Regional paleo-flow direction due NE was also reported by Hohman (1986). Therefore, it can be concluded that the bars in question are indeed migrating downstream. This is in sharp contrast to the previous study by Miall (1992), in which the same unit was identified as a laterally migrating fluvial point bar.

A cross-bar channel can be seen truncating these bars (Fig. 4.3) towards the updip side of the outcrop. This channel is approximately 3 m deep and 30 m wide. The paleoflow direction within this channel is towards the SE, with a median of 169° (n = 3). A few of the bars within the main unit also show signs of bar rotation and truncation, shown by the 4th order surfaces (Fig. 4.3). The individual bars, particularly the ones in the downstream direction, are draped by thin layers of silt and mudstone.

Above this unit, and separated by a floodplain facies, which is characterized by coaly mudstone with rootlets, lies the upper unit of the Torrivio Sandstone. This unit is approximately 12 m at its thickest updip location. This unit is characterized by multiple sub-units with different accretion directions. The 3rd order surfaces can be seen dipping to the west in the up-dip part of the section, whereas they dip downstream in the downdip part towards east. Although paleoflow from the dune-scale cross-sets is not available for the upslope dipping beds, the bar bounding surfaces can be clearly seen dipping upslope. The more eastern (downslope) bars are accreting to the east and the paleo-flow direction for these is also due east, with a median of 88° (n = 4). Therefore, this unit most probably represents a downstream migrating fluvial point bar with up-current dipping beds

representing bar rotation and /or expansion (Ghinassi and Ielpi 2015; Ghinassi et al. 2016). In the west part of the section, this is followed by ripple laminated sandstone lenses encased within mudstone, representing abandonment facies. This is followed by smaller ~4 m thick 5th order scour surfaces filled in by multiple bars migrating into the channel (Fig. 4.3).

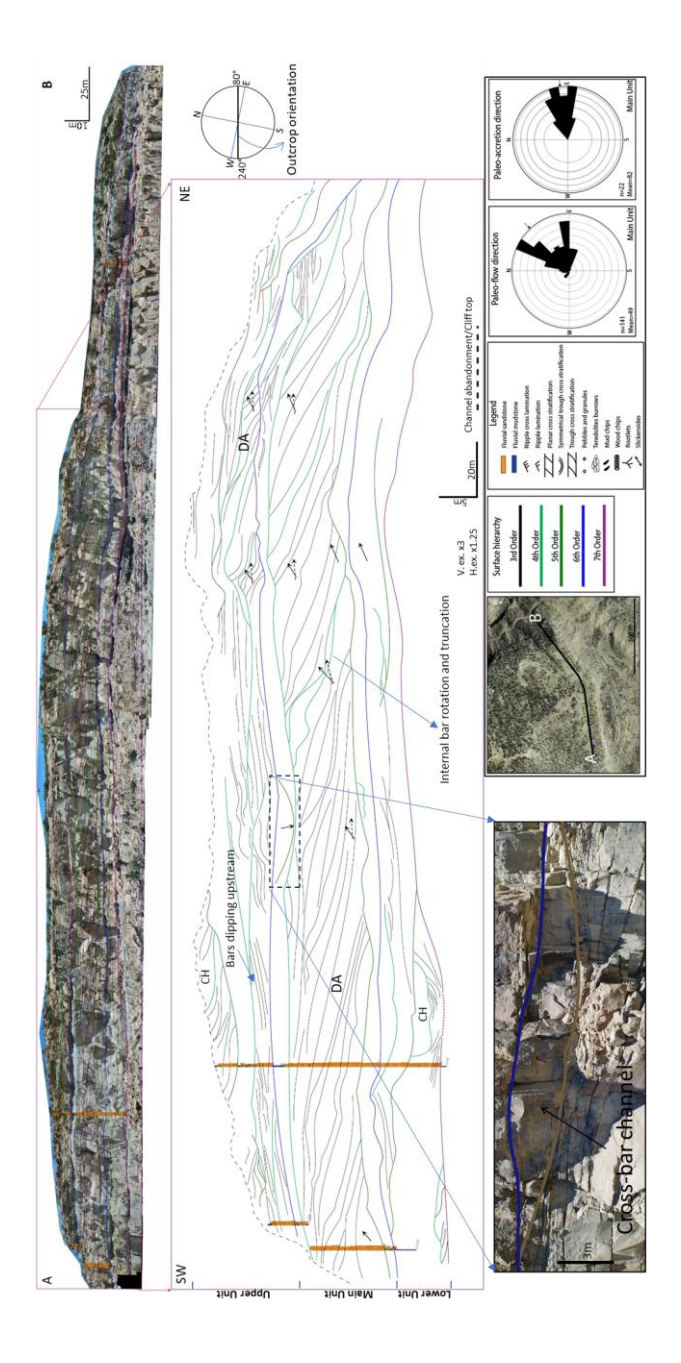


Figure 4.3. The main unit in DS-2 consists of a large downstream migrating bar. The oblique relationship between the paleo-flow and paleo-accretion direction within the

main unit is highlighted in the Rose diagrams. The upper Torrivio unit shows evidence of downstream migrating fluvial point bar. The section is oriented relative to the outcrop with the solid arrows highlighting paleo-flow direction and dashed arrows showing the paleo-accretion direction.

4.6 Scale of confluence scours in the Torrivio Sandstone

Confluence scours of different scales are seen in the outcrops of the Torrivio Sandstone. These vary from smaller scale features occurring at the junction downstream of interpreted braid bars, to the larger scale, interpreted to be where two tributaries meet, or a tributary meets a main channel. We should generally expect to find multiple bar-scale confluence scours in the deposits of a braided river. However, tributary junction scours should not be as common.

4.6.1. Confluence scours downstream of braid bars

The deposits of the confluence scours downstream of mid-channel bars can be seen at a few of the outcrops observed in this study. These are characterized by compound bars consisting of up to multiple cross-set units, although thicker deposits might be expected if not for reworking and truncation. Both the 4th order and 5th order surfaces can form the erosive base of these deposits (Bridge 2003; Smith et al. 2019). These are relatively limited in their lateral extent (Smith et al. 2019). In SS-2 (Fig. 4.4), seven cross-bedded units can be seen forming a compound bar filling the confluence scours. The total thickness of the deposit is about 2 m and the thickest unit at the bottom is about 1 m. The thickness of the rest of the cross-sets decreases upwards. The cross laminae in the bottom unit bar does not seem to be dipping into the scour at a steeper angle.

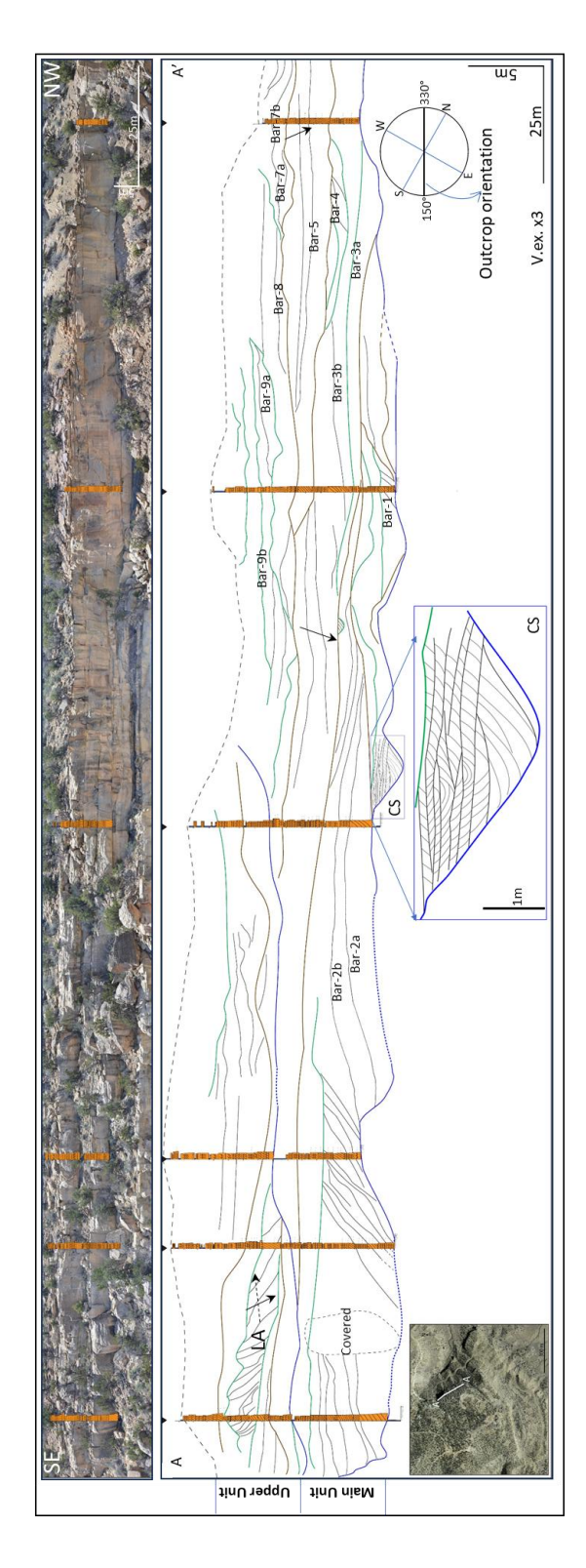


Figure 4.4. SS-2 showing braid bars with mounded geometries. Bar-scale confluence scour (CS) with 7 cross-set units. Refer to Fig. 4.3 for legends and symbols.

Similarly, in SS-3 (Fig. 4.5) a compound bar less than 2 m thick and bounded by a 4th order erosive scour can be seen. Six cross-sets can be seen, with the bottom-most unit bar approx. 1 m thick. It might be possible that more of these deposits are present in the outcrops, but truncation and reworking renders their identification difficult. However, making detailed bedding diagrams, as has been done here, makes it easier to identify at least a few of these deposits.

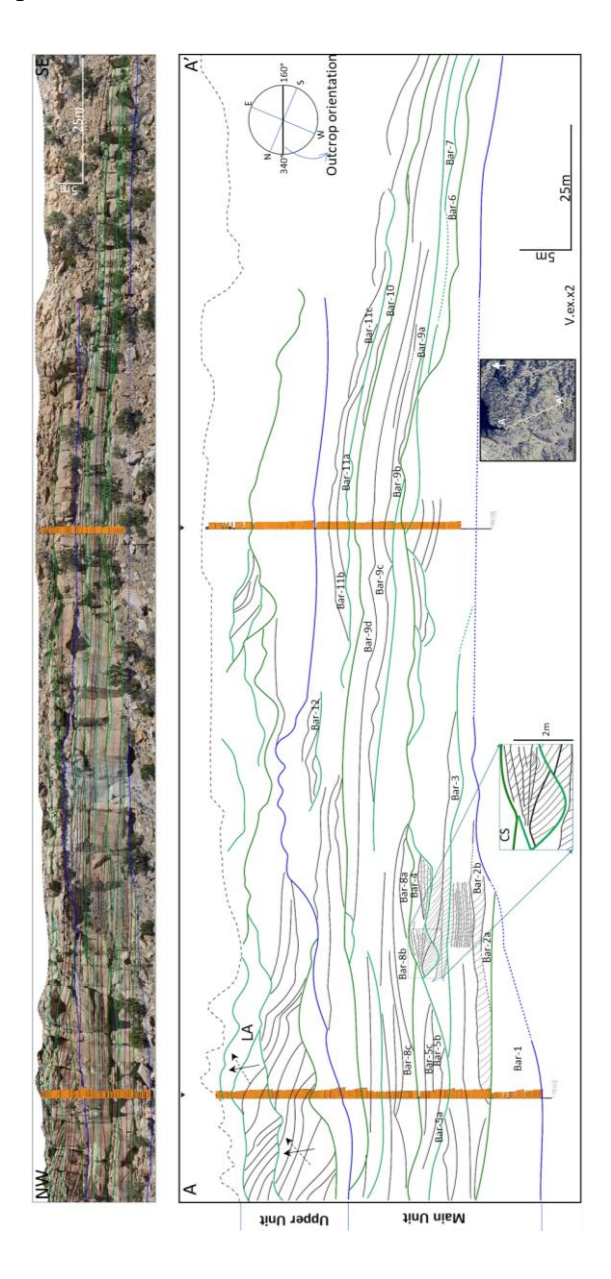


Figure 4.5. SS-3 showing bar-scale confluence (CS) fill with 6 units of cross-stratification. See Fig. 4.3 for legends and symbols.

4.6.2. Channel confluence scours

Channel confluence scours can be seen at multiple places in the Torrivio Sandstone. These can be differentiated into small-scale and large-scale confluence scours. The small-scale scour fills are characterized by a single set of oversized foresets dipping obliquely at a steeper angle into the scour (Fig. 4.6 and 4.7). The scour bases are represented by 5th order bounding surfaces while 4th order surfaces form the top of the deposits. The large foresets represent the avalanching face of a tributary mouth bar moving into the scour hole (Best 1988; Bristow et al. 1993; Smith et al. 2019). These avalanche faces dip into the scour hole at a sharp angle and are characteristic of smaller scale junctions (Parsons et al. 2008; Leite Ribiero et al. 2012). The progradation of the avalanche faces varies inversely with the junction angle and the discharge ratio and may be absent at very low confluence angles (Best 1988).

The example in Fig. 4.6 shows a single foreset, which is 2.25 m thick and dips obliquely into a scour. The erosive base of the scour represents a fifth order channel bounding surface, and the top of the fill is a fourth order macroform bounding surface (Miall 1985). Fig. 4.7A shows another such confluence with a 2.25 m thick foreset terminating at the channel base at a sharp angle. This foreset is overlain by cosets of dune-scale cross beds. The scour-fill in Fig. 4.7B is another such example represented by a foreset, which reaches up to 3.9 m in thickness. Although a bedding diagram is not available here, the measured section shows an erosive channel base below the foreset (Fig. 4.7B).

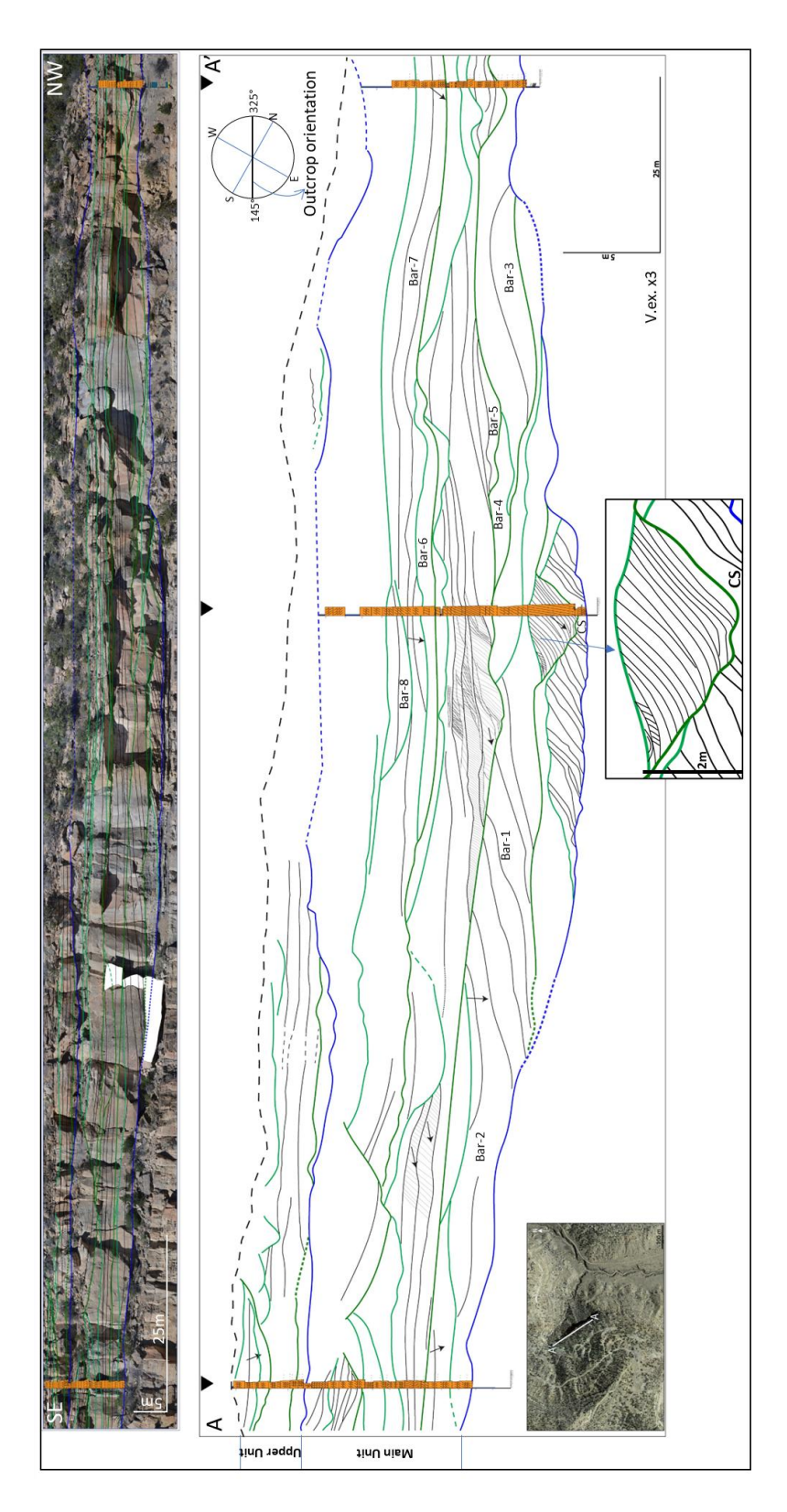


Figure 4.6. SS1 showing a 2.25 m thick foreset dipping at a steep angle into a small-scale channel-confluence scour (CS). See Fig. 4.3 for legends and symbols.

146

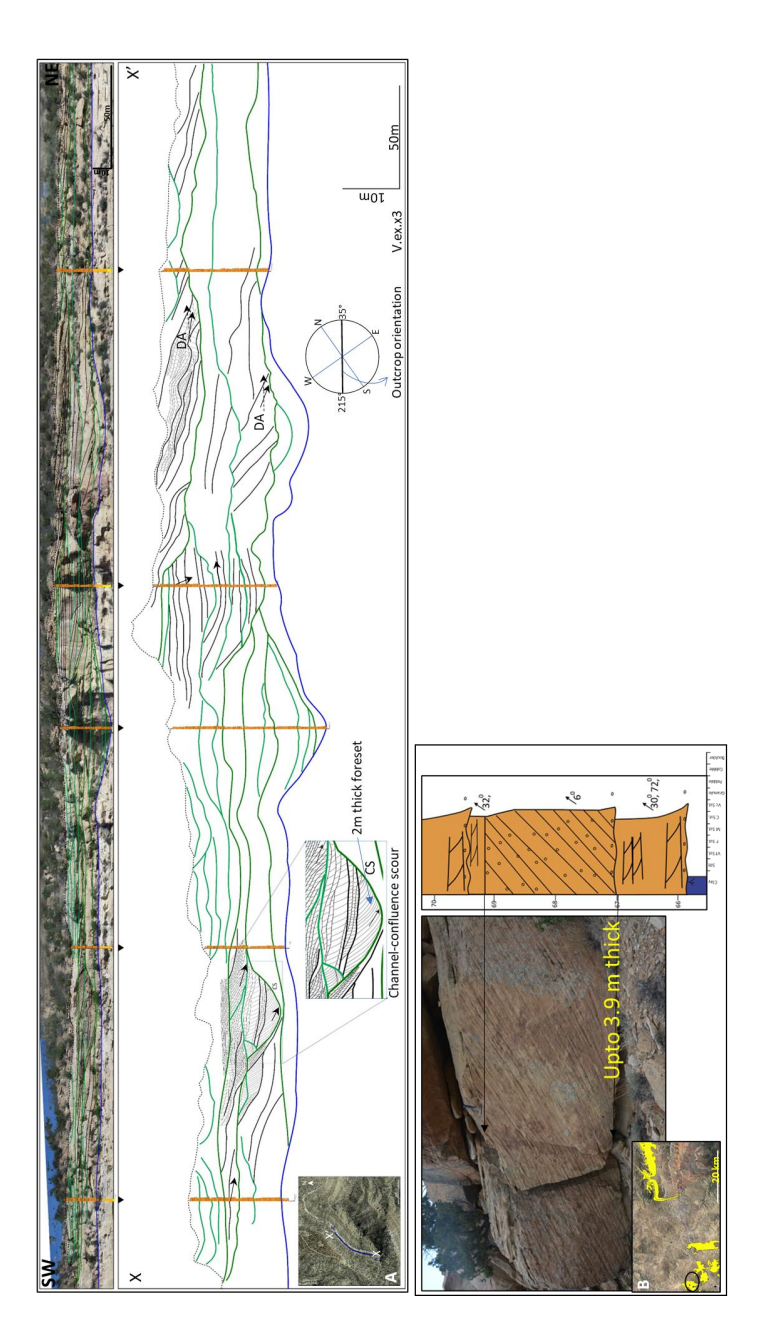


Figure 4.7. A) Oblique dip section with a 2 m thick foreset showing small-scale channel confluence. B) Steeply inclined bar, which reaches a thickness of up to 3.9 m, prograding into a channel confluence scour.

At larger scale, the channel confluence scours should be easily identifiable, as is the case here. One geographical spot (approx. 2 km east of Nose Rock Point, Fig. 4.2), shows a single 12 m thick, downstream accreting bar (Fig. 4.3). This out-sized unit is bounded at the base by a fifth-order channel bounding surface while the individual bars are bounded

by third order surfaces and are interpreted to represent deposition within a single channel (Ullah et al. 2015). As explained earlier, the scour and fill of this magnitude has not been seen anywhere in the outcrops studied, this scour is interpreted to represent a bar deposited at or downstream of a tributary confluence. The increased accommodation created here due to the confluence is also indicated by the fact that both the median cross-set thickness and the value of the thickest cross-set, is greater at this site than at any of the upstream non-confluence locations. The median value at this confluence site is ~60 cm, which is two times more than those at non-confluence locations. Also, the thickest cross-set at the tributary confluence is approximately 2.5 m while at the non-confluence location is less than a meter (Fig. 4.8).

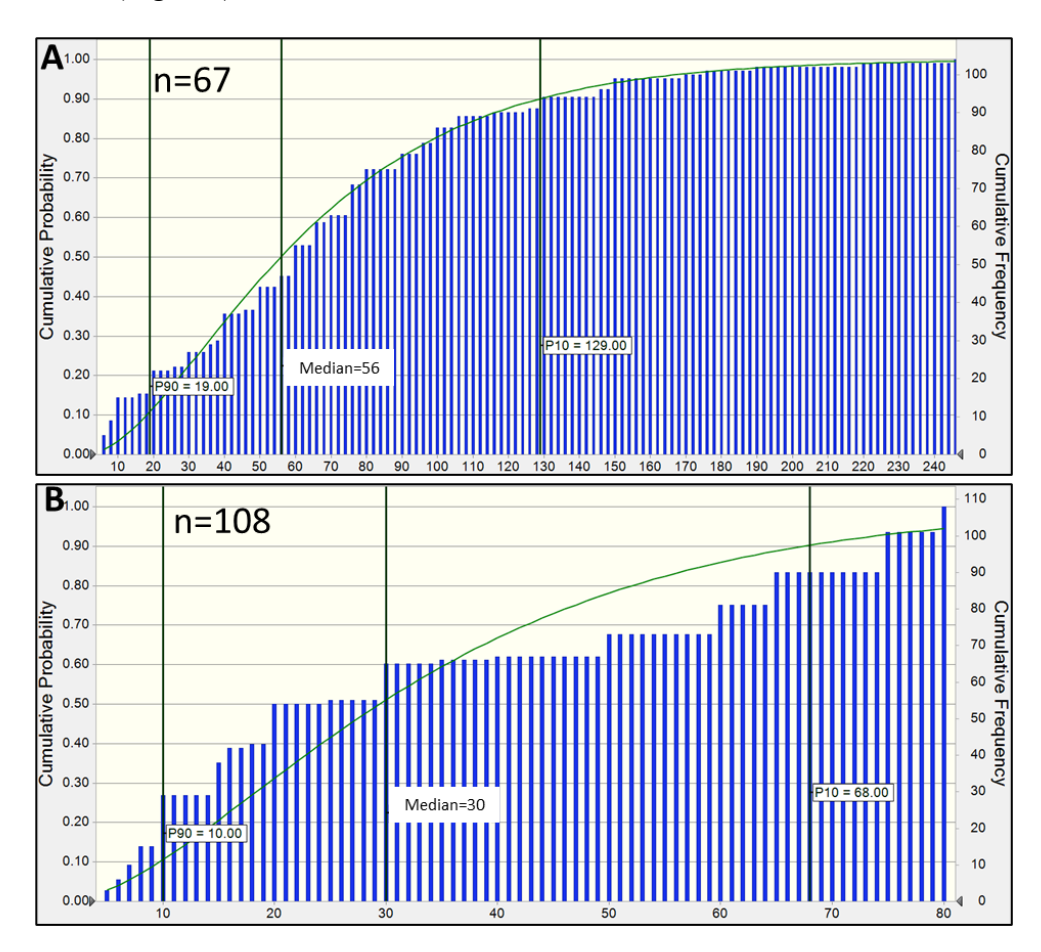


Figure 4.8. Cumulative probability distribution of the cross-set thickness at the tributary junction (A) and at upstream channels (B). The median cross-set thickness at the tributary junction is twice that at upstream channels. Also, the value of the

thickest cross-set at the tributary confluence is almost three-times that at upstream channels. All the measurements are in cm. Distribution generated by the Data Analysis tool of the Oracle Crystal ball in MS Excel.

The relative depth of scour in the Jamuna River was estimated by Klassen and Vermeer (1988) using the following equation:

$$\frac{H_S}{H} = 1.292 + 0.037\theta \tag{4.1}$$

where, H_s is the scour depth, H is the average depth of the upstream channel and θ is the confluence angle.

In their experimental studies, Mosley (1976) and Mosley and Schumm (1977) found that the relative scour depth changes as a function of the confluence angle. Although, the relationship was non-linear with some scatter, he proposed that the relative scour depth increases with increasing confluence angle from 15° to 90°. Mosely (1976) and Best (1986) found that the confluence depth is more likely to be two to four times the mean depth of the upstream channels.

Substituting 12 m and 4 m for H_s and H respectively in the above equation, results in a confluence angle of about 46° for the current study, which falls within the range of values for natural confluences between arid and humid climates of 45° and 72° respectively (Seybold et al. 2017). For the confluence depth to be more than five times the depth of the incoming channels (Best and Ashworth 1997), the confluence angle would have to be more than 100° , which might be rare in natural rivers (Seybold et al. 2017).

4.7 Discussion

4.7.1. Confluence scours or incised valleys?

Deposits of confluence scours can be misidentified as valley fills, and this might be one of the possible reasons behind the relative dearth of examples of confluence deposits in studies based on outcrops. Deposits of a single channel fill, which are much thicker than the average channel depth, are more likely to be confluence deposits. In our case for example, the 12 m thick downstream accreting bar represents the deposit of a single channel. This is considerably more than the 3 – 6 m bankfull channel depth seen in the outcrops. Moreover, there are multiple examples of smaller-scale channel confluence deposits represented by single large foresets, which are more than 2 m in thickness. Fielding (2022) presents multiple examples (their Figure 7.4 b-d) where anomalously thick single channel deposits are identified as confluence deposits and not valley fills. Similar examples have also been reported from the Ferron Sandstone of Utah, USA (Ullah et al. 2015). Studies, particularly outcrop based, which involve establishing the hierarchy of bounding surfaces and identifying architectural elements, should make the task of identifying confluence scour deposits easier (Holbrook and Oboh-Ikuenobe 2002; Miall 2006). Holbrook et al. (2001) describes valleys, bounded by 7th order surfaces, to be filled with two-to-ten channel belts bounded by sixth order surface. This is the case with our study as well, wherein the valley bounding surface (7th order) encloses at least two 6th order channel belts (Fig. 4.3).

Confluence deposits can be distinguished from incised valley fills, as they are bounded by erosive fifth order channel bases and topped by fourth order surfaces, are not regional features, and represent an out-sized deposit of a single channel episode. Incised valley deposits are bounded by seventh or higher order surfaces, are regionally extensive and are usually composed of at least two vertically stacked channel belts. Valley depth is usually controlled by the height of the exposed knickpoint, and the multistorey nature of a valley fill will reflect the ratio of valley depth to formative river depth. There are examples of continental scale rivers that are only able to incise 1.5 times the channel depth (e.g. Reijenstein et al. 2011) as the knickpoint depth is only 1.5 deeper than the river. This contrasts with an extreme example such as the Grand Canyon, where the 10 m deep Colorado River lies at the bottom of the 1800 m deep canyon. The width of a valley is controlled by duration of downcutting and the erodibility of the substrate. The distinction of valleys versus deep confluence scours can be made by careful analysis of bedding hierarchy, integrated with regional sequence stratigraphic analysis.

4.7.2. Relative scour depth

The Ganges-Brahmaputra-Meghna, or as it is called in Bangladesh, the Padma-Jamuna-Meghna fluvial system (Fig. 4.9), shows excellent examples of confluence scours ranging from bar-scale scours to much larger tributary scours (Coleman 1969; Klassen and Vermeer 1988; FAP24 1996c and 1996d; Best and Ashworth 1997; FSPB 2005 vol 5; Sambrook Smith et al. 2005 and 2019).

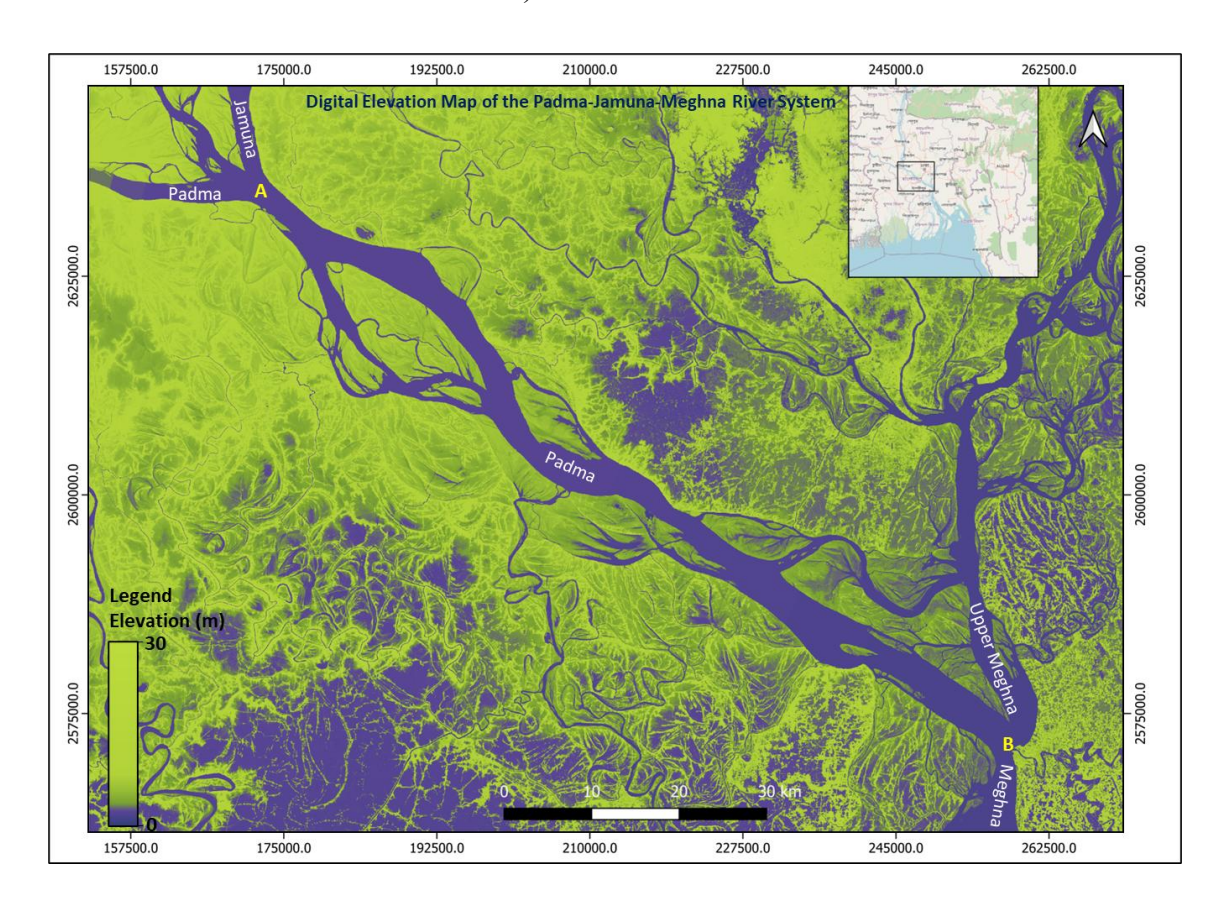


Figure 4.9. Digital elevation map showing the confluences of the Padma and Jamuna rivers (A) and Padma and Upper Meghna rivers (B) respectively. The geographical location of the area within Bangladesh is shown in the inset. The DEM used here is ASTER GDEM v3 with a resolution of 1arc.

The Jamuna and the Padma rivers have been classified as typical braided rivers (Coleman 1969; Klassen and Vermeer 1988; Sarker et al. 2003; Sarker et al. 2006; FSPB 2005 vol.5; Ashworth and Lewin 2012). The average depth of the Jamuna and Padma rivers is approx. 8 m (Klassen and Vermeer 1988; FAP24 1996a and b) and 10 m respectively (Neill et al.

2010; McLean et al. 2012; Halder and Chowdhury 2023). However, the scour depth at the confluence of the Padma and Jamuna rivers can reach up to 30 m (Fig. 4.10) while that at the confluence of the Padma and Upper Meghna rivers can reach up to 50 m (Fig. 4.11). This represents a relative scour depth ratio of more than 5 (Best and Ashworth 1997). This prompted Best and Ashworth (1997) to conclude that confluence scours should be more than five times deeper than the average channel depth.

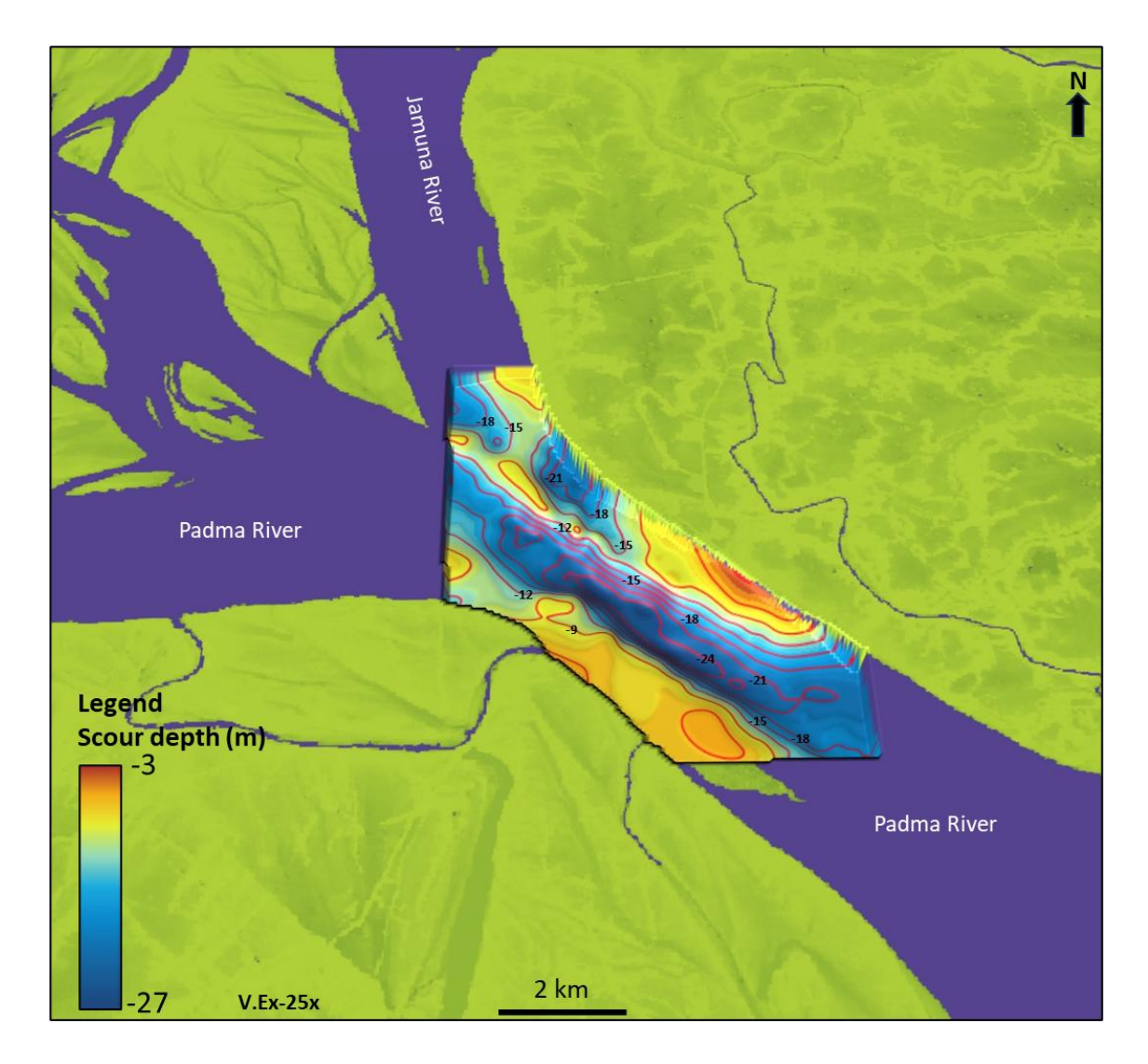


Figure 4.10. Multiple scours can be seen at the confluence of the Jamun and Padma rivers. Each of these scours is deeper than the average depth of either of the two rivers, with the main confluence being approx. 8 km long and 1.4 km wide. Data provided by British Geological Survey materials © UKRI [2013-14].

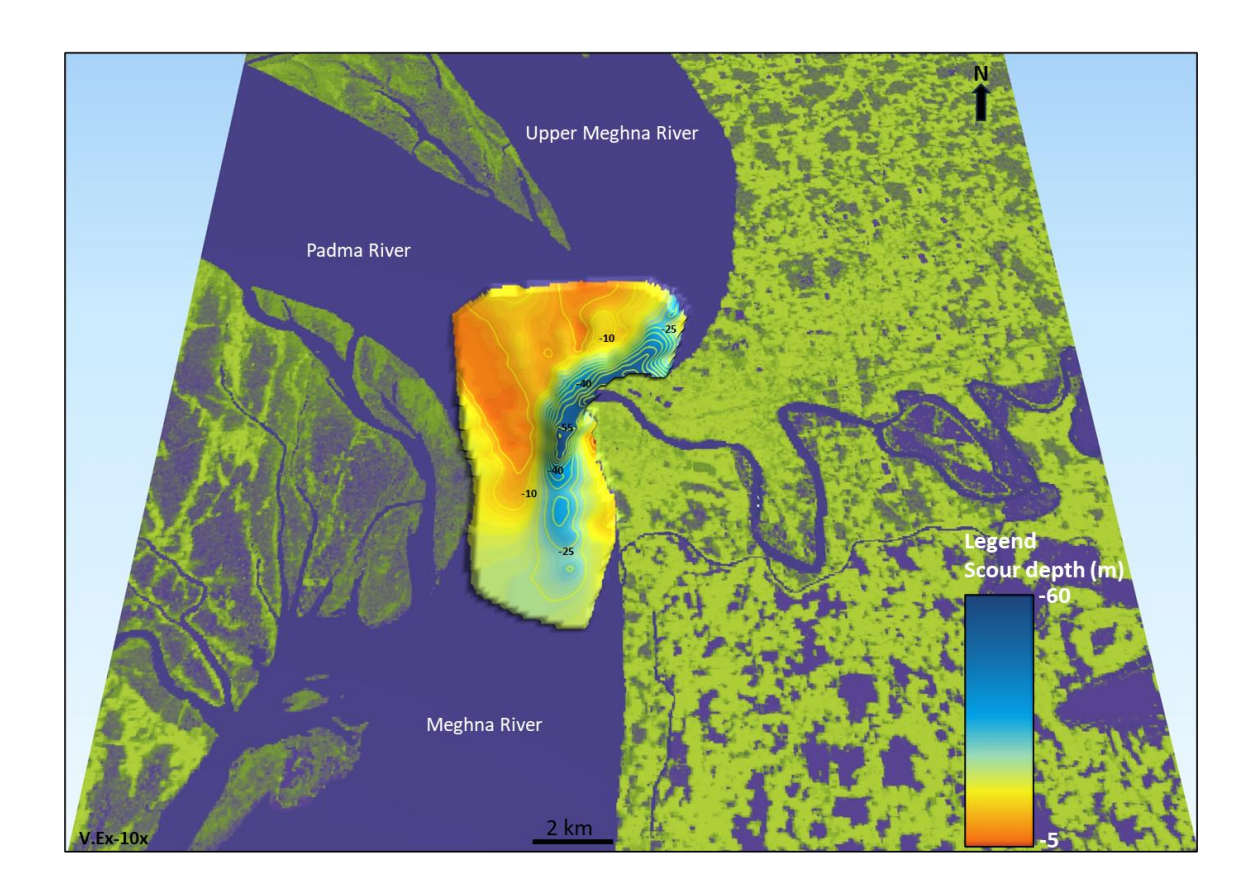


Figure 4.11. The confluence of the Padma River with the Upper Meghna tributary. The main confluence is approx. 6 km long and 900 m wide and has a scour which is close to 60 m deep. Data provided by British Geological Survey materials © UKRI [2013-14].

However, there are studies, including the current, which clearly show that this is not necessary. In their study of the confluence between the Negro (median depth of 24 - 31 m) and Solimoes (median depth of 27 - 28 m) rivers, Gualtieri et al. (2018), reported a confluence scour depth up to 70 m. This represents a relative scour depth of more than 2. While describing the confluence scours within the distributary channels of the Øyeren delta plain, Eilertsen and Hansen (2008) reported relative scour depth ranging from 2 to 3.3.

Similar values for the relative scour depth have also been reported from the rock record. In an outcrop study of the Triassic Hawkesbury Sandstone of Sydney Basin in Australia, Miall and Jones (2003) reported a scour depth (their Hollow Element) of up to 20 m while the average channel depth was reported to be 5-10 m, representing a relative scour depth of

2-5. Ullah et al. (2015) in their study of the Cretaceous Ferron Sandstone in Utah, USA, reported scour depths approximately two times deeper than the average bankfull channel depth. The current study also found that the relative scour depth is ~2.4, considering a mean channel depth of 5 m and a channel-confluence scour of 12 m.

4.8 Conclusions

The fluvial deposits of the Cretaceous Torrivio Sandstone contain clear evidence of autogenically produced scours. These scours occur downstream of mid channel braid bars as well as at a tributary junction. The scour deposit at the tributary junction is represented by a 12 m thick downstream migrating bar, which shows deposition by a single channel forming episode. The median thickness of cross-sets and the value of the thickest cross-set are both highest at this junction. The accommodation needed for such a thick deposit, and the scarcity of similar features across the outcrop belt, is best explained as being formed at a tributary junction. The erosional relief produced by the tributary junction scour is more than twice the average bankfull channel depth. This clearly shows that autogenic scours do not have to be at least five times the average channel depth.

Confluence scours represent the deepest depths in fluvial systems produced by autogenic processes. Even though confluence scour deposits have a high probability of preservation in the rock record, they have not been extensively documented in the literature. Confluence deposits can be distinguished from incised valley fills. They are bounded by erosive fifth order channel bases and topped by fourth order surfaces, are not regional features, and represent an out-sized deposit of a single channel episode. In contrast, incised valley deposits are bounded by seventh or higher order surfaces, are regionally extensive and composed of at least two channel belts. However, this distinction will only be easier if detailed architectural analysis and bounding surface hierarchy can be established on cross-sectional geometries exposed in outcrops.

References

- Ahadiyan, J., Adeli, A., Bahmanpouri, F. and Gualtieri, C., 2018. Numerical simulation of flow and scour in a laboratory junction. Geosciences, 8(5), p.162.
- Ashmore, P., 1993. Anabranch confluence kinetics and sedimentation processes in gravel-braided streams. Geological Society, London, Special Publications, 75(1), pp.129-146.
- Ashmore, P. and Parker, G., 1983. Confluence scour in coarse braided streams. Water Resources Research, 19(2), pp.392-402.
- Ashworth, P.J. and Lewin, J., 2012. How do big rivers come to be different?. Earth-Science Reviews, 114(1-2), pp.84-107.
- Best, J.L., 1986. The morphology of river channel confluences. Progress in Physical Geography, 10(2), pp.157-174.
- Best, J.L., 1988. Sediment transport and bed morphology at river channel confluences. Sedimentology, 35(3), pp.481-498.
- Best, J.L. and Ashworth, P.J., 1997. Scour in large braided rivers and the recognition of sequence stratigraphic boundaries. Nature, 387(6630), pp.275-277.Best, J.L. and Rhoads, B.L., 2008. Sediment transport, bed morphology and the sedimentology of river channel confluences. River confluences, tributaries and the fluvial network, pp.45-72.
- Best, J.L. and Rhoads, B.L., 2008. Sediment transport, bed morphology and the sedimentology of river channel confluences. River confluences, tributaries and the fluvial network, pp.45-72.
- Bhattacharya, J.P., Copeland, P., Lawton, T.F., and Holbrook, J., 2016, Estimation of source area, river paleo-discharge, paleoslope and sediment budgets of linked deeptime depositional systems and implications for hydrocarbons: Earth-Science Reviews, v. 153, p. 77-110.
- Bhattacharya, J.P., and Tye, R.S., 2004, Searching for modern Ferron analogs and application to subsurface interpretation, in Chidsey T.C. Jr., Adams, R.D., and Morris, T.H. eds., The Fluvial-Deltaic Ferron Sandstone: Regional to Wellbore Analog for Fluvial-Deltaic Reservoir Modeling: American Association of Petroleum Geologists, Studies in Geology, 50, p. 39–57.

- Biron, P., Roy, A., Best, J.L. and Boyer, C.J., 1993. Bed morphology and sedimentology at the confluence of unequal depth channels. Geomorphology, 8(2-3), pp.115-129.
- Bridge, J.S., 1997, Thickness of sets of cross-strata and planar strata as a function of formative bedwave geometry and migration: Geology, v. 25, p. 971–974.
- Bridge, J.S., 2003, Rivers and Floodplains: Forms, Processes, and Sedimentary Record: Malden, Massachusetts, Blackwell Science, 491 p.
- Bridge, J.S. and Lunt, I.A., 2006. Depositional models of braided rivers (Vol. 36, pp. 11-50). Oxford, UK: Blackwell Publishing.
- Bristow, C.S. and Best, J.L., 1993. Braided rivers: perspectives and problems. Geological society, London, special publications, 75(1), pp.1-11.
- Bristow, C.S., Best, J.L. and Roy, A.G., 1993. Morphology and facies models of channel confluences. Alluvial Sedimentation, pp.89-100.
- Coleman, J.M., 1969. Brahmaputra River: channel processes and sedimentation. Sedimentary geology, 3(2-3), pp.129-239.
- Cowan, E.J., 1991. The large-scale architecture of the fluvial Westwater Canyon Member, Morrison Formation (Upper Jurassic), San Juan Basin, New Mexico.
- Dixon, S.J., Smith, G.H.S., Best, J.L., Nicholas, A.P., Bull, J.M., Vardy, M.E., Sarker, M.H. and Goodbred, S., 2018. The planform mobility of river channel confluences:
 Insights from analysis of remotely sensed imagery. Earth-Science Reviews, 176, pp.1-18.
- Eilertsen, R.S. and Hansen, L., 2008. Morphology of riverbed scours on a delta plain revealed by interferometric sonar. Geomorphology, 94(1-2), pp.58-68.
- Feasibility Study of Padma Bridge (FSPB) in the People's Republic of Bangladesh; JICA and JMBA (2005), Volume 5: River studies.
- Fielding, C.R., 2022. Sedimentology and stratigraphy of large river deposits: recognition and preservation potential in the rock record. Large Rivers: Geomorphology and Management, Second Edition, pp.146-170.
- Flood Action Plan 24; Delft Hydraulics and DHI (1996a) FAP24 River Survey Project, Final Report, Main Volume (prepared for FPCO), Dhaka, Bangladesh, 280 pp.

- Flood Action Plan 24; Delft Hydraulics and DHI (1996b) FAP24 River Survey Project, Final Report Annex 3: Hydrology (prepared for FPCO), Dhaka, Bangladesh.
- Flood Action Plan 24; Delft Hydraulics and DHI (1996c) FAP24 River Survey Project, Final Report Annex 4: Sedimentology, (prepared for FPCO), Dhaka, Bangladesh.
- Flood Action Plan 24; Delft Hydraulics and DHI (1996d) FAP24 River Survey Project, Final Report Annex 5: Morphological Characteristics (prepared for FPCO), Dhaka, Bangladesh.
- Flores, R.M., Hohman, J.C. and Ethridge, F.G., 1991. Heterogeneity of Upper Cretaceous Gallup sandstone regressive fades, Gallup Sag, New Mexico.
- Ghinassi, M. and Ielpi, A., 2015. Stratal architecture and morphodynamics of downstream-migrating fluvial point bars (Jurassic Scalby Formation, UK). Journal of Sedimentary Research, 85(9), pp.1123-1137.
- Ghinassi, M., Ielpi, A., Aldinucci, M. and Fustic, M., 2016. Downstream-migrating fluvial point bars in the rock record. Sedimentary Geology, 334, pp.66-96.
- Gibling, M.R., 2006. Width and thickness of fluvial channel bodies and valley fills in the geological record: a literature compilation and classification. Journal of sedimentary Research, 76(5), pp.731-770.
- Gualtieri, C., Filizola, N., de Oliveira, M., Santos, A.M. and Ianniruberto, M., 2018. A field study of the confluence between Negro and Solimões Rivers. Part 1: Hydrodynamics and sediment transport. Comptes Rendus. Géoscience, 350(1-2), pp.31-42.
- Halder, A. and Mowla Chowdhury, R., 2023. Evaluation of the river Padma morphological transition in the central Bangladesh using GIS and remote sensing techniques. International Journal of River Basin Management, 21(1), pp.21-35.
- Heinz, J., Kleineidam, S., Teutsch, G. and Aigner, T., 2003. Heterogeneity patterns of Quaternary glaciofluvial gravel bodies (SW-Germany): application to hydrogeology. Sedimentary geology, 158(1-2), pp.1-23.
- Hohman, J.C., 1986. Depositional Model of Coal-bearing, Upper Cretaceous Gallup Sandstone, Gallup Sag Area, New Mexico (Doctoral dissertation, Colorado State University).

- Holbrook, J., 2001. Origin, genetic interrelationships, and stratigraphy over the continuum of fluvial channel-form bounding surfaces: an illustration from middle Cretaceous strata, southeastern Colorado. Sedimentary Geology, 144(3-4), pp.179-222.
- Holbrook, J., and Oboh-Ikuenobe, F.E., 2002. Bounding-surface hierarchies and related sources of heterogeneity in seemingly uniform fluvial sandstone sheets.
- Holbrook, J., and Wanas, H., 2014, A fulcrum approach to assessing source-to-sink mass balance using channel paleohydrologic parameters derivable from Common fluvial data sets with an example from the Cretaceous of Egypt: Journal of Sedimentary Research, v. 84, p. 349–372.
- Huggenberger, P., 1993. Radar facies: recognition of facies patterns and heterogeneities within Pleistocene Rhine gravels, NE Switzerland. Geological Society, London, Special Publications, 75(1), pp.163-176.
- Ianniruberto, M., Trevethan, M., Pinheiro, A., Andrade, J.F., Dantas, E., Filizola, N., Santos, A. and Gualtieri, C., 2018. A field study of the confluence between Negro and Solimões Rivers. Part 2: Bed morphology and stratigraphy. Comptes Rendus. Géoscience, 350(1-2), pp.43-54.
- Klassen, G.J. and Vermeer, K., 1988. Channel characteristics of the braiding Jamuna River, Bangladesh. In International Conference on River Regime. Hydraulics Research Limited, Wallingford, Oxon UK. 1988. p 173-189. 16 fig, 1 tab, 13 ref..Leclair, S.F., and Bridge, J.S., 2001, Quantitative interpretation of sedimentary structures formed by river dunes: Journal of Sedimentary Research, v. 71, p. 713–716.
- Kostic, B. and Aigner, T., 2007. Sedimentary architecture and 3D ground-penetrating radar analysis of gravelly meandering river deposits (Neckar Valley, SW Germany). Sedimentology, 54(4), pp.789-808.
- Leclair, S.F., Bridge, J.S., and Wang, F., 1997, Preservation of cross-strata due to migration of subaqueous dunes over aggrading and non-aggrading beds: Comparison of experimental data with theory: Geoscience Canada, v. 24, p. 55–66.
- Leclair, S.F., and Bridge, J.S., 2001, Quantitative interpretation of sedimentary structures formed by river dunes: Journal of Sedimentary Research, v. 71, p. 713–716.

- Leite Ribeiro, M., Blanckaert, K., Roy, A.G. and Schleiss, A.J., 2012. Flow and sediment dynamics in channel confluences. Journal of Geophysical Research: Earth Surface, 117(F1).
- Lin, W., and Bhattacharya, J.P., 2016, Estimation of Source-to-Sink Mass Balance and Depositional Systems Dominated Sediment Budgets by a Fulcrum Approach Assessment Using Channel Paleohydrologic Parameters: Cretaceous Dunvegan Formation: American Association of Petroleum Geologists, Search and Discovery article#41852.
- McLean, D.G., Vasquez, J.A., Oberhagemann, K. and Sarker, M.H., 2012, January. Padma river morphodynamics near Padma bridge. In River Flow 2012-Proceedings of the International Conference on Fluvial Hydraulics (Vol. 1, pp. 741-747).
- Miall, A.D., 1985. Architectural-element analysis: a new method of facies analysis applied to fluvial deposits.
- Miall, A.D., 1988. Architectural elements and bounding surfaces in fluvial deposits: anatomy of the Kayenta Formation (Lower Jurassic), southwest Colorado. Sedimentary Geology, 55(3-4), pp.233-262.
- Miall, A.D., 1992. Sedimentology of a sequence boundary within the nonmarine Torrivio Member, Gallup Sandstone (Cretaceous), San Juan Basin, New Mexico.
- Miall, A.D. and Jones, B.G., 2003. Fluvial architecture of the Hawkesbury sandstone (Triassic), near Sydney, Australia. Journal of Sedimentary Research, 73(4), pp.531-545.
- Molenaar, C.M., 1973. Sedimentary facies and correlation of the Gallup Sandstone and associated formations, northwestern New Mexico.
- Molenaar, C.M., 1974, January. Correlation of the Gallup Sandstone and associated formations, upper cretaceous, eastern San Juan and Acoma Basins, New Mexico. In Ghost Ranch: New Mexico Geological Society Guidebook, 25th Field Conference (pp. 251-258).
- Molenaar, C.M., 1977. The Pinedale oil seep-an exhumed stratigraphic trap in the southwestern San Juan Basin. In San Juan Basin III: New Mexico Geol. Soc. Guidebook, 28th Field Conference (p. 243).

- Molenaar, C.M., 1983. Major depositional cycles and regional correlations of Upper Cretaceous rocks, southern Colorado Plateau and adjacent areas. Rocky Mountain Section (SEPM).
- Mosley, M.P., 1976. An experimental study of channel confluences. The journal of geology, 84(5), pp.535-562.
- Mosley, M.P. and Schumm, S.A., 1977. Stream junctions; a probable location for bedrock placers. Economic Geology, 72(4), pp.691-694.
- Neill, C.R., Oberhagemann, K., McLean, D. and Ferdous, Q.M., 2010, August. River training works for Padma multipurpose bridge, Bangladesh. In IABSE-JSCE joint conference on advances in bridge engineering-II (pp. 441-448).
- Nummedal, D., 1990, Sequence stratigraphic analysis of upper Turonian and Coniacian strata in the San Juan basin, New Mexico, U.S.A., in R.N. Ginsburg and B. Beaudoin, eds., Cretaceous resources, events and rhythms: Dordrecht, Kluwer Publishing, p. 33–46.
- Nummedal, D. and Molenaar, C.M., 1995. Sequence stratigraphy of ramp-setting strand plain successions: the Gallup Sandstone, New Mexico.
- Nummedal, D. and Riley, G.W., 1991. Origin of late Turonian and Coniacian unconformities in the San Juan basin.
- Nummedal, D. and Swift, D.J., 1987. Transgressive stratigraphy at sequence-bounding unconformities: some principles derived from Holocene and Cretaceous examples.
- Parsons, D.R., Best, J.L., Lane, S.N., Kostaschuk, R.A., Hardy, R.J., Orfeo, O., Amsler, M.L. and Szupiany, R.N., 2008. Large river channel confluences. River confluences, tributaries and the fluvial network, pp.73-91.
- Reijenstein, H.M., Posamentier, H.W. and Bhattacharya, J.P., 2011. Seismic geomorphology and high-resolution seismic stratigraphy of inner-shelf fluvial, estuarine, deltaic, and marine sequences, Gulf of Thailand. AAPG bulletin, 95(11), pp.1959-1990.
- Rhoads, B.L., 2020. River dynamics: Geomorphology to support management. Cambridge University Press.

- Sambrook Smith, G.H., Ashworth, P.J., Best, J.L., Woodward, J. and Simpson, C.J., 2005. The morphology and facies of sandy braided rivers: some considerations of scale invariance. Fluvial sedimentology VII, pp.145-158.
- Sambrook Smith, G.H., Nicholas, A.P., Best, J.L., Bull, J.M., Dixon, S.J., Goodbred, S., Sarker, M.H. and Vardy, M.E., 2019. The sedimentology of river confluences. Sedimentology, 66(2), pp.391-407.
- Sarker, M.H., Huque, I., Alam, M. and Koudstaal, R., 2003. Rivers, chars and char dwellers of Bangladesh. International Journal of River Basin Management, 1(1), pp.61-80.
- Sarker, M.H. and Thorne, C.R., 2006. Morphological response of the Brahmaputra–Padma–Lower Meghna River system to the Assam earthquake of 1950. Braided Rivers: process, deposits, ecology and management, 36, pp.289-310.
- Sharma, S., Bhattacharya, J.P. and Richards, B., 2017. Source-to-sink sediment budget analysis of the Cretaceous Ferron Sandstone, Utah, USA, using the fulcrum approach. Journal of Sedimentary Research, 87(6), pp.594-608.
- Seybold, H., Rothman, D.H. and Kirchner, J.W., 2017. Climate's watermark in the geometry of stream networks. Geophysical Research Letters, 44(5), pp.2272-2280.
- Siegenthaler, C. and Huggenberger, P., 1993. Pleistocene Rhine gravel: deposits of a braided river system with dominant pool preservation. Geological Society, London, Special Publications, 75(1), pp.147-162.
- Ullah, M. S., Bhattacharya, J. P., and Dupre, W. R., 2015, Confluence scours versus incised valleys: Examples from the Cretaceous Ferron Notom Delta, Southeastern Utah, USA: Journal of Sedimentary Research, v. 85, p. 445-458.

Chapter 5

Conclusions

The objectives of the current research, as outlined in Chapter 1, have been achieved successfully. This study has successfully tested the quantitative fulcrum method by balancing sediment budgets in the previously well-studied Cretaceous Ferron Sandstone and applied the same quantitative approach to decipher the nature, size and scale and paleohydraulics of the formative rivers of the late Cretaceous Torrivio Sandstone using a field-based approach. More generally, this thesis integrates facies architectural analysis and novel use of drones to provide more accurate interpretation of ancient rivers systems, and uses a combination of physics-based, empirically-derived and statistical approaches for improved quantification of ancient river systems. The development of this quantitative approach has broad implications for prediction of source-to-sink scaling relationships, such as predicting ancient drainage areas, that can be important in paleotectonic and paleogeographic reconstructions, as well as prediction of downstream sink volumes, that can be critical for evaluating resources such as ground water and hydrocarbons. This thesis also advances models for interpreting a wide variety of fluvial scour surfaces that can include bar-top hollows, normal channel scours, and confluence scours that range from smaller bar-scale to larger tributary junctions. All these scour features are autogenic in origin, and it is critical to distinguish them from regional allogenic erosional surfaces formed as incised valleys that define sequence boundaries. This thesis thus addresses the ongoing debate as to how autogenic and allogenic scour surfaces are distinguished in ancient systems (see Holbrook and Bhattacharya 2012) and the implications for defining sequences in fluvial systems. "Sophisticated Stratigraphy" is the term recently coined by Miall (2013) for current advancement in the field of sedimentology and stratigraphy following the use of new datasets and methods. This thesis is an excellent example of this approach as it successfully integrates novel datasets, e.g. drone images and analytical processes, e.g. Monte-Carlo simulations, for new and improved quantitative analysis of ancient systems.

Chapter 2 documents successful application of the "fulcrum" approach to establish a massbalance between the feeder system and the depositional sink of the Cretaceous Ferron Sandstone in Central Utah Ferron Sandstone. Outcrop measurements (Richards 2014), such as channel depth, width, and grain size, were used to estimate paleodischarge in an identified ancient trunk channel. The bankfull channel dimensions and other paleohydraulic parameters like slope and mean flow velocity were estimated using more than one independent method for good quality control. The estimates of instantaneous discharge were first converted to mean annual discharge then integrated over the geological duration of the river to estimate the total sediment volume delivered to the downstream deltaic sinks to balance the estimated sediment flux. The mass balance across the fulcrum reveals that the average bedload sediment volume derived from the source (about 3 km³) matches with that mapped in the depositional sink within a factor of two. Probabilistic estimation, based on Monte-Carlo simulations, were used to test the sensitivity of key parameters used in converting bankfull discharge to mean annual discharge. The P10, P50 (median), and P90 values for the average annual bedload volume (Q_{mas}) are 9.1×10^4 m³, 1.7×10^5 m³ and 3.7×10^5 m³ respectively. A Q_{mas} value between P50 and P90 yields a source-to-sink balance for bedload volume. This was the first study to use a statistical approach in estimating the mean annual water and sediment discharge and to study the sensitivity of different factors used in the estimation.

Chapter 3 presents a field-based outcrop study of the late Cretaceous Torrivio Sandstone in New Mexico. The facies architecture and planform geometry of the Torrivio River were interpreted using detailed bedding diagrams built on photomosaics obtained from 2D models using GigaPan images and 3D models using UAV or drone images. These photomosaics, complimented with measured sections, produced bedding geometries used to clearly distinguish the nature of the river system. 3D models built using high resolution drone images were also used to estimate paleocurrents, that are critical to determine the orientation of cliff faces to flow directions and are the basis or interpretation of bars and channels required to characterize the fluvial style. This study used a novel 3-point technique, initially designed for use in structural geology, on 3D outcrop models for estimating paleocurrent and sandstone body dimensions.

Although earlier studies have also proposed a braided nature for the deposits of the Torrivio Sandstone (Molenaar 1973, 1974; Hohman 1986; Flores et al. 1991; Nummedal and Molenaar 1995), this is first time that the interpretation is supported by detailed bedding diagrams and architectural element analysis in flow-normal cliff sections. This study also establishes that the Torrivio Sandstone was built by a mixed-river system, which evolved over time from a weakly braided system to a more sinuous single channel system, suggesting a possible reduction in its stream power. The backwater limit of the Torrivio River is estimated for the first time in this study and is approx. 20 km. The amalgamated nature of the Torrivio deposits in this study highlights that these channels are landward of the backwater limit (Lin et al. 2019; Wu et al. 2022). Paleohydraulic analysis estimates that the braided river was about 3 m to 6 m deep and 100 m to 350 m wide. The overlying sinuous channel was approximately 4 m deep and 30 m wide. This is the first study which estimates the size and scale of the formative rivers for the Torrivio Sandstone using both direct outcrop information and independent empirical equations.

Modern analogs, suitably selected from similar climatic conditions as those of the Torrivio Sandstone, were used in the estimation of annual bedload discharge, which helped reduce the range of uncertainty in the estimation. Paleodischarge estimates of the braided section of the Torrivio Sandstone show that the average water discharge was ~1850 m³/sec, whereas the average bedload discharge was 0.27 m³/s. The average annual bedload volume was estimated to be about 30.2 x 10⁴ m³. It was also shown that the range of uncertainty in the estimation of annual water and sediment discharge can be significantly reduced by using climate-binned modern analogs. In comparison with the paleodischarge analysis of the Ferron Sandstone, the range in the estimation of the annual bedload volume was reduced to less than 4, which highlights the improvement in estimation. Independent methods were also successfully used for the estimation of drainage area of the Torrivio River, like paleogeographic reconstruction and geomorphological regional curves.

Chapter 4 documents different scales of confluence scour seen in the outcrop. These scours range from a 12 m thick downstream migrating tributary confluence scour to smaller meterscale scours typically formed downstream of a mid-channel bar. The deposit of the confluence scours downstream of mid-channel bars are characterized by compound bars

consisting of up to seven cross-set units, although thicker deposits might be expected if not for reworking and truncation. Both the 4th order and 5th order surfaces can form the erosive base of these deposits (Bridge 2003; Smith et al. 2019). The small-scale channel confluence scour fills are characterized by a single set of oversized foresets dipping obliquely at a steeper angle into the scour. The scour bases are represented by 5th order bounding surfaces while 4th order surfaces form the top of the deposits (Ullah et al. 2015). The large foresets represent the avalanching face of a tributary mouth bar moving into the scour hole (Best 1988; Bristow et al. 1993; Smith et al. 2019). At a larger scale, a 12 m thick, downstream accreting bar was identified as a tributary-confluence fill. This interpretation is in contrast with the earlier study of Miall (1992) who described the section to represent the deposit of a laterally migrating and presumably meandering channel. The revised interpretation was made possible by incorporating paleocurrent data from 3D model constructed using highresolution UAV images. This was the first time that a tributary-confluence scour has been successfully documented in an ancient system. Quantitative estimation in this study demonstrated the fact that the confluence scours are autogenic features and fundamentally different from incised valleys, which are allogenically formed. It was also established that confluence scours need not be more than five times deeper than the average channel depth, as suggested by earlier studies (Best and Ashworth 1997). Proper distinction between these scours and the average bankfull channel depth has resulted in an accurate estimation of paleohydraulic parameters that were used to determine sediment transport strength, paleodischarge, and sediment flux of a fluvial system (Holbrook and Wanas 2014; Bhattacharya et al. 2016; Sharma et al. 2017; Smith et al. 2019).

5.1 Future directions

A source-to-sink mass balance could not be established for the Torrivio Sandstone, as the sink is eroded by a regional tectonic unconformity that eroded the distal part of the sequence. However, since it has been suggested that the Torrivio Sandstone might have been reworked into the Tocito Sandstone (Jennette and Jones 1995; Valasek 1995), a

possible depositional sink can be mapped in the future by mapping the extent of the Tocito Sandstone.

Although qualitative facies models have been present for some time (Allen 1983; Miall 1988, 1996), similar progress in quantitative facies modelling is lacking. This approach however is required to put constraints on the dimensions of sandstone bodies, such as channels and channel belts. These models can be used as template for comparison, interpretation and prediction for unexplored basins. Therefore, the focus should be on developing more quantitative models in the future.

The current research work establishes that while it is still imperative to study outcrops, there needs to be increased integration with other datasets like sub-surface data and modern analogs. This integration could be particularly important in areas with poor and/or inaccessible outcrop exposures. As has been demonstrated in this study, UAV or drone photography is a highly valuable tool for making 3D models of depositional systems and obtaining information that might not be directly accessed from the outcrops and also to produce useful scaled models of ancient systems. Different scales of scour surfaces can also be identified using this approach. Another approach may involve developing virtual 3D models of the outcrops by combining UVA images with high-resolution GPR data (Fernandes jr. et al. 2015; Janocha et al. 2021). It would also be useful to integrate scaled experimental studies with the results of the outcrop studies.

Paleoclimatic reconstruction is very important in paleohydrology and sediment budget analysis, whether we use the BQART (Syvitski and Milliman 2007) or fulcrum method (Holbrook and Wanas 2014). If paleoclimatic reconstruction is sound, then suitable modern analogs can be selected to provide data on annual bankfull duration and their recurrence interval, which can help in reducing the range of uncertainty in the estimation of annual sediment load. However, there's also a need to improve the global hydrological database as most of the useful and continuous data are available mostly in the North America and Europe. A more integrated data sharing platform is also needed.

In cases where the input parameters are highly uncertain, which is normally the case with ancient systems, statistical methods like Monte-Carlo simulation could prove to be effective in capturing this uncertainty (Sharma et al. 2017).

References

- Allen, J.R.L., 1983. Studies in fluviatile sedimentation: bars, bar-complexes and sandstone sheets (low-sinuosity braided streams) in the Brownstones (L. Devonian), Welsh Borders. Sedimentary Geology, 33(4), pp.237-293.
- Best, J.L., 1988. Sediment transport and bed morphology at river channel confluences. Sedimentology, 35(3), pp.481-498.
- Best, J.L. and Ashworth, P.J., 1997. Scour in large braided rivers and the recognition of sequence stratigraphic boundaries. Nature, 387(6630), pp.275-277.Best, J.L. and Rhoads, B.L., 2008. Sediment transport, bed morphology and the sedimentology of river channel confluences. River confluences, tributaries and the fluvial network, pp.45-72.
- Bhattacharya, J.P., Copeland, P., Lawton, T.F. and Holbrook, J., 2016. Estimation of source area, river paleo-discharge, paleoslope, and sediment budgets of linked deeptime depositional systems and implications for hydrocarbon potential. Earth-Science Reviews, 153, pp.77-110.
- Bridge, J.S., 2003, Rivers and Floodplains: Forms, Processes, and Sedimentary Record: Malden, Massachusetts, Blackwell Science, 491 p.
- Bristow, C.S., 1993. Sedimentology of the Rough Rock: A Carboniferous braided river sheet sandstone in northern England. Geological Society, London, Special Publications, 75(1), pp.291-304.
- Fernandes Jr, A.L., Medeiros, W.E., Bezerra, F.H., Oliveira Jr, J.G. and Cazarin, C.L., 2015. GPR investigation of karst guided by comparison with outcrop and unmanned aerial vehicle imagery. Journal of Applied Geophysics, 112, pp.268-278.
- Flores, R.M., Hohman, J.C. and Ethridge, F.G., 1991. Heterogeneity of Upper Cretaceous Gallup sandstone regressive fades, Gallup Sag, New Mexico.

- Hohman, J.C., 1986. Depositional Model of Coal-bearing, Upper Cretaceous Gallup Sandstone, Gallup Sag Area, New Mexico (Doctoral dissertation, Colorado State University).
- Holbrook, J., and Bhattacharya, J.P., 2012, Reappraisal of the Sequence Boundary in Time and Space: Case and Considerations for an SU (Subaerial Unconformity) that is not a Sediment Bypass Surface, a Time Barrier, or an Unconformity. Earth-Science Reviews. v. 113, p. 271–302.
- Holbrook, J., and Wanas, H., 2014, A fulcrum approach to assessing source-to-sink mass balance using channel paleohydrologic parameters derivable from Common fluvial data sets with an example from the Cretaceous of Egypt: Journal of Sedimentary Research, v. 84, p. 349–372.
- Janocha, J., Smyrak-Sikora, A., Senger, K. and Birchall, T., 2021. Seeing beyond the outcrop: Integration of ground-penetrating radar with digital outcrop models of a paleokarst system. Marine and Petroleum Geology, 125, p.104833.
- Jennette, D.C. and Jones, C.R., 1995. Sequence stratigraphy of the Upper Cretaceous Tocito Sandstone: a model for tidally influenced incised valleys, San Juan Basin, New Mexico.
- Lin, W., Bhattacharya, J.P. and Stockford, A., 2019. High-resolution sequence stratigraphy and implications for cretaceous glacioeustasy of the Late Cretaceous Gallup System, New Mexico, USA. Journal of Sedimentary Research, 89(6), pp.552-575. Miall, A.D., 1985. Architectural-element analysis: a new method of facies analysis applied to fluvial deposits.
- Miall, A.D., 1980. Cyclicity and the facies model concept in fluvial deposits. Bulletin of Canadian Petroleum Geology, 28(1), pp.59-79.
- Miall, A.D., 1988. Architectural elements and bounding surfaces in fluvial deposits: anatomy of the Kayenta Formation (Lower Jurassic), southwest Colorado. Sedimentary Geology, 55(3-4), pp.233-262.
- Miall, A.D., 1992. Sedimentology of a sequence boundary within the nonmarine Torrivio Member, Gallup Sandstone (Cretaceous), San Juan Basin, New Mexico.

- Miall, A.D., 1996. The stratigraphic architecture of fluvial depositional systems. The Geology of Fluvial Deposits: Sedimentary Facies, Basin Analysis, and Petroleum Geology, pp.251-309.
- Miall, A.D., 2013. Sophisticated stratigraphy. The web of geological sciences: Advances, impacts and interactions: Geological Society of America Special Paper, 500, pp.169–190.
- Molenaar, C.M., 1973. Sedimentary facies and correlation of the Gallup Sandstone and associated formations, northwestern New Mexico.
- Molenaar, C.M., 1974, Correlation of the Gallup Sandstone and associated formations, upper cretaceous, eastern San Juan and Acoma Basins, New Mexico. In Ghost Ranch: New Mexico Geological Society Guidebook, 25th Field Conference (pp. 251-258).
- Nummedal, D. and Molenaar, C.M., 1995. Sequence stratigraphy of ramp-setting strand plain successions: the Gallup Sandstone, New Mexico.
- Richards, B.H., 2014, Fluvial to marine succession in a compound incised valley system in the Ferron Notom delta, Utah: M.Sc. Thesis: University of Houston, Houston, Texas, USA., 56 p.
- Sambrook Smith, G.H., Nicholas, A.P., Best, J.L., Bull, J.M., Dixon, S.J., Goodbred, S., Sarker, M.H. and Vardy, M.E., 2019. The sedimentology of river confluences. Sedimentology, 66(2), pp.391-407.
- Sharma, S., Bhattacharya, J.P. and Richards, B., 2017. Source-to-sink sediment budget analysis of the Cretaceous Ferron Sandstone, Utah, USA, using the fulcrum approach. Journal of Sedimentary Research, 87(6), pp.594-608.
- Syvitski, J.P. and Milliman, J.D., 2007. Geology, geography, and humans battle for dominance over the delivery of fluvial sediment to the coastal ocean. The Journal of Geology, 115(1), pp.1-19.
- Ullah, M. S., Bhattacharya, J. P., and Dupre, W. R., 2015, Confluence scours versus incised valleys: Examples from the Cretaceous Ferron Notom Delta, Southeastern Utah, USA: Journal of Sedimentary Research, v. 85, p. 445-458
- Valasek, D., 1995. The Tocito Sandstone in a sequence stratigraphic framework: An example of landward-stepping small-scale genetic sequences.

- Willis, B., 1993. Ancient river systems in the Himalayan foredeep, Chinji Village area, northern Pakistan. Sedimentary geology, 88(1-2), pp.1-76.
- Wu, T., Bhattacharya, J.P. and Jung-Ritchie, L., 2022. Sequence stratigraphic interpretation in marginal marine settings by the approach of parasequence-thickness-to-sandstone-fraction ratio: Case studies of the Gallup and Ferron outcrops in the Western Interior Basin, USA. *Journal of Sedimentary Research*, 92(2), pp.67-94.